

**Effect of II-VI Semiconductor Nanomaterials  
and Electron Irradiation on Polystyrene (PS)  
& Poly(ethylene-co-vinyl acetate) (EVA)**

*Thesis submitted to  
Cochin University of Science and Technology  
in partial fulfilment of the requirements  
for the award of the degree of  
Doctor of Philosophy  
under the  
Faculty of Technology*

*by*

**Jose Sebastian**  
Reg. No: 2958



**Department of Polymer Science and Rubber Technology  
Cochin University of Science and Technology  
Kochi- 682 022, Kerala, India**

*September 2015*

**Effect of II-VI Semiconductor Nanomaterials and Electron Irradiation  
on Polystyrene (PS) & Poly(ethylene-co-vinyl acetate) (EVA)**

*Ph. D Thesis*

*Author*

**Jose Sebastian**

Department of Polymer Science and Rubber Technology  
Cochin University of Science and Technology  
Cochin- 682 022, Kerala, India  
E-mail: joseuce@gmail.com

*Supervising guide*

**Dr. Eby Thomas Thachil**

Professor  
Department of Polymer  
Science and Rubber Technology,  
CUSAT  
E-mail: ethachil@gmail.com

Department of Polymer Science and Rubber Technology  
Cochin University of Science and Technology  
Cochin- 682 022, Kerala, India

September 2015



**Department of Polymer Science and Rubber Technology**  
**Cochin University of Science and Technology**

Cochin- 682 022, Kerala, India

---

**Dr. Eby Thomas Thachil**  
Professor (Retd.)

E-mail: ethachil@gmail.com

23/09/2015

## **Certificate**

This is to certify that the thesis entitled “**Effect of II-VI Semiconductor Nanomaterials and Electron Irradiation on Polystyrene (PS) & Poly (ethylene-co-vinyl acetate) (EVA)**” is an authentic report of the original work carried out by Mr. Jose Sebastian, under my supervision and guidance in the Department of Polymer Science and Rubber Technology, Cochin University of Science and Technology, Kochi – 682 022. No part of the work reported in this thesis has been presented for the award of any degree from any other institution. All the relevant corrections and modifications suggested by the audience during the pre-synopsis seminar and recommended by the Doctoral committee have been incorporated in the thesis.

**Dr. Eby Thomas Thachil**  
*(Supervising Guide)*

## *Declaration*

I hereby declare that the thesis entitled “**Effect of II-VI Semiconductor Nanomaterials and Electron Irradiation on Polystyrene (PS) & Poly (ethylene-co-vinyl acetate) (EVA)**” is the original work carried out by me under the guidance of Dr. Eby Thomas Thachil, Professor (Retd.), Department of Polymer Science and Rubber Technology, Cochin University of Science and Technology, Kochi 682 022, and no part of the work reported in this thesis has been presented for the award of any degree from any other institution.

Kochi – 22  
23/09/2015

**Jose Sebastian**

## *Acknowledgement*

---

*I thank God, the Heavenly Father for the great providence and abundant blessings showered on me, throughout the course of my research, and thereby allowing me to proclaim His Glory.*

*I am extremely thankful to my research guide and supervisor, Dr. Eby Thomas Thachil, Professor, Department of Polymer Science and Rubber Technology, Cochin University of Science and Technology for his enthusiastic encouragement, consistent support, valuable suggestions, inspiration, words of wisdom, personal care, which enabled me to complete my research work,*

*With great pleasure I put on record my sincere thanks to Dr. Thomas Kurian (Head of the Dept. of Polymer Science and Rubber Technology) and Dr. Sunil K Narayanan Kutty (former HOD, Dept. of Polymer Science and Rubber Technology) for providing necessary facilities for the completion of my research work. My sincere thanks to Dr. Rani Joseph (Professor Emeritus), Dr. K E George, Dr. Philip Kurian and other former faculty members of the Department of Polymer Science and Rubber Technology, for their motivation and support.*

*I express my sincere thanks to Dr. Honey John, Dr. Prasanth Krishna, Dr. Shailaja, Dr. Jayalatha, Dr. Jinu Jacob George, Dr. Jyothishkumar, Ms. Abhitha, faculty members of the Department of Polymer Science and Rubber Technology for their valuable advice and suggestions.*

*I convey my sincere thanks to Dr. Ginson P Joseph, Asst. Professor, Dept. of Physics, St. Thomas College, Pala, for sparing his valuable time with constant encouragement and timely help to conduct thermal, electrical and optical studies in his lab for the research work,*

*I express my heartfelt thanks to Dr. Josephine George, Head of the Department of Polymer Engineering, Dr. V G Geethamma, Dr. Leny Mathew, Ms. Sreeletha R, Ms. Sheeba John, Bibin Oommen, faculty members of the Department of Polymer Engineering, University college of Engineering, Muttom, Thodupuzha for their support and guidance to do the research work,*

*I am deeply thankful to Dr. Bipinpal, Mr. Abhilash, Ms. Renju and all the Research Scholars in the Dept. of Polymer Science and Rubber Technology for the valuable help and support given to me during the course of my work,*

*My sincere thanks to Mr. Augustine J Edakkara (Asst. Professor, Dept. of Physics, St .Thomas College Pala), Mr. Joby Sebastian (Asst. Professor, Dept. of Physics, St .Thomas College, Thrissur), Mr. Santoshkumar R (Asst. Professor, Dept. of Physics, St .George College, Aruvithura), Mr. Nelson Kuriakose (Asst. Professor, Dept. of Physics, St. Dominic's College, Kanjirapally), Mr. Sreekanth G (Asst. Professor, Dept. of Physics, Mangalam College of Engineering, Ettumanoor), Mr. Bitto John (Asst. Professor, Dept. of Physics, Govt. Polytechnique College, Purappuzha) for extending their helping hand to me.*

*I thank Mr. Prince Thomas, Mr. Jobin Job Mathen, Jeeba M Sunny, Research scholars in the Department of Physics, St. Thomas College Pala for their selfless cooperation and timely help at various stages of my work,*

*I convey my heartfelt thanks to Dr. Jacob Philip, (Professor, Dept. of Instrumentation, Cochin University of Science and Technology) along with Mr. Nissamuddeen Kunnath, Research Scholar, for the help provided to me for conducting the PPE studies.*

*The Library, Office and Laboratory staff of the Department of Polymer Science and Rubber Technology helped me a lot in fulfilling various requirements for completing the work, I express my sincere thanks to all of them.*

*Let me mention special thanks to my Uncle Fr. Joseph Pampara, for his prayers, motivation and constant encouragement to do Ph.D.*

*I am very grateful to all my family members especially my wife Ms. Anns and my sister Sr. Jaicy SABS and my brothers Mr. James and Mr. Mathew for their support, love and prayers. I remember with gratitude the help extended by Mr. M C Thomas and Joice Thomas for the completion of this work,*

*Let me dedicate this work to my parents, without whose prayers, encouragement and loving care for me, this work would not have become a reality.*

***Jose Sebastian***

## Preface

Organic-inorganic nanocomposites combine unique properties of both the constituents in one material. Among this group of materials, clay based as well as ZnO, TiO<sub>2</sub> nanocomposites have been found to have diverse applications. Optoelectronic devices require polymer-inorganic systems to meet certain desired properties. Dielectric properties of conventional polymers like poly(ethylene-*co*-vinyl acetate) (EVA) and polystyrene (PS) may also be tailor tuned with the incorporation of inorganic fillers in very small amounts. Electrical conductivity and surface resistivity of polymer matrices are found to improve with inorganic nanofillers. II-VI semiconductors and their nano materials have attracted material scientists because of their unique optical properties of photoluminescence, UV photodetection and light induced conductivity. Cadmium selenide (CdSe), zinc selenide (ZnSe) and zinc oxide (ZnO) are some of the most promising members of the II-VI semiconductor family, used in light-emitting diodes, nanosensors, non-linear optical (NLO) absorption etc. EVA and PS materials were selected as the matrices in the present study because they are commercially used polymers and have not been the subject of research for opto-electronic properties with semiconductor nanomaterials.

The current research investigates the possibility of using II-VI semiconductors as fillers to impart enhancement in dielectric, thermal, mechanical and optical properties of conventional polymers. To meet this requirement, nano materials were synthesized by hydro and solvothermal methods. Using solution casting and insitu polymerization, polymer nanocomposites were prepared. The morphological analysis of the nanocomposites indicated good interaction between the polymer and the



fillers. The improvement in electrical, thermal and optical properties exhibited by the composites makes them suitable for various optoelectronic applications.

The thesis entitled 'Effect of II-VI Semiconductor Nanomaterials and Electron Irradiation on Polystyrene (PS) & Poly(ethylene-*co*-vinyl acetate) (EVA)' consists of ten chapters. The first chapter is an introduction of nanocomposites, nanofillers and their significance and applications. The state-of-the-art research in the field of semiconductor based polymer nanocomposites is also presented. At the end of the chapter the main objectives of the work are mentioned.

Chapter 2 outlines the details and specifications of the materials used for the synthesis of the nanomaterial, preparation of nanocomposites as well as the equipment and procedures employed for characterizing it.

Chapter 3 discusses the effect of ZnO nanoparticles (1%, 2%, 4%) on the electrical, optical, mechanical and thermal properties of poly(ethylene-*co*-vinyl acetate) (EVA) copolymer.

Chapter 4 describes the synthesis and characterization of poly(ethylene-*co*-vinyl acetate) and EVA-nano zinc selenide (ZnSe) composite films prepared by solution casting.

Chapter 5 explains the synthesis and characterization of poly(ethylene-*co*-vinyl acetate) and EVA-nano cadmium selenide (CdSe) composite films (with 1, 2 & 4% CdSe) prepared by solution casting.

Chapter 6 is devoted to the physico-chemical properties of in situ polymerised polystyrene on dispersion of ZnO (PS / ZnO) at different concentrations.

Chapter 7 mainly focuses on the effect of zinc selenide (ZnSe) nanoparticles on the polystyrene (PS) matrix.

Chapter 8 deals with the influence of cadmium selenide (CdSe) on polystyrene polymer matrices.

The effects of electron irradiation on various properties of virgin polymers and nanocomposite derivatives are discussed in Chapter 9.

Chapter 10 summarizes the results of the studies undertaken and concludes the investigation.

# Contents

## Chapter 1

<b>INTRODUCTION .....</b>	<b>01 - 56</b>
1.1 Composites – Introduction and Types .....	01
1.1.1 Particulate reinforced composites.....	02
1.1.2 Fibre reinforced composites.....	02
1.1.3 Laminates.....	02
1.1.4 Hybrid composites.....	03
1.2 Nanocomposites .....	03
1.2.1 Classification based on matrices. ....	04
1.2.1.1 Ceramic matrix composites.....	04
1.2.1.2 Metal matrix composites.....	05
1.2.1.3 Polymer matrix composites.....	05
1.3 Nano materials- Types and properties .....	07
1.3.1 Features of nanoparticles .....	08
1.3.2 Nano materials - Major types.....	09
1.3.2.1 Nanoclays .....	09
1.3.2.2 Nanosilica .....	09
1.3.2.3 Metal and ceramic nanoparticles .....	10
1.3.2.4 Cellulose nanomaterials.....	11
1.3.2.5 Graphene.....	11
1.3.2.6 Carbon Nanotubes .....	12
1.3.2.7 Inorganic Nanoparticles.....	13
1.3.3 Synthesis of Nanoparticles.....	14
1.4 Polymer Nanocomposites- History and Development .....	17
1.4.1 Composite Preparation Techniques .....	17
1.4.1.1 Melt Blending.....	17
1.4.1.2 Solution Mixing.....	18
1.4.1.3 Chemical in situ methods.....	18
1.4.1.4 Physical in-situ methods .....	20
1.4.2 Nanocomposites – Functional properties and Applications .....	20
1.4.2.1 Mechanical Properties.....	21
1.4.2.2 Thermal Properties .....	22
1.4.2.3 Barrier Properties.....	22
1.4.2.4 Magnetic properties .....	23
1.5 Electrically active Polymer Nanocomposites .....	23
1.5.1 Intrinsically conducting polymers (ICP).....	23
1.5.2 Conductive polymer composites (CPC) .....	24
1.5.3 Polymer nanocomposites (PNC's) for opto-electronic applications .....	26

1.5.4	Major applications of opto-electro active polymer nanocomposites .....	27
1.6	Poly (ethylene-co-vinyl acetate) (EVA) and Polystyrene Matrices .....	31
1.6.1	Poly (ethylene-co-vinyl acetate) EVA .....	31
1.6.2	Nanocomposites based on poly (ethylene-co-vinyl acetate) (EVA).....	32
1.6.3	Polystyrene.....	34
1.6.4	Nano composites based on polystyrene (PS) .....	37
1.7	Semiconductor nanomaterials .....	38
1.7.1	Cadmium selenide (CdSe) .....	39
1.7.2	Zinc selenide (ZnSe) .....	40
1.7.3	Zinc oxide (ZnO) .....	40
1.8	Scope and objectives of the work:.....	41
	References.....	42

## Chapter 2

### **MATERIALS AND METHODS .....57 - 69**

2.1	Materials .....	57
2.1.1	Poly (ethylene co-vinyl acetate) EVA .....	57
2.1.2	Styrene .....	57
2.1.3	Benzoyl Peroxide .....	58
2.1.4	Chemicals for Nanomaterial synthesis .....	58
2.1.5	Equipment for nano and composite preparation.....	58
2.2	Characterization .....	59
2.2.1	Transmission electron microscopy (TEM) .....	59
2.2.2	Scanning electron microscopy (SEM).....	60
2.2.3	Fourier Transform Infrared (FT-IR) Analysis .....	60
2.2.4	Raman spectroscopy .....	61
2.2.5	UV-Vis-NIR Spectroscopy .....	62
2.2.6	Laser induced fluorescence (LIF).....	62
2.2.7	Thermogravimetry (TG) analysis .....	63
2.2.8	Photopyroelectric (PPE) Studies .....	64
2.2.9	Dielectric studies .....	65
2.2.10	Tensile strength and elongation (ASTM D 882).....	67
2.2.11	Peel resistance (ASTM D 1876).....	68
	References.....	68

## Chapter 3

### **SYNTHESIS AND CHARACTERIZATION OF POLY (ETHYLENE-*CØ*VINYL ACETATE) (EVA) / ZnO**

#### **NANOCOMPOSITES .....71 - 94**

3.1	Introduction.....	71
3.2	Synthesis of ZnO Nanoparticles.....	73
3.3	Preparation of EVA / ZnO Nanocomposite.....	73
3.4	Results and Discussions.....	74
3.4.1	Transmission Electron Microscopy (TEM).....	74
3.4.2	Scanning Electron Microscopy (SEM).....	75
3.4.3	Optical Absorption Studies.....	76
3.4.4	Laser induced fluorescence (LIF).....	78
3.4.5	FT-IR Spectroscopic Analysis.....	79
3.4.6	Dielectric Studies.....	80
3.4.7	TG - DTA Analysis.....	85
3.4.8	Photopyroelectric (PPE) studies.....	88
3.4.9	Mechanical Properties.....	89
3.5	Conclusion.....	91
	References.....	92

## Chapter 4

### **SYNTHESIS AND CHARACTERIZATION OF POLY (ETHYLENE-*CØ*VINYL-ACETATE) (EVA) / ZnSe**

#### **NANOCOMPOSITES .....95 - 116**

4.1	Introduction.....	95
4.2	Synthesis of Znse Nanoparticles.....	97
4.3	Preparation of EVA / ZnSe Nanocomposites.....	97
4.4	Characterization Techniques.....	98
4.5	Results and Discussions.....	99
4.5.1	Morphological Analysis.....	99
4.5.2	FT-IR Spectroscopy.....	100
4.5.3	Refractive Index Study.....	102
4.5.4	Optical Absorption Studies.....	104
4.5.5	Dielectric Measurements.....	107
4.5.6	Thermal Analysis.....	109
4.5.7	Mechanical Properties.....	112
4.6	Conclusion.....	114
	References.....	115

## Chapter 5

### **SYNTHESIS AND CHARACTERIZATION OF POLY (ETHYLENE-CO-VINYL ACETATE) (EVA) / CdSe**

#### **NANOCOMPOSITE.....117 - 136**

5.1	Introduction.....	117
5.2	Experimental.....	118
5.2.1	Synthesis of CdSe Nanoparticles .....	118
5.2.2	Preparation of EVA / CdSe Nanocomposite.....	119
5.3	Results and Discussions.....	119
5.3.1	TEM Analysis .....	119
5.3.2	Morphological Analysis.....	120
5.3.3	Optical Studies .....	121
5.3.4	Electrical Studies.....	124
5.3.5	Thermal Analysis .....	128
5.3.6	Mechanical Properties .....	132
5.4	Conclusion .....	134
	Reference .....	135

## Chapter 6

### **SYNTHESIS AND CHARACTERIZATION OF**

#### **POLYSTYRENE (PS) / ZnO NANOCOMPOSITES.....137 - 154**

6.1	Introduction.....	137
6.2	Experimental Procedure.....	138
6.2.1	Synthesis of ZnO Nanoparticles.....	138
6.2.2	In situ - Polymerisation of Polystyrene .....	139
6.2.3	Preparation of PS / ZnO Nanocomposite.....	139
6.3	Results and Discussions.....	140
6.3.1	Scanning Electron Microscopy (SEM).....	140
6.3.2	Optical Absorption Studies .....	141
6.3.3	FTIR Studies .....	143
6.3.4	Raman spectral studies .....	145
6.3.5	Laser induced fluorescence studies .....	147
6.3.6	Dielectric studies .....	148
6.3.7	A.C conductivity .....	151
6.3.8	Photopyroelectric studies.....	151
6.4	Conclusion .....	152
	References.....	153

## Chapter 7

### **SYNTHESIS AND CHARACTERIZATION OF POLYSTYRENE (PS) / ZnSe NANOCOMPOSITES..... 155 - 173**

7.1	Introduction.....	155
7.2	Preparation of PS / ZnSe Nanocomposites .....	157
7.3	Results and Discussions.....	157
7.3.1	Scanning Electron Microscopy (SEM).....	157
7.3.2	UV-Vis Spectroscopy .....	158
7.3.3	Raman Spectra .....	161
7.3.4	Laser induced fluorescence (LIF).....	162
7.3.5	Electrical Studies.....	163
7.3.6	Thermal Studies .....	168
7.3.7	Photopyroelectric Studies .....	170
7.4	Conclusion .....	171
	References.....	172

## Chapter 8

### **SYNTHESIS AND CHARACTERIZATION OF POLYSTYRENE (PS) / CdSe NANOCOMPOSITES..... 175 - 189**

8.1	Introduction.....	175
8.2	Experimental Procedure.....	176
8.2.1	Preparation of PS / CdSe Nanocomposite.....	176
8.3	Results and Discussions.....	176
8.3.1	Scanning Electron Microscopy (SEM).....	176
8.3.2	Transmission Electron Microscopy (TEM) .....	177
8.3.3	UV-Vis Analysis .....	178
8.3.4	Raman Studies.....	181
8.3.5	Dielectric Studies .....	182
8.3.6	TG – DTA Analysis.....	185
8.3.6	Photopyro Electric Studies (PPE).....	188
8.4	Conclusion .....	188
	References.....	189

## Chapter 9

### **EFFECT OF ELECTRON IRRADIATION ON THE PROPERTIES OF PS, EVA & THEIR NANOCOMPOSITES .....191 - 214**

9.1 Introduction.....	191
9.2 Experimental Procedure.....	193
9.3 Electrical Studies.....	194
9.4 Thermal Properties .....	204
9.4.1 Differential Scanning Calorimetry .....	204
9.4.2 TG - DTA analyses.....	208
9.5 Conclusion .....	211
Reference .....	212

## Chapter 10

### **SUMMARY AND CONCLUSION .....215 - 222**

10.1 Introduction.....	215
10.2 Summary.....	215
10.3 Conclusions.....	220

### **LIST OF ABBREVIATIONS..... 223 - 224**

### **LIST OF PUBLICATIONS..... 225 - 226**

### **CURRICULUM VITAE ..... 227**

.....*END*.....



<i>Contents</i>	<i>1.1 Composites – Introduction and Types</i>
	<i>1.2 Nanocomposites</i>
	<i>1.3 Nano Materials- Types and Properties</i>
	<i>1.4 Polymer Nanocomposites- History and Development</i>
	<i>1.5 Electrically active Polymer Nanocomposites</i>
	<i>1.6 Poly (ethylene-co-vinyl acetate) (EVA) and Polystyrene Matrices</i>
	<i>1.7 Semiconductor Nanomaterials</i>
	<i>1.8 Scope and objectives of the work</i>

### 1.1 Composites – Introduction and Types

Nature guided man to invent composites. Nature is replete with examples of composite materials in living beings and plants. Composites are heterogeneous materials created when two or more distinct components are combined. The beneficial properties of its component materials are combined, thereby producing a better product. Wood and bone are considered good examples for natural composites. Synthetic composites exhibit good strength to weight ratio and high modulus to weight ratio which makes them suitable for automobile industry and other engineering applications. Concrete used in building construction can provide superior and unique properties as it combines the most desirable properties of its constituents. Composites consist of matrix materials,

which form the continuous phase. Based on the continuous phase, composites are broadly classified into metal matrix (MMC), ceramic matrix (CMC) and polymer matrix composites (PMC). The reinforcement part of a composite may consist of fibres or fillers. Along with the presence of two or more distinct phases the composite also has got a recognizable interface or phase boundary. On the basis of the type of reinforcement used the composites are classified into particulate reinforced, fibre reinforced, laminates and hybrid composites.

### **1.1.1 Particulate reinforced composites**

A composite that contains reinforcement in the form of particles with all its dimensions roughly equal are classified as particulate reinforced composites. Particulate fillers are used to improve wear resistance, reduce friction and shrinkage and to enhance high temperature properties of the matrix [1]. Particles share load and improve stiffness of composites.

### **1.1.2 Fibre reinforced composites**

A composite whose reinforcement is having length higher than its cross section are called fibre reinforced composites. Fibrous reinforcements physically change the material to meet the required properties. Glass fibres and aramid fibres are widely used in plastics and rubbers as reinforcement.

### **1.1.3 Laminates**

A laminate is fabricated by stacking a number of layers in the thickness direction. Laminates can have unidirectional or bidirectional orientation of the fibre reinforcement. In laminated composites, synthetic fibers are used due to their physical, mechanical and thermal properties.

#### **1.1.4 Hybrid composites**

Composites with two or more different types of fillers in a single matrix are commonly known as hybrid composites. There are different types of hybrid composites; classified on the basis of the way in which the materials are incorporated. Hybrid composites are classified as sandwich type, interplay, intraply and intimately mixed materials. In a sandwich hybrid composite, one material is sandwiched between layers of another. In interplay hybrids, alternate layers of two or more materials are stacked in a regular manner. Intraply hybrid contains two or more constituents in each row which can be arranged in a regular or random manner. The constituents are mixed as much as possible in intimately mixed hybrid composites.

#### **1.2 Nanocomposites**

Nanocomposites are defined as composite materials where at least one of its constituents is having a particle size in the range of 1-100nm at least in one dimension. Nanometer is an atomic dimension and hence the properties of the nanoparticles are akin to atoms than the bulk material. Nanostructured composite materials, when using both organic polymer and inorganic nanofillers, makes composites which are truly hybrid. Organic-inorganic composites with nanoscale dimensions are of growing interest because of their unique properties, and numerous potential applications such as enhancement of conductivity [2,3], toughness [4], optical activity [5], catalytic activity [6], chemical selectivity [7] etc. In these materials, inorganic and organic components are mixed or hybridised at nanometer scale leading to the formation of hybrid/nanocomposite materials [8,9].

Nanocomposites can be broadly classified based on the type of matrix material.

### **1.2.1 Classification based on matrices.**

According to the type of matrix or continuous forms, composites are broadly classified into metal matrix (MMC), ceramic matrix (CMC) and polymer matrix composites (PMC).

#### **1.2.1.1 Ceramic matrix composites**

Ceramics have good wear resistance and high thermal and chemical stability. Their major disadvantage is that they are always brittle. The low toughness of ceramics has remained a stumbling block for their wider use. In order to overcome this limitation, ceramic-matrix nanocomposites have been receiving attention, primarily due to the significant enhancement on mechanical properties that can be achieved. The incorporation of energy-dissipating components such as whiskers, fibres, platelets or particles in the ceramic matrix would lead to increased fracture toughness. The reinforcements in the composite structure may deflect the crack hindering further opening of the crack. The incorporated phase also undergoes phase transition in conjunction with the volume expansion initiated by the stress field of a propagating crack, contributing to toughening and strengthening.

The potential of ceramic matrix nanocomposites (CMNC), mainly the  $\text{Al}_2\text{O}_3/\text{SiC}$  system, has been confirmed by the noticeable strengthening of the  $\text{Al}_2\text{O}_3$  matrix after addition of a low (i.e. ~10%) volume fraction of SiC particles of suitable size and hot pressing of the resulting mixture.

Studies have explained this toughening mechanism based on the crack-bridging role of the nanosized reinforcements. The incorporation of high strength nanofibres into ceramic matrices has allowed the preparation of advanced nanocomposites with high toughness and superior failure characteristics compared to the sudden failures of ceramic materials [10].

#### **1.2.1.2 Metal matrix composites**

Metal matrix nanocomposite (MMNC) describes materials consisting of a ductile metal or alloy matrix in which some nanosized reinforcement material is incorporated. These materials combine metal and ceramic features, i.e., ductility and toughness with high strength and modulus. Thus, metal matrix nanocomposites are suitable for production of materials with high strength in shear/compression and high service temperature capabilities. They show an extraordinary potential for application in many areas, such as aerospace and automotive industries and development of structural materials [11].

#### **1.2.1.3 Polymer matrix composites**

Polymer matrix nanocomposites (PMNC) are used in diverse fields of application. This include microelectronics which could now be referred to as nanoelectronics as the critical dimension scale for modern devices is now below 100 nm. Other areas include polymer-based biomaterials, nanoparticle drug delivery, fuel cell electrode polymer bound catalysts, layer-by-layer self-assembled polymer films, electrospun nanofibers, imprint lithography and nanocomposites. The field of nanocomposites offer many diverse properties including composite reinforcement, barrier properties, flame resistance,

electro-optical properties, cosmetic application and even bactericidal properties. Recent developments in polymer matrix based nanocomposites have led to interesting observations involving exfoliated clay. More recent investigations are progressing with carbon nanotubes, carbon nanofibers, exfoliated graphite (graphene), nanocrystalline metals and a lot of additional nanoscale inorganic filler or fiber modifications.

### Examples of polymer-matrix nanocomposites and their properties

Matrix/reinforcement	Properties
Polypropylene/montmorillonite	Improved tensile strength, stiffness, Young's modulus and tensile stress
Nylon-6/Layered-silicates	Improved storage modulus, tensile modulus, HDT, reduced flammability.
Poly lactide/Layered-silicates	Improved bending modulus, storage modulus, gas barrier properties and biodegradability.
Polyvinilidene fluoride/carbon nanotube	Dielectric permittivity and conductivity increased
Epoxy/Layered-silicates	Improved tensile strength and modulus.
Polyimide/montmorillonite	Improved tensile strength, elongation at break and gas barrier properties.
Polystyrene/Layered-silicates	Improved tensile stress and reduced flammability.
Polyethylene oxide/Layered-silicates	Improved ionic conductivity.
Poly(methyl methacrylate)/Pd	Improved thermal stability.
Polyester/TiO <sub>2</sub>	Improved fracture toughness and tensile strength.
Epoxy/SiC	Improved microhardness and storage modulus.

### **1.3 Nano materials- Types and properties**

The transition from microfillers to nanofillers yields dramatic changes in physical properties. Nanoscale materials have a large surface area for a given volume [12]. Inorganic nanoparticles can be easily prepared as metals, metal oxides, sulfides, and carbonates with diameters ranging from several hundred to a few nanometers. Due to their high surface to volume ratios, they show properties distinctly different from bulk materials. Nanoparticles can be considered as a single “crystal” of a typical size of a few nanometers consisting of 100’s to 1,000,000’s of atoms, which preserve some of the attributes of the bulk material but exhibits in addition very interesting properties due to the size quantization effect.

Typical nanomaterials currently under investigation include nanoparticles, nanotubes, nanofibres, fullerenes and nanowires. These materials are classified by their geometry as particle, layered and fibrous materials. Carbon black, silica, etc. can be classified as nanoparticles while nanofibres and carbon nanotubes are examples of fibrous materials. When the fillers have a nanometer thickness and a high aspect ratio plate like structure, it is considered as a layered nanomaterial [13].

In polymer nanocomposites (PNCs), dispersion of the nanoparticle and adhesion at the particle-matrix interface play a vital role in determining the mechanical properties of the nanocomposite. Poorly dispersed nanomaterial may shows poorer physical / mechanical properties than conventional composites [14]. Heterogeneity in composition adversely

affects the quality of the nanocomposite. Good adhesion at the interface will improve interlaminar shear strength, delamination resistance, fatigue, and corrosion resistance.

### **1.3.1 Features of nanoparticles**

Nanoparticles are particles with diameters below the micron dimension, below  $0.1\mu\text{m}$  (100 nm). The smaller the particle size, the more important would be the surface properties and the physical properties. The following are some common features of nanomaterials.

#### **(i) Properties are particle size dependent**

Nanomaterial particle size has a strong influence on the dielectric, optical, magnetic and structural properties. For example,  $\text{TiO}_2$  is a filler used to modify the optical and electrical properties of polymers. It was found that a decrease of particle size affects refractive index and band gap [15].

#### **(ii) Large specific surface area**

The large specific surface area of the filler causes the formation of an interfacial matrix (polymer) layer attached to the particle core [16]. The properties of the polymer localized in the shell are different from the bulk polymer due to immobilization. The interaction of the interfacial layer with the particle and the free bulk polymer is responsible for the changes in thermo-mechanical and electrical properties. To control the polymer-nanoparticle-composite properties and its processability, tailoring of the nanoparticle surfaces and tuning its interfacial layer is quite significant [17].



### **1.3.2 Nano materials - Major types**

#### **1.3.2.1 Nanoclays**

Among all the available nanofillers used for preparation of polymer nanocomposites, layered silicates (nanoclays) are the most studied. Clays are chemically hydrous silicates of Al, Mg, Fe, and other less abundant elements. The main structural feature of clay is that it is layered. Clay based nanocomposites were studied in detail by LeBaron et al. [18], Schmidt et al. [19] and Alexandre et al. [20]. By the addition of small amounts of clay nanofillers it is possible to achieve consistent increments in mechanical properties including elastic modulus and strength. Well dispersed nano clay can decrease the gas permeability, improve solvent and heat resistance and increase the flame retardancy characteristics in polymer matrices. Clay minerals consist of phyllosilicates which can be divided into four groups based on their crystalline structure: kaolinite group, montmorillonite/smectite group, illite group and chlorite group [21,22]. Among them, montmorillonites are the most investigated in nanocomposites, due to their potentially high aspect ratio and the unique intercalation/exfoliation properties.

#### **1.3.2.2 Nanosilica**

Nanosilica finds application in diverse fields including optoelectronics and elastomer compounding. Sol-gel technique has been used extensively in the manufacturing of nanosilica [23]. It has been used in different matrices for reinforcement and as additive for special applications. Epoxy-nanosilica composites [24] are found to give enhanced thermal and mechanical properties as the filler loading is increased. Unsaturated

polyester resins were modified by the incorporation of nanosilica to obtain enhanced mechanical and thermal properties [25].

### **1.3.2.3 Metal nanoparticles**

Metals undergo drastic property change by size reduction, and their composites with polymers are very interesting for functional properties especially for electrical applications. The enhanced properties observed in nano-sized metals are very unstable due to quantum-size effects (i.e. electron confinement and surface effect). These properties are size-dependent and can be simply tuned by altering the nanoparticles structure and dimension. Surface effects become more significant with reduction of size, as the matter consists of more surface atoms than inner ones.

Nano-sized metals have special characteristics that can be used for a number of advanced technological applications. The difficulties in handling nanomaterials have represented a strong limitation to their use. In addition, most of nano-sized metals are very unstable as they can aggregate because of the high surface free energy and can be oxidized, contaminated by air, moisture, SO<sub>2</sub>, etc. The production of nanoparticles of practically all metals has been reported, but the more widely used for polymer nanocomposites are silver, gold, platinum, iron, copper, etc.,. The main functionalities developed inside the polymer matrix by these nanomaterials are improved electrical and thermal conductivity [26], antibacterial properties [27], magnetic [28] and catalytic effects [29].

#### **1.3.2.4 Cellulose nanomaterials**

Cellulose nanomaterials (nanocellulose) denote materials composed by cellulose nanocrystals (CNC), cellulose nanofibrils (CNF), cellulose microcrystals and cellulose microfibrils. Cellulose nanocrystal also known as nanocrystalline cellulose is a type of cellulose nanofiber with pure crystalline structure with dimensions of 3–10 nm in width and an aspect ratio range of 5-50. Cellulose nanofibril is another type of cellulose nanofiber that contains both crystalline and amorphous regions with dimensions of 5–30 nm in width and aspect ratio usually greater than 50, synthesized from fibrils obtained from plant cell walls. Cellulose nanofibrils are obtained by either bacterial action or mechanical treatment of plant material.

The presence of hydroxyl groups on the surface of CNC, make it a nano material which can be further modified with various chemical groups to facilitate its incorporation and dispersion into different polymer matrices [30]. CNC are considered as one of the ideal nano reinforcements for polymer matrices because of their physio-chemical properties and have already been incorporated into many polymer matrices for different final applications such as high performance materials, electronics, catalysis, biomedical, and energy [31].

#### **1.3.2.5 Graphene**

Graphene is considered as the thinnest material in the Universe. In 2004 a group of physicists from Manchester University, UK, led by Geim and Novoselov isolated a flake of graphene for the first time [32].

They used a top-down approach, called micromechanical cleavage. The process includes extraction of a single layer graphene sheet from the three-dimensional graphite [33]. In 2006, Stankovich et al. [34] reported the use of single graphene sheets as additive for polystyrene-based composites. The two-dimensional geometry led to an extremely low percolation threshold of only 0.1%, enhancing both the conductivity and strength of the matrix. The first example of transparent and conducting ceramic graphene-based composite was graphene– silica composite spun-cast thin films with a bulk conductivity of 0.45 S/cm [35].

#### **1.3.2.6 Carbon Nanotubes**

Carbon nanotubes(CNT) consist of graphene cylinders which are available in two varieties, as single walled (SWCNT) and multi walled (MWCNT). While SWCNTs are single graphene cylinders, MWCNTs consist of two or more concentric cylindrical sheets of graphene around a central hollow core. Carbon nanotubes, are one of the allotropic forms of graphene [36], a single walled carbon nanotube (SWCNT) can be visualized as a graphene sheet rolled up into a cylinder with fullerene-like end cap having hexagonal and pentagonal faces. Based on the chirality along the graphene sheet, they can be semiconducting or metallic [37]. Both SWCNT and MWCNT shows physical characteristics of solids, with microcrystallinity and very high aspect ratios of  $10^3$ . Surface modifications of these reinforcements are carried out to obtain homogeneous distribution and also to improve interfacial bonding between the surrounding matrix and the nanosized reinforcements.

### **1.3.2.7 Inorganic Nanoparticles**

#### **Titanium Dioxide**

TiO<sub>2</sub> is known for its application in dye sensitized solar cells. Nano TiO<sub>2</sub> is used in nanomedicine and skin care products. It is often synthesized by hydrothermal, sonochemical, solvothermal, and non hydrolytic methods [38].

#### **Zinc Oxide**

Nano Zinc Oxide is used in electronic and optoelectronic device applications, gas sensors, water treatment, cosmetics, antimicrobial and anticancerous applications. Nanoparticles are synthesized by sol-gel, spray pyrolysis, thermal evaporation etc.[39]

#### **Aluminium Oxide**

Al<sub>2</sub>O<sub>3</sub> nanofillers are extensively used for the removal of heavy metal ions in the soil and waste water treatment and also for removal of pathogenic microorganisms. It is synthesized by flame spray pyrolysis, reverse microemulsion, sol-gel, and freeze drying [40].

#### **Silicon Dioxide**

SiO<sub>2</sub> synthesized widely by sol-gel, flame, and water in –oil microemulsion processes is often used in device fabrication for drug delivery, tissue engineering and biosensing [41].

#### **Silver**

Antibacterial and antifungal properties of nanosilver makes it a suitable candidate for water purification systems, paints and

household products. Its antiviral properties is utilized in biomedical use for HIV-I and monkey pox virus. Microwave processing, photochemical, ultrasonic spray pyrolysis etc are commonly used for the silver nano synthesis [42].

### **Gold**

Antibacterial and antiviral properties makes gold nanoparticle a widely used material. Biosensing and photothermal cancer therapy are other major application sectors for gold nanoparticles [43].

### **1.3.3 Synthesis of Nanoparticles**

There are a large number of techniques available to synthesize different types of nanomaterials in the form of colloids, clusters, powders, tubes, rods, wires, thin film etc. The existing conventional techniques to synthesize different types of materials are optimized to get novel nanomaterials and some new techniques are developed. The technique to be used depends upon the material of interest; type of nanostructure viz. zero dimensional (0D), one dimensional (1D) or two dimensional (2D) materials, size, quality etc.

The preparation of nanoparticles can be achieved through different approaches, either chemical or physical methods including gaseous, liquid and solid media. While physical methods generally tend to approach the synthesis of nanostructures by decreasing the size of the constituents of the bulk material (top-down approach), chemical methods tend to attempt to control the clustering of atoms/molecules at the nanoscale range (bottom-up approach).

Wet chemical processes include sol-gel method, reverse micelles method, co-precipitation method and solvothermal /hydrothermal methods of preparation, among which sol gel and hydrothermal methods are widely used. In all these methods, solutions of different ions are mixed in well-defined quantities under controlled heat, pressure and temperature, to promote formation of insoluble compounds, which are then precipitated out of the solution.

Sol-gel technology is very efficient in producing various functional materials in which particle size, porosity, thin layer thickness, separation of particles with different compositions and structures may be controlled and successful applications have been achieved. Sol-gel materials have a wide range of applications such as environmental protection, solar cell, energy storage, ceramics, sensors, magnetic devices, etc. The main advantage of the sol gel technology is the possibility to control the mechanism and kinetics of the proceeding chemical reactions, in other words, controlling each step of the sol gel processes, may affect the final structure of the materials and the modification of the processes [44].

Solvothermal process can be defined as “A chemical reaction in a closed system in the presence of a solvent (aqueous and non-aqueous solution) at a temperature higher than that of the boiling point of such solvent”. Solvothermal reactions are mainly characterized by different chemical parameters (nature of the reagents and of the solvent) and thermodynamical parameters (temperature, pressure). Consequently a solvothermal process involves high pressure. In particular, the particles

prepared by the solvothermal method were reported to have larger surface area, smaller particle size, and were more stable than those obtained by other methods [45].

Mechanical process of grinding, milling and mechanical alloying can produce a coarse powder feedstock. Physical pounding of the coarse powder was done to obtain finer and finer particles in the nanometer range. Planetary and rotating ball mills are commonly used for size reduction. The main attraction of this method is that it is very simple and only requires low cost equipments. Broad particle size distributions, contamination from the process equipment etc are its drawbacks.

Gas phase synthesis includes flame pyrolysis, electro explosion, laser ablation, high temperature evaporation and plasma synthesis. Flame pyrolysis has been used for several years for the production of carbon black and fumed silica. Laser ablation is a widely accepted technique for the manufacture of nanomaterials with the help of physical erosion and evaporation. The process is time consuming and requires high temperature and is suitable for inorganic materials.

Vacuum deposition processes such as physical vapour deposition, chemical vapour deposition, lithography and spray coatings are included in the 'form in place' processes. For the preparation of nanostructured layers and coatings, form in place technique is used.



## **1.4 Polymer Nanocomposites- History and Development**

### **1.4.1 Composite Preparation Techniques**

Polymer nanocomposites consists of a rigid nanoscale filler dispersed within a flexible polymer matrix. The difference in the inherent properties of the constituent materials (matrix and reinforcement) along with the fine particle nature of the reinforcement makes the preparation of the nanocomposite difficult. Most of the reinforcing nanomaterials are insoluble in organic solvents, and have high melting temperature which makes the preparation of nanocomposites complex.

Polymer materials have got a wide variety of properties. So finding one individual and universally accepted method for the preparation of polymer nanocomposite is not practical. Based on the processing conditions and the end product requirement of the composite, the route for preparation is determined.

#### **1.4.1.1 Melt Blending**

Melt blending method includes mixing of the nano materials in the polymer matrix at melt/softening temperature, followed by annealing. This method is environmental friendly as it does not involve the use of any organic solvents. The conventional processing of polymer products like moulding and extrusion can be used for the synthesis of nanocomposites. Table 1.1 gives some examples of polymer nanocomposites made by melt blending.

Polystyrene was the first plastic material utilized for the melt blending technique with alkyl ammonium cation modified MMT.

**Table 1.1: Examples of nanocomposites made by melt blending**

SI No	Nanocomposite	Synthesis method / outcome	Reference
1	PS-MMT	Melt blending, improved mechanical properties	46
2	PP-MMT	Utilises compatibiliser, melt intercalated	47
3	PP-CaCO <sub>3</sub>	Fine dispersion at low loadings	48
4	EPDM-Clay	Exfoliated structure rubber composite	49
5	HDPE-PP	Extrusion, PP nanofibre in HDPE matrix	50

#### 1.4.1.2 Solution Mixing

This process utilizes a filler which can swell in a predetermined solvent. The swelled filler and polymer solution were mixed to facilitate the polymer chains to displace the solvent between the filler layers. A variety of clay based nanostructures were synthesized by this method. This method is found useful to obtain intercalation of polymers with little or no polarity. The main limitation of this method is that it can be used only for certain polymer-solvent pairs. The usage of organic solvents and its economic and environmental implications restricts this method from being globally accepted.

#### 1.4.1.3 Chemical in situ methods

In this method, chemical reactions in a liquid environment are used to synthesis nanocomposites. In 1993, Ziolo et al. [51] reported a single step chemical method to synthesis fine dispersed Fe<sub>2</sub>O<sub>3</sub> nanoparticles in crosslinked polystyrene resin. Guan et al. [52] elaborated the synthesis of transparent polymer nanocomposites with PMMA- ZnS by in situ bulk

polymerization. The common feature of many of the materials is that nanoparticles are synthesized as a sol or dispersed in a solution, followed by a second step where a monomer or resin is added and polymerized. Gangopadhyay et al. [53] prepared colloidal solutions of Fe<sub>2</sub>O<sub>3</sub> nanoparticles, which then added to conducting polypyrrole. The mixture was polymerized to obtain a nanocomposite. Althues et al. [54] used a two step process to synthesise ZnO in a colloidal suspension, which was photopolymerised with poly(butanediolmonoacrylate).

According to different starting materials and fabrication processes chemical in situ synthesis can be generally classified into three types:

- a) Metal ions are preloaded within polymer matrix to serve as nanoparticle precursor. Then the precursors are exposed to corresponding liquid or gas containing S<sup>2-</sup>, OH<sup>-</sup>, or Se<sup>2-</sup> to in-situ synthesis the target nanoparticles [55].
- b) Nanoparticles are first dispersed into the monomers or precursors of the polymeric hosts and the mixture is then polymerized [56]. The well dispersed nanoparticles in the liquid monomer or precursor will avoid their agglomeration in the polymer matrix and thereafter improve the interfacial interaction between both phases.
- c) Nanoparticles and polymers can be synthesized simultaneously by blending the precursor of nanoparticles and the monomers of the polymer with an initiator in a proper solvent [57].

#### 1.4.1.4 Physical in-situ methods

The common point in physical methods is that chemical compounds are transformed into nanoparticles with the application of energy. They are mainly gas-phase methods. Vollath et al. [58] developed a reaction tube made of quartz glass crossing a microwave cavity. Volatile and water-free precursors are evaporated outside the tube and mixed with an inert carrier gas. The components are introduced as gases into the system in front of the plasma zone. Chemical reaction in gas phase and the nucleation and growth of nanoparticle occurs. The inorganic cores are formed and the organic shell of hybrid nanoparticles condense and polymerizes outside of the plasma zone on the cores synthesized in plasma.

Chemical vapour synthesis (CVS) method applied by Schallehn et al. [59] is utilized in situ polymer coating for Al<sub>2</sub>O<sub>3</sub> and SiO<sub>2</sub> nanoparticles. Srikanth et al. [60] developed a one step microwave plasma process to encapsulate iron nanoparticles with polystyrene. Qin and Coulombe [61] used a dual-plasma process for the synthesis of metal-organic core/shell nanoparticles. Copper nanoparticles were synthesized by arc evaporation and vapour condensation, and the organic coating was deposited by in-flight deposition of an organic compound through plasma polymerization.

#### 1.4.2 Nanocomposites – Functional properties and Applications

Property enhancement found in polymer nanocomposites are multi faceted. Remarkable improvement in mechanical properties including modulus, strength are shown by nanocomposites. At the same time they

exhibit flame resistance, heat resistance, reduced gas permeability, and wide variety of properties. The main reason behind the improvement in properties is the strong interfacial attraction between the matrix and the nanomaterials. With regard to application of nanocomposites, fundamental knowledge of its base properties is mandatory.

#### 1.4.2.1 Mechanical Properties

Engineering polymers require modulus and strength to meet their functional requirement as products. It is found that the tensile strength and modulus of polymers are remarkably improved by the formation of nanocomposites.

Generally it is observed that as the particle size reduces the modulus increases. This is due to the increased interaction between the matrix and the nanofiller. The incorporation of nanoparticles with poor interaction with the matrix causes reduction of tensile strength [62].

**Table 1.2: Mechanical properties of some polymer nanocomposites**

Sl No	Nanocomposite	Property	Ref
1	PP-Alumina	Increased Young's modulus	63
2	PMMA- Alumina	Tensile strength improved	64
3	Nylon 6-Clay	Young's modulus increases with 2-5% clay	65
4	PMMA-CaCO <sub>3</sub>	Improved modulus and abrasion resistance	66
5	Nylon-MMT/glass fibres	Flexural modulus and compressive strength increases	67

### 1.4.2.2 Thermal Properties

Thermal stability of the polymer nanocomposites was found to enhance with incorporation of filler. The polymer systems show thermal stability not only because of the structural difference, but also due to the restricted motion of the polymer macromolecules. The heat deflection temperature (HDT) of polymer systems can also be improved by the nanofiller interaction. The filler acts as a heat barrier, which enhances the overall thermal stability of the nanocomposite.

**Table 1.3: Thermal properties of some polymer nanocomposites**

SI No	Nanocomposite	Property	Ref
1	Epoxy-Silica	Stiffness and thermal stability increases	68
2	PMMA-MMT	Decomposition temperature increased	69
3	Nylon 6-Clay	Thermal stability improves affected by moisture	70
4	PVC-Clay	Onset of degradation delayed	71
5	Epoxy-Clay	Exfoliated structure has better stability than intercalated	72

### 1.4.2.3 Barrier Properties

Gas permeation properties of both rubber and plastic nanocomposites were found to increase by the presence of nanoparticles. Poly lactic acid (PLA) –synthetic mica system shows 150% increase in the barrier properties to oxygen [73]. PP-fumed silica [74], Epoxy-MMT [75], Polyethylene –MMT [76] exhibits gas barrier properties along with enhancement in hardness.

#### **1.4.2.4 Magnetic properties**

Regarding magnetic properties exhibited by nanocomposites, two groups of materials are most promising. The first group with metal nanoparticles and the second with  $\text{Fe}_2\text{O}_3$ ,  $\text{Fe}_3\text{O}_4$  or ferrite nanoparticles [77]. The resultant nanocomposites are free from hysteresis and show superparamagnetic properties. Superparamagnetic nanocomposites were used as microwave absorbing materials. Advanced developments of organic coated magnetic nanoparticles can be usefully applied in biomedicine (local hyperthermia) [78], biology (bio compatible ferromagnetic fluid) [79], and diagnostics as contrast agent for MRI [80]. Application is possible also in the field of biology, biomedicine and as drug carriers [81].

### **1.5 Electrically active Polymer Nanocomposites**

Most of the commercially available polymers are not conductive. Electrically conducting polymers are mainly divide as

#### **1.5.1 Intrinsically conducting polymers (ICP)**

Intrinsically conducting polymers facilitate conduction by the electronic structure of the polymer backbone. They have a  $\pi$ -conjugated structure, which enables them to be used as conductors, semiconductors or insulators based on the type of dopants. The group of materials include polyacetylene, polyaniline, polypyrrole, polythiophene, poly (para-phenylene) etc. They are used for fabricating optoelectronic devices and corrosion resistant coatings. Intrinsically conducting polymers are also used for developing sensors, actuators and separation membranes [82].

Conjugated polymers are often employed in the organic-based device light harvesting layer but have limitations in charge transport. Combinations of conjugated polymer with inorganic semiconductors have been proposed as a resolution to this deficiency. Cadmium–selenide, (CdSe) nanoparticles incorporated in poly(dithiophene)-*alt*-(benzothiadiazole) yielded power conversion efficiency of 3.13% [83]. Layer-by-layer assembly of functionalized poly(phenylene vinylene) and CdSe nanoparticle composites yielded uniform thin films with a power conversion efficiency of 0.71% [84]. Poly(3-hexylthiophene)–ZnO nanofiber composites exhibited a power conversion efficiency of 0.53% noted to be significantly better than the analogous bilayer structure of the noted components [85]. SWCNT incorporation into poly(3-octylthiophene) increased the short circuit current by two orders of magnitude [86]. Ink jet printing is a potential method for producing low cost, high volume photovoltaic and LED devices [87].

Other nanofillers employed include metal oxide nanowires, carbon nanotubes, nanoscale gold, silver, nickel, copper, platinum and palladium particles. Shape memory polymers have great potential for use in as sensors and actuators, particularly as composites with conductive fillers [88]. Deposition of Layer-by-Layer (LbL) sensor can function as a passive wireless sensor which does not require any battery power supply[89]. LbL method can also be used to fabricate high strength composites for biological implants and electrical interface materials [90].

### **1.5.2 Conductive polymer composites (CPC)**

Conducting polymer composite (CPC) materials facilitate conduction by the addition of conductive fillers to the polymer matrix. A number of



articles have been published on various aspects of CPC. It is of particular interest due to the wide variety of industrial applications. Incorporation of inorganic nanoparticles into an organic polymer matrix can significantly affect the properties of the composite. The composite material may show improved thermal, mechanical, electrical, rheological and optical properties.

Halajan et al. [91] used PVA to embed zinc selenide (ZnSe) nanoparticles into it. This inclusion helps to change the electrical and optical properties of the nanocomposite. A functionalized polystyrene containing an electroactive carbazole pendant group and an amine salt pendant group capable of electrostatic interaction with CdTe was described for potential photovoltaic applications. Poly (vinyl alcohol) matrix dispersed with lithium potassium zirconate showed that dielectric constant of the nanocomposite decreases with increase of frequency [92]. The preparation of the nanocomposite of poly(vinyl alcohol) and CdTe for electrical devices was demonstrated by Tekin et al. [93]. The dielectric properties of polymer nanocomposites (PNCs) was studied by Sun et al.[94] on epoxy-silica composites. The dielectric permittivity and loss factor were found to increase with silica incorporation. Singha et al. [95] reported that permittivity of the epoxy nanocomposites decreases with incorporation of Al<sub>2</sub>O<sub>3</sub> and TiO<sub>2</sub> fillers. The dielectric constant of crosslinked polyethylene was found to reduce with addition of nanosilica [96].

**Table 1.4: Examples of Nanofillers for Optoelectronic applications**

Sl No	Nano particle	Properties	Applications	Ref
1	SiO <sub>2</sub>	Luminescent, thermal and mechanical	Drug delivery, tissue engineering, biosensing	97
2	Ag	Plasmon resonance, thermal and electrical	Water purification, paints, antiviral applications	98
3	Au	Photothermal, magnetic properties	Biosensing, MRI, cancer therapy	99
4	Al <sub>2</sub> O <sub>3</sub>	Optical, mechanical	Gas separation, water/soil treatment	100
5	ZnO	Opto, electro, thermal properties	Device fabrication, sensors	101
6	BaTiO <sub>3</sub>	High dielectric permittivity	High energy density capacitors	102
7	Titania (TiO <sub>2</sub> , TO)	High dielectric strength	Cryogenic grid	103

### 1.5.3 Polymer nanocomposites (PNC's) for optoelectronic applications

Nanotechnology based on polymer materials concentrates on the design of advanced devices for electronic and optoelectronic applications. The dimensional range for electronic devices has entered the nanometer scale. Enhanced conductivity in organic polymers with p-type (oxidants) and n-type (reducing agents) dopants lead to the development of intrinsically conducting polymers (ICP). Redox polymers and ionically conducting polymers are two other classes of electrically conducting polymers. They are less conducting compared to ICP.

**Table 1.5: Electrical properties of some polymer nanocomposites**

SI No	Nanocomposite	Property	Ref
1	Epoxy-TiO <sub>2</sub>	Increased energy storage efficiency	104
2	Epoxy-ZnO, Al <sub>2</sub> O <sub>3</sub>	Reduction in DC volume resistivity	105
3	PVDF-MWCNT	Increase of Dielectric constant	106
4	PVDF-Ag	Improved dielectric constant and thermal conductivity	107
5	Silicone rubber- Al <sub>2</sub> O <sub>3</sub>	Low dielectric permittivity and high thermal conduction	108

In fact, the majority of organic polymers exhibit refractive index in the range 1.35- 1.5. In order to fabricate optical devices, polymers with higher refractive index are required. Polymers modified by nanoparticles have been widely investigated for applications in micro optical elements [109]. Optoelectronic devices using organic materials as active units such as organic light emitting diodes (OLEDs) and organic photovoltaic cells (OPVs) have attracted attention due to the possibility of replacing inorganic materials. The main drawback of these organic materials is their poor stability that can cause device failure even at ambient temperature. Several strategies were used to improve the stability of organic films, one main approach being the addition of inorganic nanostructures (oxides, semiconductors) to the host polymers forming composites. The presence of inorganic components, their concentration and shape have a positive effect on the optical as well as on film stability.

#### **1.5.4 Major applications of opto-electro active polymer nanocomposites**

##### **a) Microelectronic device fabrication**

It was reported that addition of nanoparticles to polymers has a strong effect on their composite dielectric properties. Dielectric constant

is found to increase by the addition of ferroelectric ceramics like BaTiO<sub>3</sub> to polymers [110]. The change of dielectric constant with nanoparticles of TiO<sub>2</sub>, SnO<sub>2</sub>, SrTiO<sub>3</sub> and others in polyester matrix were also observed [111]. Common polymers show only a low relative dielectric constant value between 2 and 4 [112]. Materials with high permittivity are required in embedded capacitors, which can be fulfilled by polymer- nanoceramic composites.

**b) Lithium-ion batteries**

The primary requirement for the use of polymer based electrolyte in modern lithium-ion batteries is high ionic conductivity in a wide range of temperature. Other requirements include mechanical stability, formation of porous solid-electrolyte-interface which is permeable for lithium ions, high lithium ion transference number and good wetting of the electrodes [113]. There are three different types of polymer based electrolytes; solvent free polymer, gel polymer and polymer composite. Nanosized ceramic particles dispersed in polymer matrix have been widely investigated [114]. Passive nanosized fillers (TiO<sub>2</sub> and Al<sub>2</sub>O<sub>3</sub>) were used for the increase of ionic conductivity in the case of polyethyleneoxide based electrolytes [115]. Active nanofillers like LiAlO<sub>2</sub> cause improvement of the ionic conductivity [116]. Hu et al. [117] prepared SnO<sub>2</sub> nanoparticles embedded polyaniline composite to function as supercapacitors.

**c) Organic solar cells**

Intrinsic conductive polymers like polyaniline (PANI), polythiophene (PTP), polypyrrole (PPy) are used in solar cells. Nanosized ceramics like SiO<sub>2</sub>, Al<sub>2</sub>O<sub>3</sub>, or TiO<sub>2</sub> are used for properties including electrical

conductivity and improved thermal resistance. It is also reported that addition of nanoceramics can improve polymer stability against photodegradation [118].

**d) Photoresists**

Poly methyl methacrylate (PMMA) positive photoresists and epoxide based negative photoresists coupled with nano sized ceramic fillers can provide sensitivity to electromagnetic radiation of a selected wavelength region. Highly agglomerated nano silver particles were used for development of an electrically conductive resist, which can be patterned by the UV-lithography process [119]. Nanocomposites also reduce coefficient of thermal expansion. This new class of nano composites allowed direct fabrication of high temperature stable optical devices by UV-lithography.

**e) Biomedicine**

The application of polymer nanocomposite in biomedical field is highly diverse. Acrylates filled with surface modified nano SiO<sub>2</sub>, in dental composite and silicone rubber- nano SiO<sub>2</sub> in catheters are a few to mention. Ferro electric poly-vinylidene fluoride (PVDF) filled with nanosized hydroxyapatite for improved biocompatibility and nanosized BaTiO<sub>2</sub>, with its high dielectric constant could be used as bioelectroactive bone regeneration composites [120].

**f) Coatings**

Nanoclay incorporated in thermoset polymer exhibit superior properties such as superhydrophobicity, improved wettability, corrosion resistance, and improved barrier properties and scratch resistance. Turri et al. [121] developed coatings based on epoxy/ nanoclay on steel substrates

to improve scratch resistance. Clay and nano silver incorporated thermoset polymer composites could be used for antibacterial properties in medical field.

**g) Sensors**

Various researchers have reported the ability of conductive polymer composites to sense vapour and liquid chemicals [122]. The mechanism of sensing is based on the increase of resistivity of the nanocomposite when exposed to organic chemicals. Dai et al. [123] reported the liquid sensing behavior of carbon black filled electrically conducting microfibrillar polymer composite. Investigations were conducted on carbon nanotube filled polycarbonate as liquid sensors for solvents like acetone and tetrahydrofuran [124].

**h) Thermoelectric materials.**

Thermoelectric materials require high electrical conductivity and low thermal conductivity. Polymer based thermoelectric materials have already replaced conventional thermoelectrics like bismuth telluride, as they possess low cost, good processability and excellent flexibility. Single walled carbon nanotubes were coated with PEDOT: POSS, to enhance the electrical conductivity of polyvinyl acetate matrix [125]. SWCNT added to polyvinylidene fluoride can also improve the electrical conductivity to behave as a thermoelectric material [126].

**i) Shape memory devices**

For conductive shape memory composites, conductive fillers are added into polymer matrices. They have a shape memory effect to recover their original shape in presence of an external stimuli.

## 1.6 Poly(ethylene-*co*-vinyl acetate) (EVA) and Polystyrene Matrices

### 1.6.1 Poly(ethylene-*co*-vinyl acetate) EVA

Poly(ethylene-*co*-vinyl acetate) commonly known as EVA, with the chemical structure as shown in Fig.1.1 is copolymer of ethylene and vinyl acetate, widely used in electrical insulation.

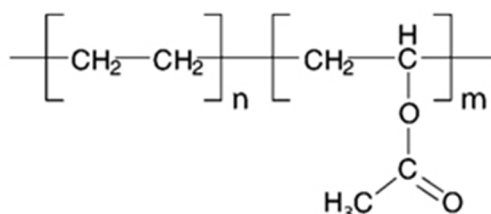


**Fig.1.1: Structure of EVA**

EVA copolymers are clear, flexible materials with high tensile strength and are mainly used in packaging and adhesive applications. EVA copolymers have improved low temperature flexibility ( $-70\text{ }^\circ\text{C}$ ) compared to low density polyethylene (LDPE), good chemical resistance, and high coefficient of friction. Films have improved clarity and weathering resistance compared to LDPE. Similar flexibility to plasticised polyvinyl chloride (PVC) may be obtained, without the problems of plasticiser migration. They have better tear resistance than LDPE and can accept high filler loadings. The disadvantages are a reduced chemical resistance compared to LDPE, reduced barrier properties, and reduced creep resistance.

Applications include stretch film for shrink-wrapping, protector strips, shoe soles, disposable medical equipment, flexible toys, tubing,

wire coating, and heat-sealing coatings on polyethylene terephthalate (PET), and aluminium foils. The vinyl acetate (VA) content of EVA determines its degree of crystallinity and melting temperature. EVA with 10% VA exhibits lower water absorption, higher tensile strength, permeability, modulus, and dielectric strength than EVA with 25% or 33% VA. It has lower heat-seal strength and flexibility and poorer low-temperature performance compared with EVA containing 25% or 33% VA. Heat-seal strength improves with VA content, as do flexibility and low-temperature performance. Increasing the VA content decreases tensile strength, resistance to heat deformation and chemicals, and barrier properties. EVA with 33% VA is useful in cable sheaths, hose, sheet, ring seals, protective caps, clips, cable binders, infusion bottles, lids, all kinds of closures, flexible panels, bellows, rail pads, and O-rings.

### **1.6.2 Nanocomposites based on poly(ethylene-co-vinyl acetate) (EVA)**

Poly(ethylene-co-vinyl acetate) (EVA) is copolymer of ethylene and vinyl acetate commonly used in cable jacketing, water proofing and component encapsulation. The presence of vinyl acetate molecules in the polymer chain reduces the polymer regularity and crystallinity. EVA has got an amorphous structure with good low temperature flexibility and toughness. It exhibits rubbery property of enhanced elongation along with the ease of processability of thermoplastics. As the vinyl acetate content in the copolymer increases, its crystallinity decreases. Flexibility, clarity and toughness increases by the increase of vinyl acetate content in the copolymer. Due to its surface gloss and impact strength EVA copolymers find market in film manufacturing. However, the lack of flame resistance



and low heat distortion temperature along with poor mechanical properties make them unsuitable for several applications.

The presence of polar vinyl acetate groups in the polymer chain improves its interactions with fillers, especially organic fillers. Inorganic fillers can also be easily dispersed in EVA matrix due to its amorphous chain structure.

Among the variety of EVA nanocomposites synthesized, the most widely studied is the EVA- nanoclay system. Organo modified montmorillonites mixed with EVA provided an intercalated nanostructure [127]. To improve the thermal properties, fine dispersion of nanoclay, exfoliated and intercalated in EVA was investigated by Zanetti et al. [128]. Synergistic effect of organically modified montmorillonite and intumescent flame retardants was reported as a flame resistant compound in EVA matrix [129].

Thermal conductivity of EVA composites was investigated by Ghose et al. [130] with the incorporation of carbon nanotubes, carbon nanofibres and expanded graphite. Electron beam irradiation of nanoclay filled EVA composites revealed that the high energy beam can crosslink the polymer matrix and thereby improve thermal resistance [131]. Not only the thermal stability, even fire retardancy of EVA can be improved by the addition of ultrafine kaolinite substituting alumina trihydrate [132].

The permeation characteristics of EVA based nanocomposites were also quite useful for the development of innovative barrier products. The study on the sorption behavior of EVA –nanoclay with benzene as the

solvent, made the inference that a small addition of nanoclay can affect the polymer morphology and reduce diffusion. Electromechanical actuators and photoactuators can be developed based on ethylene vinyl acetate filled with carbon nanotubes [133].

Mechanical properties of EVA copolymer can be tuned based on the extend and type of blending. Polyethylene –EVA blend in the ratio of 50:50 found to give inferior mechanical properties compared to pure EVA [134]. Functionalised graphene embedded in the EVA matrix can improve its tensile strength and storage modulus [135].

### 1.6.3 Polystyrene

Polystyrene (PS) is hard and rigid transparent thermoplastic with a repeating structure as shown in Fig.1.2.

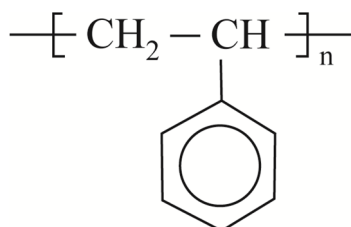


**Fig.1.2: Structure of Polystyrene**

Polystyrene was invented by E. Simson in 1839, since then it was made by different polymerization methods. Commercially polystyrene is synthesized by the dehydrogenation of ethylbenzene. The endothermic reaction of ethylbenzene produces “crude styrene” which on processing produces styrene, which on polymerization produces polystyrene. Mass and suspension polymerization are being the most important and extensively used techniques.

The mechanical properties of polystyrene depend to some extent on its molecular weight. Its optical properties includes high transmission of all wave lengths of visible light and high refractive index (1.592). The electrical insulation properties of polystyrene is good. It shows very small effect of frequency on dielectric constant and power factor upto  $10^6$  Hz. The chemical resistance of PS can be affected by solvents like benzene and chlorinated hydrocarbons. The thermal properties of PS include low thermal conductivity and low softening temperature ( $<100^0$  C). The low thermal conductivity of polystyrene makes it a good candidate for making thermal insulating foams. It is widely accepted as an easily processable and suitable plastic for packaging applications. It is a cheap and easily mouldable material with low moisture absorption. The major drawback of polystyrene is its brittleness. High impact polystyrene (HIPS) with enhanced impact resistance can be obtained by modifying polystyrene with rubber.

Considering the electrical properties of EVA, it was reported by Das et al. [136] that pure copolymer shows an electrical resistivity value of  $10^{13}$  ohm cm. Sharp decrease in the resistivity value ( $1.3 \times 10^3$  ohm cm) was obtained for EVA with surface modified graphene with 8 wt% inclusion. Silver coated wollastonite fibres were used as fillers at 8 vol% in EVA matrix to obtain electrical conductivity of  $4.8 \times 10^5$  S  $\text{cm}^{-1}$  [137]. The adhesive properties (peel strength) of the wollastonite fibre EVA matrix were found to be inferior due to poor wettability.

**Table 1.6: Nanocomposites with poly (ethylene co-vinyl acetate) EVA matrix**

Sl. No	Composition	Technique	Properties	Ref.
1	EVA-Sepiolite	Melt Blending-Twin screw extruder	Tensile Strength and Flame resistance improved	138
2	EVA/NBR-Organoclay	Internal Mixer	Youngs modulus , yield stress increased	139
3	EVA-Carbon nanotubes	Melt Mixing	Photooxidation reduced	140
4	EVA-Layered silicate	Melt processing	Combustion rate reduced	141
5	EVA-Magnesium hydroxide-MWNT	Halogen free flame retardant melt mixed	Increase of LOI values	142
6	EVA-Alumina trihydrate-MMT	Rheocord	Mechanical, thermal and flame resistance increased.	143
7	EVA-Fluorohectorite	Internal mixer	Heat release rate reduced	144
8	EVA/LDPE-Layered double hydroxides	Solution blending	Thermal resistance and tensile strength increased	145
9	EVA/Polypyrrole-MWCNT	Melt blending	Electromagnetic Interference Shielding increased	146
10	EVA-cyclodextrin nanosponge-phosphorus	Melt blending	Heat release rate decreased	147
11	HDPE/EVA-ammonium modified MMT	Melt mixing	Enhanced thermal stability	148
12	EVA-carbon black with ethylene -propylene copolymer	Melt blending	Electrical conduction improved	149
13	EVA-Graphene oxide	Solvent blending	Improved flame retardancy	150
14	EVA-CNT	Irradiated with gamma rays	Lamella structure of EVA changed	151
15	EVA-MWCNT	Brabender internal mixer	Delayed ignition and improved flame resistance	152
16	EVA/EPDM-Clay	Solution mixing with toluene	Improved thermal and mechanical properties	153
17	EVA-MMT	Solution blending	Decreased swelling	154
18	EVA-Clay	Twin screw extruder	Exfoliated structures showed improved modulus and tensile strength	155
19	EVA-clay/MWNT	Internal mixer	Mechanical, thermal and flame retardance properties improved.	156

#### **1.6.4 Nano composites based on polystyrene (PS)**

Polystyrene (PS) thermoplastics are widely used in industrial field and commercial applications. The extensive use of polystyrene is thanks to its excellent processability low cost and good dimensional accuracy, low moisture absorption and clarity. Although polystyrene has got excellent market, it lacks impact resistance, thermal resistance and electrical conductivity. Polystyrene has got its electrical conductivity in the range of approximately  $10^{-20}$  (S/cm) [157]. This inherent property of polystyrene can be altered by the incorporation of conductive fillers into its matrix. A conductive channel in the PS matrix can be made by the formation of networks with electrically connected filler particles.

Single wall carbon nanotubes have been widely investigated as an attractive candidate for improving the electrical properties of polystyrene [158]. Shah et al. [159] reported enhanced AC conductivity with increase of the MWCNT content. MWCNT-PS composite was prepared by Srivastava et al. to study the strain sensing effect of flexible films [160]. DC resistivity and AC impedance measurements were performed on carbon nanotube-PS composites by Wang et al. [161] and they observed that the low frequency resistance becomes 2 Mega ohm at 1% loading. Chen et al. [162] prepared and reported the PS-graphite nanosheets for improved electrical conductivity. Hybrid nanocomposite of graphite and MWCNT was found effective on in-situ polymerization of polystyrene for improved composite morphology [163].

**Table 1.7: Nanocomposites with polystyrene (PS) matrix**

Sl. No	Composition	Technique	Properties	Ref.
1	PS-CNT	In situ polymerisation	Electrical and thermal conductivity improved	164
2	PS-graphite	In situ polymerisation	Improved electrical and mechanical properties	165
3	PS-graphene	RAFT polymerisation	Thermal stability improved	166
4	PS-graphene	Modified with styrene maleic anhydride	Rheological and electrical properties improved	167
5	PS-clay	Supercritical CO <sub>2</sub> dispersed PS	Oxygen permeation reduced	168
6	PS-graphene-CNT	Microemulsion polymerization	Thermal, mechanical properties improved	169
7	PS-synthetic clay	Solution blending	Gas barrier increases	170
8	PS-MWCNT	Melt mixing	Thermal stability improved	171
9	PS-SWCNT	Solution mixing	Electrical conductivity increased at low percolation threshold	172
10	PS-CNT	Solution mixing	Percolated filler network formed	173
11	PS-carbon nanofibre	Melt blending	Storage modulus increases	174

## 1.7 Semiconductor nanomaterials

Semiconductor nanocrystals (NCs) bridge the gap between cluster molecules and bulk materials. As semiconductor nanoparticles exhibit size dependent properties like, scaling of the energy gap and the corresponding change in the optical properties, they are considered as front runners in technologically important materials. They are found to have novel optical, electrical and mechanical properties which result

from quantum confinement effects compared with their bulk counterparts. Semiconducting nanomaterials are made from a variety of different compounds. They are referred to as II-VI, III-V, or IV semiconductor particles, based on the periodic table groups that these elements are from. For example, silicon and germanium in Group IV, GaN, GaP, GaAs, InP and InAs are III-V semiconductors, while those of ZnO, ZnS, ZnSe, CdS, CdSe and CdTe are II-VI semiconductors. The stability of nanoparticles in polymer matrix makes their attractive for microelectronics and photonics technology.

### **1.7.1 Cadmium selenide (CdSe)**

Cadmium selenide (CdSe) is a widely investigated II-VI semiconductor nanoparticle, with a suitable band gap of 1.74 eV(300K). CdSe quantum dots can be prepared using organometallic synthesis. In recent years, hydrothermal/solvothermal method using hydrazine hydrate (HH) and ethylenediamine tetraacetic acid (EDTA) is found to be feasible and versatile [175]. It has a wide optical band gap, making it suitable for optical applications. CdSe nanoparticles with appropriate and tuned particle size can have an absorption edge and emission peak anywhere in the visible spectrum. This unique and advantageous property led to the use of CdSe for optoelectronic devices, nanosensing and biomedical imaging [176].

CdSe quantum dots were successfully used to fabricate polymer composites for electrochemiluminescence biosensing. Layer by layer construction of polyaniline matrix was found effective with graphene oxide and CdSe hybrid nanofillers [177]. Sensors made using polypyrrol

matrix with graphene oxide and CdSe were also reported recently [178]. Polyvinyl pyrrolidone (PVP) matrix composites of nanoCdSe have shown improved electrical properties for making electronic memory devices [179]. Optical activity of CdSe nanoparticles makes them fit for photo luminescent properties. Silicone [180], poly (lactic acid) [181], and poly (p-phenylenevinylene) [182] derivatives were used as matrices for cadmium selenide nanoparticles aiming at improved optical properties.

### 1.7.2 Zinc selenide (ZnSe)

Zinc Selenide (ZnSe) is an n-type semiconductor material with a wide band gap (2.58- 2.72 eV). It shows properties suitable for optoelectronic devices [183]. Nano material synthesis with controlled size, morphology and size distribution is important in tuning its physical and chemical properties. Recently, solvo-thermal process with  $ZnCl_2$  and Zinc acetate was found effective to obtain ZnSe nanoparticles ranging from 10- 15 nm [184].

ZnSe has got unique optical and electrical properties. Due to its wide band gap ( $E_g=2.7$  eV), it finds application as window layer in solar cells [185] and thin film transistors[186].The optical properties of ZnSe make it a suitable material for fluorescence quenching [187] and non linear refraction behaviour [188].

### 1.7.3 Zinc oxide (ZnO)

Zinc Oxide (ZnO) is a low cost, group II-VI direct wide band gap semiconductor ( $E_g = 3.22$  eV at 300 K) with large exciton binding energy (approx. 60 meV). It exhibits strong ultraviolet and visible



photoluminescence. These diverse properties of ZnO makes it suitable for a variety of applications. Nanosized ZnO is mixed in nanocomposites used for manufacturing coatings and sealants [189]. ZnO nanoparticles have been synthesized mainly by sol-gel method and also by solid state reaction method [190].

Nano ZnO was reported to show electrochemical activity and photocatalytic activity in poly(propylenedioxythiophene)[191]. Dielectric behavior of poly (N-vinylcarbazole)-ZnO and acetylene black nanocomposite was investigated by Ghosh et al. [192]. Low density polyethylene –ZnO showed sharp reduction in electrical resistivity at 2.8 vol % of nano ZnO incorporation [193]. Ultraviolet photo detectors of ZnO quantum dot-graphene fillers in poly (ethylene terephthalate) matrix exhibited light induced conductivity [194].

## **1.8 Scope and objectives of the work**

The literature survey carried out reveals that nanofillers in various polymer matrices generally improves mechanical, electrical, thermal, optical and other properties. Nanocomposites are useful in a variety of industries. In this thesis, EVA and PS materials were selected as the matrices. They are commercially used polymers and have not been the subject of research for optoelectronic properties with semiconductor nanomaterials. This has led to the present research interest.

Semiconductor nanomaterials of the II-VI family possess unique optoelectronic properties. The present work has been undertaken to explore the potential of different II-VI semiconductor nanomaterials like

cadmium selenide, zinc oxide and zinc selenide in amorphous polystyrene and semicrystalline EVA matrices.

EVA based nanocomposites was widely investigated for enhanced thermal conductivity and improved heat distortion temperature. Electron beam irradiation can be useful for thermal resistance of these systems. The unique properties of II-VI semiconductors coupled with EVA can make these nanocomposites suitable for device fabrication in nanosensing and biomedical imaging. Study of electrical and optical properties of the newly synthesized nanocomposites can reveal its characteristic advantages in opto-electronic device fabrication.

Improvement in conductivity behavior of polystyrene nanocomposites can be obtained with II-VI semiconductor nanomaterials. Moreover ZnSe and ZnO materials could be effective in polystyrene as they find application in solar cells and thin film transistors. The dielectric behaviour and UV photo detection of these nanocomposites can explain the material character and utility. The CdSe based polymer nanocomposites were reported for fabrication in memory devices and biosensors. The broad objective of this study is to determine the effect of filler concentration of II-VI nanomaterials on various properties of EVA and PS with prime focus on the thermal resistance, optical and electrical activation.

Structural studies (chemical and morphological) can be carried out by FTIR, Raman Spectroscopy and SEM –TEM characterisation. The physical properties of the synthesized nanocomposites can be analysed using impedance tester, photopyroelectric tester and UV characterisation.

The thermal resistance and mechanical properties can be evaluated by thermogravimetric analysis and universal testing machine.

The specific objectives of the current study are

- To synthesize II-VI semiconductor materials of zinc oxide (ZnO), zinc selenide (ZnSe) and cadmium selenide (CdSe) by hydrothermal and solvothermal methods.
- To prepare poly (ethylene-co-vinyl acetate) (EVA) and polystyrene (PS) nanocomposites with synthesized II-VI semiconductor nanofillers.
- To characterize the morphology, structure and constitution of the nanomaterials and the composites.
- To analyse the dielectric, optical, thermal and mechanical properties of the nanocomposites.

## **References**

- [1] Richardson T, Composites a design guide, Industrial Press Inc,200 Madison Avenue, Newyork,1987 Ch 1, P 18.
- [2] Coronado E, Galan-Mascaros J R, Gomez-Garcia C J and Laukhin V, Nature 2000, 408,447.
- [3] Croce F, Appetecchi G B, Persi L and Scrosati B, Nature 1998, 394, 456.
- [4] Pinnavaia T J, Science 1983, 220, 365.
- [5] Wang Y and Herron N. Science 1996, 273, 632.
- [6] Sidorov S N. J. Am. Chem. Soc.2001, 123, 10502.

- [7] Merkel T C, Freeman B D, Spontak R J, He Z, Pinnau I, Meakin P and Hill A J. *Science* 2002, 296, 519.
- [8] Sanchez C. and Ribot F. *New, J. Chem.* 1994, 18, 1007.
- [9] Lichtenha J D, Schwab J J and Reinerth W *ACChem, Innovation*, 2001, 31, 3.
- [10] She J, Inoue T, Suzuki M, Sodeoka S, Ueno K, *J. of European Ceramic Society.* 2000; 20, 12:187.
- [11] Tjong S C, Wang G S, *Mat. Sci. and Eng. A.* 2004; 386 (1-2) 48.
- [12] Luo J J and Daniel I M., *Compos. Sci. Technol.* 2003, 63, 11: 1607
- [13] Schmidt D, Shah D and Giannelis E P, *Current Opinion in Solid State and Material Science*, 6(3): 205.
- [14] Gorga R E and Cohen R E, *J. Polym. Sci., Part B: Polymer Phys*, 42, 14: 2690.
- [15] Zhang M, Lin G, Dong C, Wen L, *Surface coat Tech.* 2007, 201, 7252.
- [16] Schadler L S, Brinson L C, Sawyer W G, *J. Miner. Met. Mater. Soc.* 2007, 59, 53.
- [17] Schadler L S, Kumar S K, Benicewicz B C, Lewis S L, Harton S E, *Mat. Res. Bull.* 2007, 32, 335.
- [18] LeBaron P C, Wang Z, Pinnavaiva T J, *Appl. Clay Sci.* 1999, 15, 11.
- [19] Schmidt D, Shah D, Giannelis E P, *Curr. Opin. Solid State Mater. Sci.*, 2002, 6, 205.
- [20] Alexandre M, Dubois Ph, *Mater. Sci. Eng. R*, 2000, 28, 1.
- [21] Li X, Wang D, Cheng G, Luo Q, An J, Wang Y, *Appl. Catal. B Environ.* 2008, 81 (3-4), 267.
- [22] Vollath D, Szabo D V, Fuchs J, *Nanostruct. Mater* 1999, 12, 433.

- [23] Patel S, Bandyopadhyay A, Vijayabaskar V, Bhowmick A K, *Polymer* 2005, 46, 8079.
- [24] Chen C, Ryan S J, Schaefer D W, Jeffrey W Baur, *Polymer* 2008, 49, 17, 3805.
- [25] Martinez V M, Sanchez V P, Martin-Martinez J M, *Euro. Polym. Jour.*, 2008, 44, 3146.
- [26] Sih B C, Wolf M O, *Chem. Commun.* 2005, 27, 3375.
- [27] Dallas P, Sharma V K, Zboril R, *Adv. Colloid. Interface Sci.* 2011, 166(1-2), 119.
- [28] Wilson J L, Poddar P, Fery N A, Srikanth H, *Jour. Appl. Phys.* 2004, 95, 1439.
- [29] Crooks R M, Zhao M, Sun L, Chechik V, Yeung L K, *Acc. Chem. Res.*, 2001, 34, 181.
- [30] Fortunati E, Puglia D, Monti M, Santulli C, Maniruzzaman M, Kenny J M, *J. Appl. Polym. Sci.* 2013, 128, 3220.
- [31] Zhou C, Wu Q, in Sudheer Neralla (Ed) ISBN 978-953-51-0714-9, 2012.
- [32] Novoselov K S, Jiang D, Schedin F, Booth T J, Khotkevich V V, Morozov S V, Geim A K, *Proc. Nat. Acad. Sci.* 2005, 102, 10451.
- [33] Geim A K, Novoselov K S, *Nat. Mater.* 2007, 6, 183.
- [34] Stankovich S, Dikin D A, Dommett G H, Kohlhaas K M, Zimney E J, Stach E A, Piner R D, Nguyen S T, Ruoff R S, *Nature* 2006, 442, 282.
- [35] Watcharotone S, Dikin D A, Stankovich S, Piner R, Jung I, Chen S F, Liu C P, Nguyen S T, Ruoff R S, *Nano. Lett.* 2007, 7, 1888.
- [36] Lijima S, *Nature* 1991, 354, 56.
- [37] Dresselhaus M S, Dresselhaus G, Sugihara K, Spain I L, Goldberg H A, *Graphite Fibres and Filaments*, 1988.

- [38] Auvinen S, Alatalo M, Haario H, Jalava J P, Lammin maki R J, J of Phy. Chem. C 2011, 115, 8484.
- [39] Damonte L C, Zelis L A M, Soucase B M, Fenollosa M A H, Powder Tech. 2004, 148,15.
- [40] Ke-long H, Lian-guo Y, Su-qin L, Chao-jian L, The Transactions of Nonferrous Metals Society of China 2007, 17, 633.
- [41] Zawarah M F, El-Kheshen A A, Abd-El-Aal H M, Jour. of Ovonic Research 2009, 5, 129.
- [42] Pingali K C, Rockstraw D A, Deng S, Aerosol Sci. and Tech. 2005, 39, 1010.
- [43] Pyrpassopoulos S, Niarchos D, Nouneis G, Boukos N, Zafiropoulou I, Tzitzios V, Nanotechnology 2007, 18, 485604, 1.
- [44] Dimitriev Y, Ivanova Y, Iordanova R, J. Univ. Chem. Tech. and Metal 2008,. 43, 181.
- [45] Wang C, Ying J Y, Chem. Mater.1999, 11, 3113.
- [46] Beyer F L, Tan N C B, Dasgupta A, Galvin M E, Chem. Mater. 2002, 14, 2983.
- [47] Manias E, Touny A, Wu L, Lu B, Strawhecker K, Gilman J W, Chung T C, Poly. Mater. Sci. Eng. 2000, 82, 282.
- [48] Park C L, Park O O, Lim J G, Kim H J, Polymer 2001, 42, 7465.
- [49] Usuki A, Tukigase A, Kato M, Polymer 2002, 43, 2185.
- [50] LiJ-X, J Wu, Chan C M, Polymer 2000, 41, 6935.
- [51] Ziolo R F, Giannelis E P, Shull R D, Nanostruct. Mater 1993, 3, 85.
- [52] Guan C, Lu C L, Cheng Y R, Song S Y, Yang B, J. Mater. Chem. 2009, 19,617.
- [53] Gangopadhyay R, De A, Eur. Polymer Journal 1999, 35, 1985.

- [54] Althues H, Simon P, Philipp F, Kaskel S, J. Nanosci. Nanotechnol. 2006, 6,409.
- [55] Luo Y, Li W, Wang X, Xu D, Wang Y, Acta mater. 57(11) 2009, 3182.
- [56] Tang E, Cheng G X, Pang X S, Ma X L, Xing F B, Colloid. Polym. Sci. 2006,284, 422.
- [57] Wang Z H, Lu Y L, Liu J, Dang Z M, Zhang L Q, Wang W, J. Appl. Polym. Sci. 2011,119, 1144.
- [58] Vollath D, Szabo D V, Fuchs J, Nanostruct. Mater 1999, 12, 433.
- [59] Schallehn M, Winterer M, Weirich T E, Hahn H, Chem. Vap. Depos. 2003, 9, 40.
- [60] Srikanth H, Hajndl R, Chirinos C, Sanders J, Sampath A, Sudersan T S, Appl. Phys. Lett. 2001, 79, 3503.
- [61] Qin C, Coulombe S, Mater. Lett. 2006, 60, 1973.
- [62] Kwiatkowski, K. C. and Lukehart, C. M. in Handbook of Nanostructured Materials and Nanotechnology, Volume 1: Synthesis and Processing, Nalwa H. S. Ed. Academic Press, San Diego, CA, 2000.
- [63] Vollenberg P HT, Heikens D, Polymer 1989, 30, 1656.
- [64] Ash B J, Schadler L S, Siegal R W, Mater. Lett.2002, 55,83.
- [65] Shelly J S, Mather PT, DeVries K L, Polymer 2001, 42, 5849.
- [66] Avella M, Errico M E, Gentile G, Macromol. Symp. 2007, 247, 140.
- [67] Vlasveld D P N, Daud W, Bersee H E N, Picken S J, Compos. Part A, 2007, 38,730.
- [68] Luo J J, Daniel I M, Compos. Sci. Technol 2003, 63, 1607.
- [69] Blumstein A, Jour. Polymer Sci. A, 1965,3, 2665.
- [70] Zanetti M, Camino G, Reichert P, Mulhaupt R, Macromol. Rapid. Commun. 2002, 22, 176.

- [71] Du J X, Wang D Y, Wilkie C A, Wang J Q, Polym. Degrad. Stab. 2003, 79, 319.
- [72] D Lee K Char, Polym. Degrad. Stab. 2002, 75,555.
- [73] Zanetti M, Camino G, Reichert P, Mulhaupt R, Macromol. Rapid Commun. 2002, 22, 176.
- [74] Vladimirov V, Betchev C, Vassiliou A, Papageorgiou G, Bikiaris D, Compos. Sci. Technol.2006, 66,2935.
- [75] Ogasawara T, Ishida Y, Ishikawa T, Aoki T, Ogura T, Compos Part A- Appl S 2006,37,2236.
- [76] Picard E, Gauthier H, GerardJ-F, Espuche E, Jour. Colloid. Interface Sci. 2007, 307, 364.
- [77] Kiko Sunderland, Philip Brunetti, Leonard Spinu, Jiye Fang, Zhenjun Wang, Weigang Lu, Mat. Lett. 58, 2004, 3136.
- [78] Samantha A M, Anderson A A, Mehul S, Kimberly W A, Hilt J Z, J. Biomed. Mater. Res. Part A 2009, 91, 903.
- [79] Wang Z Y, Liu G, Sun J, Wu B Y, Gong Q Y, Song B, Ai H, Gu Z W, J. Nanosci. Nanotechnol. 2009, 9, 378.
- [80] Albornoz C, Jacobo S C, J. Magn. Magn. Mater. 2006, 305, 12.
- [81] Zhu Y, Kaskel S, Ikoma T, Hanagata N, Micropor. Mesopor Mater. 2009, 123,107.
- [82] Rajesh T Ahuja, Kumar D, Sensors and Actuators B: Chemical, 2009, 136,1,275.
- [83] Dayal S, Kopidakis N, Olson D C, Ginley D S, Rumbles G, Nano Lett., 2010,10,1, 239.
- [84] Skaff H, Sill K, Emrick T, Jour. American Chem. Soc., 2004, 126,36, 11322.



- [85] Olson D C, Shaheen S E, Collins R T, Ginley D S, *Jour. Phys. Chem. C* 2007, 111, 44, 16670.
- [86] Landi B J, Raffaele R P, Castro S C, Bailey S G, *Progress in Photovoltaics* 2005, 13, 2, 165.
- [87] Brabec C J, Durrant J R, *MRS Bulletin*, 2008, 33,7,670.
- [88] Ratna D, Karger-Kocsis J. *J. Mater. Sci* 2008; 43 (1): 254.
- [89] Loh K J, Lynch J P, Kotov N, *Int. J. Appl. Electromag Mech* 2008; 28: 887.
- [90] Shim B S, Starkovich J, Kotov N, *Compos. Sci. Technol.* 2006; 66:1174.
- [91] Halajan M, Torkamany M J, Dorranjan D, *Jour. of Phys. And Chem. of Solids* 2014, 75, 11, 1187.
- [92] Chandrakala H N, Ramraj B, Shivakumaraiah, Siddaramaiah, *Jour. of Phys. Chem. of Solids*, 2014, 75, 2, 252.
- [93] Tekin E, Smith P J, Hoepfner S, Ulrich S S, *Adv. Functional Mater.*, 2007, 17, 23.
- [94] Sun Y, Zhang Z, Wong C P, *Polymer* 2005, 46, 2297.
- [95] Singha S, Thomas M J, *IEEE Trans. Dielectr. Electr. Insul.* 2008, 15, 1, 12.
- [96] Roy M, Nelson J K, MacCrone R K, Schadler L S, *J. Mater. Sci.* 2007, 42, 3789.
- [97] Rahman I A, Padavettan V, *Journal of Nanomaterials*, 2012, 132424, 1.
- [98] Naderi S, Ghaderi A, Solaymani S, Golzan M M, *The European Physical Journal Applied Physics*, 2012, 58, 20401.
- [99] Greget R, Nealon G I, Vilenko B, Turek P P, Meny C, Ott F et al. *Chem. Phys. Chem* 2012, 13, 3092.
- [100] Sadiq I M, Pakrashi S, Chandrasekaran N, Mukherjee A, *Jour. of Nanoparticle Research*, 2011, 13, 3287.

- [101] Ugur S S, Sariisik M, Aktas A H, Ucar M C, Erden E, *Nanoscale Research Letters*, 2010, 5, 1204.
- [102] Buessem W R, Cross L E, Goswami A K, *Jour. American Ceram. Soc.*, 1992, 75, 2926.
- [103] Shao W, Nabb D, Renevier N, Sherrington I, Fu Y, Luo J, *Jour. of the Electrochemical Society*, 2012, 159, 671.
- [104] Georgia N Tomara, Ariadni P Kerasidou, Anastasios C Patsidis, Panagiota K Karahaliou, Georgios C Psarras, Stavroula N Georga, Christoforos A Krontiras, *Composites Part A*, 2015, 71, 204.
- [105] Santanu Singha, Joy Thomas M, *IEEE Trans. Dielec. Elect. Insul.*, 2008, 15, 1, 12.
- [106] Sheng-Hong Yao, Zhi-Min Dang, Hai-Ping Xu, Mei-Juan Jiang, Jinbo Bai, *Appl. Phys. Letters*, 2008, 92, 82902, 1.
- [107] Xingyi Huang, Pingkai Jiang, Liyuan Xie, *Appl. Phys. Letters*, 2009, 95, 242901, 1.
- [108] Jun-Wei Zha, Yan-Hui Zhu, Wei-Kang Li, Jinbo Bai, Zhi-Min Dang, *Appl. Phys. Letters*, 2012, 101, 62905, 1.
- [109] Kim W S, Yoon K B, Bae B S: *J. Mater. Chem.* 2005, 15, 4535.
- [110] Bhattacharya S K, Tummala R R, *J. Mater. Sci. Mater. Electron.* 2000, 11, 253.
- [111] Ritzhaupt- Kleissl H J, Johander P, Eds, *Ceramic processing in Microtechnology*, Whittles Publ. 2009, 120.
- [112] Bhattacharya S K, Tummala R R, *J. Mater. Sci. Mater. Electron.* 2000, 11, 253.
- [113] Stephan A M, Nahm K S, *Polymer* 2006, 47, 5952.
- [114] Liu H K, Wang G X, Guo Z P, Wang J Z, Konstantinov K, *J. New Mat. Electrochem. Syst.* 2007, 10, 101.

- [115] Krawiec W, Scranlon L G Jr, Fellner J P, Vaia R A, Vasudevan S, Giannelis E P, *J. Power Sources* 1995, 54, 310.
- [116] Capuano F, Croce F, Scrosati B, *J. Electrochem. Soc.*, 1991, 138, 1918
- [117] Hu Z A, Xie Y L, Wang Y X, Mo L P, Yang Y Y, Zhang Z Y, *Mater. Chem. Phys.*, 2009, 114, 990
- [118] Yang B D, Yoon K H, Chung K W, *Synth. Met.* 2004, 143, 25.
- [119] Jiguet S, Bertsch A, Hofmann H, Renaud P, *Adv. Eng. Mater.* 2004, 6, 719.
- [120] Dang Z M, Tian C Y, Zha J W, Yao S H, Xia Y J, Li Y J, Shi C Y, Bai J, *Adv. Eng. Mater-Adv. Biomater.* 2009, 11, B144.
- [121] Turri S, Torlaj L, Piccinini F, Levi M, *Journal of Applied Polymer Science*, 2010, 118, 1720.
- [122] Potschke P, Andres T, Villmow T, Pegel s, Bruuml nign H, Kobashi K, Fisher D, HaumlusserL, *Compos. Sci. Technol.*2010, 70;343.
- [123] Dai K, Xu X B, Li Z M, *Polymer*, 2007, 48, 3, 849.
- [124] Villmow T, Pegel S, Petra P, Heinrich G, *Polymer*, 2011, 52, 10, 2276
- [125] Yu C, Choi K, Yin L, Grunlan J C, *ACS Nano*, 2011, 5,10,7885.
- [126] Hewitt C A, Kaiser A B, Roth S, Craps M, Czerw R, Carroll D L, *Appl. Phys. Lett.* 2011, 98, 183110.
- [127] Alexander M, Dubois P, *Mater. Sci. Eng.* 2000 R 28, 1, 1.
- [128] Zanetti M, Camiro G, Thomman R, Mullhaupt R, 2001, *Polymer* 42, 4501.
- [129] Zhang y, Hu Y, Song L, Wu J, Fang S L, *Polym. Adv. Technol.* 2008, 19, 8, 960.
- [130] Ghose S, Watson K A, Working D C, Connell J W, Smith JrJ G., Y P Sun, *Composites Sci. Technol.* 2008, 68, 1843-1853.

- [131] Bibo Wang, Lei Song, Ningning Hong, Qilong Tai, Hongdian Lu, Yuan Hu, *Radiation Phys. Chem.*, 2011, 80, 1275.
- [132] Marcos Batistella, Belkacem Otazaghine, Rodolphe Sonnier, Anne-Sophie Caro-Bretelle, Carlos Petter, Jose-Marie Lopez-Cuesta, *Polymer Degradation and Stability*, 2014, 100, 54.
- [133] Klaudia Czanikova, Nuria Torras, Jaume Esteve, Igor Krupa, Peter Kasak, Ewa Pavlova, Dusan Racko, Ivan Chodak, Maria Omastova., *Sensors and Actuators B: Chemical*, 2013, 186, 701.
- [134] FakerM, Razavoi AghjehM K, GhaffariM, SeyyendiS A, *Euro. Polym. Journ.* , 2008, 44, 1834.
- [135] Tapas Kuila, Partha Khanra, Anata Kumar Mishra, Nam Hoon Kim, Joong Hee Lee, *Polymer Testing*, 2012, 31, 282.
- [136] Das N C, Yamazaki S, Hikosaka M, Chaki T K, Khastagir D, Chakraborty A, *Polym. Int.* 2005, 54(2), 256.
- [137] Cecen V, Boudenne A, Ibos L, Novak I, Nogellova Z, Prokes J, Krupa I, *Europ. Polym. Jour.*, 2008, 44, 3827.
- [138] Hossein Cheraghi Bidsorkhi, Mohammad Soheilmoghaddam, Raheleh Heidar Pour, Hossein Adelnia, Zurina Mohamad, *Polymer Testing*, 2014, 37 ,117.
- [139] Mohammad Razavi-Nouri, Mahmoud Karami, *Polymer*, 2014, 55, 26, 6940.
- [140] Sandrine Morlat-Therias, Elisabeth Fanton, Jean-Luc Gardette, Sophie Peeterbroeck, Michael Alexandre, Philippe Dubois, *Polymer Degradation and Stability*, 2007, 92,10, 1873.
- [141] Marco Zanetti, Luigi Costa, *Polymer*, 2004, 45, 13, 4367.
- [142] Lei Ye, Qianghua Wu, Baojun Qu, *Polymer Degradation and Stability*, 2009, 94, 5, 751.

- [143] Ming-Kuen Chang, Shyh-Shin Hwang, Sung-Po Liu, *Journal of Industrial and Engineering Chemistry*, 25 2014, 20, 4, 1596.
- [144] Marco Zanetti, Giovanni Camino, Rolf Mülhaupt, *Polymer Degradation and Stability*, 2001, 74,3, 413
- [145] Kuila T, Srivastava S K, Bhowmick A K, Saxena A K, *Composites Science and Technology*, 2008, 68,15, 3234.
- [146] Chi-Yuan Huang, Jing-Yi Wu, Keng-Yu Tsao, Chih-Lung Lin, Chien-Pang Chang, Ching-Shan Tsai, Yen-Hung Chen, Jen-Taut Yeh, Kan-Nan Chen, *Thin Solid Films*, 2011, 519,15, 4765.
- [147] Jenny Alongi, Merima Pošković, Alberto Frache, Francesco Trotta, *Polymer Degradation and Stability*, 2010, 95,10, 2093
- [148] Shahin Akhlaghi, Alireza Sharif, Mohammadreza Kalaei, Alireza Elahi, Mohammadhadi Pirzadeh, Saeedeh Mazinani, Mehdi Afshari, *Materials & Design*, 2012, 33, 273
- [149] Thomas Gkourmpis, Christer Svanberg, Senthil K. Kaliappan, Walter Schaffer, Martin Obadal, Gottfried Kandioller, Davide Tranchida, *European Polymer Journal*, 2013,49,8 ,1975.
- [150] Guobo Huang, Suqing Chen, Shouwan Tang, Jianrong Gao, *Materials Chemistry and Physics*, 2012, 135, 2-3, 938.
- [151] Kyoung-Yong Lee, Ki-Yup Kim, *Polymer Degradation and Stability* 2008, 93,7, 1290.
- [152] Riva A, Zanetti M, Braglia M, Carnino G, Falqui L, *Polymer Degradation and Stabilisation*, 2002, 77, 299.
- [153] Peeterbroeck S, Laoutid F, Swoboda B, Lopez-Cuesta J, Moreau N, Nagy J B, Alexandre M, Dubois P, *Macromol. Rapid. Commun.*, 2007, 28,260.
- [154] Pramanik M, Acharya H, Srivastava S K, *Macromol. Mater. Eng.*, 2004, 289, 562.

- [155] Duquesne S, Jama C, Le Bras M, Delobel R, Recourt P, Gloaquen J M, Compos. Sci. Technol., 2003, 63, 1141.
- [156] Peeterbroeck S, Alexandre M, Nagy J B, Pirtot C, Forseca A, Moneau N, Philippin G, Delhalle J, Mekhalif Z, Sporcken R, Bayer G, Dubois P, Compos. Sci. Technol., 2004, 64, 2316.
- [157] Kotelyanskii M, Wagner N J, Macromolecules, 1996, 29, 26, 8497.
- [158] Mitchell C A, Bahr J L, Arepalli S, Tour J M, Krishnamoorthi R, Macromolecules, 2002, 35, 8825.
- [159] Shah A H, Rizvi T Z, Measurement, 2013, 46, 1541.
- [160] Srivastava R K, Vemuru VSM, Zeng Y, Vajtai R, Nagarajaiah S, Ajayan P M et.al., Carbon 2011, 49, 12, 3928.
- [161] Zhe Wang, Mei Lu, Hu-Lin Li, Xin-Yong Guo, Materials Chemistry and Physics 100, 2006, 77.
- [162] Chen G, Wu C, Weng W, Wu D, Yan W, Polymer, 2003, 44,6,1781
- [163] Goutam Hatui, Pallab Bhattacharya, Sumanta Sahoo, Saptarshi Dhibar, Chapal Kumar Das, Composites: Part A, 56, 2014, 181.
- [164] Lahelin M, Annala M, Nykänen A, Ruokolainen J, Seppälä J, Composites Science and Technology, 2011, 71,6, 900.
- [165] Wang Z, Xie G, Wang X, Zhang Z, Jour. of Appl. Polym. Sci. 206, 100, 4434.
- [166] Renpeng Gu, William Z. Xu, Paul A. Charpentier, Polymer, 2014, 55, 21, 5322.
- [167] Zhixian He, Baoqing Zhang, Hao-Bin Zhang, Xin Zhi, Qihui Hu, Chen-Xi Gui, Zhong-Zhen Yu, Composites Science and Technology, 2014, 102, 176.
- [168] Fengyuan Yang, Mihai Manitiu, Robert Kriegel, Rangaramanujam M. Kannan, Polymer, 2014,55,16, 3915.

- [169] Archana S. Patole, Shashikant P. Patole, So-Young Jung, Ji-Beom Yoo, Jeong-Ho An, Tae-Ho Kim, *European Polymer Journal*, 2012, 48,2, 252.
- [170] Michael R. Schütz, Hussein Kalo, Thomas Lunkenbein, Josef Brey, Charles A. Wilkie, *Polymer*, 2011,52,15, 3288.
- [171] Morgan A B, Harris J D, *Polymer*, 2004, 45, 8695.
- [172] Hwu J M, Ko T H, Yang W T, Lin J C, Jiang G J, Xie W, Pan W P, *Jour. of Appl. Polym. Sci.*, 2004, 91, 101.
- [173] Mitchell C A, Bahr J L, Arepalli S, Tour J M, R Krishnamoorthi, *Macromolecules*, 2002, 35, 8825.
- [174] Zhong Y, Zhu Z, Wang S Q, *Polymer*, 2005, 46, 3008.
- [175] Yang J, Zeng J H, Yu S H, Yang L, Zhang Y H , Qian Y T, *Chem. Mater.* 2000,11,12, 3259.
- [176] Ma C, Ding Y, Moore D, Wang X, Wang, *J. Am. Chem. Soc.* 2004, 126, 708.
- [177] Hu X W, Mao C J, Song J M, Niu H L, Zhang S Y, Huang H P, *Biosens Bioelectron*, 2013, 41, 372.
- [178] Rui Ke, Xiaomei Zhang, Lei Wang, Chunyan Zhang, Shengyi Zhang, Changjie Mao, Helin Niu, Jiming Song, Baokang Jin, Yupen Tian, *Jour. of Alloys and Compounds*, 2015, 622, 1027.
- [179] Ramneek Kaur, Tripathi S K, *Microelectronic Engineering*, 2015, 133, 59.
- [180] Yang Yang Han, *Compos. Sci. Technol.*, 2011, 71, 14, 1652.
- [181] Gong X, Pan L, Tang C Y, Chen L, Hao Z, Law W C, Wang X, Tsui C P, Wu C, *Composites Part B: Engg.* 2014, 66, 494.
- [182] Bingxin Liu, Xiaodan Lu, Chunyu Wang, Cuiyan Tong, Yao He, *Changli Lu, Dyes and Pigments*, 2013, 99,1, 192.

- [183] Maria C Tamargo, II-IV Semiconductor materials and their applications, Taylor and Francis, 2002, 113.
- [184] Mollaamin F, Gharibe S and Monajjemi M, Iner. Jour. of the Physical Sci.2011, 6(6)1496.
- [185] Kale R B, Lokhande C D, Mater. Res. Bull., 2004, 39, 1829.
- [186] Wei A, Zhao X, Liu J, ZhaoY, Physica B, 2013, 410, 120.
- [187] Hamed Z B, Benchaabane A, Kouki F, Sanhoury M A, Bouchriha H, Synthetic Metals, 2014, 195, 102.
- [188] Halajan M, Torkamany M J, Dorrnian D, Jour. of Phys. and Chem. of Solids, 2014, 75,11,1187.
- [189] Xiong M, Gu G, You B, Wu L, Journal of Applied Polymer science, 2003, 90 1923.
- [190] Singh N, Mehra R M., Kapoor A., Jour. Nano. Electron. Phys. 2011, 3, 132.
- [191] Ali A, Jamal R, Shao W, Rahman A, Osman Y, Abdiryim T, Prog. In Natural Science: Materials International, 2013, 22,6, 524.
- [192] Ghosh D, Sardar P S, Biswas M, Mondal A, Mukherjee N, Materials Chem. and Phys. 2010, 123, 1, 9.
- [193] Tjong S C, Liang G D, Materials Chem. and Phys. 2006, 100, 1, 1.
- [194] Son D I, Yang H Y, Kim T W, Park W, Composites Part B: Engg. 2015, 69, 154.

.....❧.....



This chapter gives a brief description of the materials used and experimental procedures followed during this study.

### 2.1 Materials

#### 2.1.1 Poly(ethylene-co-vinyl acetate) EVA

Poly(ethylene-co-vinyl acetate), EVA copolymer was obtained from Exxon Mobil Chemicals, Singapore. The vinyl acetate content of the copolymer was 9.4 wt %. ( $M_n = 1.89 \times 10^4$ , Density  $0.931 \text{ g/cm}^3$ , Melt Flow Index-2.1g/10 min @190°C, 2.16 Kg).

#### 2.1.2 Styrene

Styrene monomer was obtained from M/s Pure chemicals, Chennai, Tamilnadu.

Molecular weight : 104.15

Density :  $0.9059 \text{ g/cm}^3$

Boiling Point : 145-146°C.

Polystyrene obtained had a molecular weight ( $M_w$ ) 24000 with polydispersity index of 3.

Density : 1.05 g/cm<sup>3</sup>.

### 2.1.3 Benzoyl Peroxide

Purchased from Sigma Aldrich.

Assay : 75 %

Melting Point : 105°C.

### 2.1.4 Chemicals for Nanomaterial synthesis

a) Zinc acetate : Purchased from Merck Millipore, Mumbai.

Assay : 99.5,

pH : 6.0-7.0

b) Sodium selenite: Purchased from Sigma Aldrich, Mumbai. .  
(Purity: 95.5)

c) Hydrazine hydrate (80% solution in water): Purchased from Merck Millipore, Mumbai.

Boiling Point : 117-119 °C.

Density : 1.02g/cm<sup>3</sup>

d) Cadmium nitrate tetrahydrate : Purchased from Sigma Aldrich.  
(Purity:99.9)

### 2.1.5 Equipment for nano and composite preparation

a) Muffle Furnace, Max. operating temperature: 1200 °C

b) Ultrasonicator

Mechanical probe ultrasonicator (Vibra cell processor VCX 750, operating at 750 W) Features: Energy monitor, Capacity: 10-250 ml, Probe tip diameter: 13mm.

The machine consists of ultrasonic power supply which converts the line voltage to high frequency electrical energy. This produces mechanical vibrations by a piezoelectric transducer within the converter. These vibrations are further intensified by the probe causing pressure waves in the solution. Probe vibration produces millions of bubbles or cavities which expand and collapse creating enormous shock waves. The extreme high energy released during this process leads to the disruption of the interaction forces between the particles, leading to a proper dispersion of the nanomaterial in the solution.

## **2.2 Characterizations**

In order to estimate the properties and morphology of nanomaterials and nanocomposites, characterization techniques are required. This will assist us to assess the macro and microstructure and also to assess and improve the quality of the composite.

### **2.2.1 Transmission electron microscopy (TEM)**

Nanomaterials used for the study were analysed using a Hitachi H7500 instrument. In a transmission electron microscope (TEM), a beam of focused high energy electrons is transmitted through a thin sample to reveal information about its morphology, crystallography, particle size distribution, and its elemental composition. It is capable of providing

atomic-resolution lattice images, as well as giving chemical information at a spatial resolution of 1 nm or better. The unique physical and chemical properties of nanomaterials depend not only on their composition, but also on their structures. TEM provides a means for characterizing and understanding such structures. TEM is unique as it can be used to focus on a single nanoparticle in a sample, and directly identify and quantify its physical structure. Perhaps the most important application of TEM is the atomic resolution real-space imaging of nanoparticles.

### **2.2.2 Scanning electron microscopy (SEM)**

Scanning electron microscopy (SEM) is perhaps the most routinely utilized instrument for the characterization of nano materials. With SEM it is possible to obtain secondary electron images of organic and inorganic materials with nanoscale resolution, allowing topographical and morphological studies to be carried out, by scanning an electron probe across the surface and monitoring the secondary electrons emitted. Compositional analysis of a material may also be obtained by monitoring the X-rays produced by the electron-specimen interaction. For the scanning electron microscopy (SEM) measurements a JEOL JSM-6390LV microscope was used. The samples were gold sputtered with 10 nm gold and the observation was made at 15-20 kV.

### **2.2.3 Fourier Transform Infrared (FT-IR) Analysis**

Fourier transform IR spectroscopy is a simple scientific technique to resolve a complex wave into its frequency components. The conventional IR spectrometers yield poor results for the far IR region, as the sources are weak and detectors are insensitive. FT-IR has made this energy-

limited region more accessible. It has also made the mid–infrared (4000–400  $\text{cm}^{-1}$ ) more useful [1]. Conventional spectroscopy, called the frequency domain spectroscopy, records the radiant power as a function of frequency. In the time domain spectroscopy, the change in radiant power is recorded as a function of time. In the Fourier transform spectrometer, a time domain plot is converted into a frequency domain spectrum [2]. The FT-IR spectra were recorded in the range of 4000 - 400  $\text{cm}^{-1}$  using the instrument Thermo-Nicolet Avatar 370. Shimadzu IRAffinity 1S was also used for the study.

#### **2.2.4 Raman spectroscopy**

In the present study, a mobile Raman microspectrometer (HE 785, JY Horiba) was used. The excitation source is a cw diode laser, emitting at 786 nm (maximum power on the sample, 50 mW), fibre-optically coupled to an optical head that enables focusing of the beam by means of a number of objective lenses ( $\times 10$   $\times 20$   $\times 50$ ) which provide variable focusing of the beam [3] (and thus magnification of the work area) down to a few microns on the sample surface. A white light illumination system and a high-resolution color camera (video microscope) are also part of the optical head and offer a very clear view of the area under investigation, necessary for positioning the beam on nanocomposites. The scattered Raman radiation is collected through the focussing objective and sent through an optical fiber to a compact spectrograph, equipped with a concave grating, which provides spectral coverage up to 3,200  $\text{cm}^{-1}$  at a spectral resolution of about 10–15  $\text{cm}^{-1}$ . Spectra are recorded on a high-sensitivity, Peltier-cooled CCD detector (1,024 $\times$ 256 pixels, Synapse, JY

Horiba). In a typical measurement, the entire fragment is placed under the microscope objective and with the help of an XYZ micro-positioner and the video microscope the spot to be analysed is selected. The beam power on the sample depends on the material investigated, in the range of 0.05–5.5 mW. Typical exposure time of the CCD was 20s per scan, while normally 10 to 20 scans were averaged.

### **2.2.5 UV-Vis-NIR Spectroscopy**

UV-Vis-NIR spectroscopy might be defined as the measurement of the absorption or emission of radiation associated with changes in the spatial distribution of electrons in atoms and molecules. In practice, the electrons involved are usually the outer valence or bonding electrons, which can be excited by absorption of UV or visible or near IR radiation. Excitation of a bound electron from the highest occupied molecular orbital increases the spatial extent of the electron distribution, making the total electron density larger and more diffuse, and often more polarizable. A vibrational excited state of the molecule contains rotational excitation and electronic excited state of a molecule also contains vibrational excitation [4]. Varian Cary 5E / Varian Cary 5000 UV-Vis-NIR Spectrophotometer were used for the measurements.

### **2.2.6 Laser induced fluorescence (LIF)**

The fluorescence of the samples can be conveniently monitored by laser-induced fluorescence (LIF). The irradiation is performed with a nanosecond excimer laser (Lambda Physik EMG 201 MSC) operating at 248nm in ambient atmosphere (Flaser  $\sim 5 \text{ mJ cm}^{-2}$ ). The laser beam is

focused perpendicularly onto the sample at a 1.5mm<sup>2</sup> surface. The induced emission is collected by an optical fiber oriented almost perpendicularly to the sample, 2cm away from its surface, and is spectrally analyzed in a 0.20m grating spectrograph. The spectrum is recorded on an ICCD – Andor camera, interfaced to a PC. Cut-off filters are used to block any probe beam scattered light.

### **2.2.7 Thermal analysis**

Thermoanalytical methods involve the measurement of various properties of materials subjected to dynamically changing environments under predetermined conditions of heating rate, temperature range and gaseous atmosphere or vacuum. In many cases, the use of a single thermo analytical technique may not provide sufficient information to solve the problem on hand and hence, the use of other thermal techniques, either independently or simultaneously for complementary information becomes necessary.

Thermoanalytical analysis incorporates three closely related techniques.

- i) Thermogravimetric (TGA) [5] analysis is a technique in which the mass of a substance is measured as function of temperature or time, while the substance is subjected to a controlled temperature program.
- ii) Differential thermal analysis (DTA), which involves comparing the precise temperature difference between a sample and an inert reference material, while heating both.

- iii) Differential scanning calorimetry (DSC), similar to DTA except that electrical energy is used to restore the cooler of the two materials to the same temperature as the other. This allows direct measurement of energy changes.

### 2.2.8 Photopyroelectric (PPE) Studies

In this section, the experimental set up for the photopyroelectric technique is described. The applications of this technique for the determination of thermal diffusivity ( $\alpha$ ), thermal effusivity ( $e$ ), thermal conductivity ( $k$ ) and heat capacity ( $C_p$ ) are outlined in detail.

Since the strength of the PPE signal is found to be proportional to the intensity of radiation, optical source should have a high spectral radiance. The optical heating source employed in the present work is 120 mW He-Cd laser of wavelength  $\lambda=442$  nm.

For the generation of PPE signal, modulation of the incident light beam is essential, most commonly, amplitude modulation. The depth of modulation using a mechanical chopper is nearly 100%. In the present experiment a mechanical chopper (Model No.SR 540) is used for the intensity modulation of the laser beam.

A 28  $\mu\text{m}$  thick PVDF film with pyroelectric coefficient  $P = 0.25 \times 10^{-8}$  V/cm-K at room temperature has been used as the pyroelectric detector in our measurements. The room temperature values of pyroelectric detector resistance and capacitance are 50 G $\Omega$  and 750 pF respectively.



The present study employs a dual phase lock-in amplifier (Stanford Research System, Model SR 830) for measurements. The block diagram of the PPE set up is shown in Figure 2.1.

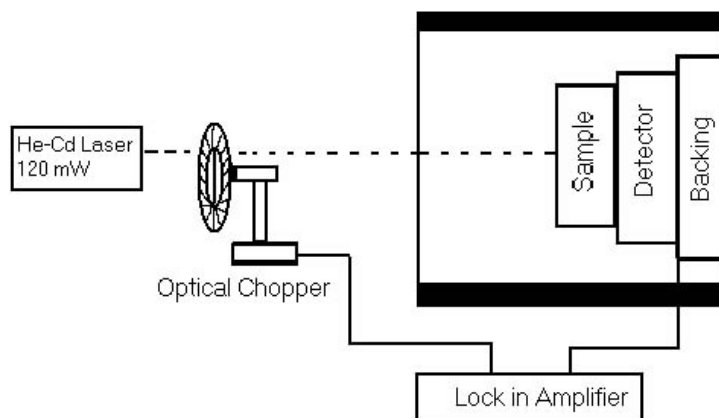


**Fig. 2.1: Block diagram of the PPE setup**

### 2.2.9 Dielectric studies

One of the useful characterizations of electrical response of solids is the dielectric measurement. A study of the dielectric properties of solids gives information about the electric field distribution within the solid. The frequency dependence of these properties provides information about the material's applications. The range of measurement depends on the properties and the materials of interest.

#### a) Dielectric constant

From the study of dielectric constant as a function of frequency and temperature, the different polarization mechanisms in solids can be understood.

The relative permittivity or the relative dielectric constant  $\epsilon_r$  may be defined as:

- i) The ratio of the electric field density produced in the medium to that produced in vacuum by the same electric field strength.
- ii) The ratio of the capacitances of a condenser containing a given dielectric to the same condenser with vacuum as the dielectric.

Therefore the relative dielectric constant  $\epsilon_r$  is

$$\epsilon_r = \frac{\epsilon}{\epsilon_0} \dots\dots\dots (2.1)$$

we know that 
$$\epsilon = \frac{Cd}{A} \dots\dots\dots (2.2)$$

$$\epsilon_r = \frac{Cd}{\epsilon_0 A} \dots\dots\dots (2.3)$$

where A is the area of the sample and d is the thickness of the sample. The relative permittivity ( $\epsilon_r$ ) is usually known as permittivity. It is always greater than unity. Suppose a parallel plate condenser has a capacitance of  $C_0$  in air, then its capacitance when the space between the plates is filled by a medium of permittivity  $\epsilon_r$  is given by  $C = \epsilon_r C_0$ ,  $\epsilon_r$  can be found out from the measurement of the capacitance.

**b) Dielectric loss**

The dielectric loss is a measure of the energy absorbed by a dielectric. It is known that in a capacitor, the dielectric usually has a resistance R and impedance Z which are related to the phase angle.

Assuming R to be very large

$$\tan \delta = \frac{1}{\omega RC} \dots\dots\dots (2.4)$$

$\tan \delta$  is referred to as the dielectric loss. The dielectric loss depends very much on temperature and frequency. The instrument used for the dielectric measurement was HIOKI 3532-50 LCR Impedance analyzer.

### 2.2.10 Tensile strength and elongation (ASTM D 882)

The test method covers tensile properties of plastic films and sheeting with less than 1mm thickness. Test specimen shall consist of strips of uniform width and thickness at least 50 mm longer than the grip separation. The nominal width of the specimen shall be not less than 5 mm or greater than 25.4 mm. [6]

Tensile strength is calculated by dividing the maximum load by the original minimum cross sectional area of the specimen. Percent elongation at break is calculated by dividing the extension at the moment of rupture of the specimen by the initial gauge length of the specimen and multiplying by 100.

The machine used for tensile studies is Instron 3366. The machine has got one fixed and one moving member carrying grips holding the test specimen. The drive mechanism provides uniform speed for separation of the moving grip from the stationary one. If the percentage of elongation is more than 100, the rate of grip separation is kept at 500 mm/min.

### 2.2.11 Peel resistance (ASTM D 1876)

The peel resistance test is intended to determine the relative peel resistance of adhesive bond between flexible adherends by means of a T-type specimen. Peel strength is defined as the average load per unit width of the bondline required to separate progressively a flexible member from a rigid member or another flexible member.

Laminated test panels consist of two flexible adherents properly bonded together. The panel dimension with 152 mm width and 305 mm length, bonded to 229 mm length was used for making the test samples [7]. Samples with 25 mm width was cut from the panel and the unbonded end (2 X 76mm) was used for clamping with the testing machine. Load was applied at a constant head speed of 254mm (10 in) per minute. The autographic recoded load versus head movement was used to find the peel resistance. The peeling curve after the initial peak upto 127mm was obtained and the average peeling load in pounds per inch of the specimen width was reported.

### References

- [1] Griffiths P R, de Haseth J A, Fourier Transform Infrared Spectrometry, Wiley, New York, 1986.
- [2] Silverstein R M, Webster F X, Spectrometric Identification of Organic Compounds, Wiley, New York, 1997.
- [3] Ian R. Lewis, Howell Edwards, Handbook of Raman Spectroscopy: From the Research Laboratory to the Process Line, Taylor and Francis, 2001.

- [4] Burgess C, Knowles A, Standards in absorption Spectrometry, Techniques in Visible and Ultraviolet Spectrometry, Chapman & Hall, London, 1981.
- [5] Emadi, D, L V Whiting, S Nafisi. R Ghomashchi,. Journal of Thermal Analysis and Calorimetry, 2005, 81, 1: 235–242.
- [6] ASTM D 882.
- [7] ASTM D 1876.



**SYNTHESIS AND CHARACTERIZATION OF POLY  
(ETHYLENE-*CO*-VINYL ACETATE) (EVA) / ZnO  
NANOCOMPOSITES**

<i>Contents</i>	3.1 <i>Introduction</i>
	3.2 <i>Synthesis of ZnO Nanoparticles</i>
	3.3 <i>Preparation of EVA / ZnO Nanocomposite</i>
	3.4 <i>Results and Discussions</i>
	3.5 <i>Conclusion</i>

**3.1 Introduction**

Composites have attracted the attention of material scientists as it combines the advantages of different materials. In recent years, material scientists are looking for nano-composites based on polymer matrix due to several added advantages. The advantages include balanced physical and mechanical properties, ease of processability and low production cost [1]. Much work has already been carried out to improve the optical and electrical properties of polymers through suitable doping [2, 3]. Polymer based dielectric materials can be used to fabricate flexible and light weight electrical devices. It is now known that nano-particles like Al<sub>2</sub>O<sub>3</sub>, TiO<sub>2</sub>, SiO<sub>2</sub> etc heterogeneously distributed within the polymer matrix can enhance dielectric properties [4]. Murugaraj and co-workers [5] have fabricated polymer – alumina nano-composites with improved dielectric characteristics. Carbon nanotubes (CNTs), carbon black, carbon

nanofibres (CNF) as well as single and multi walled carbon nano tubes (SWNTs & MWNTs) have been incorporated in polymer matrix to be used as antistatic coatings [6].

In recent years, colloidal and semiconducting nano particles have attracted a great deal of attention for both researchers and industrialists. Different types of Group II-VI nanoparticles including ZnSe, CdS, CdSe and CdTe are found to be used extensively for light-emitting diode [7], solar cell [8], biomedical tag [9] and laser [10] applications. Nanocrystals (NCs) of semi conducting materials are used in optoelectronic devices like lasers and transistors [11,12]. The ZnO used in this study is one such type of nanopowder having excellent ultraviolet property and visible photoluminescence [13], and it is a semiconductor having large exciton binding energy (~60 meV). It has got diverse applications in photovoltaic cells, variable resistors, as fully transparent thin film transistors and in short wavelength light emitting diodes.

A wide variety of polymers are used in the synthesis of nanocomposites. They form a continuous phase termed as the matrix of the composite. Polymer matrix composites (PMC) with ceramics and metals as fillers have been developed to improve electrical properties like dielectric permittivity [14,15]. Poly methylmethacrylate [16,17], epoxy [18], poly(vinyl alcohol) [19], polyaniline [20,21] etc are extensively used as the matrix for composites.

Poly(ethylene-co-vinyl acetate), EVA, was used as the base polymer in this work as they are compatible even with inert fillers. EVA is noted for its rubbery nature along with gloss, permeability and good impact

strength. EVA-TiO<sub>2</sub> nanocomposites were investigated for the effect of TiO<sub>2</sub> particle size on the co-efficient of thermal expansion [22]. Ethylene vinyl acetate is particularly used in electrical industry as cable insulating material due to good stress cracking resistance.

The II-VI group semiconducting materials show significant properties from the optoelectronic point of view [23]. In the bulk form and in the quantum dot form, these materials exhibit high density and quantum confinement. This chapter deals with the effect of ZnO nanopowder on the electrical, optical and mechanical properties of EVA polymer matrix.

### **3.2 Synthesis of ZnO Nanoparticles**

A solution of 0.2M-[CH<sub>3</sub>COO)<sub>2</sub> Zn.2H<sub>2</sub>O], Zinc acetate (dihydrate), was prepared by dissolving 4.39 gm of zinc acetate in 100 ml of methanol (in a beaker) and the mixture was kept stirred for 15 minutes. Another mixture of 0.5M- NaOH and methanol was prepared by dissolving 0.5 gm of NaOH in 25 ml of methanol and was kept stirring for 15 minutes. Then the NaOH- methanol mixture was added to the basic solution and the reaction mixture was stirred for 30 minutes. The prepared solution was kept in an autoclave for drying at 180°C for 5 hours to obtain nano-sized ZnO particles. After drying, white ZnO nanoparticles were obtained. The size of the nano powder determined using TEM was found to be around 20 nm (Fig.3.1).

### **3.3 Preparation of EVA / ZnO Nanocomposite**

Ethylene vinyl acetate- ZnO nanocomposites were prepared for different weight percentages (1%, 2%, and 4%) of ZnO by direct probe



sonicator method. Initially pure EVA film was made in a glass mould by solution casting method using toluene. Then 1% by weight of ZnO nanoparticles was added to EVA- toluene mixture taken in a beaker and was subjected to direct probe sonication. Finally the polymer was dried in a glass mould for 3-4 hours at 50°C and thus polymer nanocomposite with 1% ZnO was formed. Similarly, nanocomposites for remaining weight percentages, (2% and 4%) of ZnO were prepared.

### 3.4 Results and Discussions

#### 3.4.1 Transmission Electron Microscopy (TEM)

In Transmission Electron Microscope imaging, Hitachi H7500 TEM was used to analyse the ZnO nanoparticle. A thin specimen is irradiated with an electron beam of uniform current density, the electron energy is in the range of 60 -150 keV (usually, 100 keV). TEM micrograph shown in Fig 3.1, confirmed that the synthesized ZnO particles are solid in nature and the particle size is about 20nm.

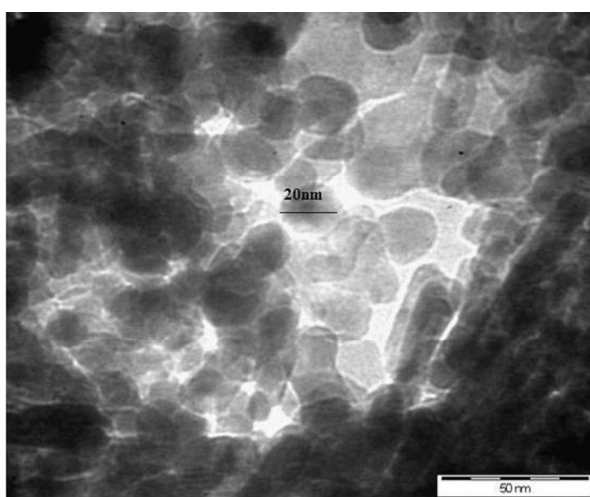


**Fig. 3.1: TEM Micrograph of ZnO nanoparticles**

### 3.4.2 Scanning Electron Microscopy (SEM)

SEM micrographs have a very large depth of field yielding a characteristic three dimensional appearance useful for understanding the surface structure of the sample. A JEOL JSM-6390 LV microscope was used to identify the relative differences in surface characteristics of EVA and its nanocomposites. The ZnO particle distribution and its influence on the EVA copolymer morphology were also investigated. Micrographs at  $1\mu\text{m}$  and  $10\mu\text{m}$  (Fig: 3.2b and 3.2c) showed the developed shape of the EVA particles and the filler distribution in EVA. A homogeneous dispersion of ZnO in the EVA matrix was observed in Fig 3.2a. The nano ZnO dispersion in the EVA surface was evident with higher magnification at  $100\text{nm}$  (Fig. 3.2d).

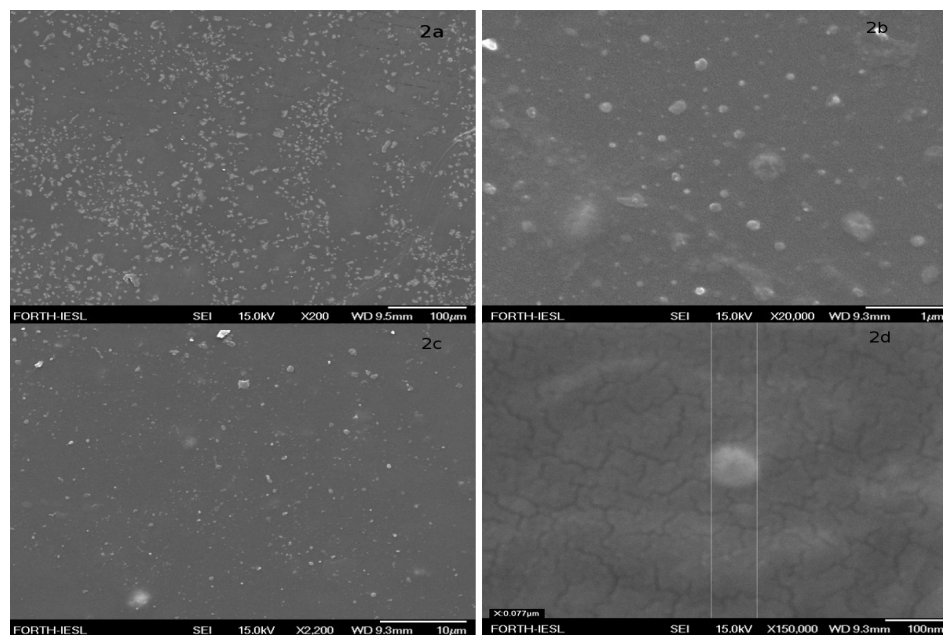


**Fig. 3.2a - 3.2d: SEM Micrographs of EVA / ZnO nanocomposites under different magnifications**

### 3.4.3 Optical Absorption Studies

The instrument used in ultraviolet-visible-NIR spectroscopy is VARIAN CARY 5000 spectrophotometer, recorded in the region of 200 to 2000 nm. The simplest type of absorption spectrometer is based on single-beam operation in which a sample is examined to determine the amount of light absorbed at a given wavelength. The results are then compared with a reference obtained in a separate measurement. The optical absorption spectra of the nanocomposites are shown in Fig. 3.3. The spectra show large transparency window between 500 nm and 1600 nm. But there is absorption at 1200 and 1450 nm. It is observed that the intensity of the absorption peak is increased with increase in the filler concentration. The band gap of the prepared nanocomposites has been determined using the Tauc-relation.

$$\alpha h\nu = A (h\nu - E_g)^{n/2} \dots\dots\dots (3.1)$$

where  $h\nu$  is the photon energy,  $\alpha$  is the absorption co-efficient,  $E_g$  is the band gap,  $A$  is a constant and  $n=1$  for the direct band gap. For allowed direct transition, a graph between  $(\alpha h\nu)^2$  and  $h\nu$  is plotted and extrapolation of the straight line to  $(\alpha h\nu)^2 = 0$  axis gives the value of the band gap. The tauc plot of the EVA / ZnO nanocomposites is shown in Fig.3.4. The band gaps of 1%, 2% and 4% EVA / ZnO PNC's are found to be 4.56eV, 4.18eV and 3.97eV respectively, which decrease with increase in filler concentrations. This may be due to the formation of another discrete quantum level in the microscopic scale which reduces the pure intrinsic band gap of the virgin material.

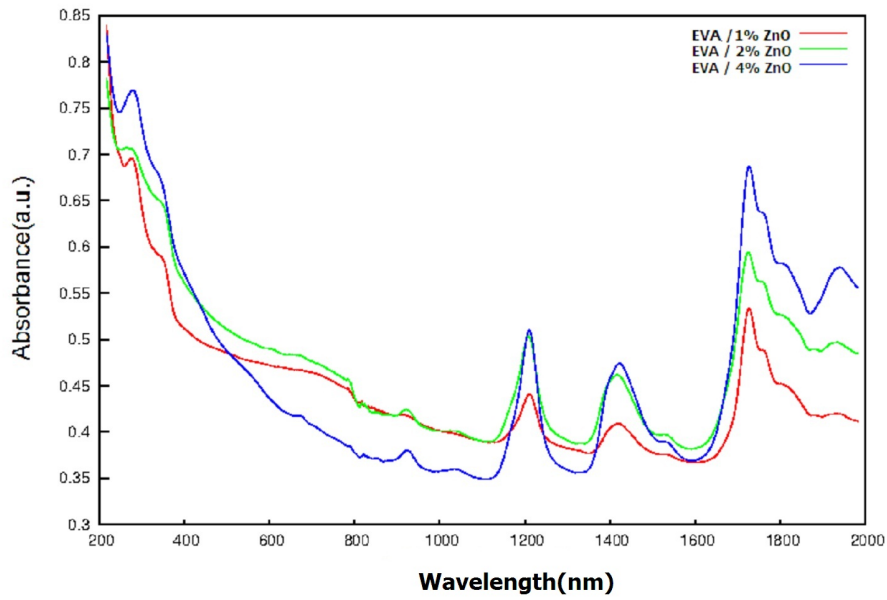


Fig. 3.3: UV-Vis- NIR spectra of EVA / ZnO nanocomposite with different filler concentrations

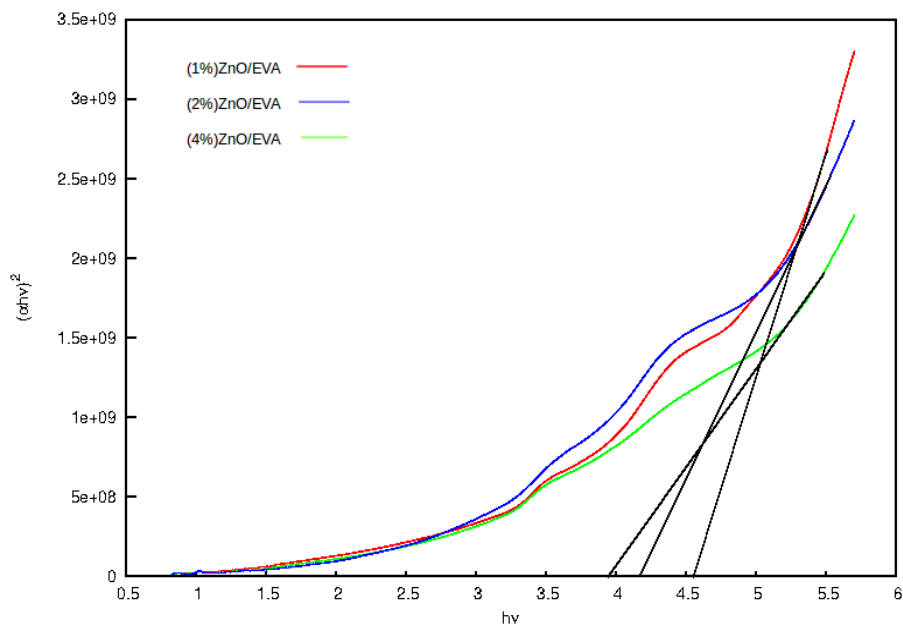
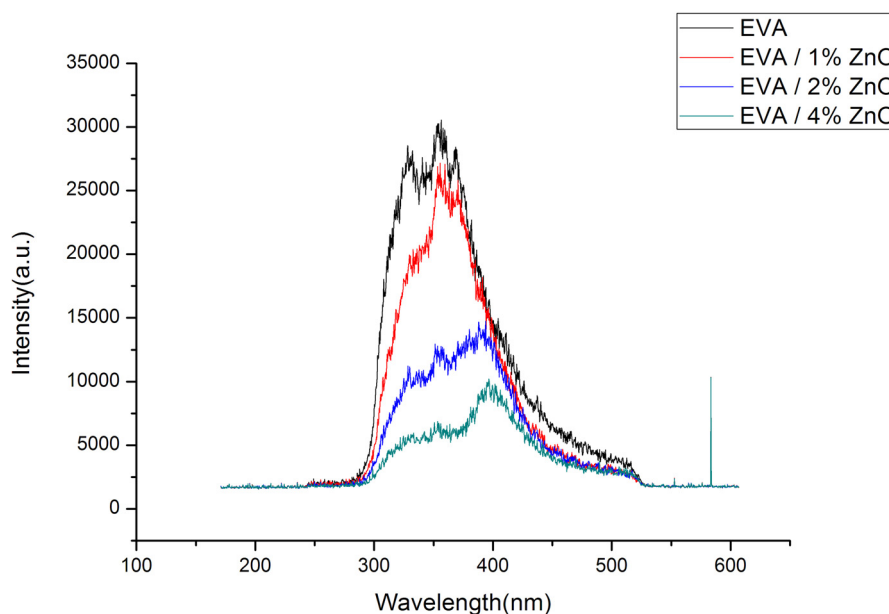


Fig.3.4: Tauc plot of EVA / ZnO nanocomposite with different filler concentrations

### 3.4.4 Laser induced fluorescence (LIF)

The fluorescence of the samples was conveniently monitored by laser-induced fluorescence (LIF). The irradiation was performed with a nanosecond excimer laser (Lambda Physik EMG 201 MSC) operating at 248 nm in ambient atmosphere (Flaser  $\sim 5 \text{ mJ cm}^{-2}$ ). The laser beam was focused perpendicularly onto the sample on a  $1.5 \text{ mm}^2$  surface. The induced emission was collected by an optical fiber oriented almost perpendicularly to the sample, at 2 cm away from its surface, and was spectrally analyzed in a 0.20 m grating spectrograph. The spectrum was recorded on an ICCD – Andor camera, interfaced to a PC. Cut-off filters were used to block any probe beam scattered light. Fig.3.5. shows the LIF spectra of the nanocomposites.



**Fig.3.5: LIF spectra of pure EVA and EVA / ZnO nanocomposites**

From the figure one can easily find that the fluorescence intensity decreases with increase in filler concentration. This may be due to the fact that the filled ZnO atoms tend to destabilize the molecular bonding structure of the EVA matrix, especially -C-O-C-, -C=O, by weakening the orbital  $\sigma$ , the  $\pi$  bonding electron density. As the concentration of the filler increases this destabilization also increases thereby decreasing the intensity.

### **3.4.5 FT-IR Spectroscopic Analysis**

The analysis of Fourier transform infrared (FT-IR) spectra of the samples has been carried out using a Thermo Nicolet Make Avatar 370 FTIR Spectrometer in the wave number range  $400 - 4000 \text{ cm}^{-1}$ . DTGS detector was used for signal detection. Fig. 3.6 shows the FT-IR spectra of pristine EVA and EVA / ZnO composites. The C=O stretching and C-C-O stretching of vinyl acetate, at  $1738 \text{ cm}^{-1}$ , and  $1241 \text{ cm}^{-1}$  are quite clear. C-H stretch of EVA was observed in the peak at  $2920 \text{ cm}^{-1}$  and  $2850 \text{ cm}^{-1}$ . Other characteristic peaks of vinyl acetate are at  $1021 \text{ cm}^{-1}$  and  $608 \text{ cm}^{-1}$ .  $\text{CH}_2$  bending mode peaks occur at  $1465 \text{ cm}^{-1}$ . C- $\text{CH}_3$  bending absorption peak is obtained at  $1375 \text{ cm}^{-1}$ . This characteristic transmittances were observed for pure EVA and its nanocomposites. The presence of ZnO caused slight change in the characteristic peak of EVA. The presence of ZnO in the EVA matrix produced peaks at  $434 \text{ cm}^{-1}$ ,  $664 \text{ cm}^{-1}$ ,  $3431 \text{ cm}^{-1}$  for the nanocomposites.

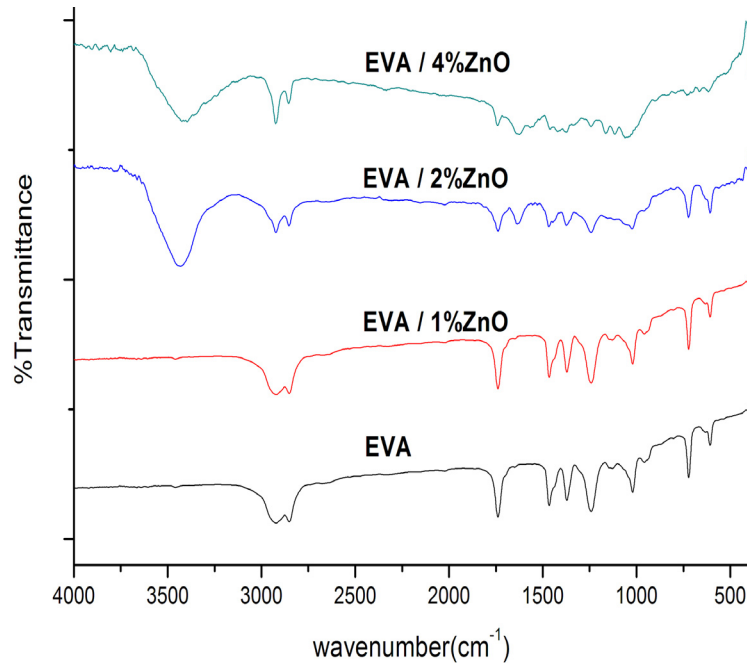


**Fig. 3.6: FT-IR Spectra of pure EVA, and its ZnO nanocomposites.**

### 3.4.6 Dielectric Studies

Dielectric studies are carried out using HIOKI 3532-50 LCR HITESTER. The LCR HITESTER can be connected to a computer via RS-232 interface (frequency range: 50Hz to 5MHz). The EVA / ZnO polymer nanocomposite of area  $9.5 \times 10^{-5} \text{ mm}^2$  having silver coating on the opposite faces was introduced between two copper electrodes. The dielectric constant of the sample is calculated using the relation  $\epsilon_r = Cd / \epsilon_0 A$ ; where the nanocomposite acts as a dielectric with  $\epsilon_0$  the absolute permittivity, C is the capacitance, d is the thickness and A is the area ( $\text{mm}^2$ ) of the EVA / ZnO composite. Fig.3.7 shows the variation of dielectric constant of EVA / ZnO with different filler concentrations. From the figure, one can easily examine the behaviour of dielectric

constant of nanocomposites with frequency from 100 Hz to 5MHz. It is observed that dielectric constant has larger values at lower frequencies and then decreases with increase in frequency for all films. However, there is an increase in the dielectric constant of the nanocomposites as the percentages of the filler concentration increase. The values of dielectric constant at 1 kHz for 1%, 2% and 4% ZnO are around 3.62, 4.1 and 4.7 respectively. The dielectric constant remains almost constant for all samples in the higher frequencies. At low frequencies, all the four polarizations are active. The space charge contribution depends on the purity and perfection of the material and its influence is noticeable in the low frequency region. The orientational effect can sometimes be seen in some materials even up to  $10^{10}$  Hz. Ionic and electronic polarizations always exist below  $10^{13}$  Hz. Hence, the larger values of dielectric constant and dielectric loss exhibited by nanocomposite at low frequencies may be attributed to space charge polarization due to impurities and defects present in the nanocomposites. Fig.3.8 shows the variation of dielectric loss of nanocomposites as a function of frequency. In the lower frequency region, dielectric loss shows larger values due to the loss associated with ionic mobility. The trend in the variations of both dielectric constant and dielectric loss as a function of frequency is the same. Temperature has a striking effect on the dielectric properties. Interestingly, the variations of both dielectric constant and dielectric loss as a function of frequency are the same for all temperatures. It is observed that the dielectric constant and dielectric loss slightly decrease with the temperature which may be due to the reduction in charge carriers. The variation of dielectric constant and loss with temperatures for 1 kHz and 2 kHz frequency are shown in Fig.3.9-3.12.



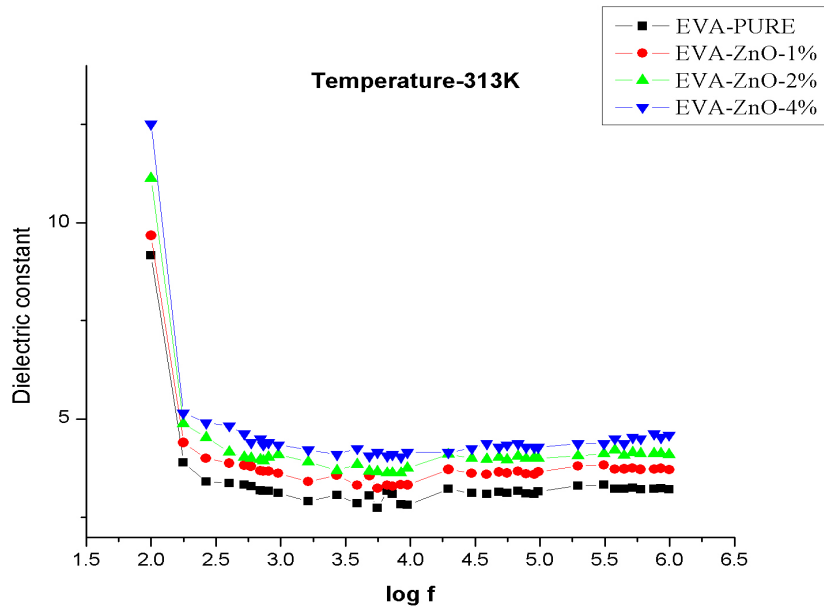


Fig. 3.7: Variation of dielectric constant of EVA / ZnO with different filler concentrations as a function of frequency

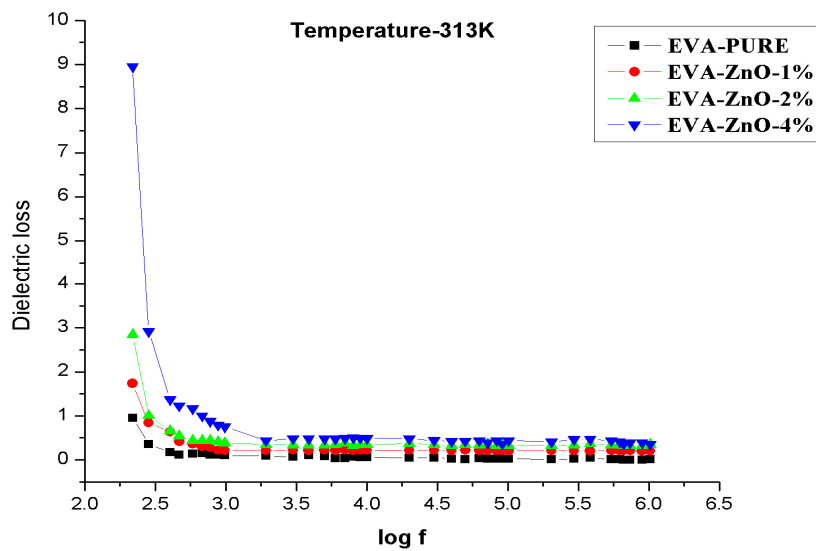


Fig. 3.8: The dielectric loss variation of EVA / ZnO with different filler concentrations as a function of frequency

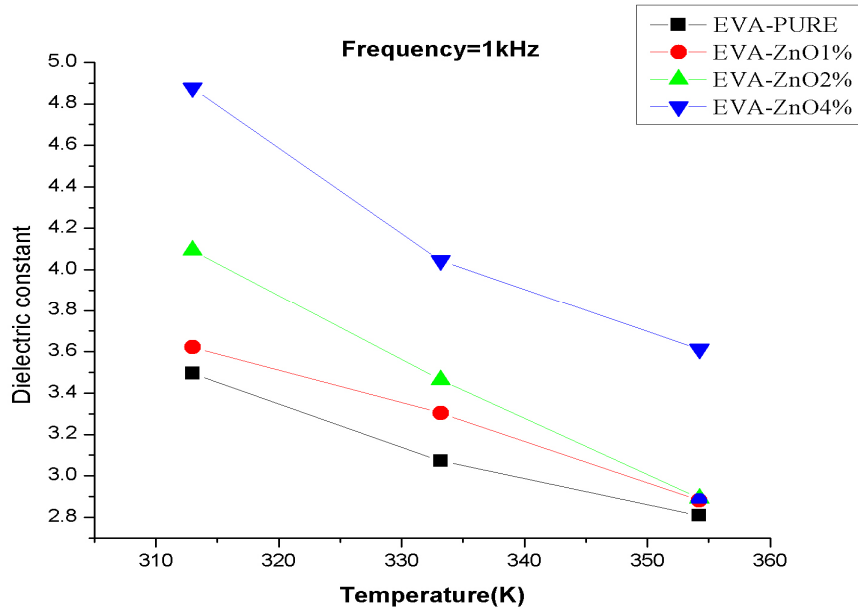


Fig. 3.9: Variation of dielectric constant of EVA / ZnO with different temperature at 1 kHz frequency

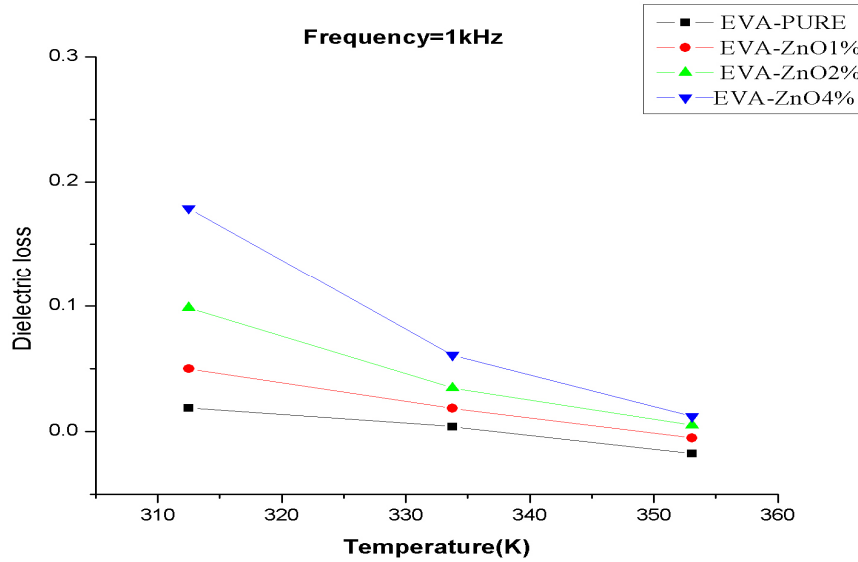
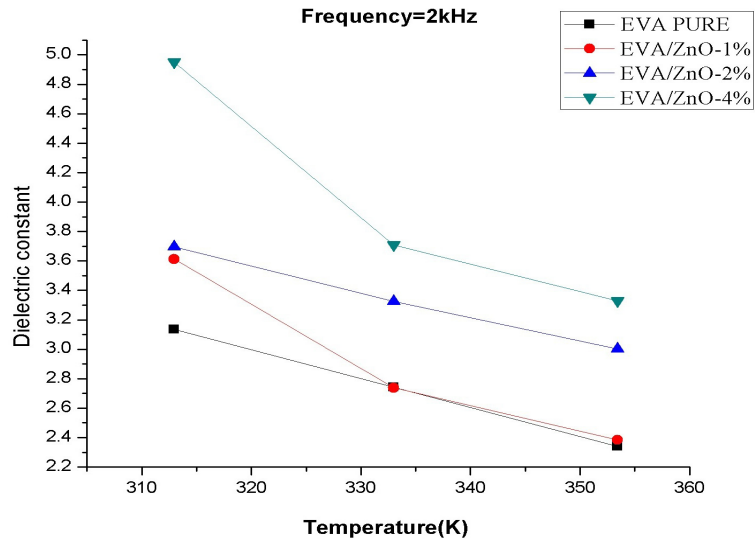
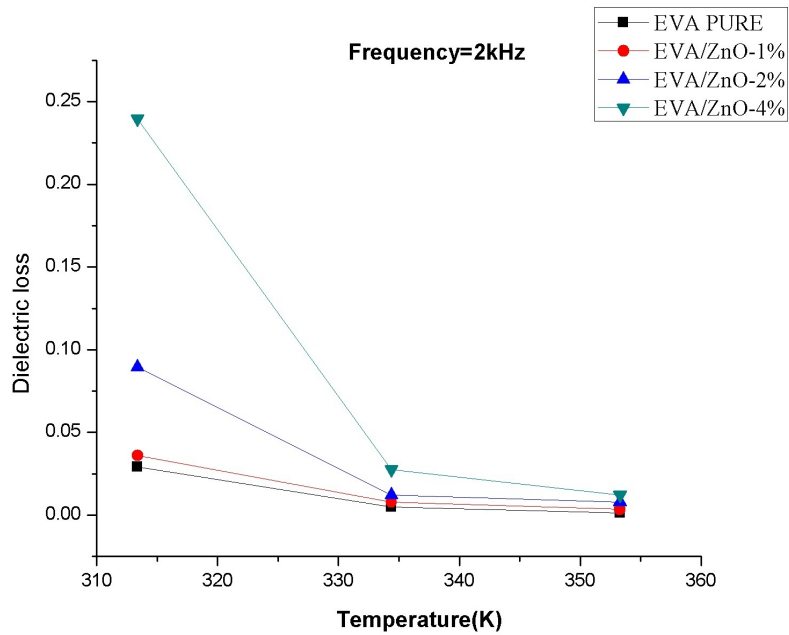


Fig.3.10: Variation of dielectric loss of EVA / ZnO with different temperatures at 1 kHz frequency



**Fig.3.11: Variation of dielectric constant of EVA / ZnO with different temperatures at 2 kHz frequency**



**Fig. 3.12: Variation of dielectric loss of EVA / ZnO with different temperature at 2 kHz frequency**

### **3.4.7 TG - DTA Analysis**

The TGA and DTA analysis of polymer nanocomposites was carried out between 28°C and 750 °C at a heating rate of 20 K/min using the instrument NETSZCH STA 409C. The TGA - DTA curves are shown in Fig.3.13a - 3.13d, which confirm the decomposition of the nanocomposites in two steps. 28.9 % and 28.5 % of weight is lost for pure EVA and EVA / 1% ZnO respectively in the first stage while that is 14% and 13 % respectively for 2 % and 4% of filler concentrations. It is also observed that the thermal stability of the polymer nanocomposites increases by increase in filler concentrations and the onset decomposition temperature of the pure EVA, 1%, 2% and 4% EVA / ZnO are around 290°C, 295°C, 318°C and 337°C respectively. There isn't much difference in the thermogram of pure and 1% doped EVA / ZnO.

The increment in the thermal stability may be due to the increase in resistance of the nanocomposites by increase in interfacial area. The significant improvement in the resistance to thermal decomposition of the nanocomposites can be due to the increase in the interfacial interaction between the ZnO nanofiller and the polymer which can increase the activation energy of decomposition and lead to the enhancement of the thermal stability of the composites [24]. The homogeneous distribution and dispersion of the nanofiller might have hindered the diffusion of oxygen and volatile decomposition products, compared to pure polymer [25].

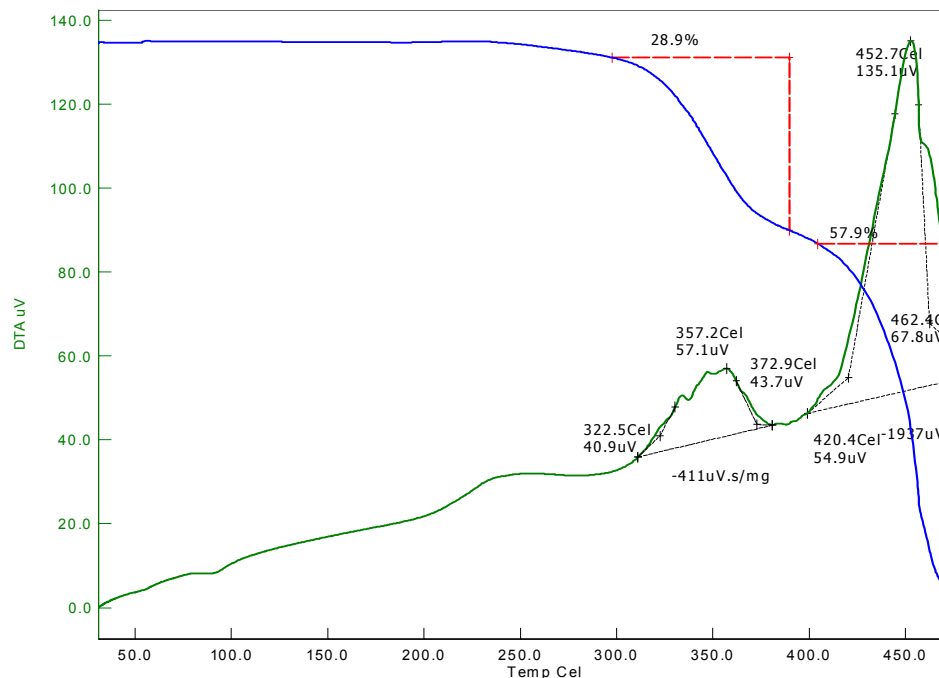


**Fig.3.13a: TG-DTA Curve of pure EVA**

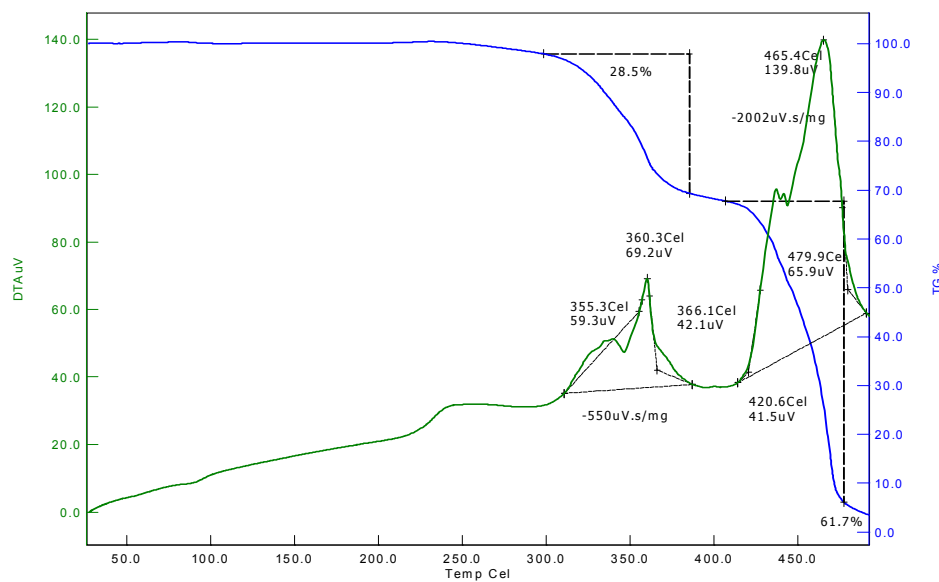


**Fig.3.13b: TG-DTA curve of EVA/ 1% ZnO nanocomposite**

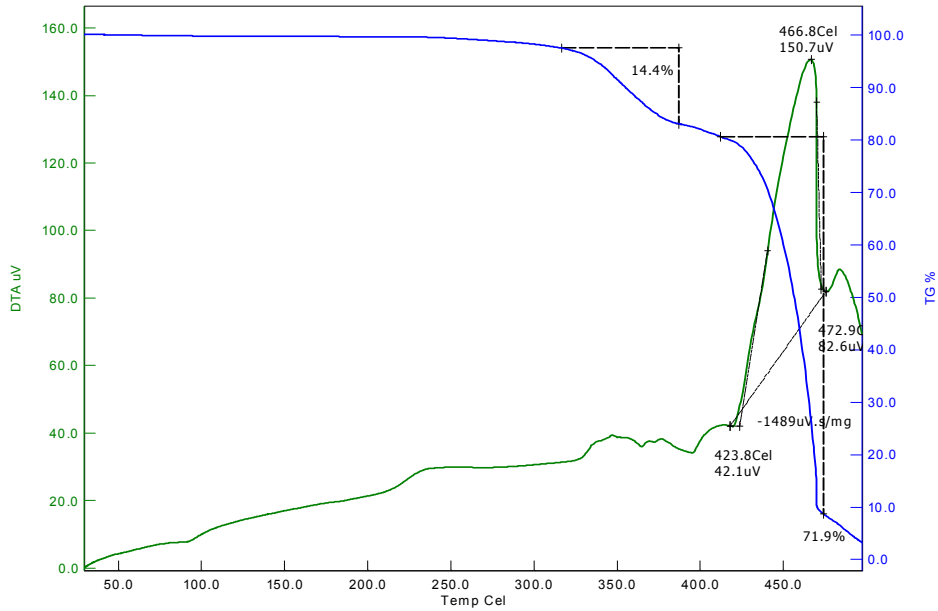


Fig.3.13c: TG-DTA curve of EVA / 2%ZnO nanocomposite

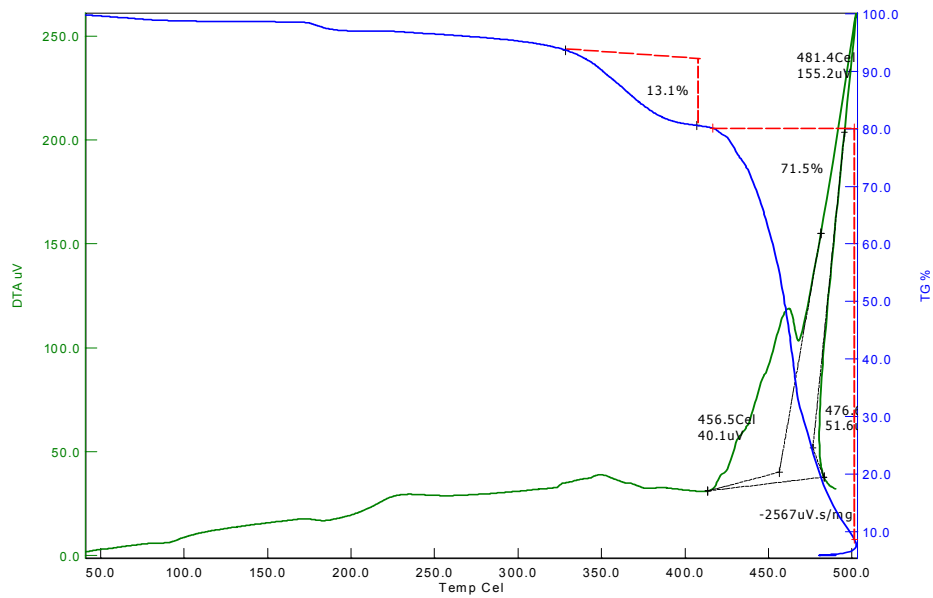


Fig.3.13d: TG-DTA curve of EVA / 4%ZnO nanocomposite

### 3.4.8 Photopyroelectric (PPE) studies

The thermal parameters such as thermal diffusivity ( $\alpha$ ), thermal effusivity ( $e$ ), thermal conductivity ( $k$ ) and specific heat capacity ( $C_p$ ) were determined by the technique developed Preethy C Menon et al. [26]. During the measurement, the sample, the pyroelectric detector and the backing should be thermally thick. The sample was illuminated by an intensity-modulated beam of light, which gives rise to periodic temperature variations by optical absorption. The thermal waves so generated propagate through the sample and were detected by the pyroelectric detector. A He-Cd laser of (wavelength  $\lambda=442$  nm KIMMON) output power 120 mW was used as the optical heating source. A polyvinylidene fluoride (PVDF) film of thickness 28  $\mu\text{m}$  was used as the pyroelectric detector. The sample was attached to the pyroelectric detector by means of a thermally thin layer of a compound whose contribution to the signal was negligible. The signal output was measured using a lock-in amplifier (SR830). The frequency of modulation of the light was kept above 40 Hz to ensure that the detector, the sample and the backing medium were thermally thick during measurements.

Thermal parameters such as thermal effusivity ( $e$ ) and thermal diffusivity ( $\alpha$ ), the thermal conductivity ( $k$ ) and specific heat capacity are tabulated in the Table 3.1. From the table, it is clear that the thermal conductivity increases with increase in filler concentration. This may be due to the Brownian motion of nanoparticle [27,28]. The Brownian motion effect of nanoparticles is more prominent at low mass fraction of nanoparticles [29].

**Table 3.1: Thermal parameters of EVA / ZnO nanocomposites**

Sample Code	Thermal effusivity, $e$ ( $W s^{1/2}/m^2K$ )	Thermal diffusivity, $\alpha$ ( $\times 10^{-6} m^2/s$ )	Thermal conductivity, $k$ (W/mK)	Sp. heat capacity, $C_p$ (J/kgK)
EVA	$446 \pm 32$	$0.2334 \pm 0.15$	$0.1425 \pm 0.12$	$1530 \pm 31$
EVA / 2% ZnO	$1937 \pm 18$	$0.24154 \pm 0.14$	$0.263 \pm 0.010$	$1431 \pm 33$
EVA / 4% ZnO	$2758 \pm 35$	$0.85113 \pm 0.18$	$0.298 \pm 0.015$	$1300 \pm 28$

### 3.4.9 Mechanical Properties

The tensile strength and elongation at break measurement of the pure EVA and EVA nanocomposites samples was performed using an Instron 3366 testing machine according to ASTM D882. Each sample had a width of 6.4 mm. The average thickness of the samples was about 0.16 mm. The tensile test was conducted using a cross head speed of 500 mm/min. The stress- strain graph and elongation at various stages of the test were recorded and tensile strength and elongation at break values are shown in Fig.3.14. Ethylene vinyl acetate (EVA) films show good tensile strength (30 MPa) and stretches 430% more than its original dimension before break. Thin films of EVA- ZnO nanocomposites have got comparable tensile and deforming properties to that of the pristine polymer. The tensile strength improves to 33MPa on addition of 1% of ZnO nanoparticles. The nano sized particles might be having a reinforcing effect to tie up the EVA molecules, leading to greater resistance to tensile deformations. Further increase in ZnO reduces the tensile strength and the strain deformations. The chain flexibility of the macromolecules is found reduced with the incorporation of ZnO nanoparticles, leading to reduction of elongation.



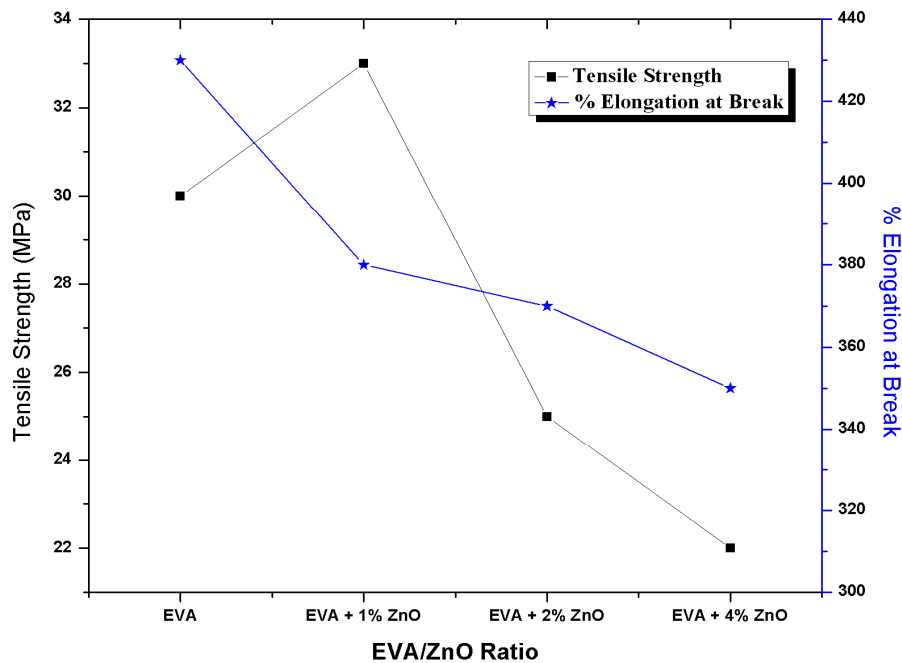


**Fig.3.14: Tensile strength and elongation at break of EVA / ZnO nanocomposites**

Peel resistance of the nanocomposites was tested using an Instron tensile testing machine at a peel speed of 250 mm/min. Peel test with 180° stripping was carried out as per ASTM D 1876. Peel test involves stripping away of substrate joined by the adhesive. The substrates (glass paper, cotton and polyester) were flexible enough to permit a 180° turn near the point of loading. Peel strength values were recorded in Newtons per millimeter (N/mm) width of the bonded specimen. Peel resistance of the EVA nanocomposites on various substrates is shown in Fig.3.15. The inclusion of the ZnO nanoparticles to the EVA matrix improves its peel strength on 2% of nano ZnO loading on all substrates. When ZnO was incorporated more, it was found that the peel adhesion properties get

reduced compared to the virgin EVA. The surface finish and smoothness of the glass paper might have attributed to its inferior adhesion compared to cotton and polyester fabric. Cotton fabric gives maximum peel adhesion (2.4 N/mm) as the EVA copolymer impregnates its porous surface.

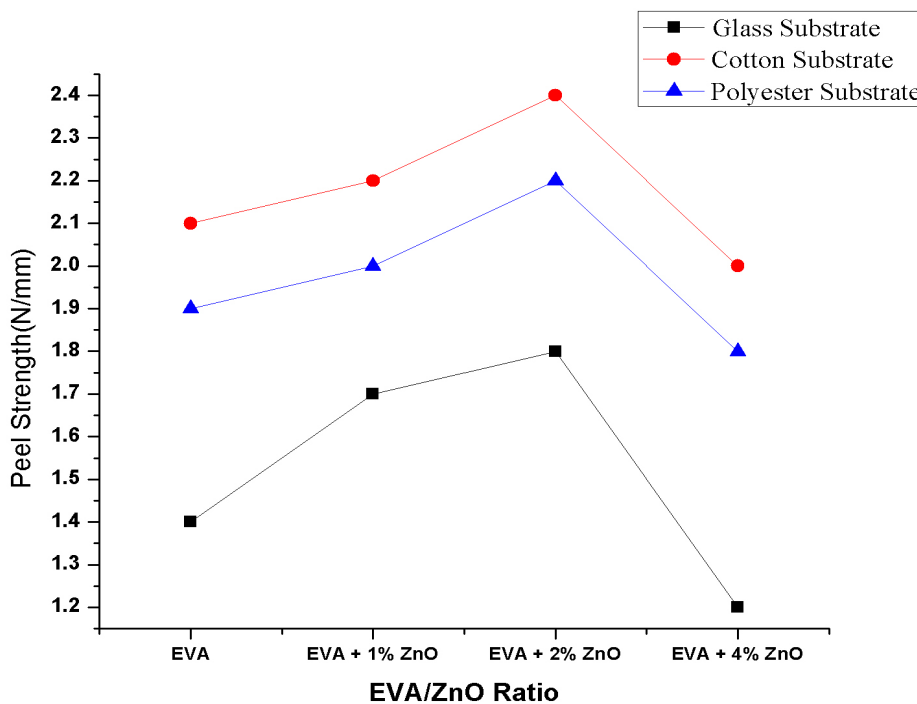


**Fig. 3.15: Peel Strength v/s EVA / ZnO ratio**

### 3.5 Conclusion

The EVA/ZnO nanocomposites of different concentrations of ZnO nanoparticle (1%, 2% and 4%) have been prepared successfully by ultrasonic probe method. The ZnO nanoparticles used in the synthesis of polymer nanocomposite were synthesized by solvothermal method. The investigations on the electrical properties of the nanocomposites revealed

that conductivity increases with increase in the filler concentrations and resistivity increases when temperature increases. The band gap of the nanocomposites is found to decrease with increasing filler concentration. The thermal stability of the nanocomposites was also found to be increasing with filler concentration. Photopyroelectric technique is used to find the thermal parameters such as thermal diffusivity ( $\alpha$ ) and thermal effusivity ( $e$ ), thermal conductivity ( $k$ ), heat capacity ( $C_p$ ) and except heat capacity all others are found to increase with increasing filler concentration. The tensile strength and peel strength of the nanocomposites are found to increase initially with the addition of ZnO nanoparticles.

### References

- [1] Ray S, Eastal A J, Cooney R P, Edmonds N R, Mater. Chem .Phys. 2009, 113, 829.
- [2] Blom P W M, Schoo H F M, Matters M, Appl. Phys. Lett. 1998,73, 3914.
- [3] Kiesow A, Morris J E, Radehaus C, Heilmann A, J. Appl. Phys. 2003, 94, 6988.
- [4] Siegel R W, Schadler-Feist L, Ma D, Hong J I, Martensson E, Onneby C, Publication No: WO2005036563,2005, 28.
- [5] Murugaraj P, Mainwaring D, Mora-Huertas N, J. Appl. Phys.2005, 98, 054304.
- [6] Victoria Tishkova, Pierre-Ivan Raynal, Pascal Puech, Antoine Lonjon, Marion Le Fournier, Philippe Demont, Emmanuel Flahaut, Wolfgang Basca, Compos. Sci. Technol. 2011, 71, 1326.

- [7] Lee J., Sunder V C, Heine J R, Bawendi M G, Jensen K F, *Adv. Mater.* 2000, 12, 1102.
- [8] Shaheen S E, Brabec C J, Sariciftci N, *Appl. Phys. Lett.* 2001, 78, 841.
- [9] Wang H., Branton D, *Nat. Biotechnol.* 2001, 19, 622.
- [10] Artemyev M., Woggon U, Langbein W, *Phys. Status Solidi* 2002, 229, 423.
- [11] Klein D, Roth R, Lim A K L, Alivisatos A P , MeEuen P L, *Nature* 1997,389, 699
- [12] Klimov V I, Milkhailovsky A A., Su Xu, Leatherdale C A, Eisler H J, Bawendi M G., *Science* 2000, 290, 314.
- [13] Konenkamp R., Word R., Schlegel C., *Appl. Phys. Lett.* 2004, 85, 6004.
- [14] Dang Z M, Zhou T, Yao S H , Yuan J K., Zha J W, Song H T, *Adv. Mater.* 2009, 21, 2077.
- [15] Zhi-Min Dang, Jin-Kai Yuan, Jun-Wei Zha, Tao Zhou, Sheng-Tao Li, Guo-Hua Hu, *Prog. in Mater. Sci.* 2012, 57, 660.
- [16] Monti O L A, Fourkas J T, Nesbitt D J, *J. Phys. Chem. B*, 2004, 108, 1604.
- [17] Sui-Ming Yuen, Chen-Chi M. Ma, Chia-Yi Chuang, Kuo-Chi Yu, Sheng-Yen Wu, Chen-Chien Yang, Ming-Hsiung Wei, *Comp. Scien. and Tech* 2008,68, 963.
- [18] Stankovich S, Dikin D A, Dommett G H B , Kohlhaas K M, Zimney E J, Stach E A, Piner R D, Nguyen S T, Ruoff R S, *Nature* 2006, 442,282.
- [19] Khanna P K, Narendra Singh, Shobhit Charan, Mulik U P, *Mat. Chem. and Phy.* 2005, 93,117.
- [20] Sambhu Bhadra, Dipak Khastgir, Nikhil K. Singha, Joong Hee Lee, *Prog. in Poly. Sci.* 2009, 34, 783.

- [21] Subramanian S, Pathinettam Padiyan D, Mat. Chem. and Phys. 2008, 107, 392.
- [22] Gonzalex-Benito J, Castillo E, Caldito J F, Europ. Poly. Journal 2013, 49, 1747.
- [23] Kasap S, Springer Handbook of Electronic and Photonic Materials, Springer, Berlin, 2007.
- [24] Marosfoi B B, Marosi A S G, Tabuani D, Camino G, Pagliari S, Jour. Therm. Anal. Calorim 2006, 86, 669.
- [25] Al-Ghamadi A A, El-Tantawy F, Compos. Part A, 2010,41, 3, 1693.
- [26] Preethy Menon C and Philip S, Meas. Sci. Technol. 2000, 111,744.
- [27] Xiao B, Yang Y, Chen L, Powder Technol. 2013, 239, 409.
- [28] Wan M, Yadav R, Yadav K, Yadaw, Exp. Therm. Fluid Sci. 2012, 41, 158.
- [29] Haddad Z, Abu-Nada E, Oztop H F, Mataoui Int. J. Therm. Sci. 2012, 57, 152.

.....❧.....

**SYNTHESIS AND CHARACTERIZATION OF POLY  
(ETHYLENE-CO-VINYL-ACETATE) (EVA) /  
ZnSe NANOCOMPOSITES**

<i>Contents</i>	<i>4.1 Introduction</i>
	<i>4.2 Synthesis of ZnSe Nanoparticles</i>
	<i>4.3 Preparation of EVA / ZnSe Nanocomposites</i>
	<i>4.4 Characterization Techniques</i>
	<i>4.5 Results and Discussions</i>
	<i>4.6 Conclusion</i>

**4.1 Introduction**

Thermoplastics and thermosetting plastics have been found useful for a variety application in the field of electronic and electrical technology. Fabrication of nanostructures in polymer matrices has attracted researchers due to the advantages of readily tunable bandgaps, electroactivity, excellent flexibility and good processability compared to conventional materials [1-4]. The optical and electronic properties of the polymer matrices can be altered by a judicious selection of nanomaterials [5,6]. Polymer-semiconductor nanocomposites with non linear optical properties are used in fibre-optic communication systems such as optical storages, optical limiters and for digital signal restoration [7-9].

Poly (ethylene-co-vinyl acetate), EVA is a commercial plastic with good low temperature flexibility and toughness. EVA exhibits rubbery property of enhanced elongation along with ease of processability of thermoplastics. Due to its surface gloss and impact strength, EVA copolymers find market in film manufacturing. The presence of vinyl acetate molecules in the polymer chain reduces the polymer regularity and crystallinity. EVA-clay nanocomposites are widely used in wires, cables and food packaging [10].

The II-VI semiconducting materials show significant properties from the optoelectronic point of view [11]. Among polymer –inorganic nanocomposites, SiO<sub>2</sub>, TiO<sub>2</sub>, ZnO and clay based filler systems have been widely investigated [12, 13]. In the bulk form and in the quantum dot form these materials exhibit high density and quantum confinement. Zinc selenide (ZnSe) is an n-type semiconductor material with wide band gap (2.58-2.72 eV) [14-15]. The band gap was found to increase as the particle size decreases. The incorporation of semiconducting ZnSe nanoparticles to the amorphous EVA structure was found to alter the properties of polymer films.

The present chapter mainly focuses on the preparation of nanocomposite films based on EVA with varying ratio of ZnSe particles and studies the effect of ZnSe on the optical, thermal and mechanical properties of EVA.

## **4.2 Synthesis of ZnSe Nanoparticles**

Materials such as zinc acetate and sodium selenite used for the preparation of ZnSe nanopowder are Merck GR grade of purity  $\geq 98\%$ . Zinc acetate of 4.388 g was dissolved in 100 ml of direct Millipore water and 0.519g of sodium selenite ( $\text{Na}_2\text{SeO}_3$ ) was dissolved in 30 ml of hydrazine hydrate ( $\text{N}_2\text{H}_4 \cdot \text{H}_2\text{O}$ ). Both the prepared solutions were mixed up by vigorous stirring with external heat energy. Then these solutions were transferred into a Teflon lined sealed stainless steel autoclave and heated at  $240^\circ\text{C}$  for 5hrs in a muffle furnace. It was washed two times using Millipore water for removing impurities.

## **4.3 Preparation of EVA / ZnSe Nanocomposites**

Ethylene vinyl acetate (EVA) copolymer used for the experiment was obtained from Exxon Mobil Chemicals, Singapore. The copolymer was first dissolved in toluene. Then synthesized ZnSe nanoparticles were dispersed in a sonication bath for 2 hours on the basis of the desired weight fraction (2% and 4%) of ZnSe nanoparticle at room temperature. In order to make the resultant neat nanoparticles filled polymer samples, it was transferred to a teflon coated glass mould and spread with uniform thickness. The mixture was heated at  $40^\circ\text{C}$  for 18 hours in an air oven to evaporate the solvent completely and finally, we got a thin film of pure and EVA / ZnSe nanocomposite.



#### 4.4 Characterization Techniques

ZnSe nanoparticles were analyzed using Hitachi H7500 TEM and the nanocomposites were analysed by JEOL JSM – 6390 LV SEM. The Fourier transform infrared (FT-IR) spectra of the samples are taken in the wave number range 400- 4000 $\text{cm}^{-1}$  using a Thermo Nicolet Make Avatar 370 FTIR Spectrometer and for signal detection, DTGS detector is used. The refractive indices of the samples were determined using HIOKI 3532-50 LCR IMPEDANCE ANALYZER and program version 4.03E was used to record the refractive indices of the samples by varying the frequencies from 100 Hz to 5MHz. VARIAN CARY 5000 spectrophotometer was used to determine the optical absorption spectrum of the samples and recorded in the region of 200 to 2000 nm. The TG and DTA analyses of EVA / ZnSe were carried out between 28 and 1300 °C at a heating rate of 20 K/min using the instrument NETSZCH STA 409C. The tensile strength and elongation at break of the virgin EVA and EVA nanocomposites were tested by an Instron 3366 testing machine according to ASTM D882. Peel strength was performed using an Instron tensile testing machine at a peel speed of 250 mm/min. Peel test with 180° stripping was carried out as per ASTM D 1876. Peel test involves stripping away of substrate joined by the adhesive. The substrates (glass paper, cotton and polyester) were flexible enough to permit a 180° turn near the point of loading. Peel strength values were recorded in Newton per millimeter (N/mm) of width of the bonded specimen.

## **4.5 Results and Discussions**

### **4.5.1 Morphological Analysis**

Transmission electron microscopy (TEM) is a vital characterization tool for directly imaging nanomaterials to obtain quantitative measures of grain size, size distribution, and morphology. TEM of ZnSe nanoparticles are shown in Fig. 4.1. The image reveals that the shape of the particles is spherical and the average size of particles is about 80nm. The dark images show that nanoparticles are solid in nature.

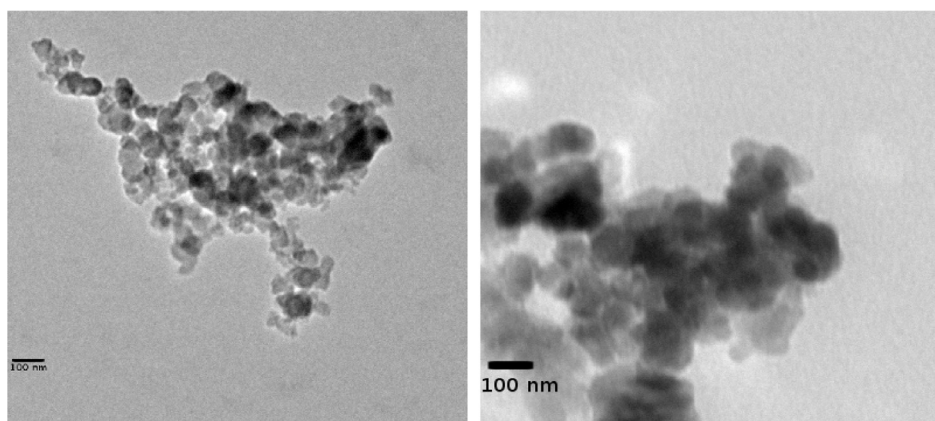


**Fig. 4.1: TEM images of ZnSe nanoparticles**

The relative surface characteristics of EVA and its composites were compared using SEM micrographs. ZnSe nanoparticles reinforced the host EVA matrix and the dispersion of the nanoparticles was confirmed by JEOL JSM-6390LV microscope. The developed shape of EVA and filler distribution can be observed by SEM (Fig.4.2a-d).

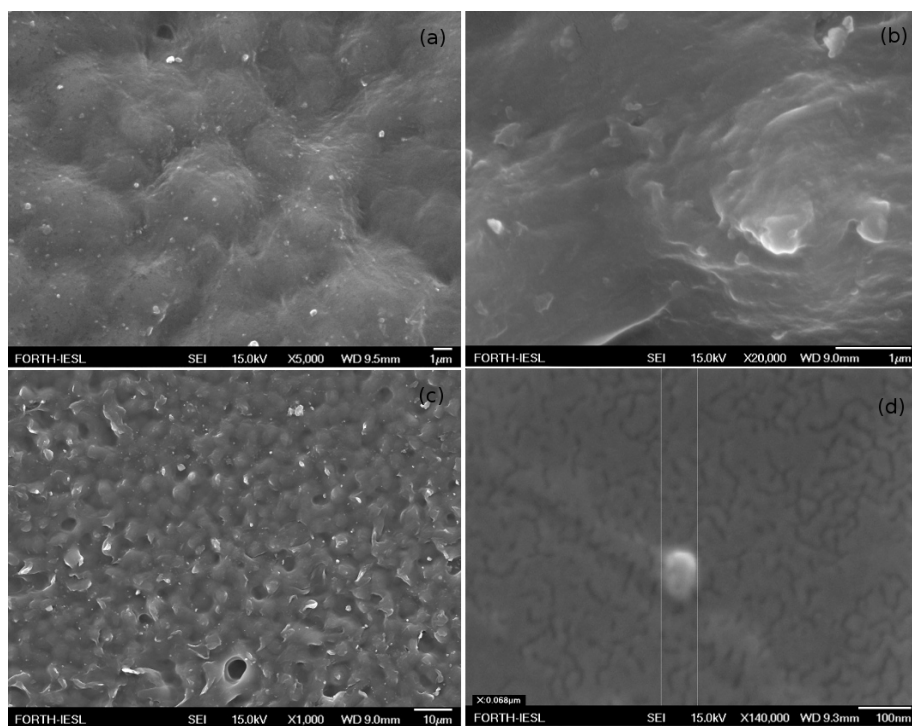


**Fig.4.2a-d: SEM Micrographs of EVA / ZnSe composites at different magnifications**

#### 4.5.2 FT-IR Spectroscopy

The FTIR spectra of the ZnSe / EVA nanocomposites are shown in Fig.4.3. The comparison of pristine, 2% and 4% ZnSe doped EVA has been done and the polymeric group identification and the effect of ZnSe in EVA could be established. The bands observed at  $1738\text{ cm}^{-1}$ ,  $1241\text{ cm}^{-1}$ ,  $1021\text{ cm}^{-1}$  and  $608\text{ cm}^{-1}$  are attributed to the vinyl acetate content in EVA. The bands at  $2921\text{ cm}^{-1}$ ,  $2851\text{ cm}^{-1}$ ,  $1465\text{ cm}^{-1}$ ,  $722\text{ cm}^{-1}$  are attributed to the character of ethylene group. The peaks produced around  $1639\text{ cm}^{-1}$  and  $3430\text{ cm}^{-1}$  are the characteristic absorption peaks of ZnSe. Additional peaks obtained in the nanocomposites at  $1427\text{ cm}^{-1}$  and  $2327\text{ cm}^{-1}$  might be due to the presence of adsorbed species on the surface of ZnSe nanoparticles.

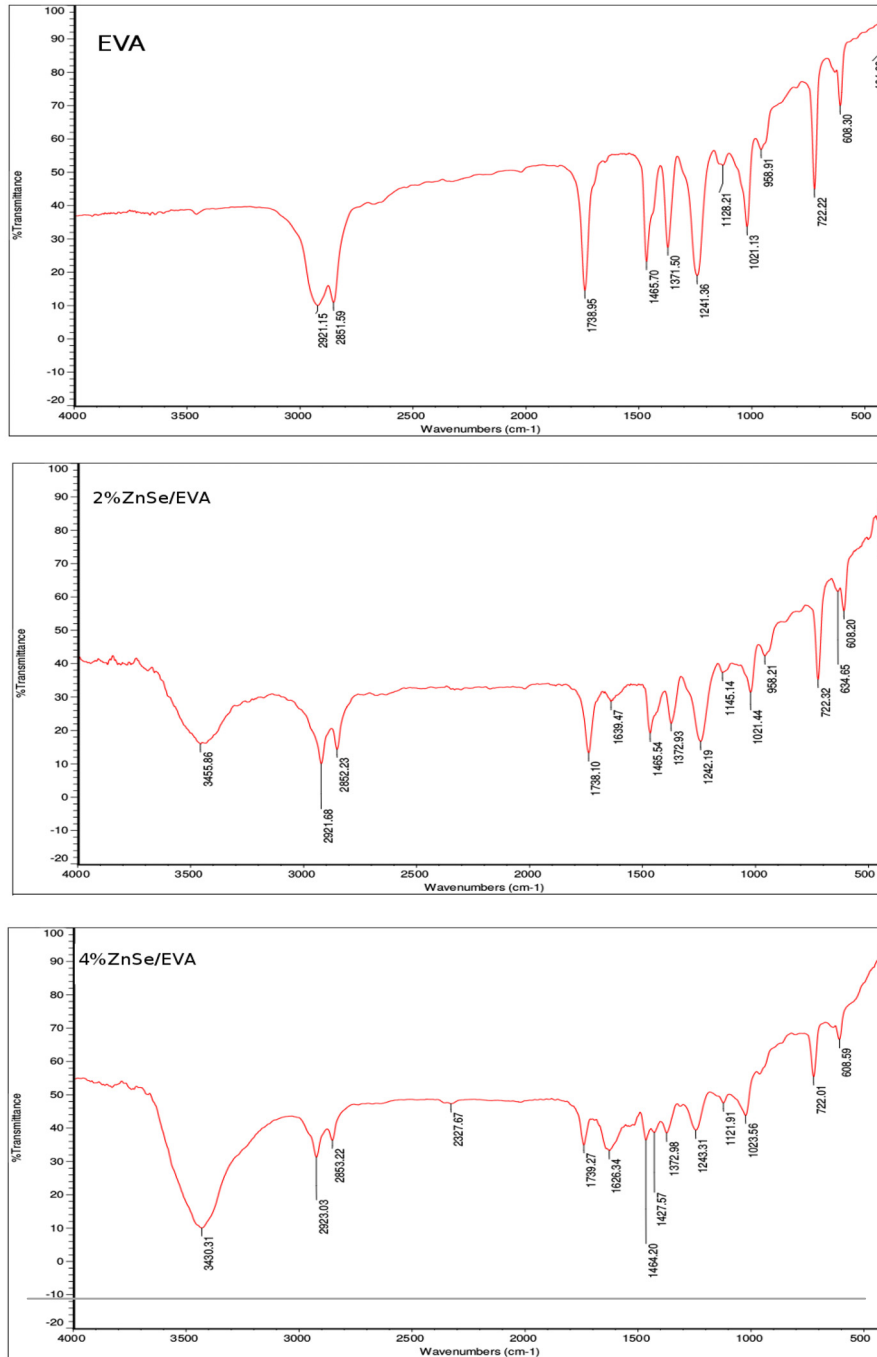


Fig. 4.3: FT-IR Spectra of pure EVA and EVA / ZnSe anocomposites

### 4.5.3 Refractive Index Study

The refractive index of EVA / ZnSe has been determined from the measurement of dielectric constant with the help of LCR Impedance analyzer using Maxwell's rule [16,17],

$$n = \sqrt{(\epsilon_r \mu_r)} \dots \dots \dots (4.1)$$

where  $\epsilon_r$  is the relative permittivity and  $\mu_r$  is the relative permeability.  $\mu_r$  is 1 for non-magnetic materials. The dielectric constant of the sample is calculated using the relation  $\epsilon_r = Cd / \epsilon_0 A$ ; where the nanocomposite acts as a dielectric with  $\epsilon_0$ , absolute permittivity, C is the capacitance, d is the thickness and A is the area ( $\text{mm}^2$ ) of the ZnSe / EVA composite.

In this study, we investigated the variation of refractive index by varying frequency from 100Hz to 1MHz. The results of the variation of refractive index as a function of frequency for samples of different ZnSe nanoparticle concentration dispersed in EVA matrix are shown in Fig.4.4. It is observed that the index value of pure EVA is increased with increasing filler concentrations. This may be due to the absorption of energy by the increased concentration charge carriers, which reduces the frequency of the incident wave. However, pure and nanocomposite samples found almost constant refractive index in the region from 300 Hz to 1 MHz. Commonly, the micro-structured coating of EVA and EVA / ZnSe nanocomposites allow a rough approximation for uniform index value in entire varied frequency region except for very low frequencies. It is seen that the value of index could go up to 5.7 below 500Hz. Fig 4.5 shows variation of refractive index with frequency at

different temperatures. We examined the results using EVA / 4% ZnSe nanocomposite and found that there was a slight decrement in these values on increasing temperature. The calculations are carried out from room temperature to 353K and the sample possessed reproducibility.

In short, the average index profiles of samples could be tuned from 1.52 to 2.28 by homogeneous dispersion of ZnSe nanoparticle in threshold concentration. The index difference of about 0.8 could be achieved easily from the pristine matrix. By the inclusion of composites with different refractive indices, multi-layer anti-reflective coating and photovoltaic modules can be effectively modelled.

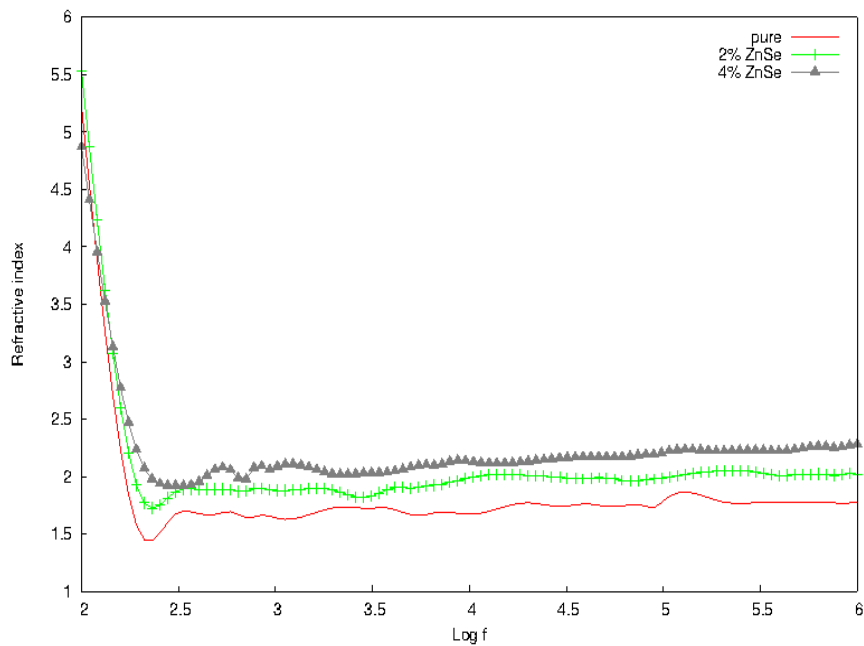


**Fig. 4.4: Variation of refractive index with frequency of EVA and its ZnSe nanocomposites at room temperature**

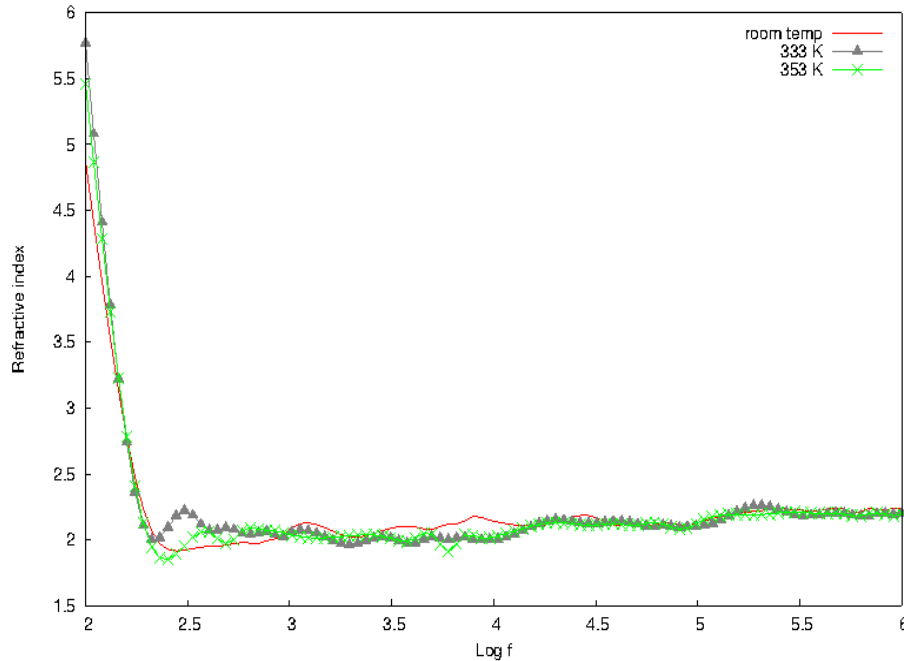


**Fig. 4.5: Variation of refractive index with frequency of EVA / 4% ZnSe at different temperatures**

#### 4.5.4 Optical Absorption Studies

The UV-Vis-NIR spectra of the EVA / ZnSe nanocomposites are recorded in the region 200 to 2000 nm as shown in Fig 4.6. The bandgap of the prepared nanocomposites has been determined using the Tauc-relation [18].

$$\alpha h\nu = A (h\nu - E_g)^{n/2} \dots\dots\dots (4.2)$$

where  $h\nu$  is the photon energy,  $\alpha$  is the absorption co-efficient,  $E_g$  is the band gap,  $A$  is a constant and  $n=1$  for the direct band gap [19]. For allowed direct transition, a graph between  $(\alpha h\nu)^2$  and  $h\nu$  is plotted, extrapolation of the straight line to  $(\alpha h\nu)^2 = 0$  axis gives the value of the

band gap. The estimated band gap of pure EVA and 2% and 4% ZnSe nanoparticles dispersed in EVA host matrix is found to be around 4.74 eV, 4.44 eV and 4.08 eV respectively. The band gap of the prepared composites showed a marked decrement when the percentage of nanoparticles is increased. This may be due to the enhancement of charge carriers in the valence band by the addition of ZnSe nanoparticles.

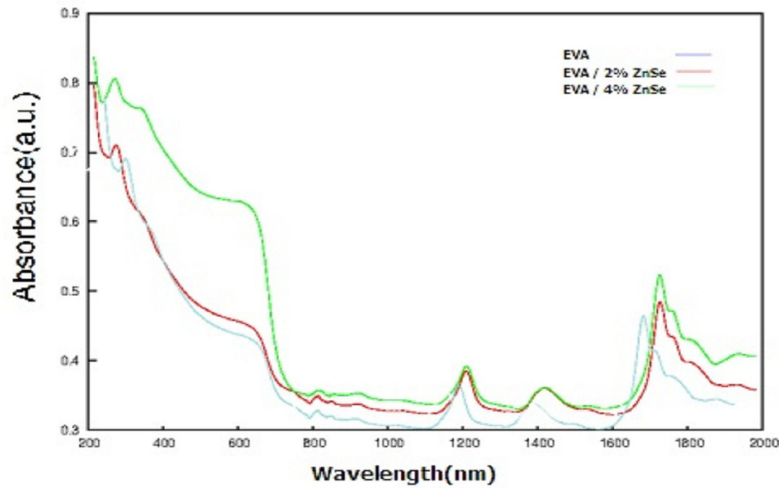


**Fig. 4.6: UV-Vis-NIR Spectra of EVA and EVA / ZnSe nanocomposites**

The exponential character of the absorption coefficient of the nanocomposites near the fundamental absorption edge is expressed by the Urbach rule,  $\alpha = \alpha_0 \exp [hv/E_u]$ , where  $\alpha$  is the absorption coefficient,  $\alpha_0$  depends on the material,  $h\nu$  is the incident photon energy, and  $E_u$  is the Urbach energy. Fig. 4.7 shows the Tauc and Urbach plot of the nanocomposites. The linear region in the Urbach plot is the direct manifestation of the structural disorder in the EVA matrix caused by the addition of ZnSe nanofillers. The enhancement in Urbach energy



confirms the microscopic uniformity of the dispersity in the ZnSe nanoparticles in EVA. The band gap of the nanocomposites decreased whereas Urbach energy increased by increasing the filler concentration. It may be due to the modification of the electronic structure of EVA matrix by the ZnSe nanoparticles which led to the formation of various polaronic and defect levels. The internal potential fluctuations caused by structural disorder due to the presence of nano fillers may be the reason for the increase in Urbach energy.

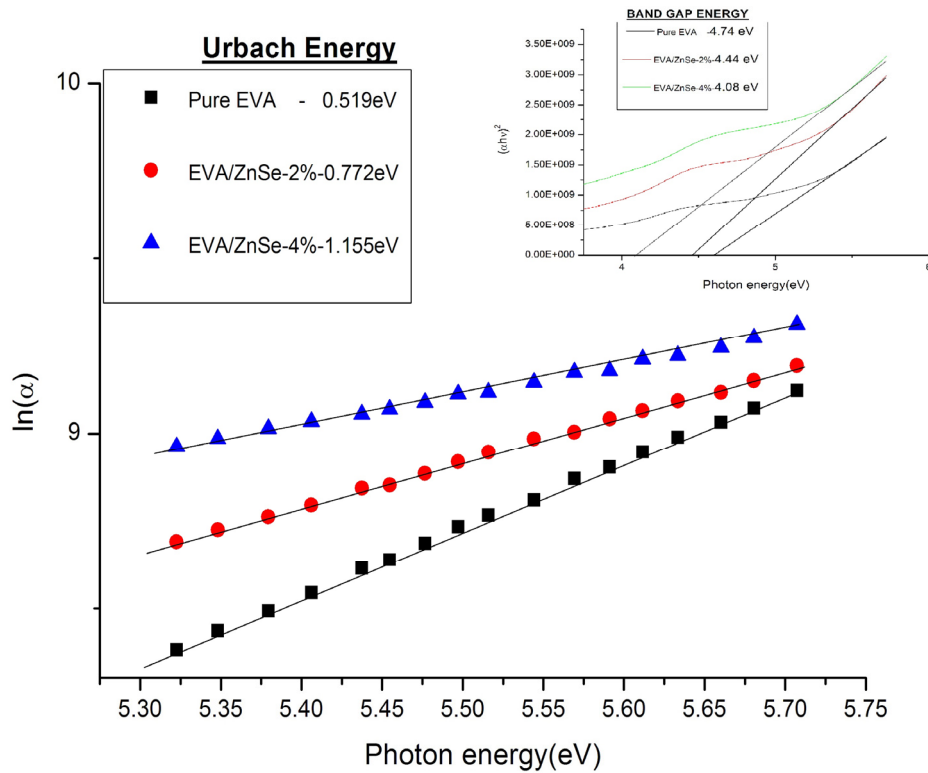
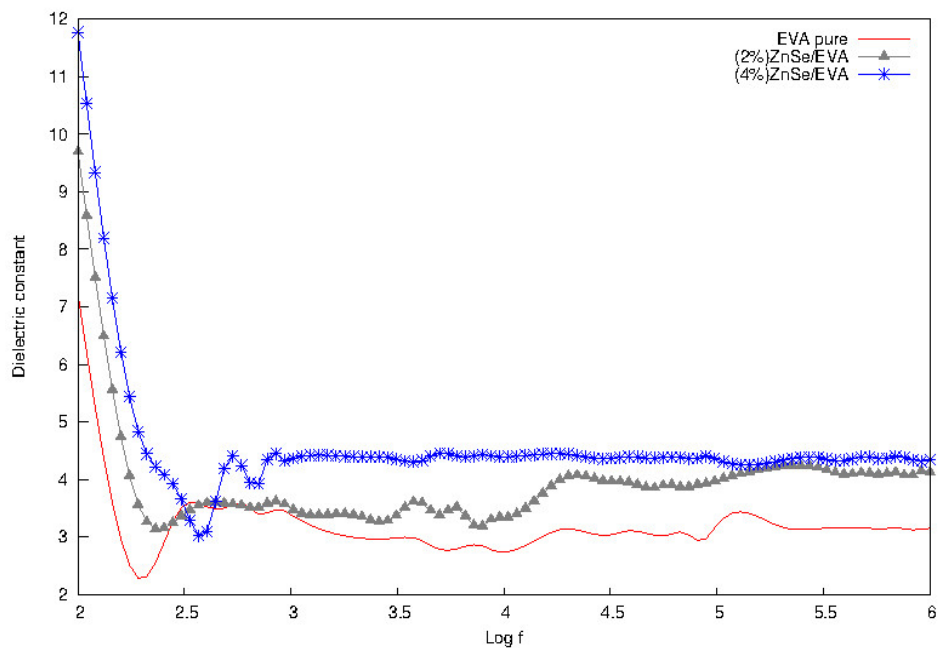


Fig. 4.7: Urbach and Tauc plot of the EVA / ZnSe composites

#### **4.5.5 Dielectric Measurements**

The study of dielectric behaviour of different samples of EVA / ZnSe nanocomposite was carried out using HIOKI 3532-50 LCR HITESTER. Fig. 4.8 shows dielectric constant of EVA / ZnSe composites as a function of frequency. It can be seen from the graph that dielectric constant of pristine EVA and EVA nanocomposites increases with decreasing frequency. At lower frequencies all the free dipolar functional groups in the nanocomposites orient themselves in the direction of applied field, which causes a large value of dielectric constant. As the frequency increases these dipolar groups find it hard to align at the same pace of alternating field, so that the dielectric constant has small values at higher frequencies. Usually nanocomposites have high dielectric constant at low frequencies and large electrical conductivity when semiconducting fillers are dispersed with low percolation threshold. There is a sharp decrement in the dielectric constant between 100 Hz and 1000 Hz. Beyond that frequency dielectric constant is almost constant. But the dielectric constant is found to increase with increasing filler concentration. The values of dielectric constant at 1 kHz are 3.4, 3.7 and 4.5 respectively for pristine, 2% ZnSe and 4% ZnSe filled EVA nanocomposites. Fig. 4.9 shows dielectric loss of EVA / ZnSe composites as a function of frequency. The loss factor of nanocomposites decreased when the frequency and concentration of filler in polymer matrix increased. It may be due to the reduction in the moving dipoles in the nanocomposite as compared to pristine EVA which confirmed strong interaction between EVA and nano fillers.



**Fig. 4.8: Dielectric constant of EVA/ZnSe composites as a function of frequency**

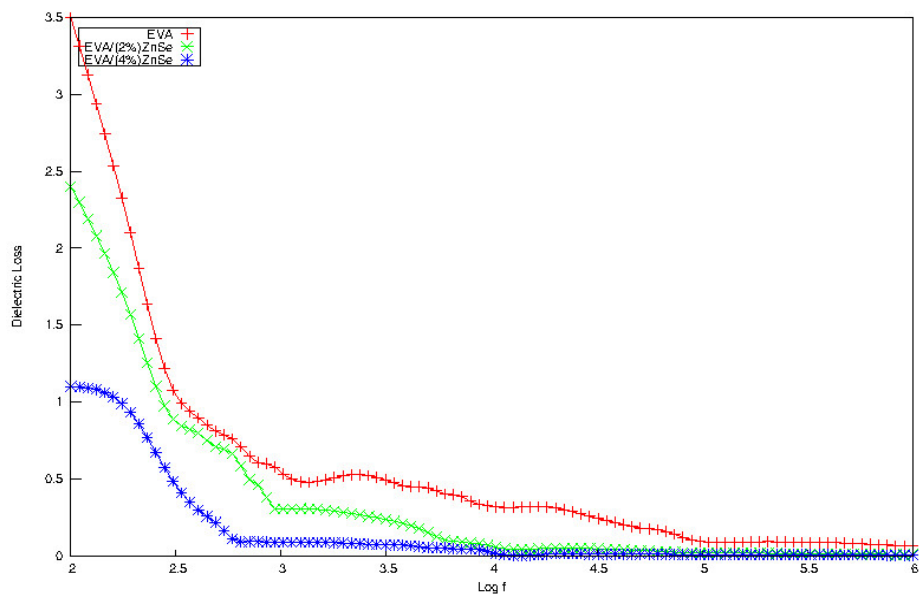


**Fig. 4.9: Dielectric loss of EVA/ZnSe composites as a function of frequency at room temperature**

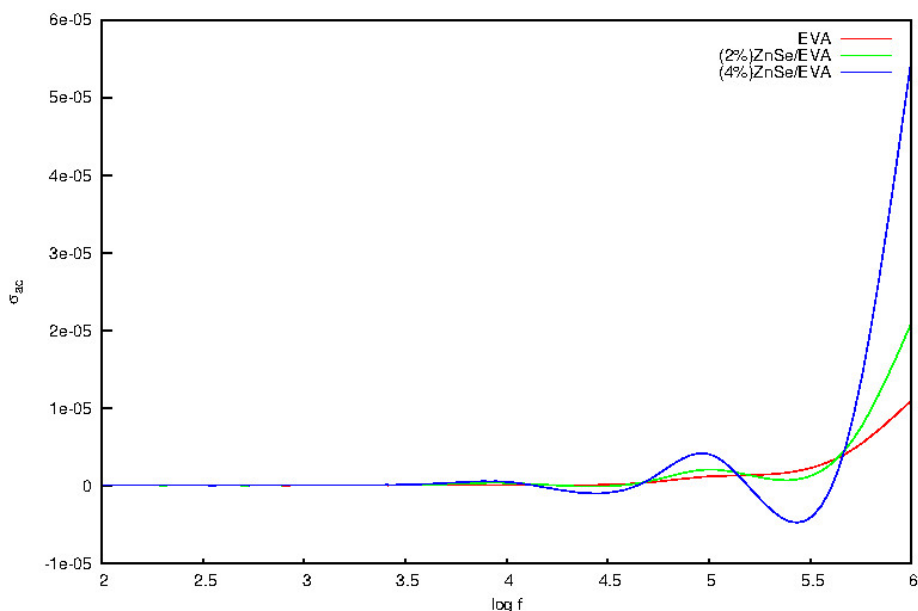


**Fig. 4.10: The AC conductivity of EVA/ZnSe composites as a function of frequency at room temperature**

Fig. 4.10 shows AC conductivity of the nanocomposites. From the figure, it is clear that the conductivity has almost constant value between 100 Hz to 100 kHz and further increase of frequency results in a sharp increase of the conductivity. The AC conductivity was also found to increase with increasing concentration of ZnSe nanoparticles.

#### **4.5.6 Thermal Analysis**

EVA undergoes both physical and chemical changes while heating so that a clear distinctive thermal analysis is needed. The thermogravimetric (TG) and Differential thermal analysis (DTA) on pure and EVA / ZnSe composites were carried out from room temperature to 500<sup>0</sup>C. The TG-DTA traces of pure and doped samples are shown in Fig 4.11a – 4.11c.

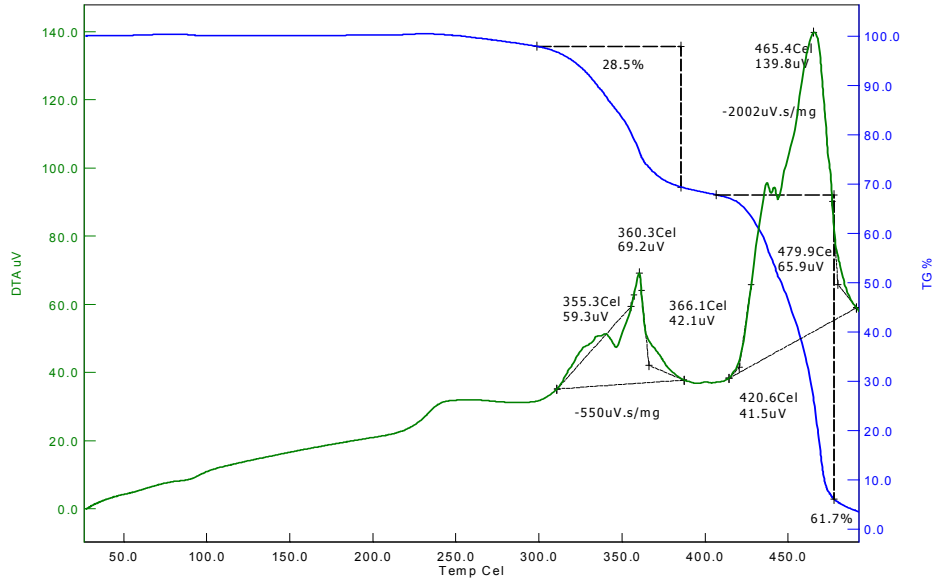


**Fig.4.11a: TG-DTA Curve of EVA co-polymer**

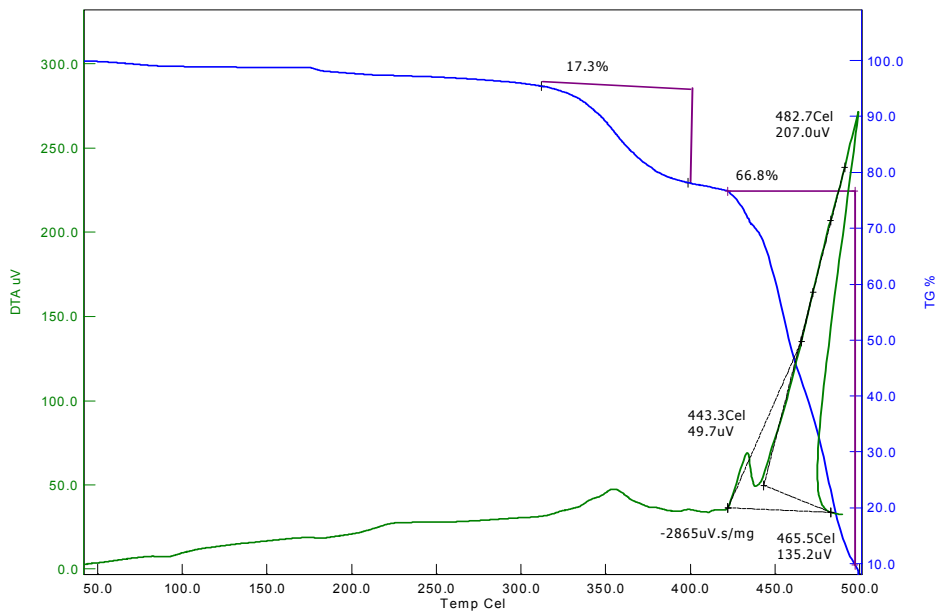


**Fig. 4.11b: TG-DTA Curve of EVA / 2% ZnSe nanocomposite**

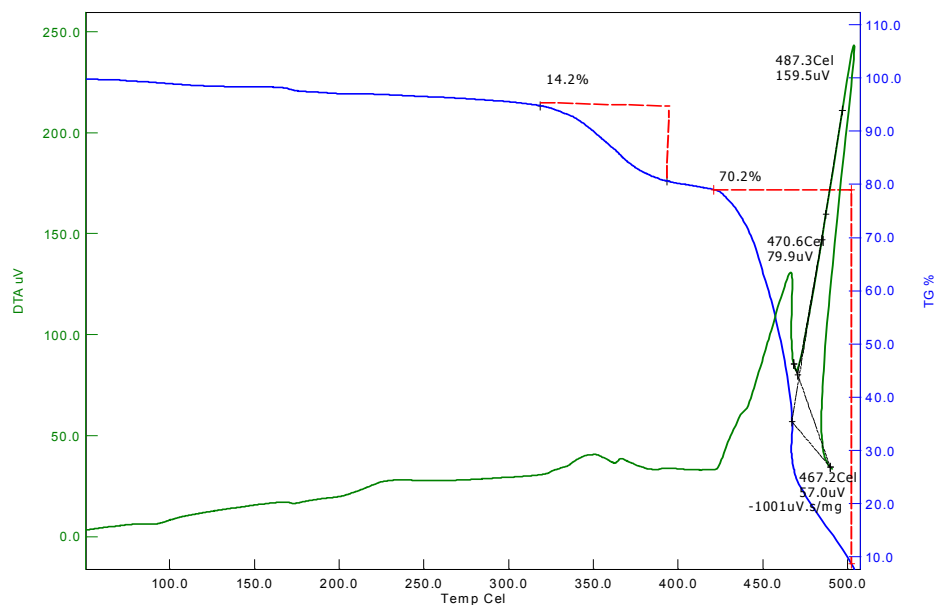


**Fig. 4.11c: TG-DTA Curve of EVA / 4% ZnSe nanocomposite**

They show almost the same behaviour for the three samples with two steps decomposition between 290<sup>0</sup>C to 500<sup>0</sup>C. It is clear that pure EVA is thermally stable upto 298<sup>0</sup>C whereas 2% ZnSe and 4% ZnSe doped EVA are stable upto 309<sup>0</sup>C and 315<sup>0</sup>C respectively. Thus the thermal stability of the EVA nanocomposite increases along with the increase of filler concentration. 28.5% of weight is lost in the first stage decomposition of pure EVA, but it is found that the weight loss in the first stage decomposition decreases as filler concentration increases and found is to be 17.3% and 14.2% for 2% and 4% ZnSe / EVA respectively.

An improved photopyroelectric technique has been used to determine the thermal parameters of nanocomposites. A He-Cd laser of (wavelength  $\lambda=442$  nm KIMMON) output power 120 mW was used as

the optical heating source. The light from the laser was intensity-modulated using a mechanical chopper (SR 540). A polyvinylidene fluoride (PVDF) film of 28  $\mu\text{m}$  thickness was used as the pyroelectric detector. The sample was attached to the pyroelectric detector by means of a thermally thin layer of a compound whose contribution to the signal was negligible. The signal output was measured using a lock-in amplifier (SR830). The frequency of modulation of light was kept above 30 Hz to ensure that the detector, the sample and the backing medium were thermally thick during measurements. The thermal parameters of the nanocomposites are presented in Table 4.1. The thermal conductivity of the EVA increases where as specific heat capacity decreases with increase in the amount of ZnSe nanoparticles. The enhancement in the thermal conductivity of the nanocomposite may be due to the movement of fillers in the amorphous part of the EVA matrix.

**Table 4.1: Thermal parameters of EVA / ZnSe nanocomposites**

Sample Code	Thermal effusivity, $e$ ( $\text{Ws}^{1/2}/\text{m}^2\text{K}$ )	Thermal diffusivity, $\alpha$ ( $\times 10^{-6}\text{m}^2/\text{s}$ )	Thermal conductivity, $k$ ( $\text{W}/\text{mK}$ )	Sp. heat capacity, $C_p$ ( $\text{J}/\text{kgK}$ )
EVA / 2% ZnSe	$2048 \pm 30$	$1.3974 \pm 0.10$	$0.246 \pm 0.10$	$2127 \pm 40$
EVA / 4% ZnSe	$1445 \pm 16$	$3.9369 \pm 0.15$	$0.280 \pm 0.11$	$1021 \pm 25$

#### 4.5.7 Mechanical Properties

Tensile strength and Elongation at break of EVA / ZnSe nanocomposites are shown in Fig.4.12. The pristine EVA sample showed good extension of 430% and tensile strength in the range of 30 MPa. The addition of 2% ZnSe nanoparticle is found to reduce the tensile properties of the

composite compared to the virgin EVA. The reduction of tensile strength at higher ratio of nano loading was due to the stress concentration at the interface where the ZnSe particles agglomerate. As the loading level increases, the dispersion and distribution of nanomaterials get reduced. Percentage stretch possible with the nanocomposite samples reduces with ZnSe loading. This phenomenon is already reported with polymer based nanocomposites as the matrix molecular orientation is negatively affected by the reinforcement particles.

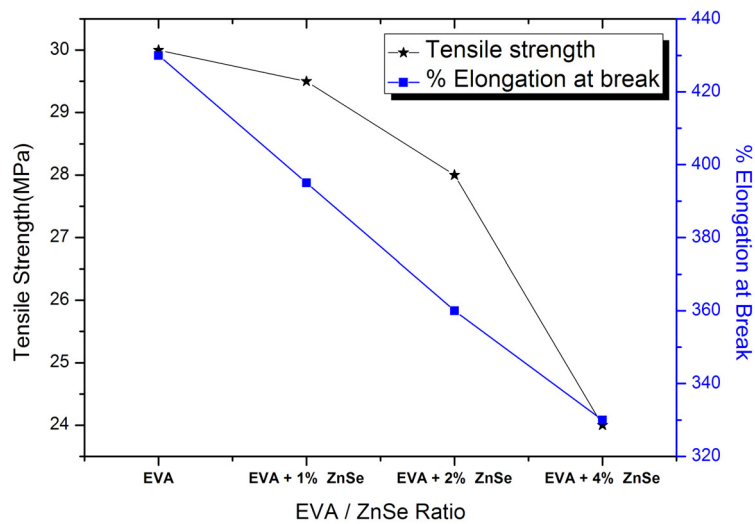


**Fig.4.12: Tensile strength and Elongation at break of EVA / ZnSe nanocomposite**

Peel strength increases for EVA / ZnSe composites on all substrates on 2% incorporation. The adhesion properties differ, based on the molecular interactions of the adhesive with the adherent. Fig.4.13 shows that the molecular flexibility of EVA is not affected by 2% of ZnSe on all substrates. The improvement in cohesive strength resulting from the



presence of ZnSe might be responsible for the improvement in peel strength. The lack of distribution with increased amount of nanoparticles might be the underlying reason for the reduction of peel strength at 4% loading. It can also be inferred that there is a maximum ratio (2%) for ZnSe, above which the inherent polymer property is adversely affected.

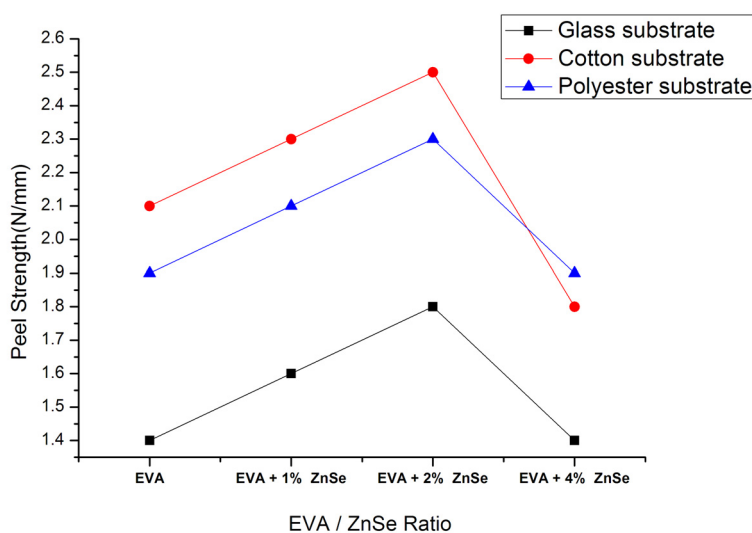


**Fig. 4.13: Peel Strength v/s EVA / ZnSe ratio**

## 4.6 Conclusion

An easier approach towards the synthesis of ZnSe nanoparticles and EVA/ ZnSe nanocomposites was established. The synthesized ZnSe nanoparticle size was estimated as 80nm. FT-IR analysis confirmed the presence and uniform dispersion of ZnSe nanoparticles in EVA. The value of index of refraction of the composite could be easily controlled by varying the amounts of dispersed ZnSe nanoparticles. The band gaps of the pure, 2% and 4% ZnSe / EVA were found to be 4.74 eV, 4.44 eV

and 4.08 eV respectively confirming the increase in the conductivity of EVA by increasing the filler concentrations. The thermal stability of the samples also increases on increasing the filler concentration. The mechanical property evaluation of the samples showed that the tensile strength and the percentage of elongation decrease by the incorporation of nano ZnSe. Peel resistance showed improvement in properties at 2% ZnSe incorporation on all substances.

## References

- [1] Jiahua Zhu, Minjiao Chen, Honglin Qu, Xi Zhang, Huige Wei, Zhiping Luo, Henry A. Colorado, Suying Wei, ZhanhuGuo, *Polymer* 2012, 53 5953.
- [2] Thurn Albrecht T, Schotter J, Kastle G A, Emley N, Shibauchi T, KrusinElbaum L, Guarini K, Black C T, Tuominen M T, Russell T P, *Science* 2000, 290, 2126.
- [3] Pyun J, Matyjaszewski K, *Chem. Mater.* 2001, 13, 3436.
- [4] Brabee C J, Sariciftci N S, Hummelen J C, *Adv. Funct. Mater.* 2001, 11, 15.
- [5] Blom P W M, Schoo H F M, Matters M, *Appl. Phys. Lett.* 1998, 73, 3914.
- [6] Kiesow A, Morris J E, Radehaus C, Heilmann A, *J. Appl. Phys.* 2003, 94, 6988.
- [7] Subbaiah Y P V, Prathap P, Devika M, Reddy K T R, *Phys B* 2005, 365, 240.
- [8] He T, Wang C, Pan X, Wang Y, *Phys. Lett. A* 2009, 373, 592.
- [9] Ma G, He J, Tang S, *Phys. Lett. A* 2003, 306, 348.
- [10] Gonzalex-Benito J., Castillo E., Caldito J F, *European Polymer Journal* 2013, 49, 1747.

- [11] Kasap S, Springer Handbook of Electronic and Photonic Materials, Springer, Berlin, (2007).
- [12] Rhee S H, Choi J Y, Journal of the American Ceramic Society 2002, 85, 1318.
- [13] Camargo P, Satyanarayana K, Wypych F, Materials Research 2009, 12,1.
- [14] Homann T, Hotje U, Binnewies M, Borger A, Becker K D, Bredow T, Solid State Sci. 2006, 8, 44.
- [15] Hodes G, Chemical Solution Deposition of Semiconductor Films, Taylor and Francis, New York, 2004, 362.
- [16] Ashcroft, N. W. and Mermin, N. D., Solid State Physics, 11<sup>th</sup> Indian Reprint, 2011.
- [17] <http://large.stanford.edu/courses/2007/ap272/brockman1>.
- [18] Tauc J., Amorphous and Liquid Semiconductor (Plenium Press, New York, 1974).
- [19] Kumar S. and Chandra R, Optical Mater.2005, 27, 1346.



**SYNTHESIS AND CHARACTERIZATION OF POLY  
ETHYLENE CO-VINYL ACETATE (EVA) /  
CdSe NANOCOMPOSITE**

<i>Contents</i>	<i>5.1 Introduction</i>
	<i>5.2 Experimental</i>
	<i>5.3 Results and Discussions</i>
	<i>5.4 Conclusion</i>

**5.1 Introduction**

Inorganic semiconductor nanocrystals show physical properties suited for the manufacture of LEDs [1], solar cells [2-3] and instrumentation for biomedical imaging [4]. Cadmium selenide (CdSe) is one of the widely investigated II-VI Group semiconductor materials. Excellent optical conductivity makes it useful for several optoelectronic applications, including thin film transistors [5], gamma ray detectors [6], photoelectron–chemical cells [7], photoconductors [8] etc. Nanomaterials of CdSe have been found useful in various fields. Drastic increase in the surface to volume ratio of CdSe nanoparticles helps it to attain properties different from the macroscopic counterparts. These properties largely depend on the particle size and shape [9-10]. Recently, CdSe based polymer nanocomposites were reported for memory devices [11] and biosensors [12].

Ethylene vinyl acetate copolymer (EVA) is an extensively used versatile material [13]. The vinyl acetate (VA) content in the copolymer determines its applications as rubber, thermoplastic elastomers and plastic [14]. Ease of processability coupled with low density and flexibility makes EVA one of the widely accepted polymer matrices to fabricate polymer nanocomposites (PNC). The matrix polymer in the PNC influences the range and strength of the interaction between the filler materials [15]. EVA was chosen as the matrix due to its ability to be homogeneously compounded with nanofillers and also because of its good mechanical properties.

A thin film of CdSe in the EVA matrix was obtained by solution casting, after ultrasonication which ensures proper dispersion. The optical and electrical properties of nanocomposites were determined. The variation of mechanical and adhesive strength with the incorporation of nano fillers was also measured. TG-DTA analysis was utilized for obtaining the thermal properties of the composite.

## **5.2 Experimental**

### **5.2.1 Synthesis of CdSe Nanoparticles**

Solvothermal technique is a promising synthesis method because of the low process temperature and easy to control of particle size. Stringent symmetry of nano-particles can be controlled by chemical concentration, reaction temperature and kinetic control. From several trial and error methods, we selected 0.1 molar cadmium nitrate tetrahydrate ( $\text{CdNO}_3)_2 \cdot 4\text{H}_2\text{O}$  which was dissolved in 100 ml of double distilled water,

0.3 molar sodium selenite ( $\text{Na}_2\text{SeO}_3$ ) was dissolved in 30 ml of hydrazine hydrate ( $\text{N}_2\text{H}_4 \cdot \text{H}_2\text{O}$ ). Both the prepared solutions were mixed up under vigorous stirring with external heat energy at  $60^\circ\text{C}$ . Then these solutions were poured into a Teflon lined sealed stainless steel autoclave and heated at  $240^\circ\text{C}$  for 5 hrs in a muffle furnace. It was washed two times using distilled water for removing impurities. Then it is dried to obtain a black coloured nano CdSe powder.

### **5.2.2 Preparation of EVA / CdSe Nanocomposite**

The copolymer was first dissolved in toluene. Then synthesized CdSe nanoparticles were dispersed in a sonication bath for 2 hours on the basis of the desired weight fraction (1%, 2% and 4%) of CdSe nanoparticle at room temperature. In order to obtain nanoparticles filled polymer samples, it was put into a Teflon coated glass mould and spread in uniform thickness. Afterwards, the mixture was heated at  $40^\circ\text{C}$  for 18 hours in an air oven to evaporate the solvent completely and finally, a thin film of pure EVA and EVA / CdSe nanocomposite was formed.

## **5.3 Results and Discussion**

### **5.3.1 TEM Analysis**

TEM images of CdSe nanoparticles are shown in Fig.5.1. The image reveals that most of the nano-CdSe particles have a diameter 40-55nm, and these particles tend to aggregate together. The shape of the particles is spherical and the average size of particles is about 50nm. The dark images show that nanoparticles are solid in nature.

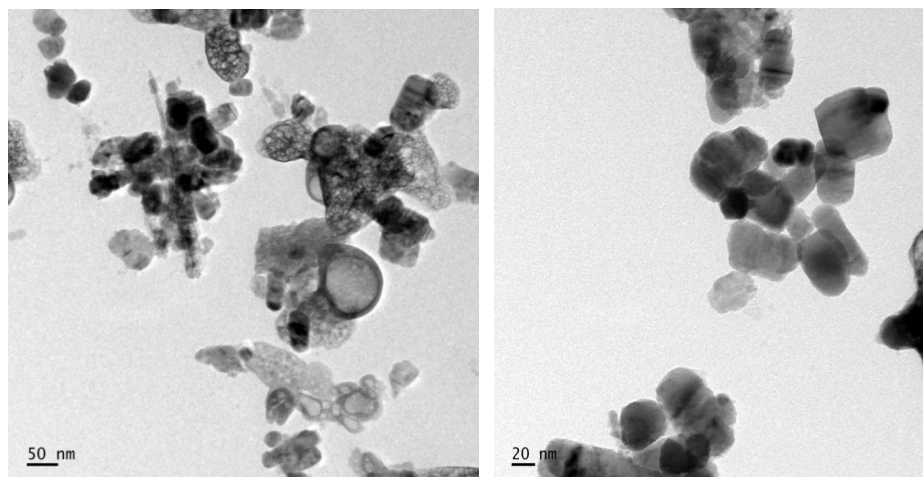


**Fig. 5.1: TEM images of CdSe nanopowder**

### 5.3.2 Morphological Analysis

The morphology of selectively extracted EVA / 4 % CdSe nanocomposite with magnifications x 20,000 and x 200,000 are shown in Fig.5.2.

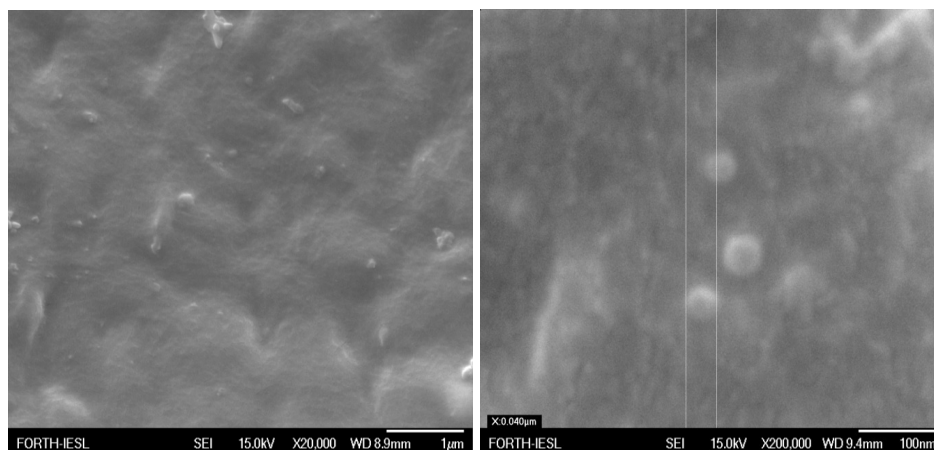


**Fig. 5.2: SEM micrographs of EVA / 4% CdSe nanocomposites**

The CdSe particle distribution and its influence on the EVA copolymer morphology were investigated. A compatible interaction could have taken place between CdSe and host matrix and the surface micelles were homogeneous. The developed shape of the EVA particles and the filler distribution in EVA are clear from scanning electron microscopy. The particle size was about 50nm, and in good agreement with the TEM result.

### 5.3.3 Optical Studies

The absorption spectra of the samples were obtained out using a VARIAN CARY 5000 spectrophotometer, in the region of 200 to 1000 nm and are shown in Fig.5.3.

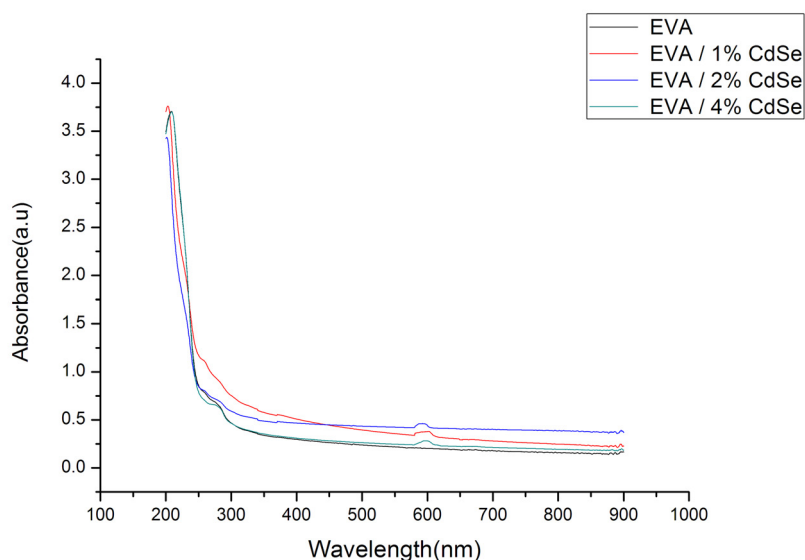


**Fig.5.3: The absorbance as a function of wavelength of CdSe doped EVA films of different concentrations**

From the figure, one can easily find that the absorption increases as the CdSe percentage increases. The addition of the filler material to the polymer does not change the chemical structure of the polymer but



physical properties of the samples change. There are no absorption bands in the visible region since the samples are transparent and this result agrees with previous studies. The cut off wavelength of the samples are around 250 nm.

Fig.5.4 shows the dependence of  $(\alpha h\nu)^2$  on the photon energy ( $h\nu$ ) for direct allowed transitions. The optical energy gap was estimated from the extrapolation of the linear portion of the graph to the photon energy axis. It is to be noticed that the curve is characterized by the presence of an exponentially decaying tail at low photon energy. It is observed that  $E_g$  decreases with increasing dopant concentration.

The variation of the calculated values of the optical energy gap may reflect the role of CdSe in modifying the electronic structure of the EVA matrix due to appearance of various polaronic and defect levels. The decrease in the optical energy band gap with filler concentration may be explained on the basis of the fact that the incorporation of small amounts of dopant forms charge transfer complexes in the host matrix. These charge transfer complexes increase the electrical conductivity by providing additional charges, which results in the decrease of optical energy gap. As the dopant concentration is increased, the dopant molecules start bridging the gap separating the two localized states and lowering the potential barrier between them, thereby facilitating the transfer of charge carrier between two localized states [16]. From Fig.5.5, it can be inferred that the increase of Urbach energy  $E_u$ , values by increasing the concentration of CdSe in EVA / CdSe nanocomposites. This can be attributed to the effect of internal potential fluctuation associated

with the structural disorder. The band gap energy and Urbach energy of samples are shown in Table 5.1.

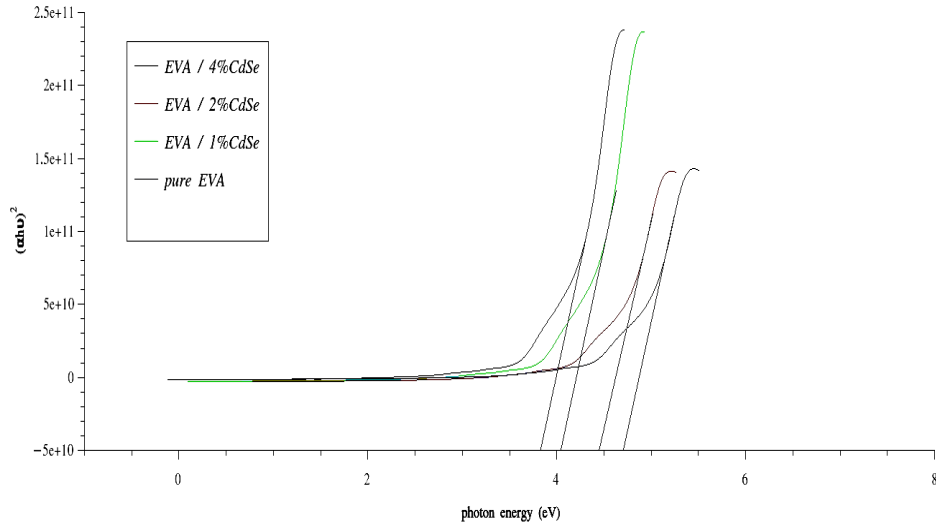


**Fig.5.4: Tauc Plot for EVA with different CdSe concentration**

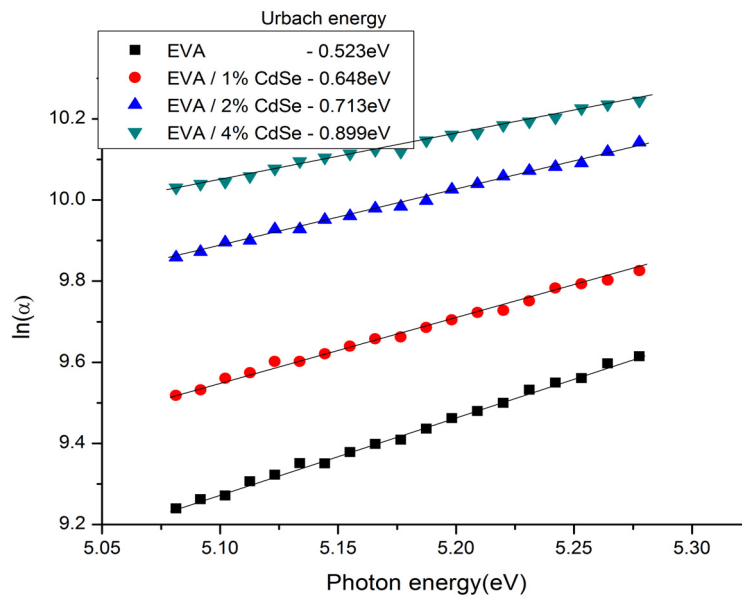


**Fig.5.5: Relation between  $\ln(\alpha)$  and  $h\nu$  for EVA at different CdSe concentration.**

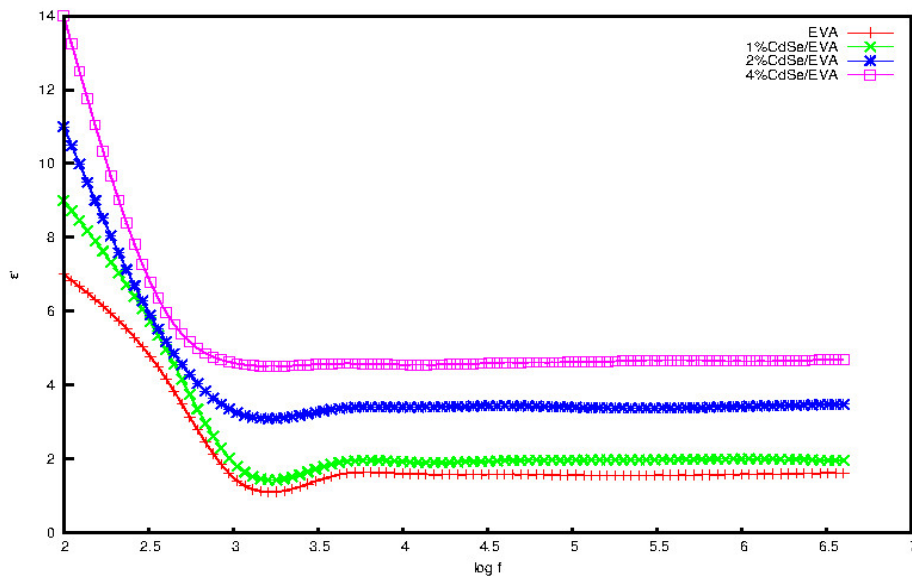
**Table 5.1: Direct optical energy gap and Urbach energy of EVA doped with CdSe.**

Samples	Band Gap in eV ( $E_g$ )	Urbach Energy in eV ( $E_u$ )
Pure	4.651	0.523
EVA / 1% CdSe	4.249	0.648
EVA / 2% CdSe	4.04	0.713
EVA / 4% CdSe	3.984	0.899

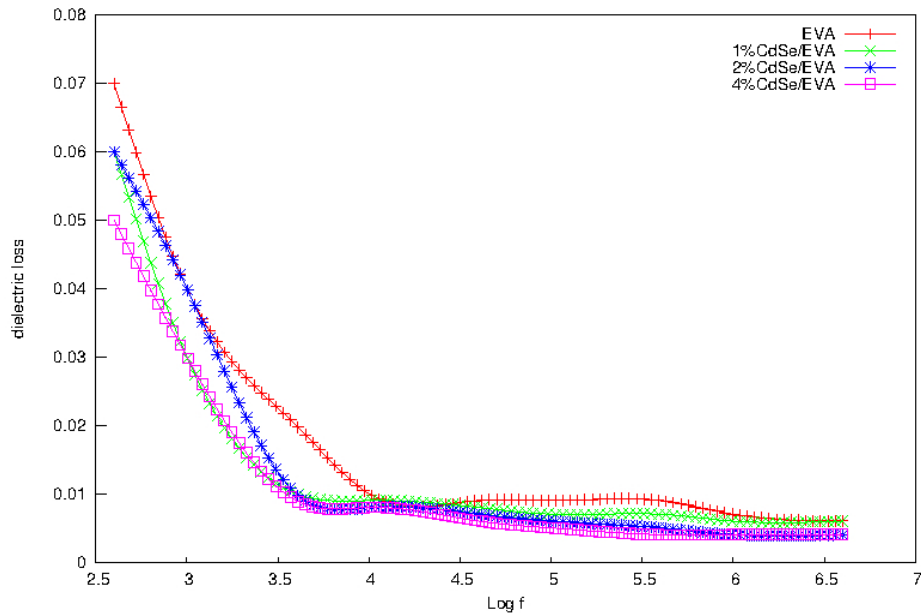
### 5.3.4 Electrical Studies

A well polished sample of polymer nanocomposites of dimension  $9.5 \times 10^{-5} \text{ mm}^2$  having silver coating on opposite faces was introduced between two copper electrodes and then connected to HIOKI 3532-50 LCR HITESTER. We can directly measure parameters like capacitance, resistance, inductance, impedance, dielectric loss and quality factor in the frequency region of 50Hz to 5MHz. Fig.5.6 shows the frequency dependence of dielectric permittivity of the samples at room temperature. The magnitude of dielectric constant is increased with increasing concentration of CdSe nanoparticles. The value is higher at lower frequencies and become stable above 1 kHz. It is a typical characteristic of disordered polymers [17-19] and may be attributed to the dependence on the electronic, ionic, orientational or space charge polarization. That is, all the four polarizations are active. At very low frequencies, dipoles follow the field and with increase in frequency, it begins to lag behind the field and permittivity decreases. The space charge contribution depends on the purity and perfection of the material.

The complex permittivity is related to the free dipole oscillation in an alternating field [20]. Fig.5.7 shows the variation of the dielectric loss with frequency of EVA / CdSe films for different concentrations of CdSe at room temperature. For all samples, dielectric loss shows larger values due to the loss associated with ionic mobility in the low frequency region. The strength and frequency of relaxation depend on the characteristic property of dipolar relaxation. On the addition of CdSe nanoparticles, there is an increase in semiconducting impurities and these charge carriers speed up the segmental motion in available free volume. The relatively fast segmental motion coupled with charge carriers enhances the transport and thus electrical properties of EVA.

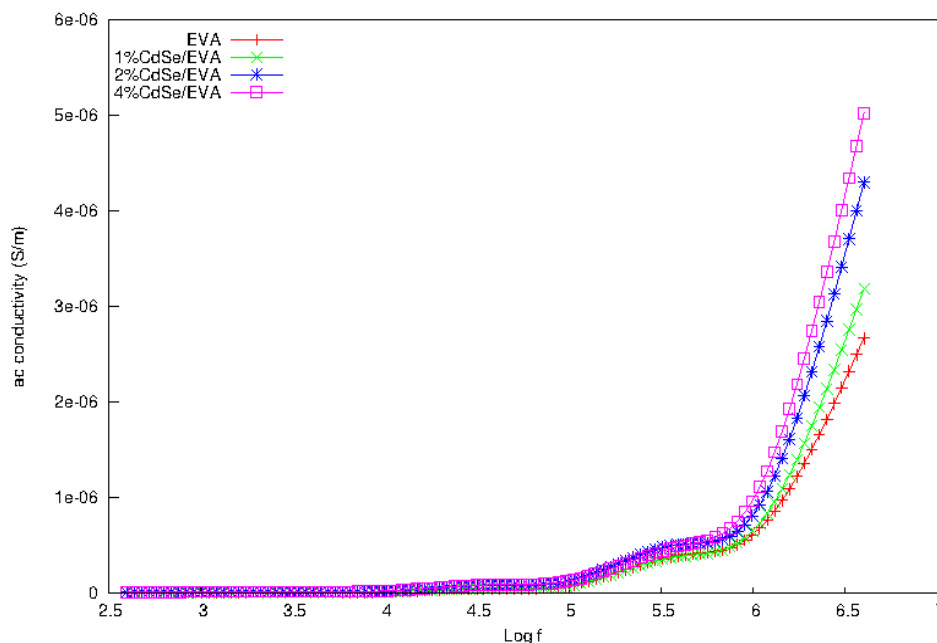


**Fig.5.6: Dielectric constant of pure EVA and EVA / CdSe PNC**



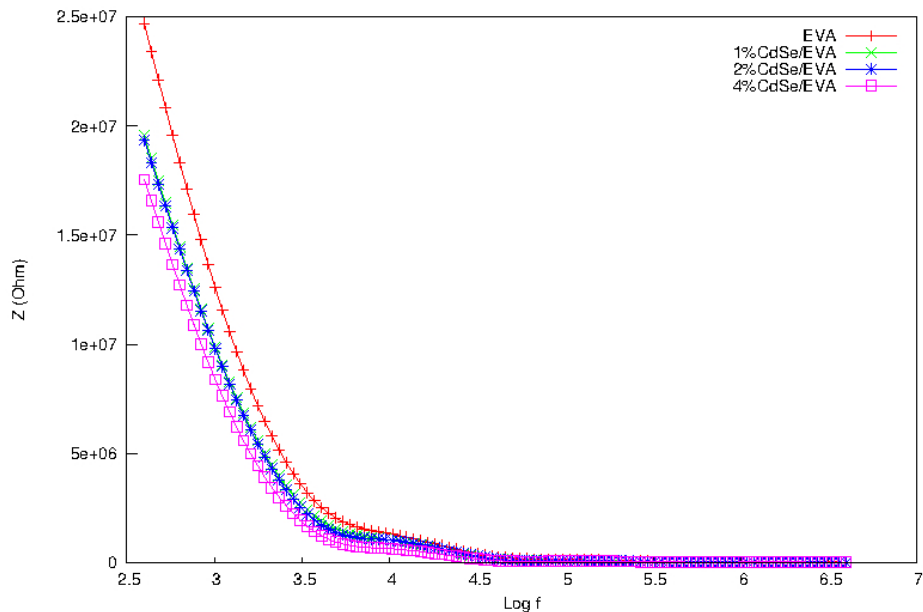
**Fig.5.7: Dielectric loss of pure EVA and EVA / CdSe nanocomposites**

Fig.5.8 depicts the variation of A.C. conductivity of EVA / CdSe as a function of frequency. The A.C. conductivity patterns show a frequency independent plot in the low frequency region and exhibit dispersion at higher frequencies. Conductivity increases as frequency increases, obeys universal power law [21,22] and universal dynamic response. This has widely been observed in disordered materials and is believed to be reflected in the mechanism of charge transport behaviour of charge carriers. This is due to the reduction in space charge polarization at high frequency. Pure EVA has low conductivity when compared to the EVA / CdSe's of different concentrations. As the concentration of CdSe nanoparticles increases, conductivity also increases.



**Fig.5.8: A.C conductivity of Pure EVA and EVA / CdSe nanocomposite**

Fig.5.9 shows the variation of impedance of EVA / CdSe on varying frequency. Impedance decreases as frequency increases. The frequency dependence is similar for all the doped samples. Pure sample has more impedance than the doped samples at lower frequencies and it decreases with increase in the percentage of doping. These results can be correlated with AC conductivity, where an increase of conductivity gives reduced impedance and vice-versa.



**Fig.5.9: Impedance spectra of pure EVA and EVA / CdSe nanocomposites**

### 5.3.5 Thermal Analysis

Thermo gravimetric (TG) and differential thermal analysis (DTA) of virgin EVA and EVA / CdSe nanocomposites were carried out between room temperature and 600°C which are shown in Fig.5.10 - 5.13. TG-DTA showed almost similar behaviour for all four samples with two stages decomposition, but the thermal stability was found to be increasing with increasing filler concentration. The weight percentage of decomposition in the first stage decreases when the amount of the filler is increased. The same phenomena are observed for all the thermograms. The onset decomposition temperature of pure EVA, EVA / 1% CdSe, EVA / 2% CdSe and EVA / 4% CdSe are 298°C, 326°C, 338°C and 352°C respectively.

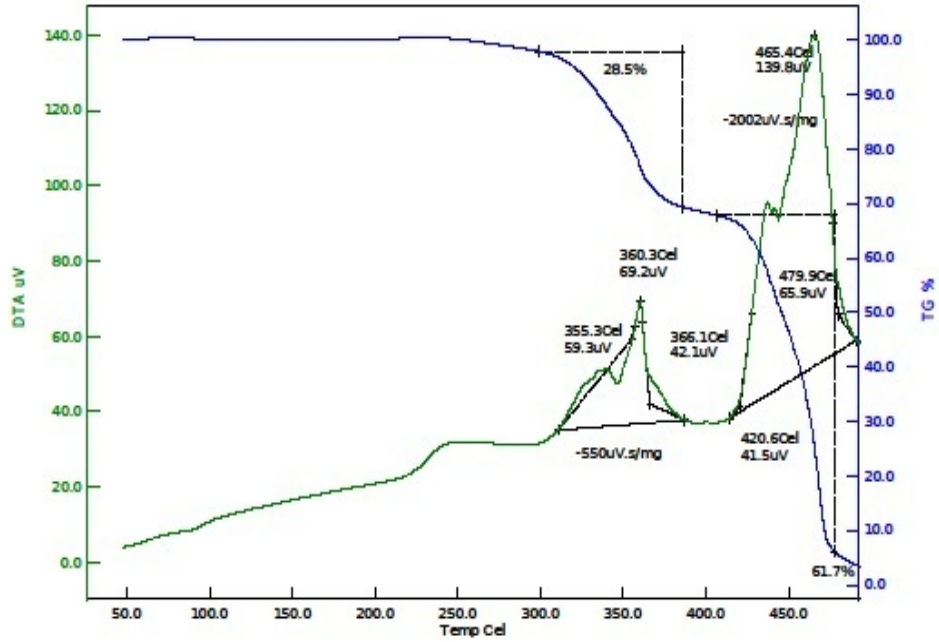


Fig. 5.10: TG-DTA curve of pure EVA

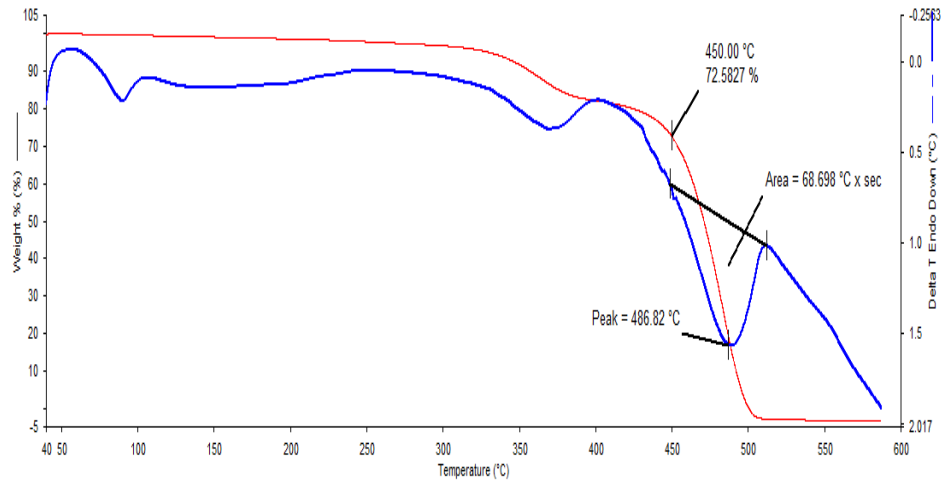
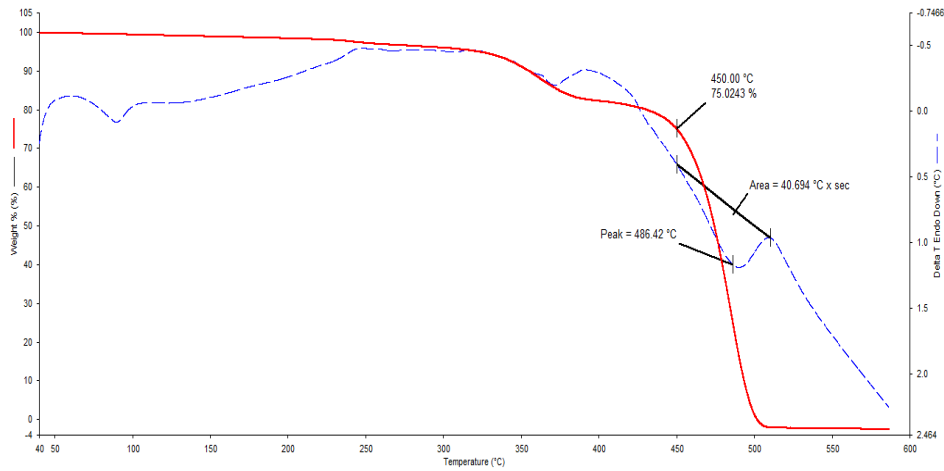
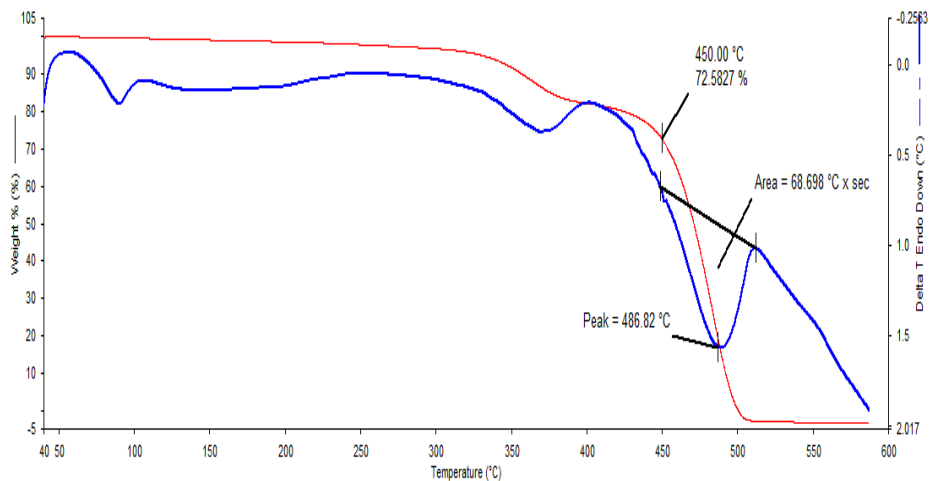


Fig.5.11: TG-DTA curve of EVA / 1% CdSe



**Fig.5.12: TG-DTA curve of EVA / 2% CdSe****Fig.5.13: TG-DTA curve of EVA / 4 % CdSe**

In order to carry out the PPE studies, the samples of EVA and EVA / CdSe at different filler concentrations of thickness varying from 0.10 to 0.22 mm were used. In this measurement, a thermally thick pyroelectric detector is attached to one side of the sample, which is also thermally thick and the combination is mounted on a thermally thick backing medium.

Intensity modulated light from a 120 mW He-Cd laser (KIMMON) of wavelength  $\lambda=442$  nm has been used as optical heating source.

The pyroelectric detector used in this measurement was polyvinylidene fluoride (PVDF) film of thickness 28  $\mu\text{m}$ , with both sides coated with Ni-Cr film, and its pyroelectric coefficient is  $p = 0.25 \times 10^{-8} \text{ Vcm}^{-1} \text{ K}^{-1}$ . The sample-detector-backing assembly was enclosed in a chamber, which was maintained at room temperature. The frequency of modulation of light was kept in the range 40-65 Hz to ensure that the detector, the sample and the backing medium are thermally thick during the measurement. Measurement of the PPE signal phase and amplitude enables one to determine the thermal diffusivity (defined as  $\alpha = k/\rho C_p$ ,  $\rho$  being the sample density) and thermal effusivity (defined as  $e = (kC_p \rho)^{1/2}$ ) respectively. From the measured values of  $\alpha$  and  $e$ , the thermal conductivity ( $k$ ) and heat capacity ( $C_p$ ) of the samples were calculated, and are presented in Table 5.2. It is seen from the table that the values of thermal diffusivity ( $\alpha$ ) and effusivity ( $e$ ), the thermal conductivity ( $k$ ) of the samples increase with increase in the filler concentration whereas specific heat capacity ( $C_p$ ) decreased with increasing filler concentration.

**Table 5.2: Thermal parameters of EVA and EVA / CdSe nanocomposites**

Sample	Thermal effusivity ( $\text{Ws}^{1/2}/\text{m}^2\text{K}$ )	Thermal diffusivity ( $\text{X } 10^{-7}\text{m}^2/\text{s}$ )	Thermal conductivity ( $\text{W/mK}$ )	Sp.Heat capacity( $\text{J/KgK}$ )
EVA	446	0.2334	0.14	1530
EVA /1% CdSe	469	0.2547	0.17	1395
EVA /2% CdSe	481	0.2677	0.21	1228
EVA/4% CdSe	523	0.3165	0.24	1187

### 5.3.6 Mechanical Properties

Fig.5.14 shows the tensile strength and elongation at break of EVA and EVA / CdSe at different filler concentrations. The virgin EVA sample showed tensile strength in the range of 29-31 MPa, with 430% elongation. The addition of 1% CdSe nanoparticles reduced the tensile strength, whereas the percentage elongation reduced to 410 % from 430 %. Further addition of the nanoparticle further reduces the tensile strength of the samples. The reduction of tensile strength with incorporation of nano loading was due to stress concentration at the interface of CdSe particles. As the loading level increases, the effect of dispersion and distribution of nanomaterials gets reduced. Percentage stretch possible with the nanocomposite sample reduces with CdSe loading. The inherent chain flexibility and the deforming ability of EVA was found to be absent in the nanofilled systems. It has led to the drastic reduction of elongation to 340% with the incorporation of 4% of nano CdSe. The tensile strength of EVA / CdSe nanocomposites depends on the degree of strain induced crystallization which in turn depends on the EVA chain length and its flexibility. Longer chains show higher strain induced crystallization and strength. The nano filler incorporation might have reduced the strain induced effect and led to reduction of tensile strength with nano CdSe incorporation [23].

Peel strength increases for EVA / CdSe composites on all substrates upto 1% incorporation. The adhesion properties differ, based on the molecular interactions of the adhesive with the adherent. Fig.5.15 shows that the molecular flexibility of EVA is not negatively affected by

1% of CdSe on all substrates. The improvement in cohesive strength resulting from the presence of CdSe might be responsible for the improvement in peel strength. The lack of distribution with increased amount of nano particles might be the underlying reason for the drastic reduction of peel strength at 4% loading. Nanoparticles in the polymer matrix could have reduced the surface interaction of the adhesive layer between the adherents to reduce the peel resistance. In the cotton substrate the peel resistance was reduced to 2.0 N/mm from 2.1 N/mm. The reduction of elongation at break of the nanocomposite may be due to the restricted mobility of the molecular chain due to the presence of the nanoCdSe [24].

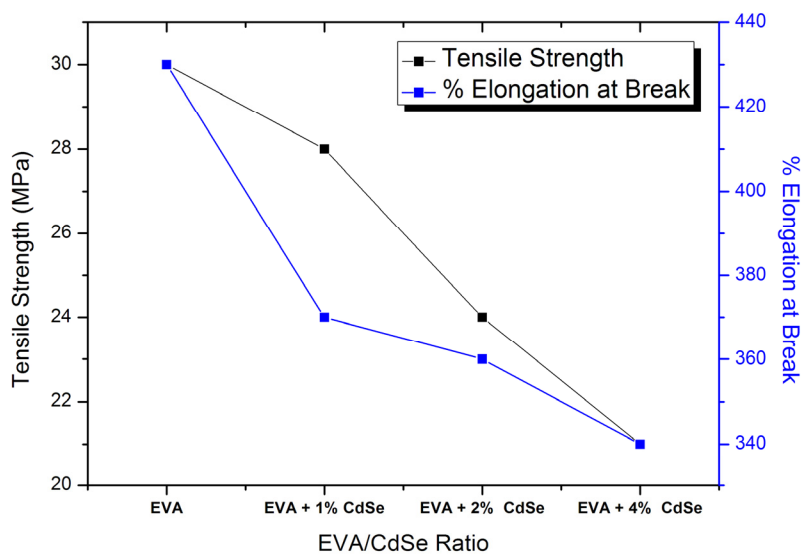


**Fig.5.14: Tensile strength and Elongation at break of EVA/ CdSe nanocomposite**

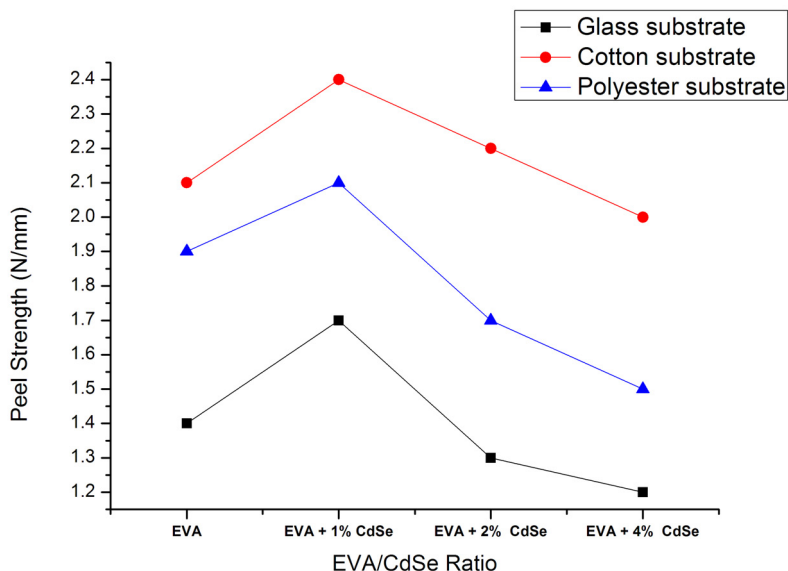


Fig.5.15. Peel Strength v/s EVA/ CdSe ratio

## 5.4 Conclusion

EVA/CdSe nanocomposite materials of different concentrations of CdSe nanoparticle (1%, 2% and 4%) have been prepared successfully by ultrasonication solution casting. The CdSe nanoparticles were synthesized using solvo-thermal method and the size of the particles was found to be around 50nm. The dielectric constant and dielectric loss were found to decrease with increasing frequency being almost constant at higher frequencies. Dielectric constant and loss increase with increase in filler concentration. The band gap of the nanocomposites decreases on increasing the amount of CdSe, whereas the Urbach energy was found to increase. The onset decomposition temperature of pure EVA, EVA / 1% CdSe, EVA / 2% CdSe and EVA / 4% CdSe are 298°C, 326°C, 338°C and 352°C respectively. The thermal conductivity of the nanocomposites

was found to be increasing with increasing filler concentration. The tensile strength of the nanocomposites was found to decrease with the addition of CdSe nanomaterials. On addition of CdSe, the elongation properties also get reduced. Peel resistance increased with 1% CdSe and afterwards, strength of adhesion on all substrates was found to be reduced.

## **Reference**

- [1] Hodes G, Yaron A A, Decker F , Motisuke P, Phys. Rev. B, 1987, 36, 4215.
- [2] Huynh W U, Dittmer J J, Libby W C, Whitting G L, Alivisatos A P, Adv. Funct. Mater. 2003, 13, 73.
- [3] Song J H, Wang X D, Riedo E, Wang Z L, Jour. Phys. Chem. B, 2005, 109, 9869.
- [4] Masotti A, Pitta A, Ortaggi G, Corti M, Innocenti C, Lascialfari A, Mag. Resonan. Mat. in Phys. Bio. and Med. 2009, 22, 77.
- [5] Claster A V, Veraet A, Rycke I D, Bates J D, Jour. Cryst. Growth, 1988, 86, 624.
- [6] Roth M, Nucl. Instrum. Methods A, 1989, 283, 291.
- [7] Lade S J, Uplane M D, Lokhande C D, Mater. Chem. Phys. 2001, 68, 36.
- [8] Nair M T S, Nair P K, Zingaro R A, Meyers E A, Jour. Appl. Phys. 1993, 74, 1879.
- [9] Murray C B, Kangan C R, Bawendi M G, Science 1995, 270, 13335.
- [10] Alivisatos A P, Jour. Phys. Chem. 1996,100, 13226.
- [11] Ramneek Kaur, Tripathi S K, Microelectronic Engineering, 2015, 133,59-65.

- [12] Ke R, Zhang X, Wang L, Zhang C, Zhang S, Mao C, Niu H, Song J, Jin B, Tian Y, J. of Alloys and Compounds, 2015, 622, 15 , 1027.
- [13] Holmes M, Plastic Addit. Compd. 2004, 6, 3, 32.
- [14] Wang B, Wang X, Shi Y, Tang G, Tang Q, Song L, Hu Y, Radiation Phys. Chem. 2012, 81, 308.
- [15] Mutiso R M, Winey K I, Prog. In Polymer Sci. 2015, 40, 63.
- [16] Sangawar V S, Dhokne R J, Ubale A U, Chikhalikar P.S, .Meshram S D, Bull. Mater. Sci. 2007, 30 163.
- [17] Himanshu A K. Ray D K & Sinha T P, Indian J Phys. 2005, 79, 787.
- [18] Matteeva E S, Synth Met 1996, 79, 127.
- [19] Lian A. Besner S & Dao L H. Synth Met 1995,74, 21.
- [20] Bottcher C F S & Bordewijik P. Theory of Electric Polarization, 2<sup>nd</sup> Ed Elseiver Amstetdam.1998.
- [21] Jonscher A K, Dielectric Relaxation in Solids, Chelsea Dielectric Press, London (1983).
- [22] Jonscher A K, Nature 1977, 267,673.
- [23] Datta S K, Chaki T K, Khastgir D, Die Angew. Makromol. Chem. 1996, 238,105.
- [24] Lyons B J, Radiation Phys. Chem. 40, 6, 489.



## **SYNTHESIS AND CHARACTERIZATION OF POLYSTYRENE (PS) / ZnO NANOCOMPOSITES**

<i>Contents</i>	6.1 <i>Introduction</i>
	6.2 <i>Experimental Procedure</i>
	6.3 <i>Results and Discussions</i>
	6.4 <i>Conclusion</i>

### **6.1 Introduction**

Polymer nanocomposites (PNCs) have received great attention in both academic and industrial fields due to their peculiar and unique properties. Incorporation of nanofillers to polymer matrices in quantities below 5% imparts enhanced mechanical, optical, barrier and flame resistant properties. Electrical properties of PNCs can also be tuned based on the required end product properties. In an electroactive polymer nanocomposite, the polymer matrix can be either intrinsically conducting or insulating. Polystyrene (PS) is a hard, rigid, transparent thermoplastic with good electrical insulation properties. Polystyrene matrix nanocomposites have been widely studied with metal, metal oxide, nonmetal oxide and other nano materials. Carbon nanotubes[1-2], carbon black [3], silica [4], titanium arsenate [5], quantum dots [6] etc. show specific property enhancement in polystyrene matrices. Addition



of graphite nanoplatelets can convert polystyrene into a semiconducting material [7].

Metal oxides have been found effective in polymer matrices for improving electrical properties.  $\text{TiO}_2$  [8] and  $\text{Al}_2\text{O}_3$  [9] nanoparticles exhibit improvement in electrical properties and fracture toughness of polyethylene and polyester resin. Electrical conductivity of polyethylene modified with single walled carbon nanotubes [10] and poly vinylcarbazole with titanium dioxide [11] has also been investigated. ZnO nanoparticles have got tremendous attention in recent years due to their chemical stability, high luminous transmittance, ultraviolet absorption and low dielectric constant [12-13]. The semiconducting nature of ZnO was utilized to develop short wave length light emitting diodes (LEDs), piezo and pyro electric varistors and thin film transistors [14]. PS / ZnO nanocomposites were investigated for applications in organic LEDs [15] and light transmitters [16].

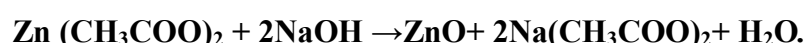
The present chapter focuses on the effect of ZnO on the electrical, thermal and optical properties of insitu polymerized polystyrene.

## **6.2 Experimental Procedure**

### **6.2.1 Synthesis of ZnO Nanoparticles**

ZnO nanoparticles were prepared by hydrothermal method. A solution of 1M NaOH was prepared by dissolving 2g of NaOH in 50ml of deionized water and the mixture was kept stirring for 15 minutes. A solution of 0.5M zinc acetate was prepared by dissolving 5.48g zinc acetate in 50ml deionized water and the mixture was kept stirred for

15 minutes. Then the zinc acetate solution was added to the basic solution and the reaction mixture was stirred for 15 minutes. The prepared solution was kept in a Teflon lined sealed stainless steel autoclave and maintained at a temperature of 200<sup>0</sup>C for 6 hours under autogenous pressure. The overall reaction can be written as:



### **6.2.2 Insitu - Polymerisation of Polystyrene**

Styrene monomer was taken in a separating funnel and 5% NaOH solution was added into it. The mixture was shaken for 10 minutes to remove the inhibitor along with the alkali layer. This was done four times to purify the monomer. Deionised water was then mixed with styrene and washed to remove the traces of NaOH. Purified styrene was then transferred to a three necked round bottom glass reactor. Reflux condenser and nitrogen inlet were connected to the reactor and the assembly was kept on a hot plate magnetic stirrer. Benzoyl peroxide (1 wt%) was then added as the initiator to the monomer in the reactor. The temperature was then increased to 80<sup>0</sup>C along with stirring. Bulk polymerization was allowed for 5 hrs. Then the mixture was transferred to a Teflon coated mould and dried in an air oven at 60<sup>0</sup>C for 18 hrs. The polystyrene film (80% yield) obtained was then peeled off from the mould.

### **6.2.3 Preparation of PS / ZnO Nanocomposite**

To synthesize insitu polymerized nanocomposite, the required amount of nano ZnO was first dispersed in the purified styrene monomer (for 2 wt percentage nanocomposite, 0.8 gm of ZnO in 50 ml of styrene).

The ZnO-styrene mixture was ultrasonicated for one hour at room temperature to obtain good dispersion. This solution was then polymerized at 80<sup>0</sup>C in the three necked reactor for 5hrs after adding the benzoyl peroxide initiator. The polymerized PS / ZnO nanocomposite was then poured into the teflon coated mould and kept in air oven to obtain thin film of approximately 0.1 mm thickness.

### 6.3 Results and Discussions

#### 6.3.1 Scanning Electron Microscopy (SEM)

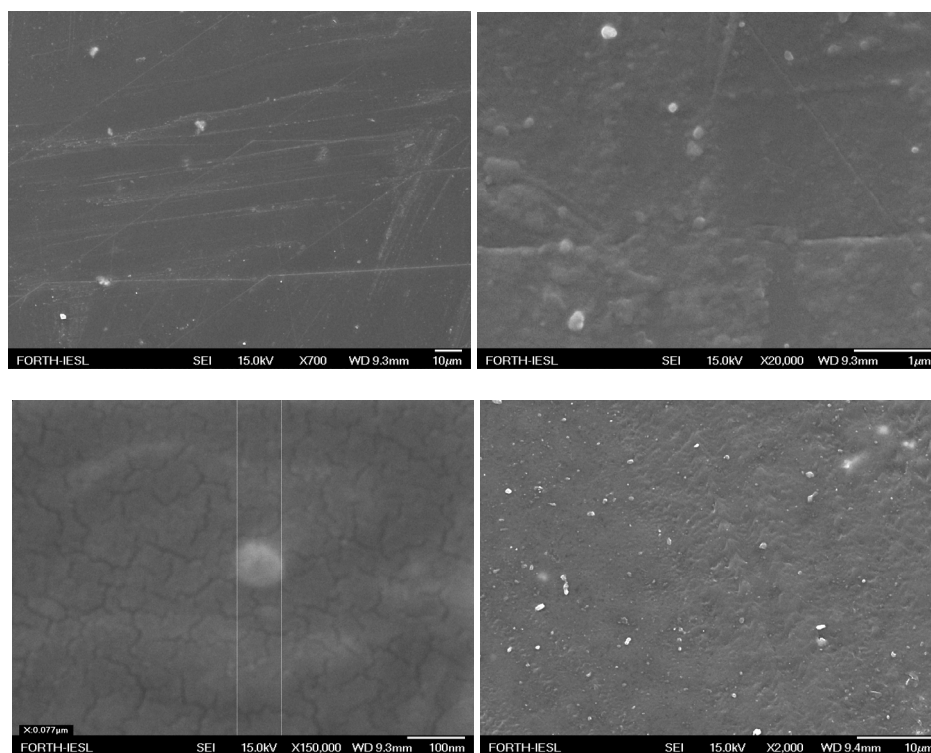


**Fig.6.1: SEM Micrographs of PS / ZnO nanocomposites under different magnifications**

For scanning electron microscopy (SEM), a JEOL JSM-6390LV microscope was used. The samples were gold sputtered with 10 nm gold and the observation was made at 15-20 kVolts. The dispersion pattern of ZnO in polystyrene was confirmed by scanning electron microscope (Fig.6.1).

### 6.3.2 Optical Absorption Studies

The optical absorption spectra of the samples were recorded in the region between 200 and 700 nm, using a UV-1800 Shimadzu spectrophotometer and are shown in Fig.6.2. It was observed from the spectra that samples have a large transmission window starting from 275 to 700 nm without any absorption peak. The values of cut off wavelength of the samples were found to be almost the same for all filler concentrations.

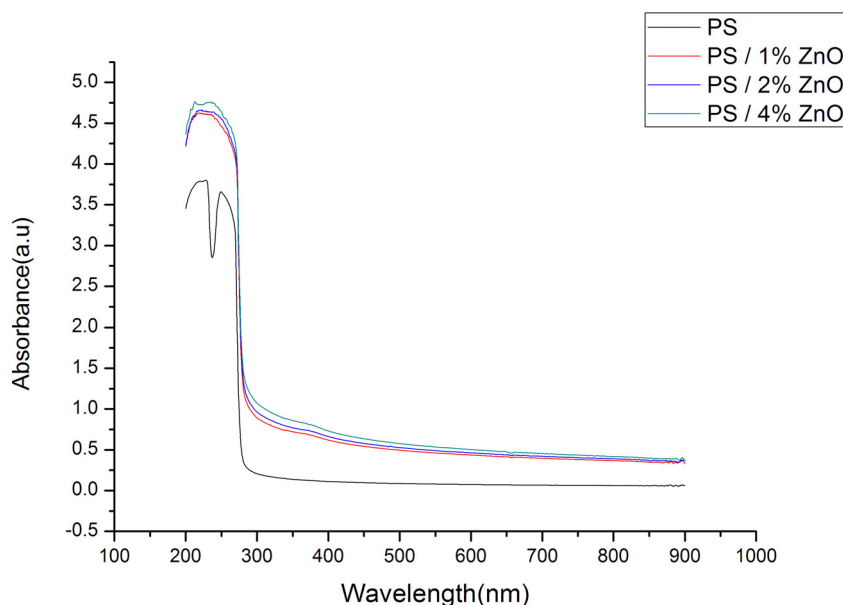


**Fig.6.2: Optical absorption spectra of PS / ZnO nanocomposites**

The band gap ( $E_g$ ) of the PNC's was calculated using Tauc plotting technique and is shown in Fig.6.3. The band gaps of PS and 1%, 2% and 4% PS/ZnO PNC's were found to be 4.418 eV, 4.342 eV, 4.266 eV and 4.071 eV respectively. The decrement in the band gap of the materials reveals the increment in the conductivity as the filler concentration increases.

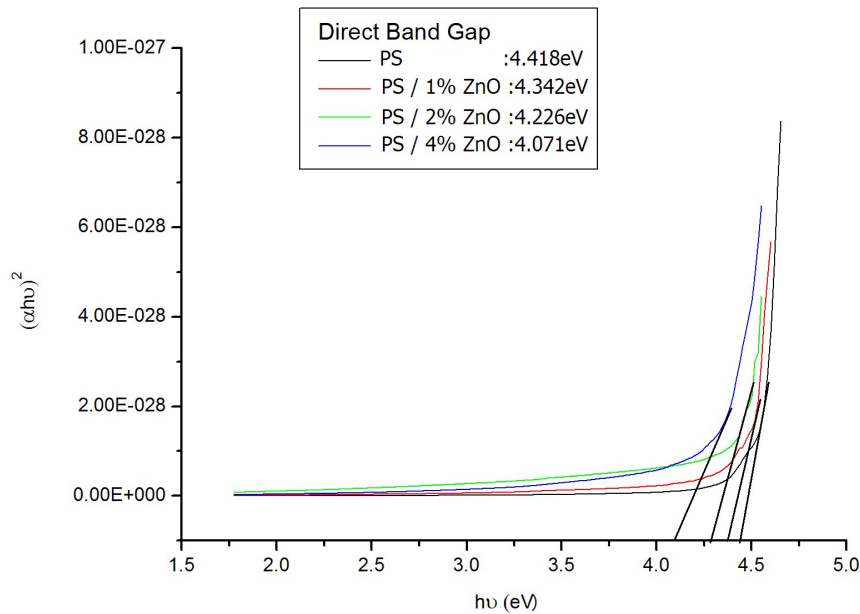


**Fig. 6.3: Tauc – Plot of PS / ZnO nanocomposites**

The exponential character of the absorption coefficient of the nanocomposites near the fundamental absorption edge is expressed by the Urbach rule [17]  $\alpha = \alpha_0 \exp [hv/E_u]$ , where  $\alpha$  is the absorption coefficient,  $h\nu$  is the incident photon energy, and  $E_u$  is the Urbach energy. Fig.6.4 shows Urbach plot of the nanocomposites. Urbach energy was found to increase with increasing filler concentration. It may

be due to the modification of electronic structure of PS matrix by the ZnO nano particles which led to the formation of various polaronic and defect levels [18]. The internal potential fluctuations caused by structural disorder due to the presence of nano fillers may be the reason for the increase in Urbach energy [19].

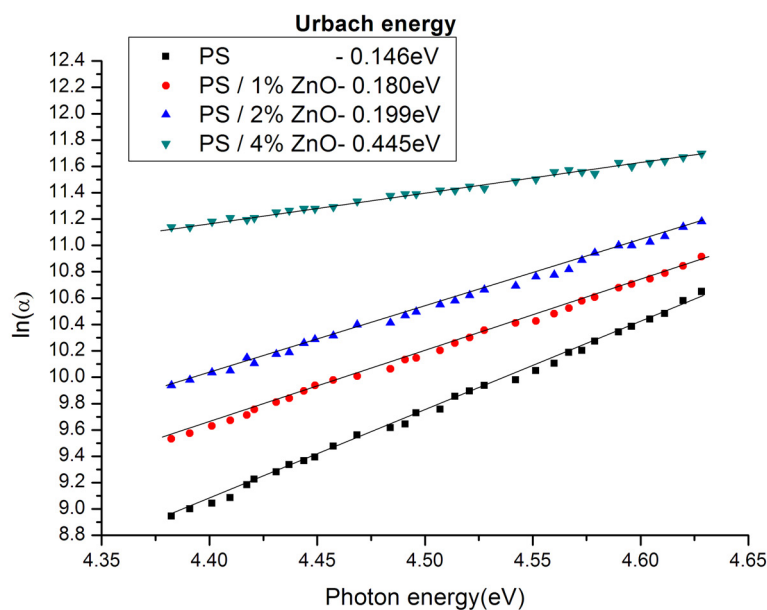


**Fig. 6.4: Relation between  $\ln(\alpha)$  and  $h\nu$  for PS at different ZnO concentration.**

### 6.3.3 FTIR Studies

The FTIR spectra of the samples were carried out in the wave number range  $400 - 4000 \text{ cm}^{-1}$ . The FTIR spectra of filler and polymer composites (PNC) are shown in Fig.6.5. The polystyrene material shows all its characteristic peaks in the pure and the doped composites. C-H out of the plane bending was observed between  $900-690 \text{ cm}^{-1}$ . Strong

absorption peaks were noticed at  $699\text{ cm}^{-1}$  and  $755\text{ cm}^{-1}$  due to the presence of mono substituted ring structure. Overtone and combination bands were seen between  $2000\text{ cm}^{-1}$  and  $1667\text{ cm}^{-1}$ . The C-H stretch was observed at around  $2850\text{ cm}^{-1}$  whereas the aromatic C-H stretch provided a peak at  $3026\text{ cm}^{-1}$ . The ZnO incorporated in polystyrene produced additional peaks at  $622\text{ cm}^{-1}$  and  $3431\text{ cm}^{-1}$ . Table 6.1 shows the observed bands and vibrational assignments of pure PS, ZnO and its composites.

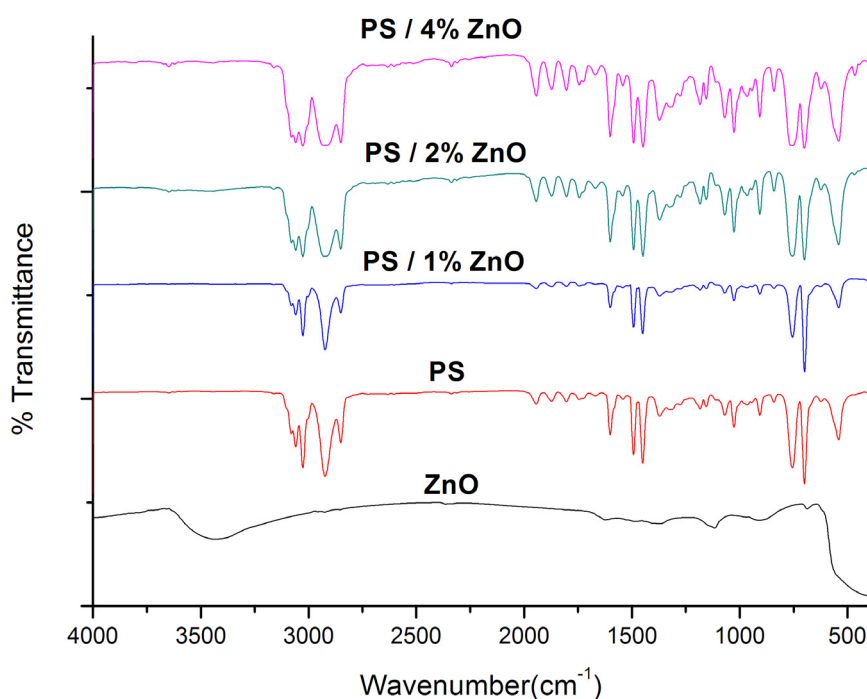


**Fig.6.5: FTIR spectra of ZnO, pure PS and PS / ZnO composites**

**Table 6.1: Polymeric group identification of PS and PS / ZnO nanocomposites from FT-IR analysis**

Pure PS	ZnO / 1%PS	ZnO / 2%PS	ZnO / 4%PS	Assignments
1449.46	1449.91	1448.51	1448.19	Aromatic
1492.34	1492.31	1492.05	1492.06	C=C
1600.86	1600.65	1600.68	1600.80	
1183.49	1183.45	1183.47	1183.61	C-H
1155.07	1155.01	1155.13	1155.13	
3059.72	3059.66	3059.65	3059.66	Aromatic C-H stretching
3026.37	3026.24	3026.32	3026.33	
2850.61	2850.52	2850.52	2850.28	

#### **6.3.4 Raman spectral studies**

In the present study, a mobile Raman microspectrometer (HE 785, JY Horiba) was used. The excitation source is a cw diode laser, emitting at 786 nm (maximum power on the sample, 50 mW), fibre-optically coupled to an optical head that enables focusing of the beam by means of a number of objective lenses ( $\times 10$ ,  $\times 20$ ,  $\times 50$ ) which provide a variable focusing of the beam (and thus magnification of the work area) down to a few microns on the sample surface. A white light illumination system and a high-resolution colour camera (video microscope) are also part of the optical head and offer a very clear view of the area under investigation, necessary for positioning the beam on nanocomposites. The scattered Raman radiation is collected through the focussing objective and sent through an optical fiber to a compact spectrograph, equipped with a concave grating, which provides spectral coverage up to  $3,200 \text{ cm}^{-1}$  at a spectral resolution of about  $10\text{--}15 \text{ cm}^{-1}$ . Spectra are



recorded on a high-sensitivity, aircooled C detector (1,024×256 pixels, Synapse, JY Horiba). In a typical measurement, the entire fragment is placed under the microscope objective and with the help of an XYZ micro-positioner and the video microscope the spot to be analysed is selected. The beam power on the sample was, depending on the material investigated, in the range of 0.05–5.5 mW. Typical exposure time of the CCD was 20s per scan, while normally 10 to 20 scans were averaged.

Raman spectra of PS and PS / ZnO nanocomposites are shown in Fig.6.6. The peaks at  $621.672\text{ cm}^{-1}$ ,  $1001.677\text{ cm}^{-1}$ ,  $1607.606\text{ cm}^{-1}$  are the most intense bands. These bands represent the ring deformation ( $621.672\text{ cm}^{-1}$ ), aromatic ring breathing ( $1001.677\text{ cm}^{-1}$ ), and C=C aromatic ring stretching ( $1607.606\text{ cm}^{-1}$ ).

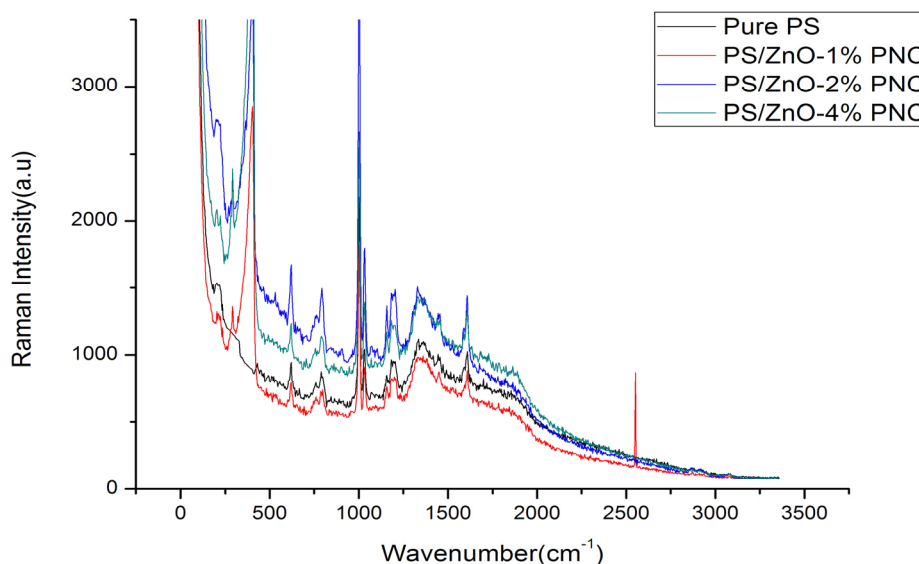


**Fig. 6.6: Raman spectra of PS and PS / ZnO nanocomposites**

These peaks are also present in PS / ZnO nanocomposites but the relative intensity of these peaks in the spectra of different concentrations of PS / ZnO are different. The peaks at 406.135 cm<sup>-1</sup> in PS / 1% ZnO, 399.177 cm<sup>-1</sup> in PS / 2% ZnO and 406.135 cm<sup>-1</sup> in PS / 4% ZnO confirm the presence of ZnO in the composite. Table 6.2 shows the observed bands and the vibrational assignments of PS / ZnO composites.

**Table 6.2: Raman spectra analysis of PS and PS / ZnO nanocomposites**

Pure PS (cm <sup>-1</sup> )	PS / 1% ZnO (cm <sup>-1</sup> )	PS / 2% ZnO (cm <sup>-1</sup> )	PS / 4% ZnO (cm <sup>-1</sup> )	Assignments
	406.135	399.177	406.135	ZnO vibration
621.672	621.672	622.457	621.672	Ring deformation
1001.677	1001.677	999.567	1001.677	Aromatic ring breathing
1607.606	1617.99	1608.394	1607.606	C=C aromatic ring stretching

### 6.3.5 Laser induced fluorescence studies

The fluorescence of the samples was conveniently monitored by laser-induced fluorescence (LIF). The irradiation was performed with a nanosecond excimer laser (Lambda Physik EMG 201 MSC) operating at 248 nm in ambient atmosphere (Flaser ~ 5 mJ cm<sup>-2</sup>). Fig.6.7 shows the LIF spectra of the nanocomposites. From the figure, one can easily find that the fluorescence intensity increases with increase in filler concentrations. The ZnO filler atoms incorporated into the PS through -CH<sub>2</sub>-CH- bonding of the compound may enhance stability of the molecular orbital electron density. As the filler concentration increases, the electron density becomes more and more stable which means the number of effective

transitions increases. This may be the reason for the enhancement in the intensity of the fluorescence when the filler concentration increases.

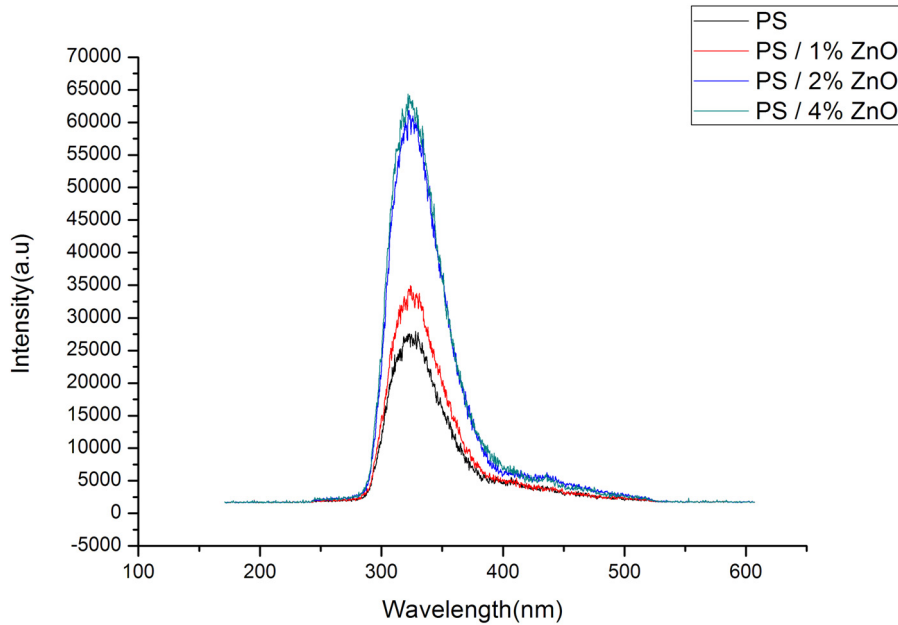


**Fig.6.7: LIF spectra of pure PS and its composites**

### 6.3.6 Dielectric studies

A well-polished sample of polymer nanocomposite of dimension  $9.5 \times 10^{-5} \text{ mm}^2$  having silver coating on the opposite faces was introduced between two copper electrodes and then connected to HIOKI 3532-50 LCR HITESTER to measure parameters such as capacitance, resistance, inductance, impedance, dielectric loss and quality factor of the material by varying the frequency from 100 Hz to 5MHz. Fig.6.8 shows the variation of dielectric constant of PNC's at different frequencies. It is observed that initially the dielectric constant has larger values at lower

frequencies and then decreases with increase in frequency; the dielectric constant remains almost constant at higher frequencies. The decrease in dielectric constant of PNC at high frequencies may be attributed to the dependence on the electronic, ionic, orientational and space charge polarizations. At low frequencies, all the four polarizations are active. The space charge contribution depends on the purity and perfection of the material. Its influence is noticeable in the low frequency region. The low frequency dielectric constant is found to increase with increase in filler concentration. The orientational effect can sometimes be seen in some materials even up to  $10^{10}$  Hz. Ionic and electronic polarizations always exist below  $10^{13}$  Hz. Hence, the larger values of dielectric constant and dielectric loss exhibited by PNC at low frequencies may be attributed to space charge polarization. Fig.6.9 shows the variation of dielectric loss of samples as a function of frequency. In the lower frequency region, dielectric loss shows larger values due to loss associated with ionic mobility. The trend in the variations of both dielectric constant and dielectric loss as a function of frequency is almost the same in all frequency regions especially in low frequency range. From the figures, it is quite clear that there is a larger increment in both dielectric constant and dielectric loss for the PNC's as filler concentration increases in the low frequency region.

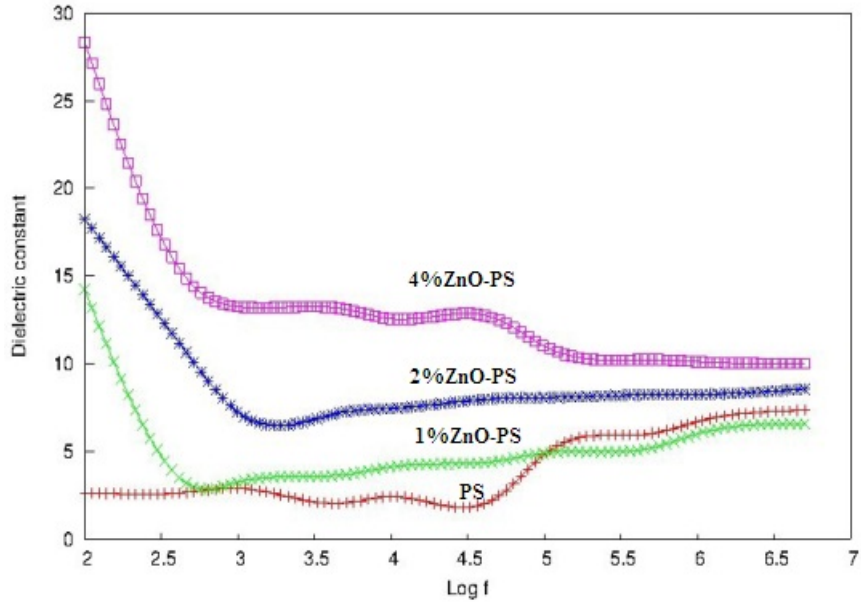


**Fig.6.8:** Variation of dielectric constant of PS and PS / ZnO nanocomposites as a function of frequency at room temperature

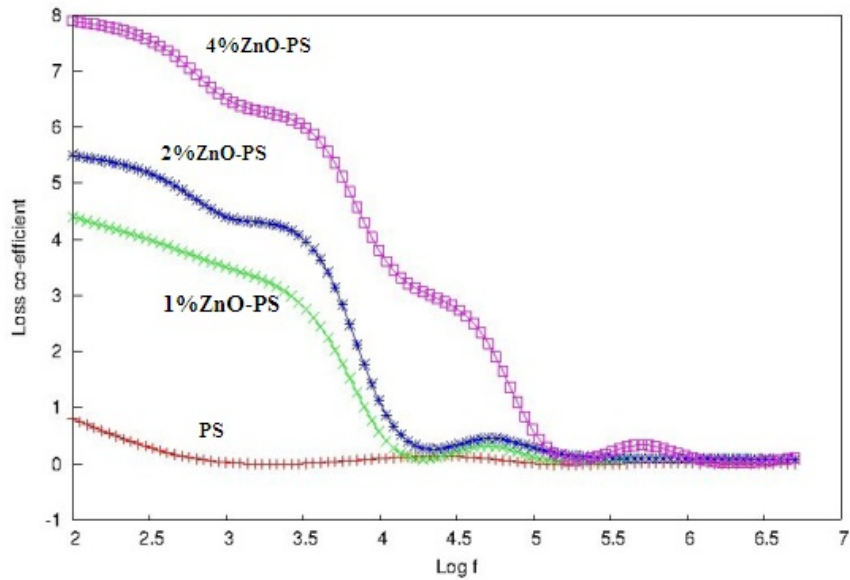


**Fig.6.9:** Variation of dielectric loss variation of PS and PS / ZnO composites as a function of frequency at room temperature.

### 6.3.7 A.C conductivity

Fig.6.10 depicts the variation of a.c conductivity of PNC's as a function of frequency. Conductivity increases as frequency increases. As the weight percentage increases conductivity shows a markable increase at high frequency. This is due to the reduction in space charge polarization at high frequency. The pure PS has low conductivity compared to PS / ZnO PNCs of different concentrations, but up to a particular frequency all the samples show the same constant conductivity. As the concentration of ZnO nanoparticles increases conductivity also increases.

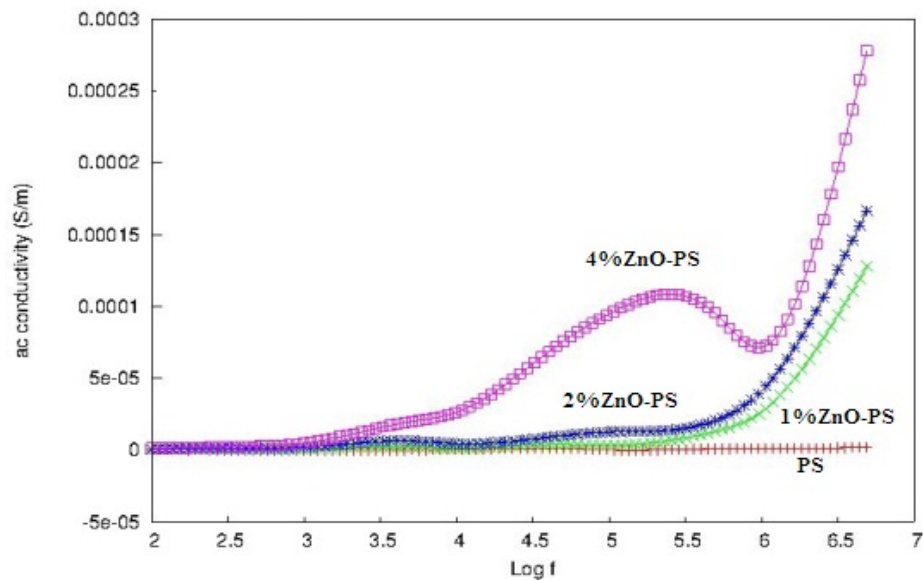


Fig.6.10: AC conductivity of PS and PS / ZnO nanocomposites as a function of frequency

### 6.3.8 Photopyroelectric studies

Thermal parameters of PS and ZnO doped polystyrene of thickness ranging from 0.16mm to 0.20 mm have been determined by

photopyroelectric technique. Using the data of PPE signal phase and amplitude, the values of the thermal diffusivity ( $\alpha$ ) and thermal effusivity ( $e$ ) were determined. From the measured values of  $\alpha$  and  $e$ , the thermal conductivity ( $k$ ) and heat capacity ( $C_p$ ) of nanocomposites have been calculated and presented in Table 6.3.

**Table 6.3: Thermal parameters of PS and PS / ZnO nanocomposites**

Sample	Thermal effusivity (Ws <sup>1/2</sup> /m <sup>2</sup> K)	Thermal diffusivity (X 10 <sup>-7</sup> m <sup>2</sup> /s)	Thermal conductivity (W/mK)	Sp.Heat capacity (J/Kg)
PS	961	0.5914	0.704	1250
PS / 1% ZnO	751	0.5882	0.549	980
PS / 2% ZnO	705	0.5403	0.494	960
PS / 4% ZnO	686	0.5118	0.468	960

## 6.4 Conclusion

In this study PS/ZnO nanocomposites with different concentrations of ZnO nanoparticles (1%, 2% and 4%) have been prepared successfully by adding a certain amount of nanosized ZnO into monomer solution followed by stirring, ultrasonication and polymerisation. The ZnO nanoparticles were synthesized by hydrothermal method. The particle size of the ZnO is found to be close to 20 nm. The prepared nanocomposites were subjected to optical and electrical characterization studies. The optical properties of PS / ZnO nanocomposite films were investigated using UV-Vis spectroscopy and band gap of the films were found to decrease with increase in the filler concentrations. The dielectric constant and dielectric loss of the compound showed almost the same

behavior and both decrease with increase in frequency. The fluorescence intensity was also found to increase with increase in filler concentration.

## **References**

- [1] Shah A H, Rizvi T Z, Measurement, 2013, 46, 1541.
- [2] Lahelin M, Annala M, Nykanen A, Ruokolainen J, Seppala J, Comp. Sci. Tech., 2011, 71,5, 900.
- [3] Erasto Armando Zaragoza-Contreras, Claudia Alejandra Hernandez-Escobar, Alfredo Navarrete-Fontes, Sergio Gabriel Flores-Gallardo, Micron, 2011, 42, 263.
- [4] Maxim N Tchoul, Matthew Dalton, Loon-Seng Tan, Hongchen Dong, Chin MiongHui, Krzysztof Matyjaszewski, Richard A Vaia, Polymer, 2012, 53, 79.
- [5] Tanvir Arfin, Faruq Mohammad, Jour. Indus. Engg. Chem. 2013, 19, 2046.
- [6] Tripathi S K, Ramneek Kaur, Jyothi, Optics Commun., 2015, 352, 55.
- [7] Chen G H, Wu D J, Weng W G, J. Appl. Polym. Sci. 2001, 82, 2506.
- [8] Ma D, Hugener T A, Siegel R W, Christerson A, Martensson E, Onneby C, Schadler L, Nanotechnology, 16, 2005, 724.
- [9] Zhang M, Singh R, Materials Letters, 2004, 58, 408.
- [10] Haggemueller R, Guthy C, Lukes J R, Fisher J E, Winey K I, Macromolecules 2007, 40, 2417.
- [11] Cho B, Kim T W, Choe M, Wang G, Song S, Lee T, Org Electron 2009, 10, 473.
- [12] Velayutham T S, Abd Majid W H, Gan W C, Khorsand Zak A, Gan S N, J. Appl. Phys. 2012, 112; <http://dx.doi.org/10.1063/1.4749414>.



- [13] Xiong M N, Gu G X, You B, J. Appl. Polym. Sci. 2003, 90, 1923.
- [14] Kokabi M, Sirousazar M, Hassan Z, Eur. Polym. J. 2007, 43, 773.
- [15] Lee J, Bhattacharya D, Easteal A J, Metson J B, Curr. Appl. Phys. 2008, 8, 41.
- [16] Nenna G, De Girolamo A Del Mauro, Massera E, Bruno A, Fasolino T, Minarini C, J. Nano. Mat. 2012, doi: 10.1155/2012/319398.
- [17] Chae D W, Kim B C, Polymer. Adv. Tech., 2006, 16, 846.
- [18] Urbach F, Phys. Rev. 1953, 92, 1324.
- [19] El-Khodary A, Physica B: Condensed Matter. 2010, 405, 16, 4301.

.....❧.....

## SYNTHESIS AND CHARACTERIZATION OF POLYSTYRENE (PS) / ZnSe NANOCOMPOSITES

Contents	7.1	<i>Introduction</i>
	7.2	<i>Preparation of PS / ZnSe Nanocomposites</i>
	7.3	<i>Results and Discussions</i>
	7.4	<i>Conclusion</i>

### 7.1 Introduction

Conducting polymer composites (CPC) made by the incorporation of conducting fillers like carbon fibres [1], metallic particle fillers [2] carbon nanotubes [3,4] have been extensively investigated. Nano composites based on semiconductor nano materials in polymer systems show peculiar electronic and optical properties [5]. It is advantageous to embed the semiconductor nanoparticles like metal selenides in thin polymer films because the polymer matrix serves as a medium to assemble the nanoparticles and stabilize them against aggregation [6,7]. Metal selenide nano-particles heterogeneously distributed in the polymer matrix can improve its dielectric behaviour.

The choice of selecting the host polymer matrix mainly depends on its processability, electrical, thermal and optical properties [8].

Thermoplastics like polyvinyl chloride (PVC) [9], poly butylene terephthalate (PBT) [10], polycarbonate (PC) [11] etc. were used as matrix for various investigations. Polystyrene (PS) is a rigid transparent thermoplastic with good electrical insulation properties. It can be insitu polymerized with nano particles to obtain a uniform thin film on casting. Exfoliated polystyrene- nano clay composites [12] and polystyrene-multiwalled carbon nanotube (MWCNT) [13] have been studied for thermal and electrical features.

The electrical conductivity of carbon nanotubes in insulating polymers has also been a topic of considerable interest. The percolation threshold for conduction is about 1.5 wt% of MWCNTs in the composites, and a maximum conductivity of about  $1 \text{ Sm}^{-1}$  can be achieved [14]. Potential applications include electromagnetic interference shielding, transparent conductive coatings, electrostatic dissipation, supercapacitors, electromechanical actuators and various electrode applications. Zinc selenide (ZnSe) thin films were deposited on different substrates like glass, stainless steel, ITO for solar cell applications [15-17]. Zinc Selenide is an important direct band gap material used for fabricating laser diodes [18]. Polyvinyl alcohol (PVA) - ZnSe based nanocomposites were reported for their nonlinear optical effects [19].

This chapter reports the preparation and characterization of nanocomposites of polystyrene with ZnSe nano fillers at varying loading levels and to evaluate the electrical properties offered by the nanofiller. The mechanical and optical properties with increasing ratios of ZnSe (1-4%) to virgin PS were also adjudged.

## **7.2 Preparation of PS / ZnSe Nanocomposites**

To synthesize insitu polymerized nanocomposite, the required amount of synthesised nano ZnSe was first dispersed in purified styrene monomer (for 1wt % nanocomposite, 0.4gm of ZnSe in 50 ml of styrene). The nano ZnSe-styrene mixture was ultrasonicated for one hour at room temperature to obtain good dispersion. The mixed solution was then transferred to a three necked round bottom glass reactor. Reflux condenser and nitrogen inlet were connected to the reactor and the assembly was kept on a hot plate magnetic stirrer. This solution was then polymerized at 80<sup>0</sup>C in the three necked reactor for 5hrs after adding initiator-benzoyl peroxide. The polymerizing PS-ZnSe mixture was then poured into a Teflon coated mould and kept in air oven to obtain a thin film of approximately 0.1-0.25 mm thickness.

## **7.3 Results and Discussion**

### **7.3.1 Scanning Electron Microscopy (SEM)**

The size and morphology of the synthesized products were determined at 15 kV by scanning electron microscope (SEM). Fig.7.1 shows the SEM images of PS / ZnSe film, showing the dispersion of ZnSe in the polystyrene. The size was about 50 nm, and the shape, spherical. A homogeneous dispersion is observed.

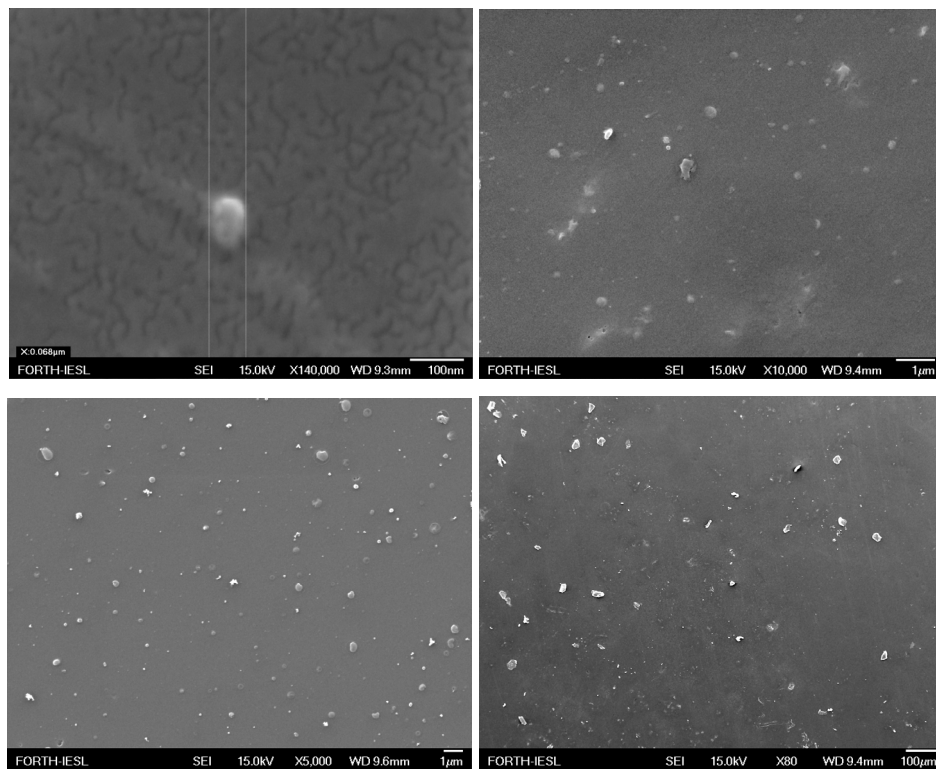


**Fig.7.1: SEM Micrograph of PS / 4% ZnSe nanocomposites under different magnification**

### 7.3.2 UV-Vis Spectroscopy

UV analysis of PS / ZnSe nanocomposites was done by UV-1800 Shimadzu UV-VIS spectrophotometer and is shown in Fig.7.2. The spectra show large transparency window between 200 nm and 1000nm. Absorption peaks are noticed between 200nm and 300nm for all samples. It is observed that the intensity of the absorption peak is increased with increase in filler concentration.

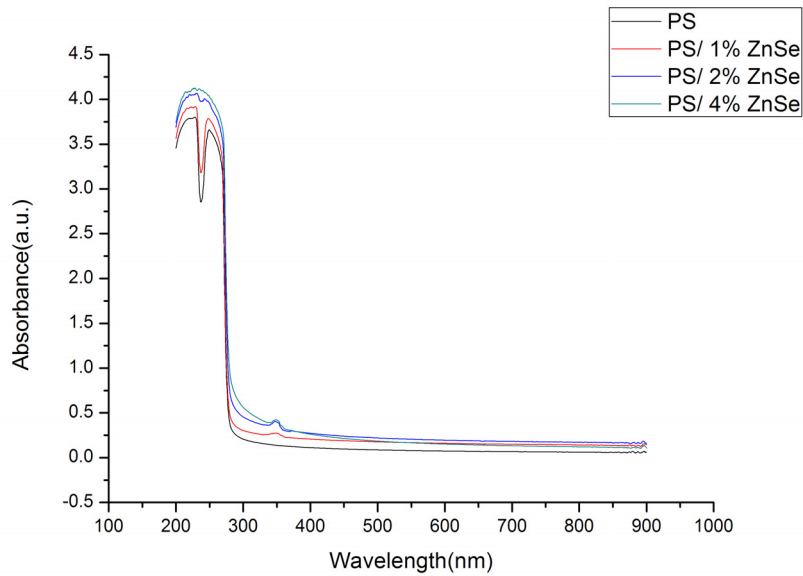


**Fig.7.2: Absorbance as a function of wavelength of ZnSe doped PS films at different concentrations**

The bandgap of the prepared nanocomposites has been determined using the Tauc-relation and is shown in Fig.7.3. Urbach plot of the nanocomposites is shown in Fig.7.4. The estimated band gap energy and Urbach energy of pure PS and PS / ZnSe nanocomposites are given Table 7.1. From the table it is evident that the bandgap energy decreases whereas the urbach energy increases with increase in the filler concentrations.

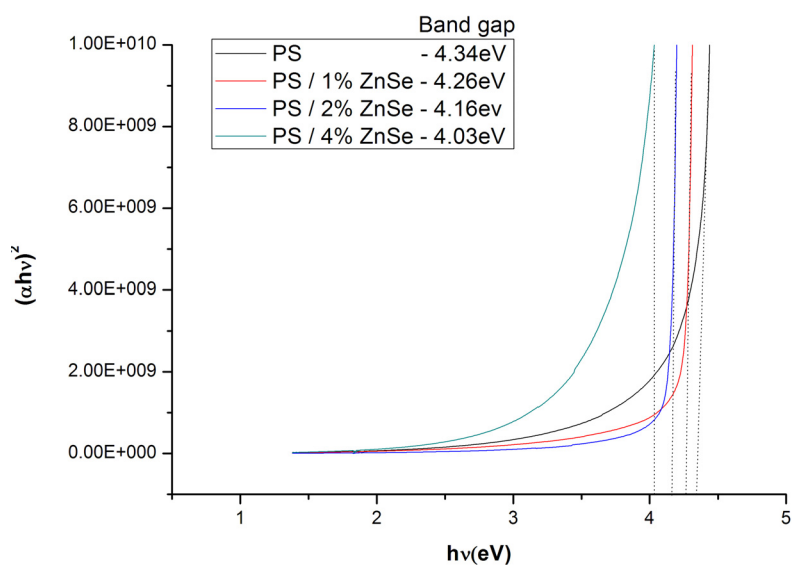


**Fig. 7.3: Tauc – Plot of PS / ZnSe nanocomposites**

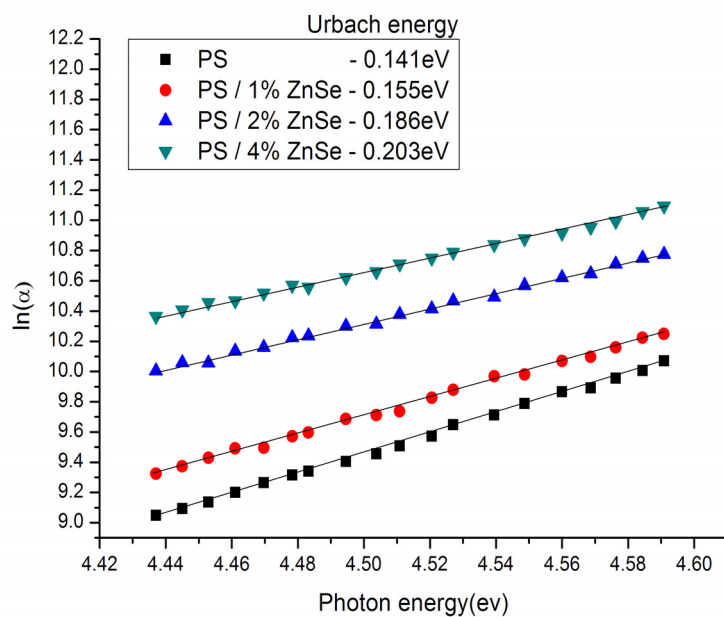


**Fig.7.4. Relation between  $\ln(\alpha)$  and  $h\nu$  for PS at different ZnSe concentration.**

**Table 7.1: Direct optical energy gap and Urbach energy of PS doped with ZnSe.**

Samples	Band Gap in eV ( $E_g$ )	Urbach Energy in eV ( $E_u$ )
Pure	4.34	0.141
EVA / 1% CdSe	4.26	0.155
EVA / 2% CdSe	4.16	0.186
EVA / 4% CdSe	4.03	0.203

### 7.3.3 Raman Spectra

Fig.7.5. shows the Raman spectra of polystyrene (PS) and PS / 1% ZnSe, PS / 2% ZnSe, PS / 4% ZnSe nanocomposites.

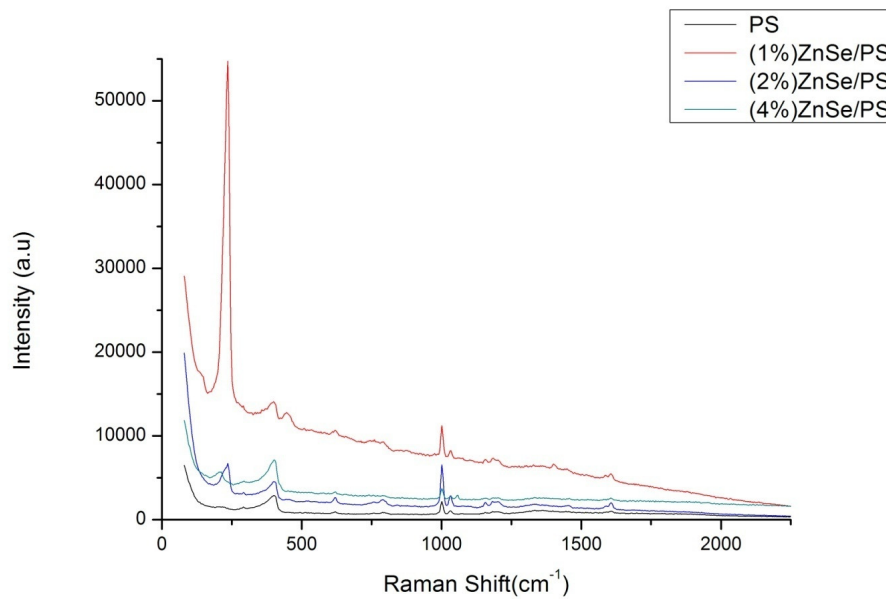


**Fig.7.5: Raman spectra of pure PS and PS / ZnSe nanocomposites**



The peaks at  $250\text{cm}^{-1}$  and  $415\text{cm}^{-1}$  are attributed to the scattering of the nano ZnSe by longitudinal optical (LO) photon and transverse optical photon modes [20,21] respectively. The other shifts observed correspond to polystyrene. The ring deformation of polystyrene matrix corresponds to  $621\text{cm}^{-1}$  and  $615\text{cm}^{-1}$  peaks. The shift in the peak at  $1001\text{cm}^{-1}$  to  $991\text{cm}^{-1}$  for pure and ZnSe filled polystyrene corresponds to aromatic ring breathing. The peaks at  $1607\text{cm}^{-1}$  and  $1617\text{cm}^{-1}$  in the nanocomposite are attributed by the C=C aromatic ring stretching.

#### 7.3.4 Laser induced fluorescence (LIF)

The fluorescence spectra of the composites have been obtained with a nanosecond excimer laser (Lambda Physik EMG 201 MSC) operating at 248 nm in ambient atmosphere (Flaser  $\sim 5\text{ mJ cm}^{-2}$ ). The laser beam was focused perpendicularly onto the sample at a  $1.5\text{ mm}^2$  surface. The spectrum was recorded on an ICCD –Andor camera, interfaced to a PC. Cut-off filters were used to block any probe beam scattered light. Fig.7.6. shows the LIF spectra of the nanocomposites. From the figure one can easily find that the fluorescence intensity increases with increase in filler concentration which means that as concentration of the filler increases, the molecular electron density of the pristine sample becomes stabilized.

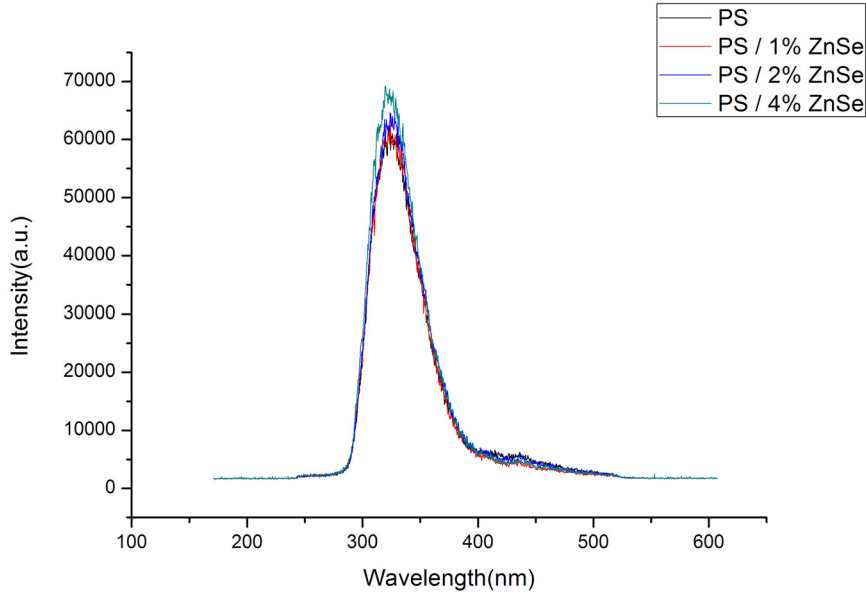


**Fig.7.6: LIF spectra of pure PS and PS / ZnSe composites**

### 7.3.5 Electrical Studies

The dielectric properties of PS/ZnSe nanocomposite in the present work were measured in a range of 100 Hz to 5 MHz using HIOKI 3532-50 LCR HITEST2ER. The dielectric parameter as a function of frequency is described by the complex permittivity

$$\epsilon^i = \epsilon' - j\epsilon'' \dots\dots\dots (7.1)$$

where  $\epsilon'$  is the real part for energy storage and  $\epsilon''$  is the imaginary part for energy loss. The measured capacitance C is used to calculate the dielectric constant using the equation

$$\epsilon' = \frac{Cd}{\epsilon_0 A} \dots\dots\dots (7.2)$$

where  $d$  is the thickness,  $A$  is the area and  $\epsilon_0$  is the permittivity of free space.

Fig.7.7.a-c shows the variation of relative permittivity (real part) of nanocomposites with frequency for different temperatures. From the figure, it is clear that the effective permittivity of unfilled PS and PS / ZnSe composite increases with decreasing frequency. An increase in the effective permittivity with filler concentration is also noted may be due to the introduction of ZnSe. As the filler concentrations increase the number of nanoparticles in the matrix increases thereby increasing permittivity.

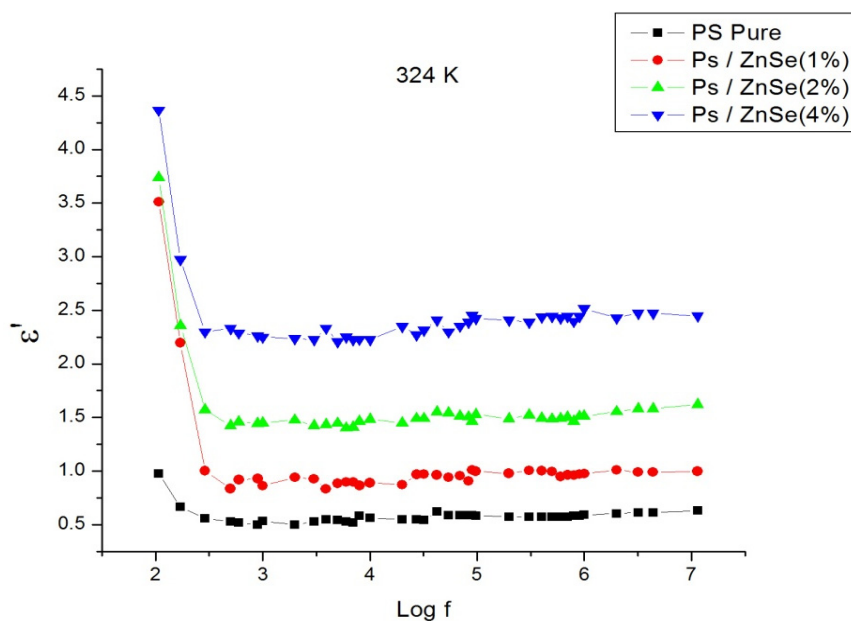


Fig.7.7a: Variation of dielectric constant with frequency at 324 K

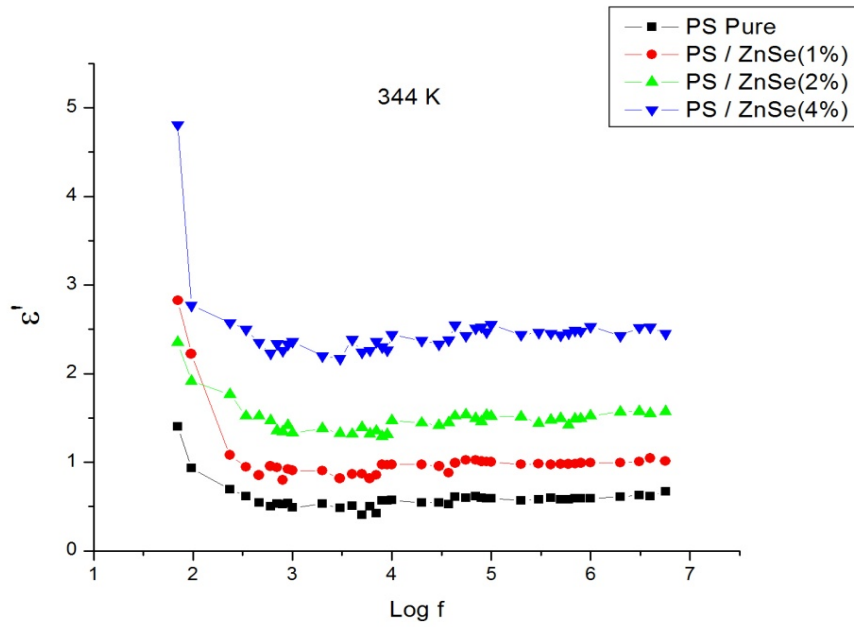


Fig.7.7b: Variation of dielectric constant with frequency at 344 K

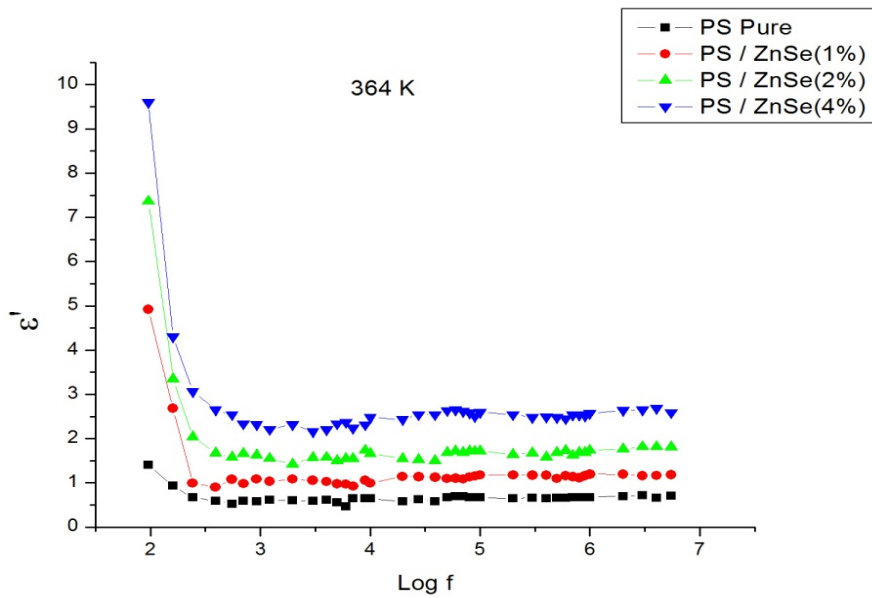
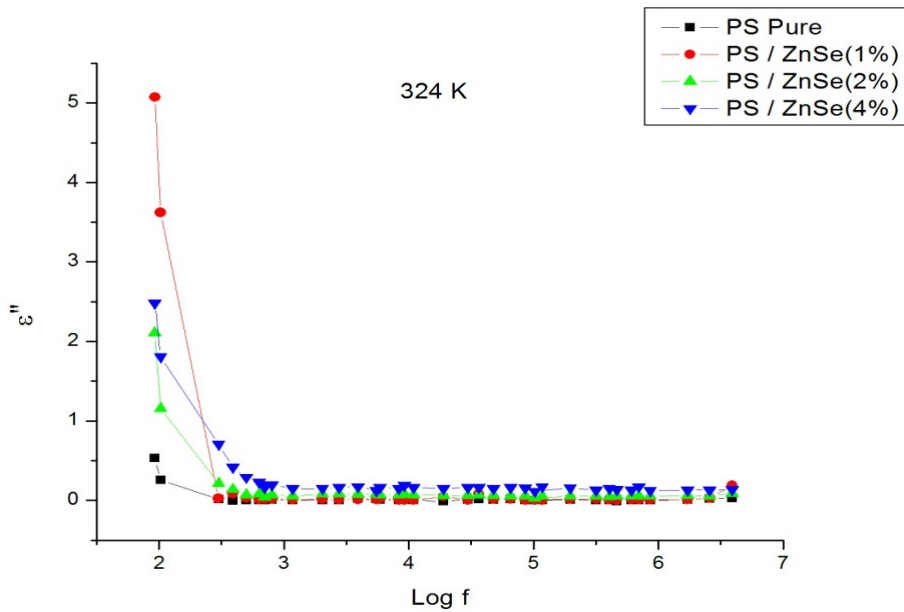


Fig.7.7c: Variation of dielectric constant with frequency at 364 K

The dielectric loss ( $\epsilon''$ ) is described by

$$\epsilon'' = \epsilon' \tan \delta \dots\dots\dots(7.3)$$

The variation of relative permittivity (imaginary part) of PS/ZnSe nanocomposites with frequency at different temperatures are presented in Fig.7.8a - c. From the figure it is clear that when ZnSe nano-filler concentration increases, the dielectric loss is also increases.



**Fig.7.8a: Variation of dielectric loss with frequency at 324 K**

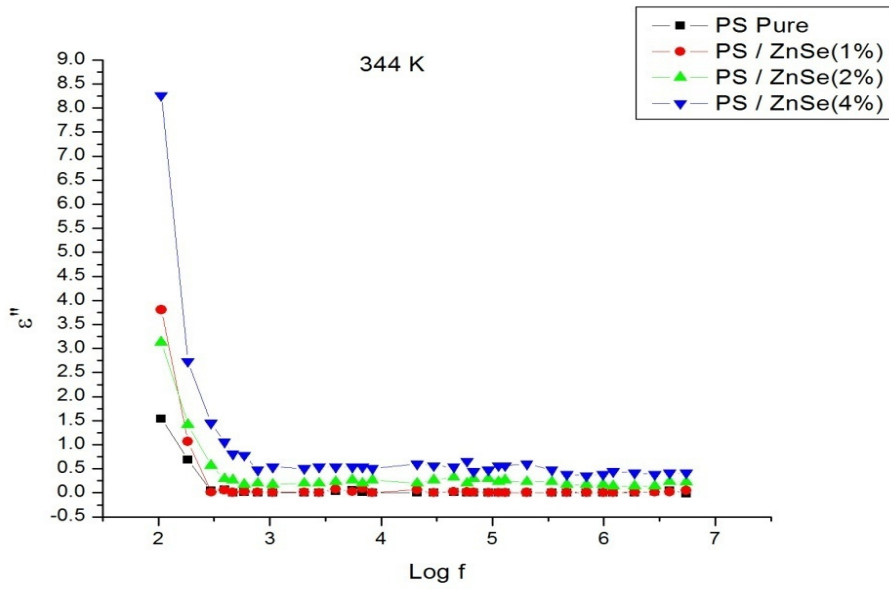


Fig.7.8b: Variation of dielectric loss with frequency at 344 K

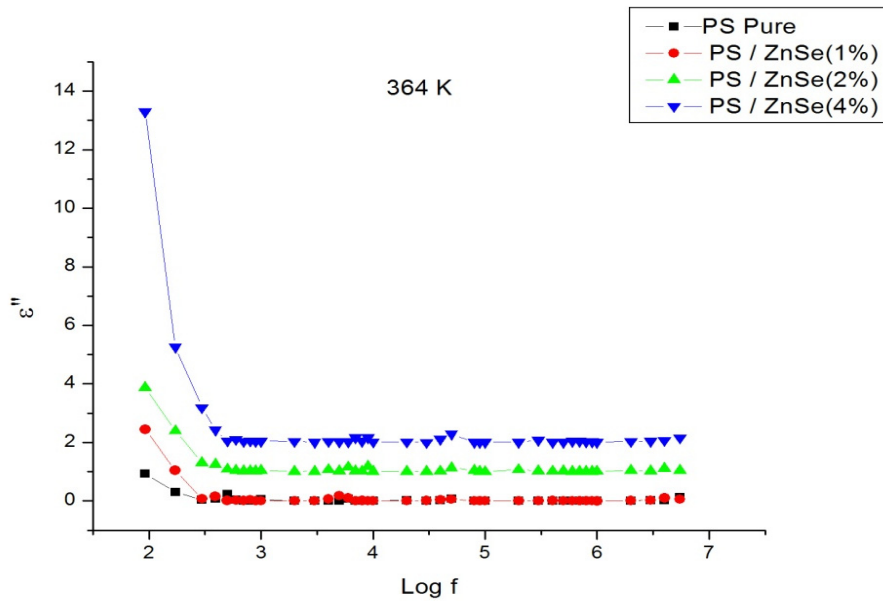


Fig.7.8c: Variation of dielectric loss with frequency at 364 K

### 7.3.6 Thermal Studies

The TGA/DTA analyses of PS / ZnSe were carried out using a Perkin Elmer Simultaneous Thermal Analyser – STA 6000. The samples were heated in the temperature range between 40°C and 700°C at a heating rate of 10°C/min under N<sub>2</sub> atmosphere with a nitrogen flow rate of 20 ml/min. The TGA curve and DTA curve obtained for pure polystyrene and PS / ZnSe nanocomposite with different loading levels are shown in Fig.7.9 a-d.

TGA measures the change in weight of samples as it is heated. Clearly, there is only one major weight loss step. For pure PS, degradation commences near 290°C and continues rapidly until about 450°C. Hence it is stable upto 290°C in nitrogen atmosphere. From thermograms, it is clear that the thermal stability of PS / ZnSe nanocomposite is greater than that of virgin PS, and among nanocomposites, it increases with increase in loading level. DTA signal gives a peak in the endothermic direction. From the Fig. 7.9a, it is observed  $\Delta T$  endo down peak at 416°C and the onset of this peak is the transformation temperature and is at 360°C. The peak of DTA curve gives the temperature corresponding to maximum degradation ( $T_{max}$ ).

The significant improvement in the resistance to thermal decomposition of the nanocomposites may be attributed to the formation of thermal insulating and low permeable char residue of ZnSe and polystyrene during decomposition at the outer surface of the nanocomposite which acts as a protective barrier reducing the heat and mass transfer between the flame and polystyrene [22]. The presence of inorganic nanofiller could make the polymer resistant from getting volatilized and restrict polymer

chain flexibility for thermal conduction. ZnSe's heat sink property and the ability to reduce the defects of organic structure would have caused the enhancement in thermal resistance [23].

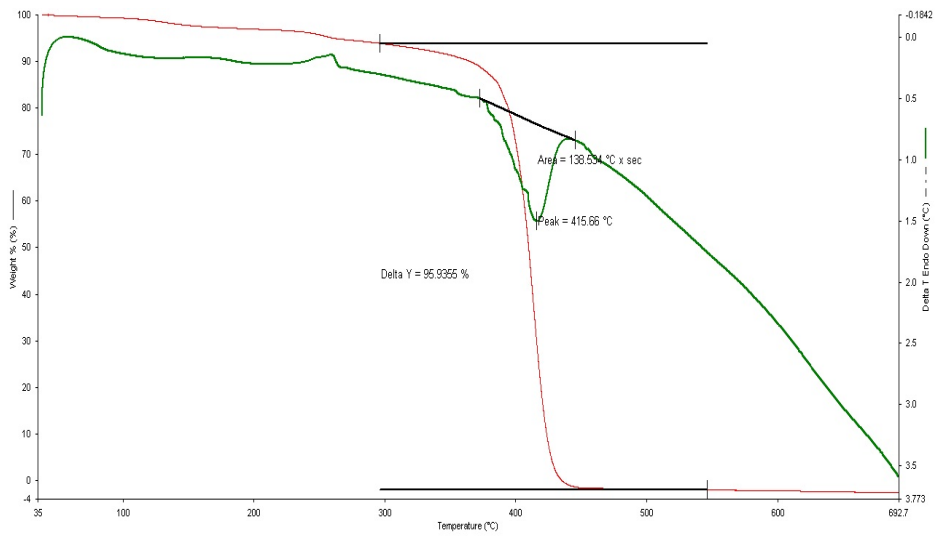


Fig.7.9a: TGA/DTA curves of pure PS

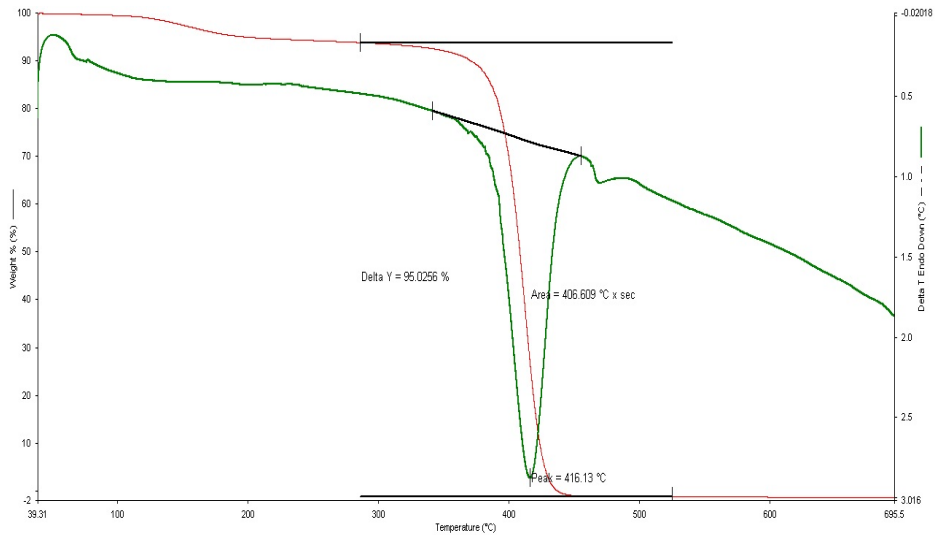
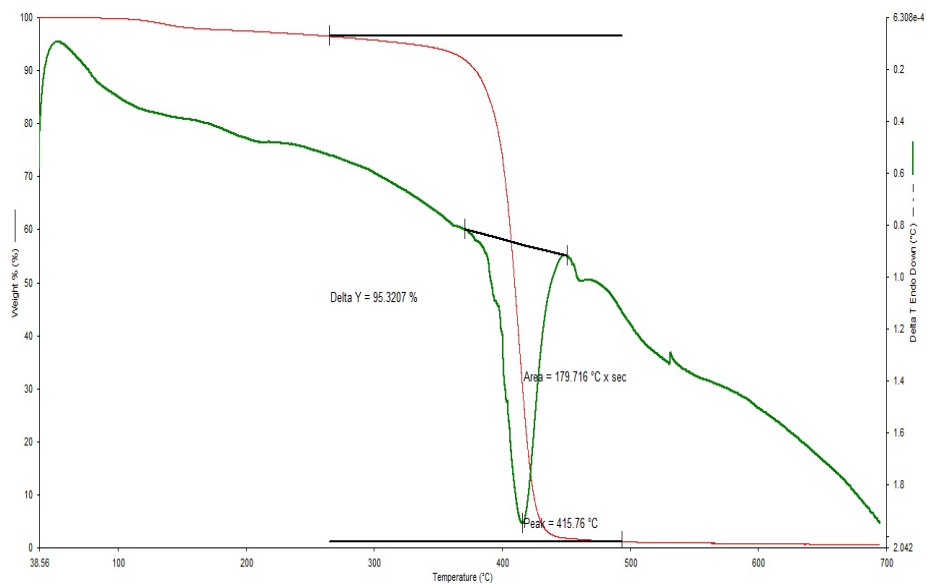
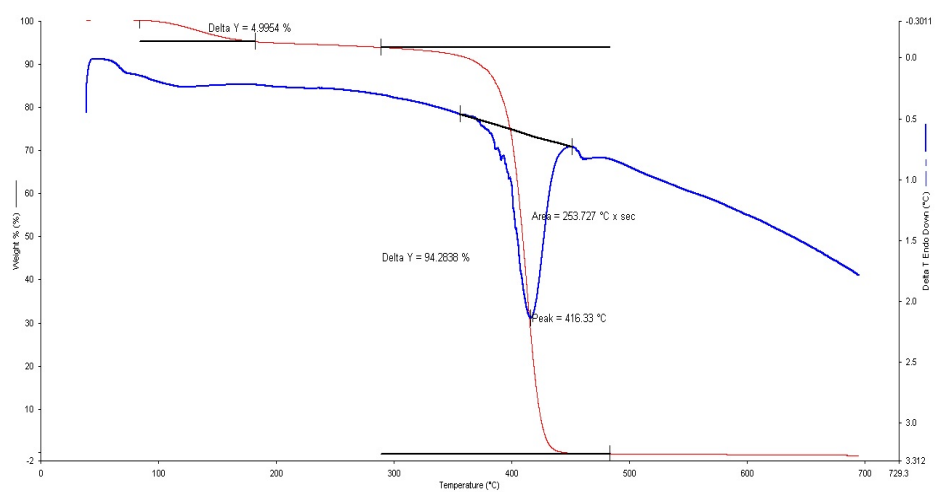


Fig.7.9b: TGA/DTA curves of PS / 1% ZnSe





**Fig.7.9c: TGA/DTA curves of PS / 2% ZnSe**



**Fig.7.7d: TGA/DTA curves of PS / 4% ZnSe**

### 7.3.7 Photopyroelectric Studies

Thermal parameters of PS and PS / ZnSe composites have been determined by photopyroelectric technique using a sample of average

thickness 0.94 mm. Using the data of PPE signal phase and amplitude, the values of the thermal diffusivity ( $\alpha$ ) and thermal effusivity ( $e$ ) were determined. From the measured values of  $\alpha$  and  $e$ , the thermal conductivity ( $k$ ) and heat capacity ( $C_p$ ) of samples are calculated and tabulated in the Table 7.2.

**Table 7.2: Thermal parameters of PS & PS / ZnSe composites**

Sample	Thermal effusivity	Thermal diffusivity	Thermal conductivity	Sp.Heat capacity
	(Ws <sup>1/2</sup> /m <sup>2</sup> K)	(X 10 <sup>-7</sup> m <sup>2</sup> /s)	(W/mK)	(J/KgK)
PS	961	0.59136	0.704	1250
PS /1% ZnSe	740	0.5374	0.517	1010
PS /2% ZnSe	720	0.5346	0.502	986
PS /4% ZnSe	707	0.5159	0.484	985

## 7.4 Conclusion

Polystyrene / zinc selenide nanocomposites have been successfully prepared using insitu polymerization method. The homogeneity of the dispersion of the ZnSe in the matrix was confirmed by a scanning electron microscope. It was found that dielectric constant decreases with increasing frequency and almost remained constant on further increase in frequency. Onset decomposition temperature of the samples is found to increase with increase in filler concentration. Fluorescence intensity has also been found to increase with increase filler concentration. Thermal conductivity and specific heat capacity decrease with increase in filler concentration.

## References

- [1] Bardash L, Boiteux G, Seytre G, Hakme C, Darere N, Rybak A, et al. *e-Polymers* (2008) 155 1
- [2] Micusik M, Omastova M, Krupa I, Prokes J, Pissis P, Logakis E, et al. *J. Appl. Polym. Sci.* (2009) 113, 2356.
- [3] Sinsawat A, Anderson K L, Vaia R A, Farmer B L, *J. Polymer. Sci. B Polym. Phys.* 41 (2003) 3272.
- [4] Xu W, Ge M, Pan W P. *J. Therm. Anal. Calorim.* (2004)78:91.
- [5] Roy B, Roy S, Chakravorty D, *J. Mater. Res.* 9 (1994) 2677.
- [6] Boyd R W, Gehr R J, Fisher G L, Sipe J E, *Pure Appl. Opt.* 5 (1996) 505.
- [7] Takele H, Greve H, Pochstein C, Zaporojtchenko V, Faupel F, *Nanotechnology* 17 (2006) 3499.
- [8] Baibarac M, Baltog I, Lefrant S, Mevellec J Y, Chauvet O, *Chem. Mater.* 15 (2003) 4149.
- [9] Guo M, Chen J, Li J, Tao B, Yao S, *Anal. Chem. Acta.*532 (2005) 71.
- [10] Chang J H, Mun M K, Kim J C. *J Appl. Polym. Sci.* (2007)106:1248.
- [11] Bohning M, Goering H, Hao N, Mach R, Oleszak F, Schonhals A, *Rev. Adv. Mater. Sci.* (2003) 5:155.
- [12] Uthirakumar P, Nahm K S, Hahn Y B, Lee Y S. *Eur. Polym. J.* (2004) 40:2437.
- [13] Junrong Yu, Kangbo Lu, Erwan Sourty, Nadia Grossiord, Cor E Koning, Joachim Loos, *Carbon* 45, 15 (2007) 2897.
- [14] Junrong Yu, Kangbo Lu, Erwan Sourty, Nadia Grossiord, Cor E Koning, Joachim Loos, *Carbon* 45, 15 (2007) 2897.

- [15] Hankare P P, Chate P A, Chavan P A, Sathe D J, J. Alloys Compd. 461 (2008) 623.
- [16] Kumaresan R, Ichimura M, Arai E, Thin Solid Films 414 (2002) 25.
- [17] Chaparro A M, Maffiotte C, Gutierrez M T, Herrero J, Thin Solid Films 358 (2000) 22.
- [18] Harris L M C, Chang Y H, Chen Y F, Hsu J W, Lin J M, Cho W C, Appl. Phys. Lett. 70 (1997) 2256.
- [19] Soliman Selim M, Seoudi R, Shabaka A A, Materials Letters 59 (2005) 2650.
- [20] Lu G, An H, Chen Y et.al Jour. Of Crystal Growth, 2005, 274, 530.
- [21] Taj Muhammed Khan, Tayyaba Bibi, Chin. Phys. B, 2012, 21,9, 097303
- [22] Blumstein A, Jour. of Polymer Sci. A, 1965,3,2665
- [23] Lee C W, Renaud C, Hsu C S, Nguyen T P, Nanotechnology, 2008, 19,455202.

.....✪✪.....

## SYNTHESIS AND CHARACTERIZATION OF POLYSTYRENE (PS) / CdSe NANOCOMPOSITES

Contents	8.1 <i>Introduction</i>
	8.2 <i>Experimental Procedure</i>
	8.3 <i>Results and Discussions</i>
	8.4 <i>Conclusion</i>

### 8.1 Introduction

In this chapter, we used polystyrene (PS), rigid commercial thermoplastic with good electrical insulation properties as matrix. It is a transparent plastic with ease of processability such that it can be insitu polymerized with nano particles to obtain a uniform thin film on casting. Exfoliated polystyrene- nano clay composites [1], polystyrene- multiwall carbon nanotube (MWCNT) [2] have been studied for thermal and electrical features. Vollenberg and Heikens [3] performed a wide range of tests on composites with matrices made of polystyrene, styrene–acrylonitrile copolymer (SAN) and nano-sized glass or alumina inclusions.

Cadmium selenide (CdSe) and its nanoparticles attracted researchers because of their unique optical properties, including extended optical absorption in the ultra-violet region, bright photoluminescence(PL),

narrow emission band, size tunable PL and photostability [4-7], and as promising PL materials for optical electronic device applications [8-9]. The room temperature electrical properties of poly(butyl acrylate)-CdSe nanocomposites have been investigated for their bright green photoluminescence [10].

In this chapter, the effect of CdSe on the electrical, thermal and optical properties of polystyrene has been studied.

## **8.2 Experimental Procedure**

### **8.2.1 Preparation of PS / CdSe Nanocomposite**

To synthesize insitu polymerized nanocomposite, the required amount of nano CdSe was first dispersed in the purified styrene monomer (for 2 wt percentage nanocomposite, 0.8 gm of CdSe in 50 ml of styrene). The CdSe-styrene mixture was ultrasonicated for one hour at room temperature to obtain good dispersion. This solution was then polymerized at 80<sup>0</sup>C in the three necked reactor for 5hrs after adding the benzoyl peroxide initiator. The polymerized PS / CdSe nanocomposite was then poured into the teflon coated mould and kept in air oven to obtain thin film of approximately 0.1 mm thickness.

## **8.3 Results and Discussions**

### **8.3.1 Scanning Electron Microscopy (SEM)**

Fig.8.1 shows the SEM micrographs of PS / CdSe composite surfaces at different magnifications. A uniform distribution of CdSe with clear particle profiles and interface boundary was seen on the surface of polystyrene. At higher magnification, the size and shape of the particles

embedded in the matrix were visible and found to be around 50 nm. It is in good agreement with the result obtained from transmission electron microscopy (TEM) analysis.

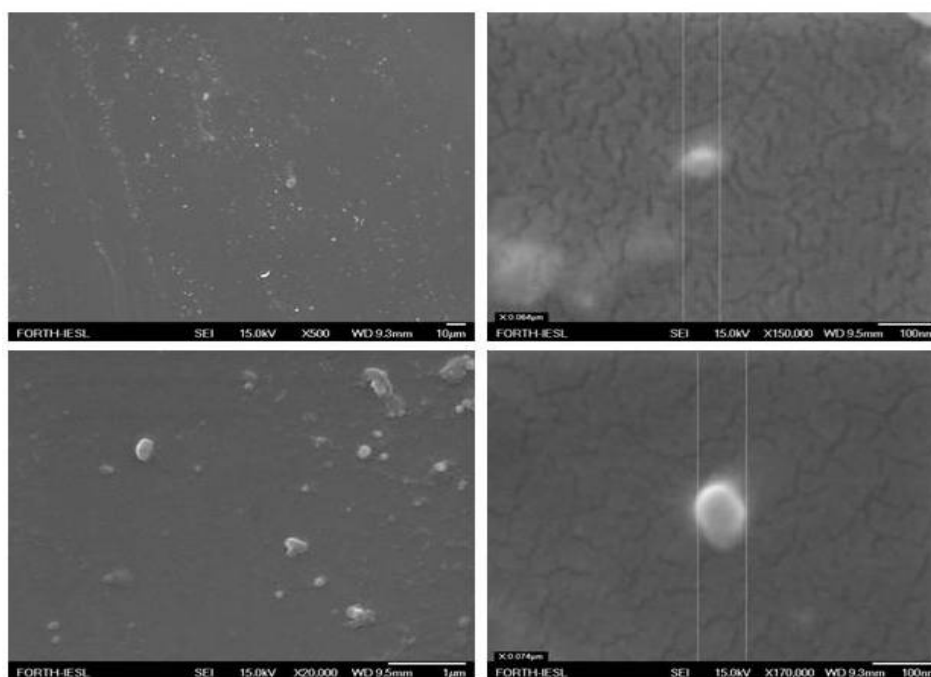


**Fig.8.1: SEM Micrographs of PS / CdSe nanocomposite.**

### **8.3.2 Transmission Electron Microscopy (TEM)**

TEM is a vital tool for quantitative measures of grain size and morphology. TEM of CdSe nanoparticles are shown in Fig.8.2a-b. The images reveal that the shape of the particles is almost spherical and the average size of particles is about 50 nm. The dark images show that nanoparticles are solid in structure.

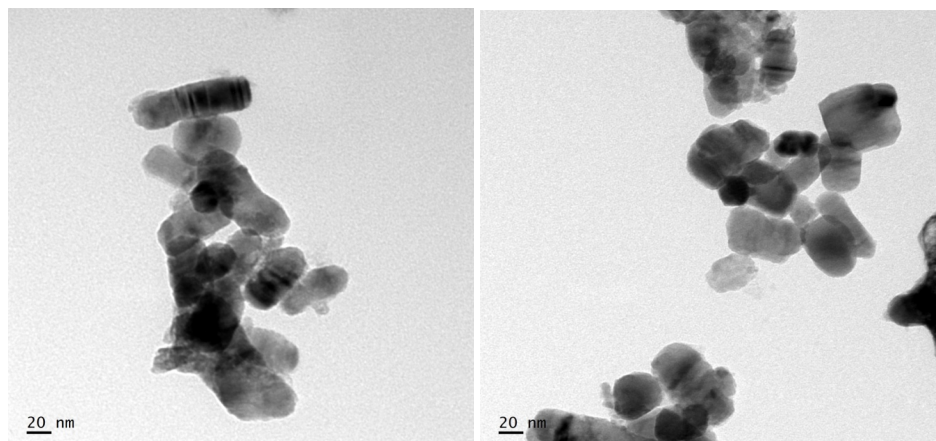


Fig. 8.2a-b: TEM images of CdSe nanoparticles

### 8.3.3 UV-Vis Analysis

The optical absorption spectra of the samples were recorded in the region 200 to 700 nm, using a UV-1800 Shimadzu spectrophotometer and are shown in Fig.8.3.

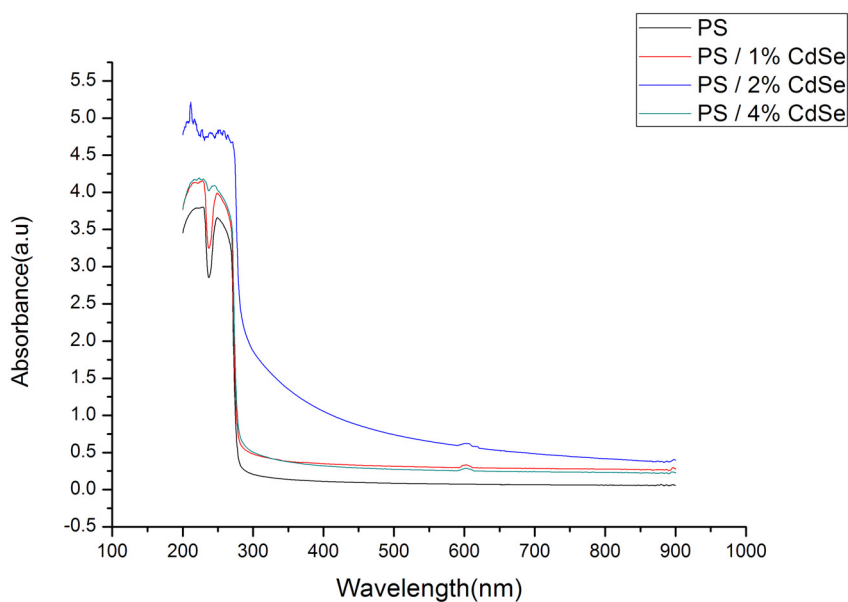
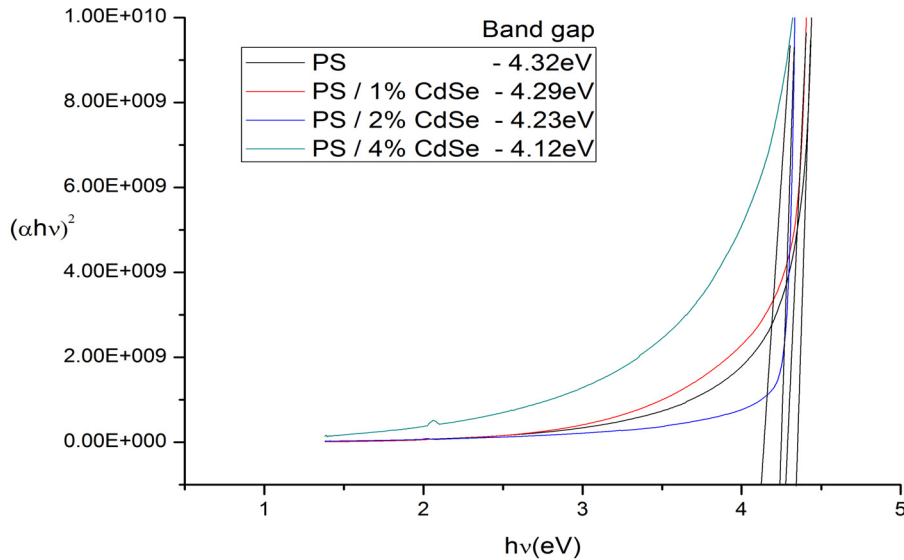


Fig.8. 3: UV –Vis Absorption spectra of pure PS and PS / CdSe composites



It is observed from the spectra that samples have a large transmission window starting from 275 nm without a specified absorption peak. The UV cut-off wavelength is around 275nm for all the samples and the intensity of UV absorption increases with the increase of CdSe content in the composite. The presence of nano sized CdSe enhances the uv absorption so that PS possesses a better uv shielding properties.

Fig.8.4 shows Tauc-plot for allowed energy band transitions. The extrapolation of the linear portion of the plot on the photon energy axis provides the optical energy gap. The curve was characterized by the presence of an exponentially decaying tail at low photon energy. It is evident from the Tauc plot that  $E_g$  (Band Gap) is decreased with increase in dopant concentration. It may be due to the modification in the electronic structure of the PS matrix due to the appearance of various polaronic and defect levels due to CdSe nanoparticles [11]. The decrement in the optical band gap may be attributed to the generation of excess charge carriers and formation of charge transfer complexes. When dopant concentration is increased, the dopant molecules start bridging the gap separating the two localized states and lowering the potential barrier between them, thereby facilitating the transfer of charge carriers between two localized states.



**Fig. 8.4: Tauc-plot of PS with different CdSe concentration**

The Urbach plot is presented in Fig.8.5, in which the natural logarithm of absorption coefficient,  $\alpha$  is plotted as a function of photon energy ( $h\nu$ ). The magnitudes of the Urbach energy,  $E_u$  were estimated by taking the reciprocal of the slopes of the linear portion of these curves. The values of optical band gap and Urbach energy for nanocomposites are tabulated in Table 8.1. The  $E_u$  values are found to be increasing with the concentration of CdSe in PS. The increase of  $E_u$  values by increasing the concentration of CdSe in the nanocomposites may be due to the effect of internal potential fluctuation associated with the structural disorder [12].

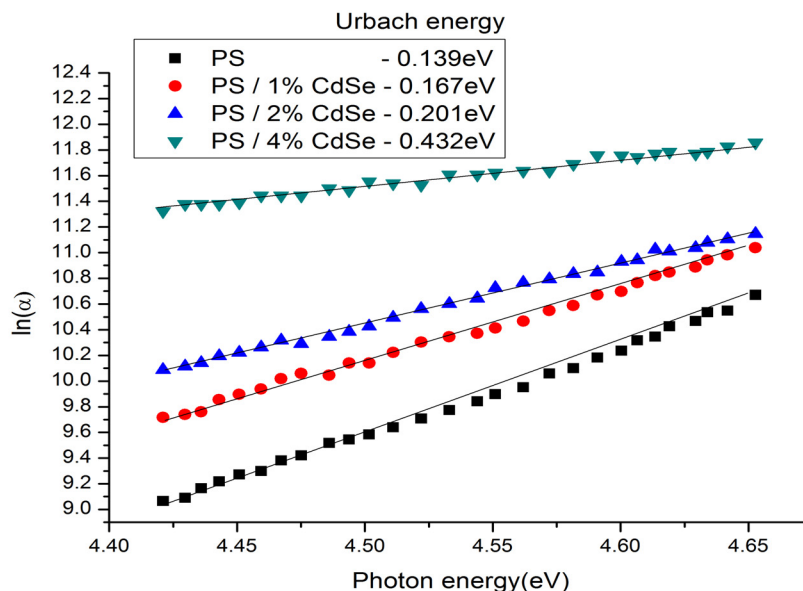


Fig.8.5: Relation between  $\ln(\alpha)$  and  $h\nu$  for PS and PS / CdSe composites

Table 8.1: Band gap ( $E_g$ ) and Urbach energy ( $E_u$ ) values of PS / CdSe nanocomposites

Samples	$E_g$ (eV)	$E_u$ (eV)
Pure PS	4.32	0.139
1% PS / CdSe	4.29	0.167
2% PS / CdSe	3.23	0.201
4% PS / CdSe	4.12	0.432

### 8.3.4 Raman Studies

Fig. 8.6 shows the Raman spectra of polystyrene (PS) and PS / CdSe composites at different filler concentrations. Appearance of the peaks at  $210\text{cm}^{-1}$  and  $401\text{cm}^{-1}$  in the nanocomposite corresponds to the CdSe vibration. The peaks are related to the scattering of the nanoCdSe by

longitudinal optical (LO) phonon and its first overtone. The ring deformation of polystyrene corresponds to  $621\text{ cm}^{-1}$  and  $615\text{ cm}^{-1}$  peaks of the composite. Weak vibrations of C-C bonds give peak at  $800\text{ cm}^{-1}$ . The shift in the peak at  $1001\text{ cm}^{-1}$  to  $1012\text{ cm}^{-1}$  for pure and CdSe filled polystyrene corresponds to aromatic ring breathing. The peaks at  $1607\text{ cm}^{-1}$  and  $1618\text{ cm}^{-1}$  in the nanocomposite are attributed to the C=C aromatic ring stretching.

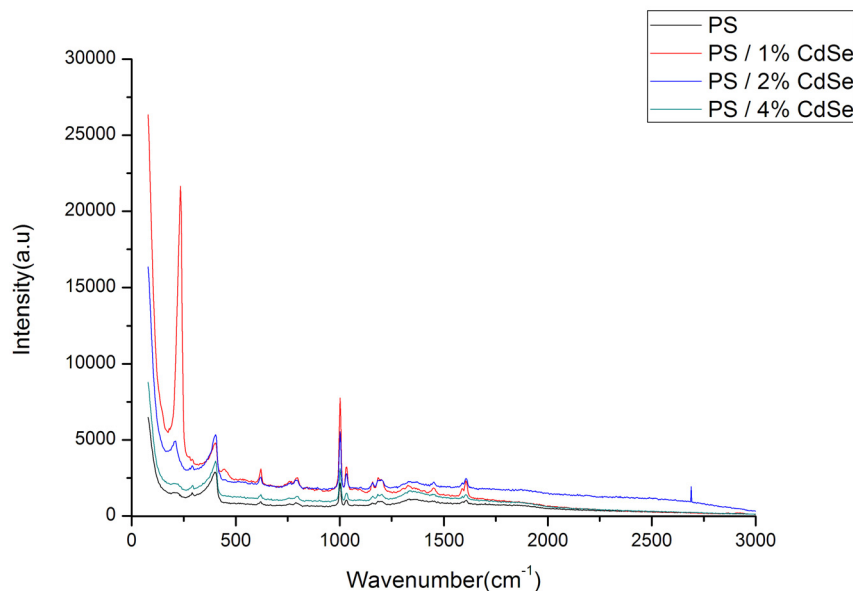
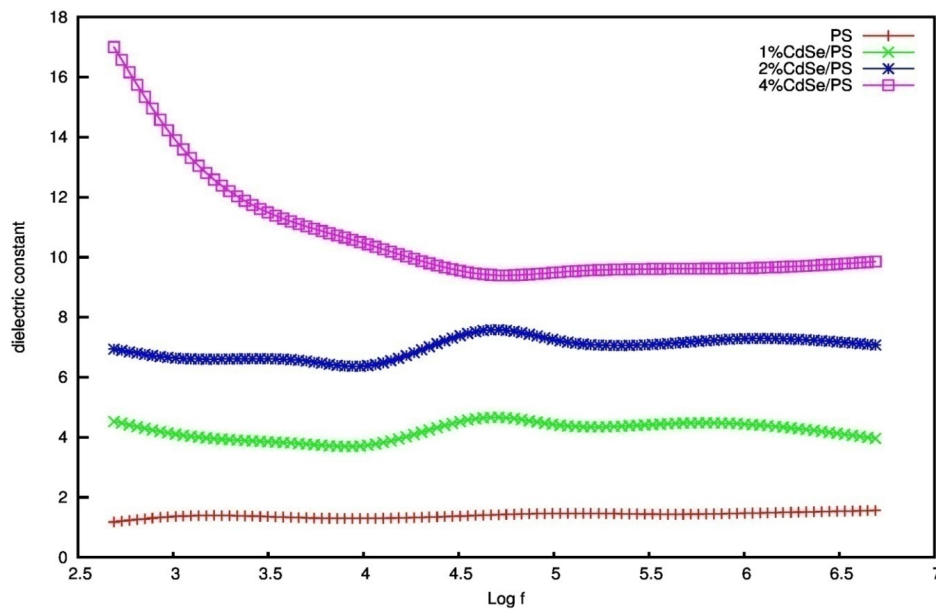


**Fig.8.6: Raman spectra of polystyrene (PS) and PS / CdSe composites**

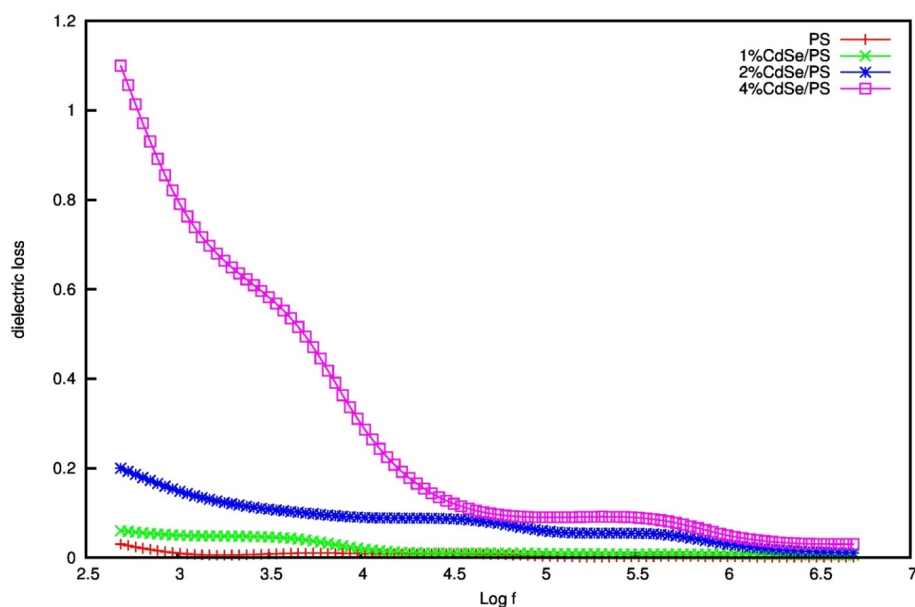
### 8.3.5 Dielectric Studies

Fig.8.7 shows the variation of dielectric constant of PNC's at different frequencies. It is observed that initially the dielectric constant has larger values at lower frequencies, decreases with increase in frequency and remains almost constant at room temperature. The

decrease in dielectric constant of PNC on increasing the frequencies may be attributed to the dependence on the electronic, ionic and orientational polarizations. At low frequencies, all the four polarizations' influence is noticeable. The space charge contribution depends on the purity and perfection of the material. Hence, the larger values of dielectric constant and dielectric loss exhibited by PNC at low frequencies may be attributed to space charge polarization.



**Fig.8.7:Variation of dielectric constant as a function of frequency of PS and PS / CdSe composites.**



**Fig.8.8: Variation of dielectric loss  $\epsilon''$  as a function of frequency of PS and PS / CdSe composites**

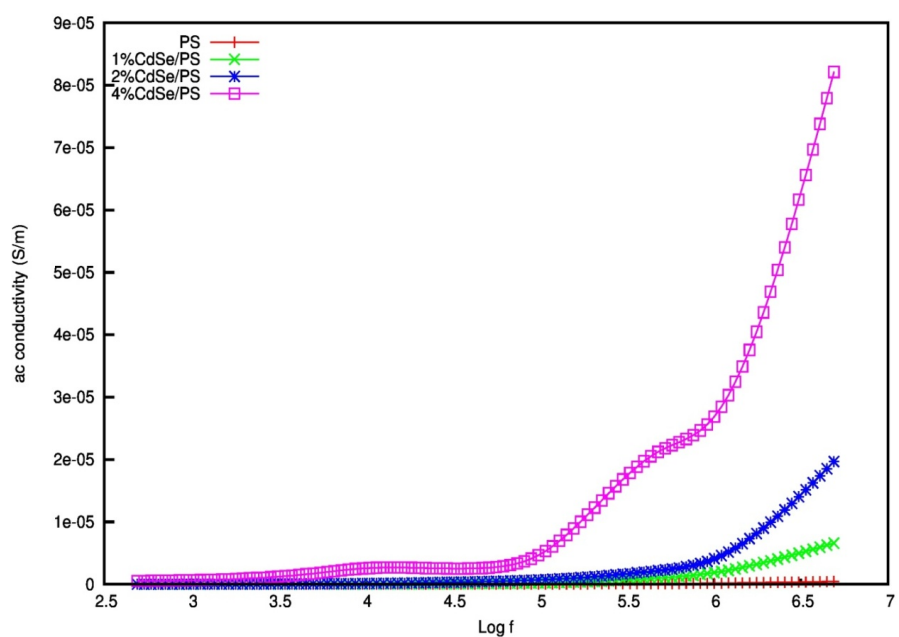


**Fig.8.9: A.C Conductivity of pure PS and PS / CdSe composites**

Fig.8.8 shows the variation of dielectric loss of samples as a function of frequency. The trend in the variations of both dielectric constant and dielectric loss as a function of frequency is almost the same. Fig.8.9 depicts the variation of AC conductivity of PNC's on varying frequency. Conductivity is increased with increase in frequency, may be due to the reduction in space charge polarization at high frequency. The pure PS has low conductivity when compared to the PS / CdSe composites of different concentrations. As the concentration of CdSe nanoparticles increases conductivity also increases.

### **8.3.6 TG – DTA Analysis**

Thermo gravimetric (TG) and differential thermal analysis (DTA) on pure PS and its composites were carried out from room temperature to 600°C. A neat distinctive TG-DTA trace of pure and doped samples are shown in Fig.8.10a –d. Almost the same thermal behaviour is observed for all the samples. However, there is a change in the onset temperature, almost same behavior is seen for the four samples with single step decomposition between 350°C to 460°C. It is clear that pure PS is thermally stable up to 298°C whereas the thermal stability of 2% CdSe and 4% CdSe / PS increases up to 309°C and 315°C respectively. That is, the thermal stability of the PS nanocomposite increases with increase in the filler concentrations.

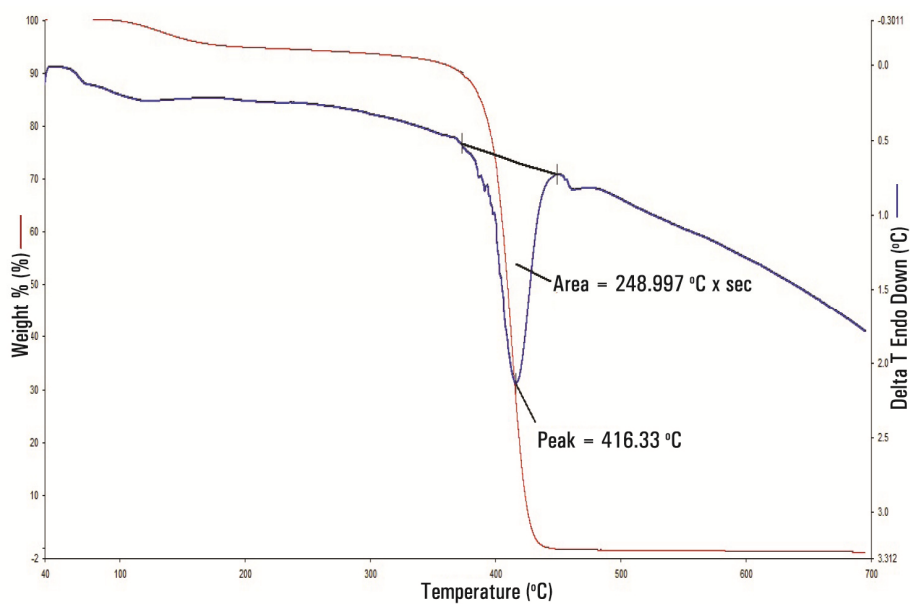


Fig.8.10a: TGA and DTA trace of pure PS

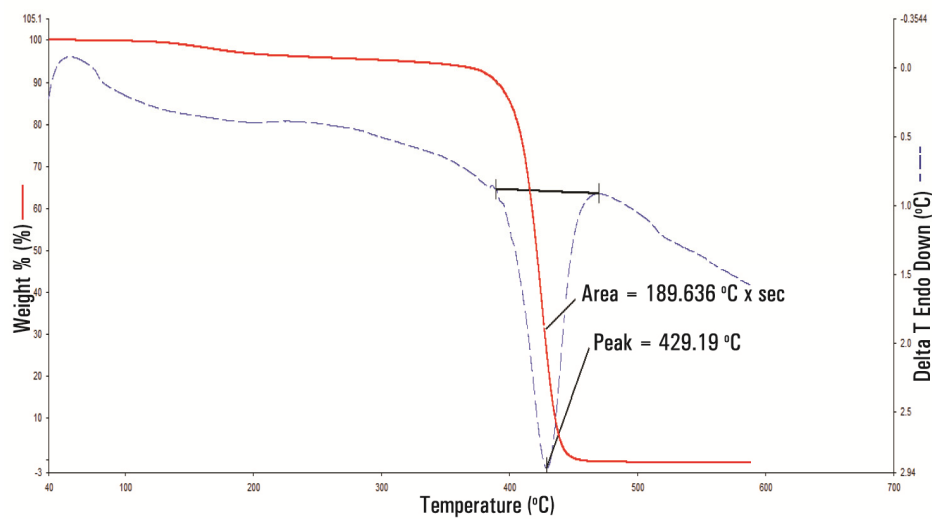


Fig.8.10b: TGA and DTA trace of PS / 1 % CdSe



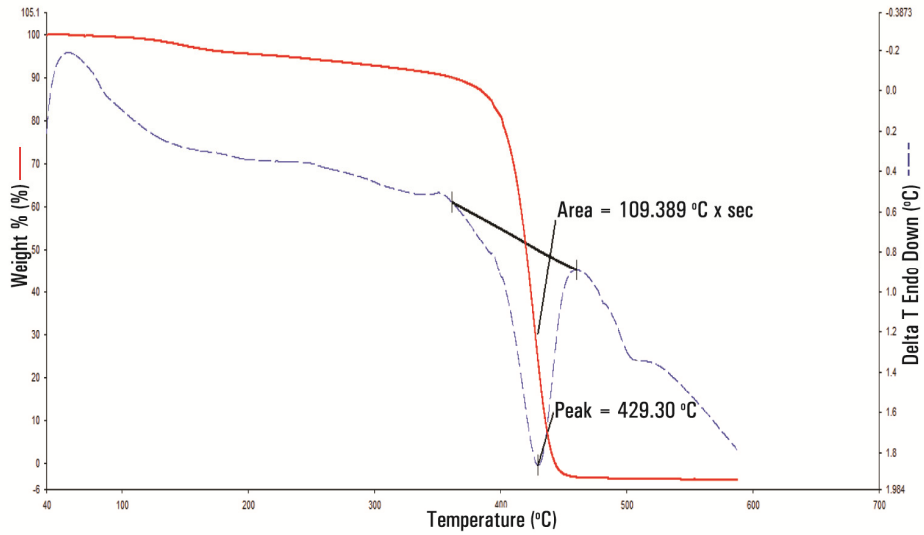


Fig.8.10c: TGA and DTA trace of PS / 2 % CdSe

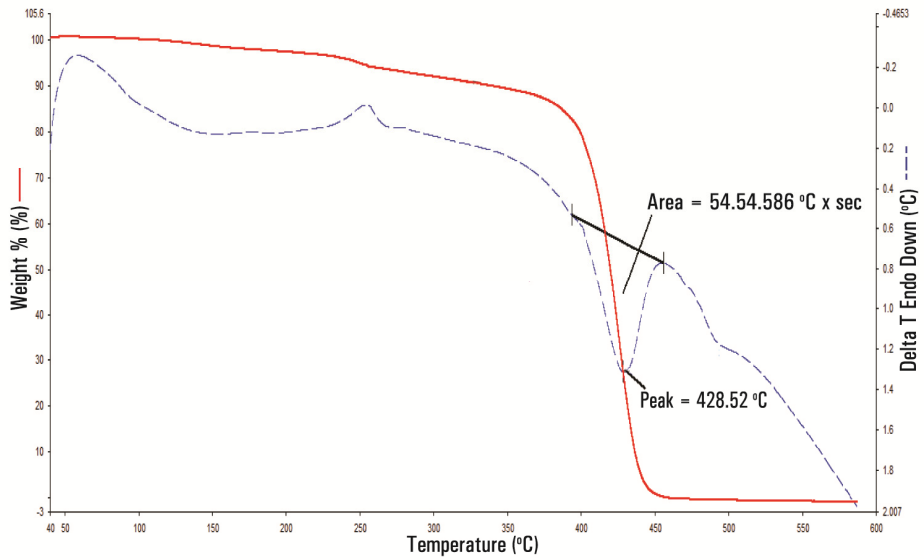


Fig.8.10d: TGA and DTA trace of PS / 4 % CdSe

### 8.3.7 Photopyro Electric Studies (PPE)

An improved photopyroelectric technique has been used to determine the thermal parameters of the samples. The necessary criterion that needs to be satisfied for such a measurement is that, the sample, the pyroelectric detector and the backing should be thermally thick during measurements. The sample was illuminated by an intensity-modulated beam of light, which gives rise to periodic temperature variation by optical absorption. The thermal waves so generated propagate through the sample and were detected by the pyroelectric detector. Measurements of PPE signal phase and amplitude enable one to determine the thermal diffusivity and thermal effusivity. From the measured values of  $\alpha$  and  $e$ , the thermal conductivity  $k$  and heat capacity  $C_p$  of the samples were calculated and presented in Table 8.2.

**Table 8.2: Thermal parameters of PS and PS / CdSe nanocomposites**

Sample	Thermal effusivity (Ws <sup>1/2</sup> /m <sup>2</sup> K)	Thermal diffusivity (X 10 <sup>-7</sup> m <sup>2</sup> /s)	Thermal conductivity (W/mK)	Sp.Heat capacity (J/KgK)
PS	961	0.59136	0.704	1250
PS /1% CdSe	746	0.5807	0.542	990
PS /2% CdSe	686	0.4809	0.4535	980
PS /4% CdSe	665	0.4652	0.432	975

## 8.4 Conclusion

Polystyrene / CdSe composites of different filler concentrations have been prepared successfully using ultrasonication method. The bandgap and Urbach energy of the samples were calculated and it is found that bandgap energy decreases with increase in filler concentration

while Urbach energy increases. Both dielectric constant and dielectric loss decrease with increase in frequency. The thermal stability of the composites was found to increase by the presence of CdSe nanoparticles whereas thermal conductivity decreased.

## **References**

- [1] Uthirakumar P, Nahm KS, Hahn Y B, Lee Y S. Eur. Polym. J. 2004, 40,2437.
- [2] Uthirakumar P, Nahm KS, Hahn YB, Lee YS. Eur Polym J 2004, 40, 2437.
- [3] Vollenberg P H T, Heikens D, Polymer 1989, 30, 1656.
- [4] Alivisatos A P, J. Phys. Chem. 1996, 100, 13226..
- [5] Alivisatos A P, Science 1996, 271, 933
- [6] Murraray C B, Kagan C.R, Bawendi M G, Annu. Rev. Mater. Sci. 2000, 30, 545.
- [7] Dabbousi B O, Rodriguez-Viejo J, Mikulec F.V, Heine J R,. Mattoussi H, Ober R, Jensen K F, Bawendi M G, J. Phys. Chem. B 1997, 101,9463.
- [8] Chaudhary S, Ozkan M, Chan W C W, Appl. Phys. Lett. 2004, 84, 2925.
- [9] Klein D, Roth R, Lim A, Alivisatos A P, McEuen P L, Nature 1997, 389, 699.
- [10] Walker G W, Sundar V C, Rudzinski C M, Wun A W, Bawendi M G, Nocera D G, Appl. Phys. Lett. 2003, 83, 3555.
- [11] Peres M, Costa L C, Neves A, Soares M J, Monteiro T, Esteves A C, Barros-Timmons A, Trindade T, Kholkin A, Alves E, Nanotechnology 2005, 9, 1969.
- [12] El-Khodary, Physica B: Condensed Matter, 2010, 405 (16), 4301.

.....✉.....

## EFFECT OF ELECTRON IRRADIATION ON THE PROPERTIES OF PS, EVA & THEIR NANOCOMPOSITES

Contents	9.1	<i>Introduction</i>
	9.2	<i>Experimental Procedure</i>
	9.3	<i>Electrical Studies</i>
	9.4	<i>Thermal Properties</i>
	9.5	<i>Conclusion</i>

### 9.1 Introduction

Recently, material scientists are increasingly attracted to designing polymer dielectric materials due to their better signal progression for waveguide applications and inter-layer dielectrics that can reduce resistance-capacitance (RC) time delays [1]. Nanoparticles intercede with polymer matrix and electron beam irradiation offer an alternative in fabricating materials of synergistic properties with ease of processing and can be readily geared towards miniaturization of electronic device fabrication [2,3]. Among many polymer matrices, poly(ethylene-co-vinyl acetate (EVA) captures much attention because of its superior qualities like tunable electrical properties, flexibility, environmental stability and ease of preparation. Polystyrene can also be employed as the matrix material as it has got excellent processability, chemical resistance and optical transparency [4]. ZnSe nanofiller makes a continuous network in

the polymer and impart a greater polarization in an applied electric field, thereby increasing the dielectric constant. The unique optical and electrical properties of ZnSe [5] play a considerable role in the conduction mechanism [6,7] of nanocomposite.

High energy radiation can modify the structure of polymers and can cause changes in chemical, electrical and optical properties [8,9]. Irradiation can also result in bond rupturing and atomic displacement in the polymer so that the displaced atoms can migrate through polymeric network until they are trapped in the lattice leaving deficiency regions [10]. Chain scission, cross linking and chemical transformations are the possible events that affect the variation of electrical properties [11,12].

In order to assess the applicability of ethylene vinyl acetate and polystyrene as dielectric materials, it is necessary to study their dielectric parameters. In the present day environment, electrical engineering materials using dielectrics pave a new path for progress in radio-electronics, automatics, nuclear engineering etc [13]. Modulation of dielectric properties and the ease with which polymers can be shaped into complex multi-polymer systems are the reasons why industrialists looking for novel applications. The dispersion of nanoparticles and subsequent electron irradiation could make considerable progress in this area. Organically modified nano-clay reinforced EVA [14], nano-hydroxyapatite modified LDPE [15], glass fibre reinforced polyamide 6 [16] etc. were some of the electron irradiated polymer composites recently explored for enhancement in thermal and mechanical properties. Electron beam irradiation was found to be a useful method for improving the

dielectric behaviour and AC conductivity of polyethylene –glycol [17] and polyethylene-oxide based electrolyte films [18].

The present chapter deals with the effect of electron irradiation on the electrical and thermal properties of virgin polystyrene (PS) and PS / 2% ZnSe nanocomposites & virgin poly(ethylene-co-vinyl acetate) (EVA) and EVA / 2% ZnSe nanocomposites at 2 kGy and 4 kGy doses.

## **9.2 Experimental Procedure**

The procedure for the synthesis of ZnSe nanoparticles and the preparation of EVA / ZnSe and PS / ZnSe composites etc. are the same as described in Chapter 4 and Chapter 7 respectively.

A variable energy microtron facility available at Microtron center, Mangalore University was made use of for the experiment. The facility provides electrons of 4 - 12 MeV energy and bremsstrahlung radiation of energy 3 - 10 MeV.

The prepared virgin polymer and nano composite films were exposed to 8 MeV electrons in the free air environment. The films were kept at a distance of 30 cm from the beam exit point where almost uniform electron beam distribution exists for an area of 8cm x 8cm. The dose rate was adjusted with a current of 20 mA and the accelerator was operated in pulsed mode at a repetition frequency of 50 Hz and the samples were exposed to a graded electron beam dose of 2 and 4 kGy. The salient features of the Microtron accelerator are detailed elsewhere [19]. The delivered doses were measured using a current integrator calibrated against appropriate radiation dosimeters.

### 9.3 Electrical Studies

LCR Impedance analyzer, HIOKI 3532-50, was used to study the dielectric behavior of the prepared composites in the range of 100 Hz to 5 MHz. Here the polarized molecules or atoms can align in accordance with the applied field and cause electromagnetic energy to be transferred into materials. The dielectric properties of materials are characterized by

$$\epsilon = \epsilon_0 (\epsilon' - j \epsilon'') \dots\dots\dots(9.1)$$

where  $\epsilon_0$  is the permittivity of the free space,  $\epsilon'$  is the real part of permittivity of medium and  $\epsilon''$  is the imaginary part of relative permittivity, which gives the amount of energy dissipated in the dielectric. Amount of energy dissipated to energy stored in an applied electric field, called the loss co-efficient. These results reveal the sensitive effect on molecule's electrical polarizability.

The complex capacitance and dielectric loss are estimated in frequency range of 100Hz to 1MHz. The complex capacitance which relates to a sample of planar geometry of area A and thickness d is

$$C(\omega) = (A/d) \epsilon(\omega) \dots\dots\dots(9.2)$$

$\epsilon(\omega)$  is the permittivity of material. Relative permittivity can be thus obtained.

Fig.9.1 and 9.2 show the variation of dielectric constant as a function of frequency for pure EVA and EVA / 2 % ZnSe with electron irradiation of 2 kGy and 4 kGy doses at room temperature. At lower

frequencies, the samples possess a high relative permittivity and drops down around 1KHz region, then reaches a constant value. The sharp decrease in the value of dielectric constant on increasing the frequency is due to the inability of the dipolar molecules in the polymer to adjust to changes in the orientation direction. The high values of dielectric constant at low frequencies may be due to the accumulation of charges at the interface between the sample and electrodes. The dielectric constant is found to be enhanced by increasing irradiation doses in both the cases. The enhancement in the dielectric constant by electron irradiation may be due to the creation of some defect sites in the band gap of samples. These defects are the result of confinement of charge carriers in the band gap of polymer [14].

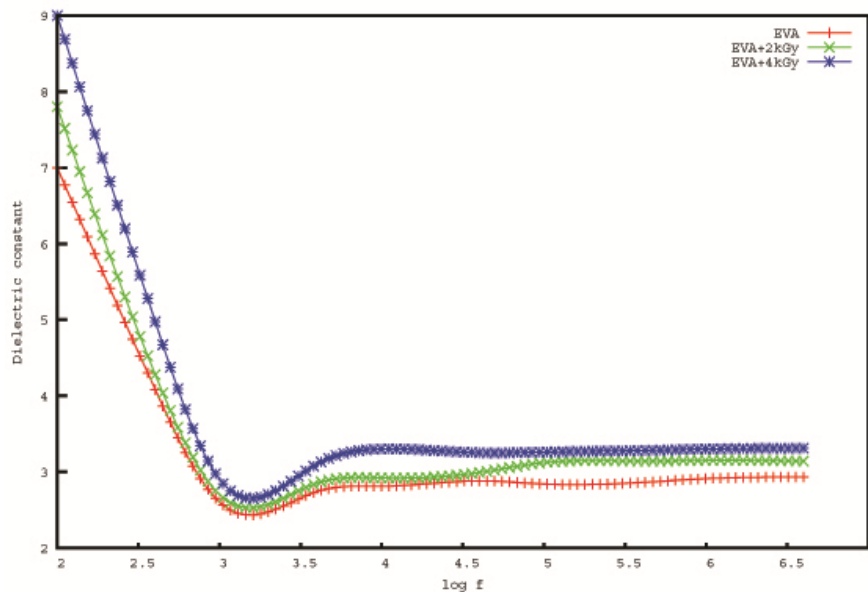


**Fig.9.1: Variation of dielectric constant as a function of frequency at room temperature for pure and irradiated EVA**



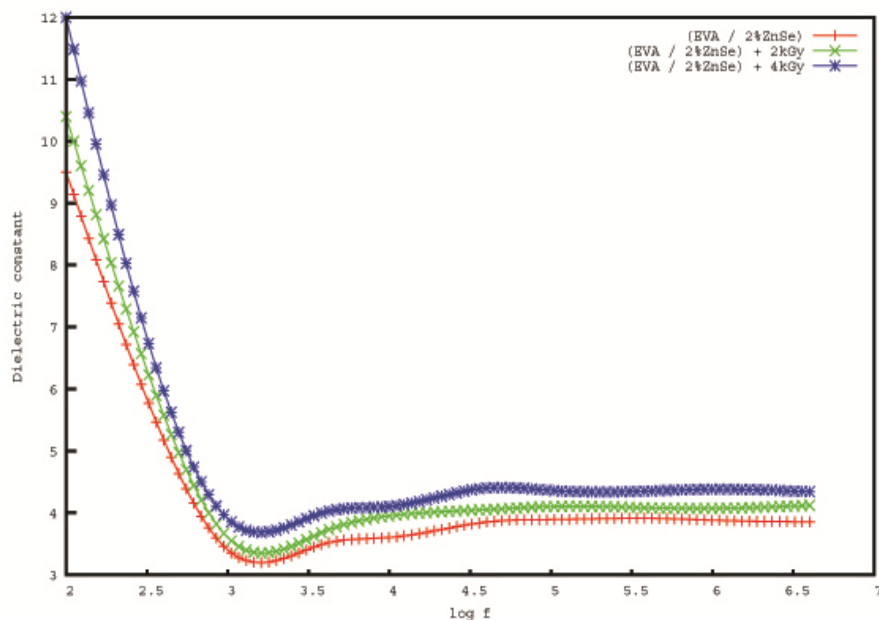


**Fig.9.2:** Variation of dielectric constant as a function of frequency at room temperature for EVA / 2 % ZnSe and irradiated EVA / 2 % ZnSe

The values of dielectric constant at 2 KHz are tabulated in the Table.9.1. From the table it is clear that the value of dielectric constant of pure EVA increases with increase of filler concentration and irradiation doses.

**Table 9.1:** The values of dielectric constant at 2 KHz for pure and irradiated EVA

Sample	Dielectric constant
EVA	2.5
EVA + 2 kGy	2.6
EVA + 4 kGy	2.8
EVA / 2% ZnSe	3.375
EVA / 2% ZnSe+ 2 kGy	3.5
EVA / 2% ZnSe+ 4 kGy	3.8125

The percentage of enhancement in the dielectric constant of polymer composites are compared with pure EVA and tabulated in Table 9.2. From the table it is observed that concentration of ZnSe plays a major role in tuning the pure EVA to a semiconductor. The electron irradiation enhances the dielectric constant of EVA, however there is a drastic enhancement in the dielectric constant when there is a presence of filler. From the above studies it is clear that the effect of electron irradiation is more in the EVA / ZnSe composite than in the virgin EVA. In the pure EVA electric field is created due to electron irradiation only, however in the case of EVA composites the creation of electric field is not only due to irradiation but also due to filler. The variation of dielectric loss with frequency of the pure EVA and EVA / 2% ZnSe at different doses of electron irradiation is shown in the Fig.9.3 and Fig.9.4 respectively. As in the case of dielectric constant, dielectric loss also found to be decreasing with increase in frequency. But there is a slight increase in the dielectric loss as the doses of the electron irradiation increases.

**Table 9.2: Comparison of the percentage of enhancement in the dielectric constant of polymer / composites with pure EVA**

Sample	% of enhancement
EVA & EVA + 2 kGy	4.0
EVA & EVA + 4 kGy	12.0
EVA & EVA / 2% ZnSe	35.0
EVA & EVA / 2% ZnSe + 2 kGy	40.02
EVA & EVA / 2% ZnSe + 4 kGy	52.5

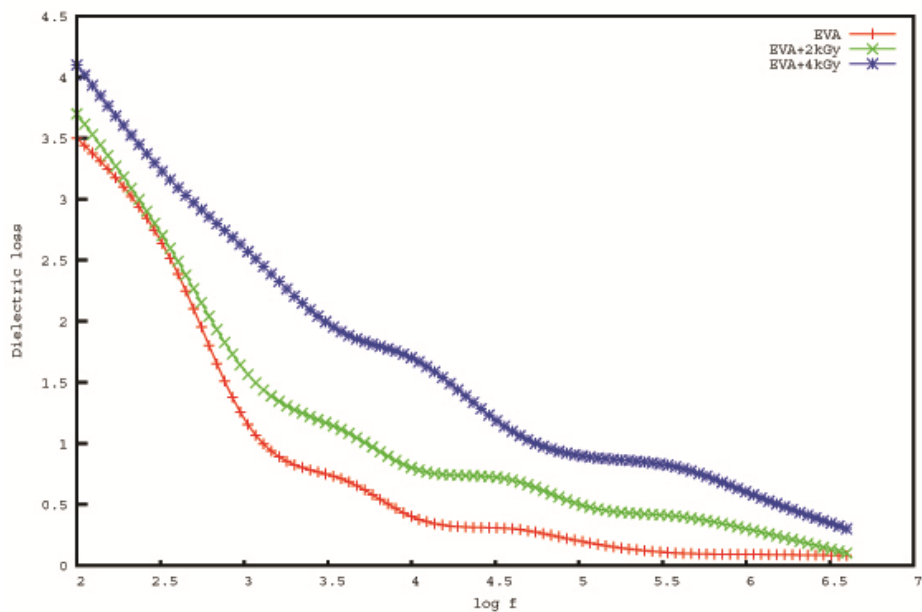


**Fig.9.3: Variation of dielectric loss as a function of frequency at room temperature for pure and irradiated EVA**

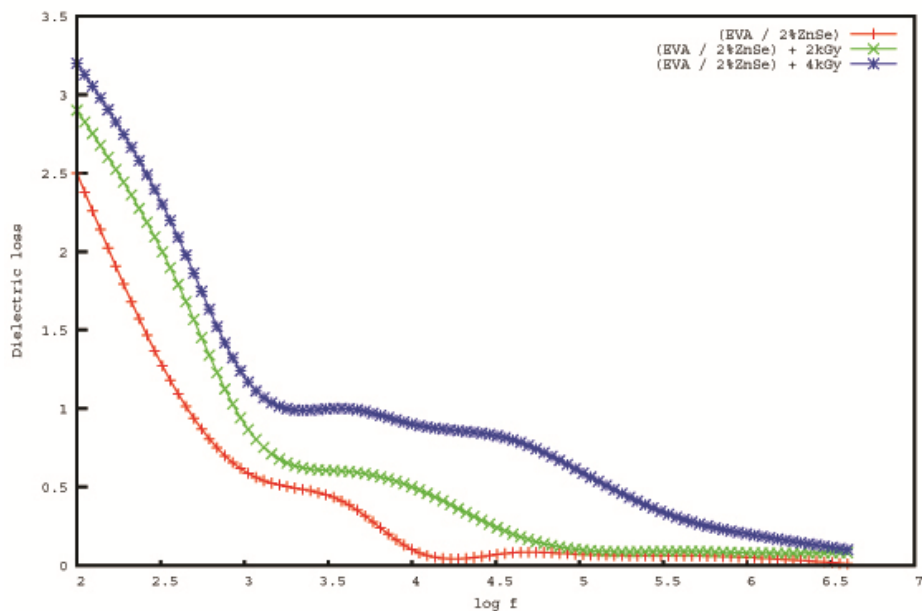


**Fig.9.4: Variation of dielectric loss as a function of frequency at room temperature for EVA / 2% ZnSe and irradiated EVA / 2% ZnSe**

The electrical conductivity in the presence of an alternating current field was also measured using LCR meter at ambient temperature for a frequency range of 100 Hz to 3 MHz. The ac conductivity ( $\sigma_{ac}$ ) of the samples was calculated using the formula  $\sigma_{ac} = \omega \epsilon_r \tan \delta \epsilon_0$ . Fig.9.5 and Fig.9.6 show the plot of log f versus  $\sigma$ . Figures show the frequency dependent electrical conductivity of unirradiated and irradiated films. The AC conductivity of the polymer film increases with frequency which is the common characteristics of disordered materials [20]. Further, the enhancement in conductivity with electron beam is found to be increased with increasing electron beam dose index. There is not much change in conductivity with frequency within  $10^5$  Hz for all films, thereafter an increase in frequency leads to an increase in conductivity [18]. This is due to the fact that trapped charges by e-irradiation are activated at higher frequencies in the disordered EVA polymer chain and are attributed a gradual approach towards the resonance frequency of the charge carriers along the polymeric chain. There may be large energy loss along beam trajectories by the formation of single or multiple helices in the host matrices, thereby increasing the free charge carriers [21]. However, the frequency dependent A.C conductivity of EVA / 2%ZnSe nanocomposite increases with electron beam dose. It may be due to the degradation of the polymer chains [22,23].

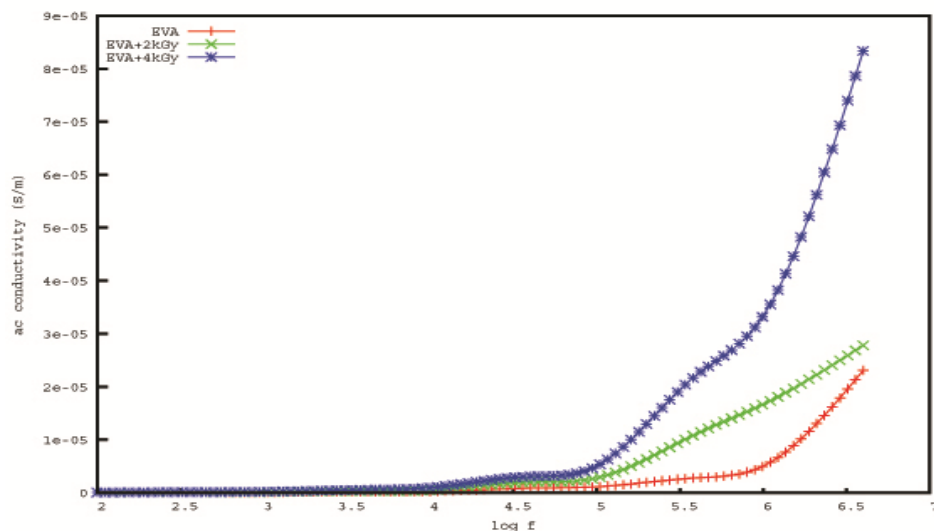


**Fig.9.5: Variation of AC conductivity as a function of frequency for pure EVA and irradiated EVA**

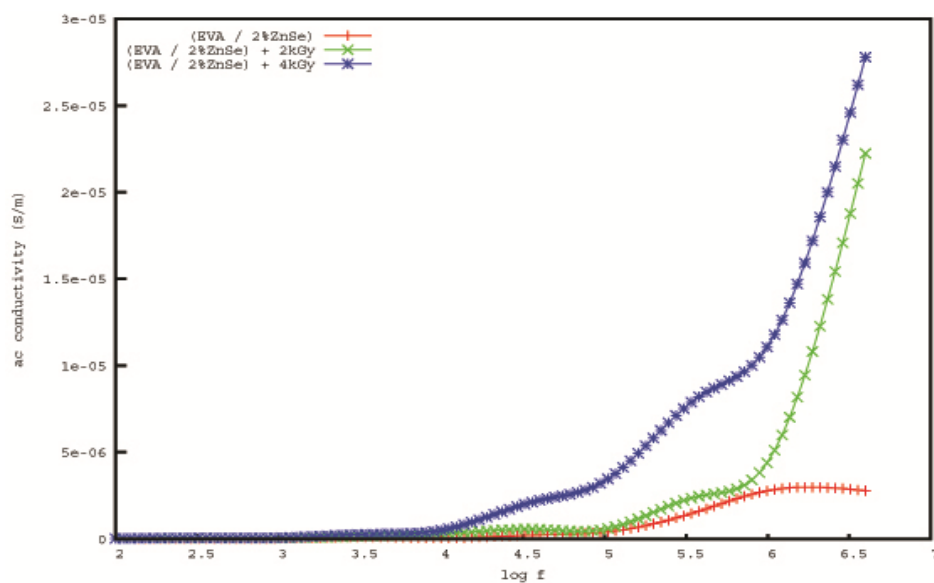


**Fig.9.6: Variation of AC conductivity as a function of frequency for EVA / 2% ZnSe and irradiated EVA / 2% ZnSe**

Fig.9.7 and Fig.9.8 show the variation of dielectric constant with frequency at room temperature for 2 kGy and 4 kGy doses of electron irradiation for pure and PS / 2 % ZnSe polystyrene. The trend in the variation of dielectric constant with frequency is same as in the case of EVA. Dielectric constant in both cases found to decrease with increase in frequency. But there is an increment in the value of dielectric constant when the doses of the electron irradiation increases, which may be attributed to the increment in the charge carriers by electron irradiation. The variation of AC conductivity with frequency for pure PS and PS / 2% ZnSe for 2kGy and 4kGy doses are shown in Fig. 9.9 and 9.10 respectively. From the figure it is clear that AC conductivity is almost constant in the low frequencies and increases in the higher frequencies. Conductivity also increases with the increase of electron irradiation dose. This may be due to the formation of single on multiple helices, thereby increasing the free charge carriers in the polymer film. The values of AC conductivity of PS and PS / 2 % ZnSe at different doses are given in Table 9.2.

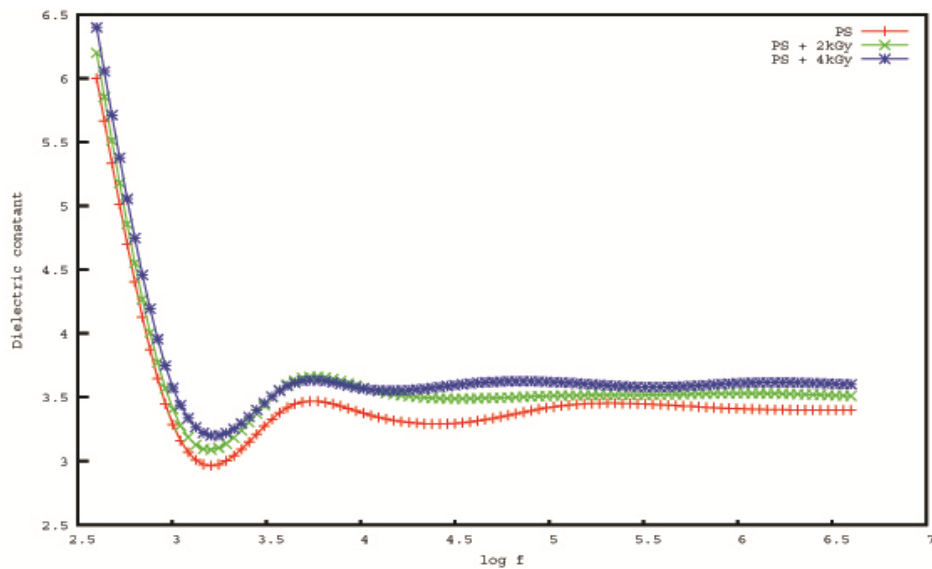


**Fig.9.7:** Variation of dielectric constant as a function of frequency at room temperature for pure and irradiated PS

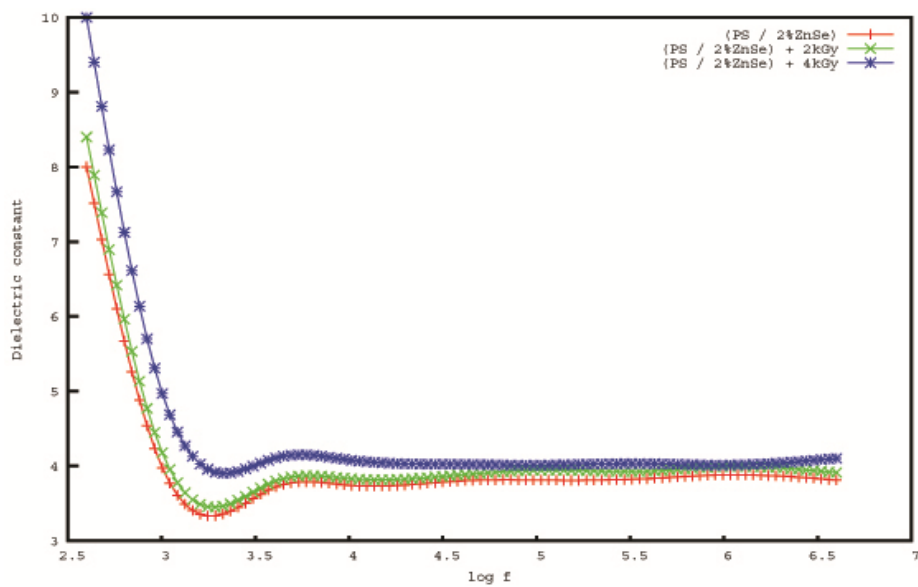


**Fig.9.8:** Variation of dielectric constant as a function of frequency at room temperature for PS / 2% ZnSe and irradiated PS / 2% ZnSe

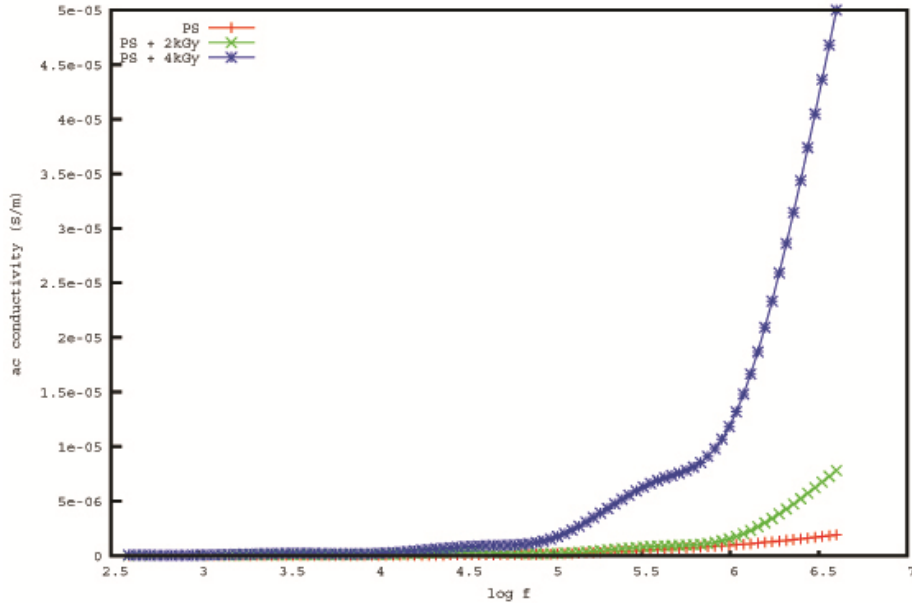


**Fig.9.9: Variation of AC conductivity with frequency for pure and irradiated PS**

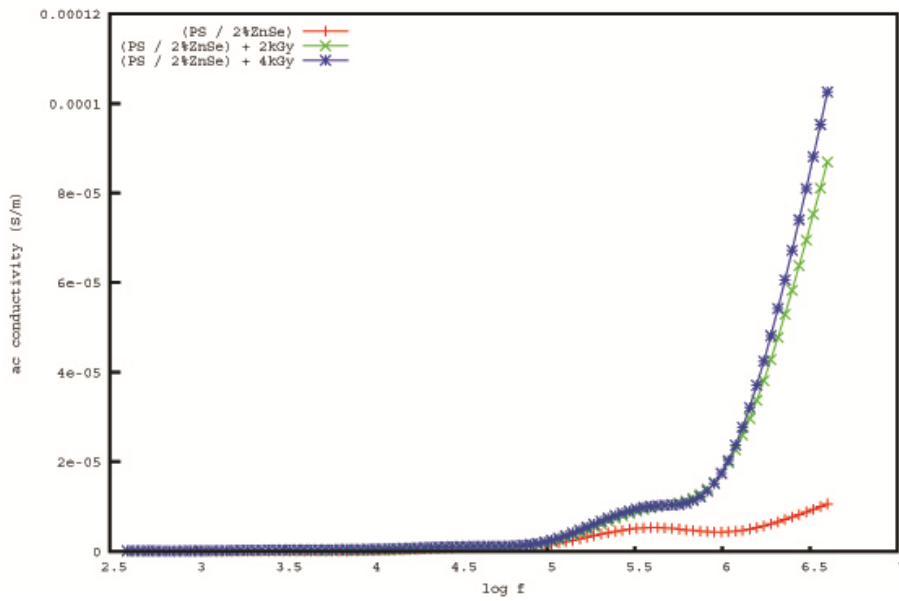


**Fig.9.10: Variation of AC conductivity with frequency for PS / 2% ZnSe and irradiated PS / 2% ZnSe**



**Table 9.2: AC conductivity values of PS and PS / 2 % ZnSe composites with different irradiation doses at 316 kHz frequency.**

Sample	AC conductivity (S/m)
PS	$0.0625 \times 10^{-5}$
PS + 2 kGy	$0.125 \times 10^{-5}$
PS + 4 kGy	$0.625 \times 10^{-5}$
PS + 2% ZnSe	$0.46 \times 10^{-5}$
PS + 2% ZnSe + 2 kGy	$0.76 \times 10^{-5}$
PS + 2% ZnSe + 4 kGy	$1.07 \times 10^{-5}$

## 9.4 Thermal Properties

The thermal properties of composites depend on the fillers and interfacial compatibility of the composite system [15]. Perkin Elmer's STA 6000, simultaneous thermal analyzer is used for the thermal analysis of the samples

### 9.4.1 Differential Scanning Calorimetry

The differential scanning calorimetry (DSC) curves of pure EVA, irradiated EVA (2KGy & 4KGy) are shown in Fig.9.11. It shows an endothermic peak at  $97^{\circ}\text{C}$ , representing the melting temperature of the crystalline phase of EVA [24]. The pure EVA samples as well as the irradiated samples have shown an exothermic peak starting at  $350^{\circ}\text{C}$ . The exothermic peak of the virgin EVA has been found to be larger indicating liberation of heat by molecular rearrangement or crystallization. The increased molecular order or crosslink formation might have reduced the exotherm for irradiated samples. EVA nanocomposites show endotherm peak at around  $500^{\circ}\text{C}$ , representing the complete decomposition of EVA

nanocomposite. The decomposition proceeds around 450<sup>0</sup>C, almost in a similar fashion for both irradiated and virgin EVA.

The 2% ZnSe filled EVA nanocomposite showed similar pattern for the DSC curve (Fig. 9.12). The thermal behaviour of the irradiated and unirradiated nanocomposites showed variation in the exothermic curve starting at 325 <sup>0</sup>C. Unirradiated samples showed larger peak due to the increased crystallization effect at higher temperature. The thermal decomposition behaviour of all the nanocomposites remain the same.

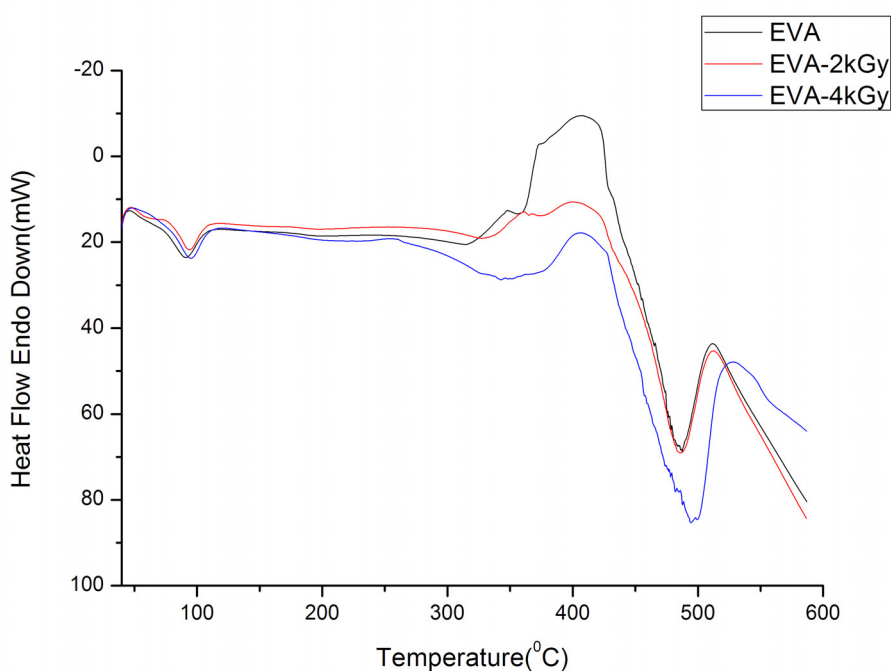


**Fig. 9.11: DSC curves of pure EVA and irradiated EVA**

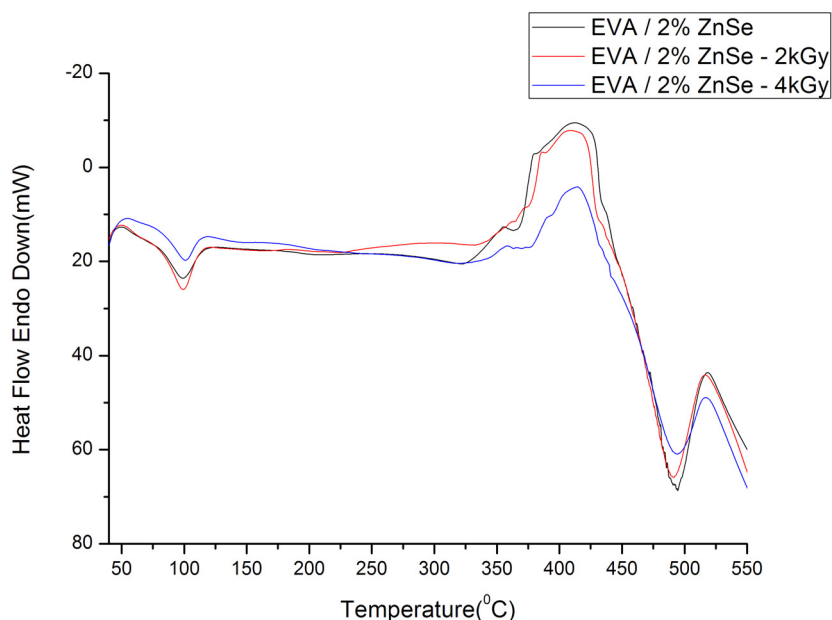


**Fig. 9.12: DSC curves of EVA / 2 % ZnSe and irradiated EVA / 2 % ZnSe.**

The DSC curves of pure polystyrene and the irradiated samples (Fig 9.13) shown similar characters on heating from 15<sup>0</sup>C. The glass transition endothermic peaks of polystyrene were produced at around 100<sup>0</sup>C [25]. The melt behaviour shown by the virgin polystyrene and 2kGy irradiated polystyrene were similar, 4kGy irradiated sample exhibited more resistance to melting at around 140<sup>0</sup>C. The thermal decomposition of all the samples became uniform at around 400<sup>0</sup>C.

DSC curves of 2% ZnSe filled polystyrene nanocomposite exhibited the same pattern of the virgin material and shown in Fig.9.14. Irradiation of the polystyrene nanocomposites exhibited characteristic peaks of virgin and non-irradiated samples, except the 4kGy irradiated nanocomposite. The 2% ZnSe filled nanocomposite with 4kGy irradiation shows higher decomposition peak at around 425<sup>0</sup>C.

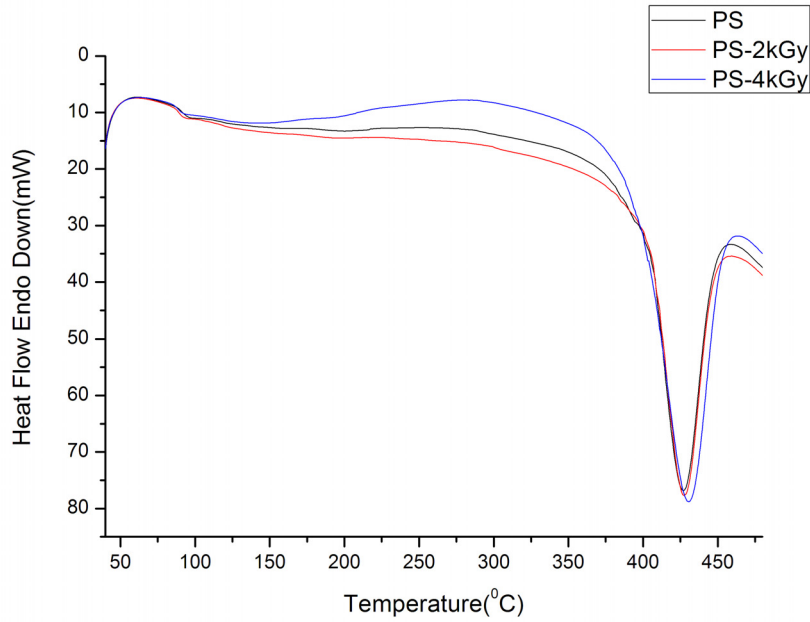


**Fig. 9.13: DSC curves of pure PS and irradiated PS**

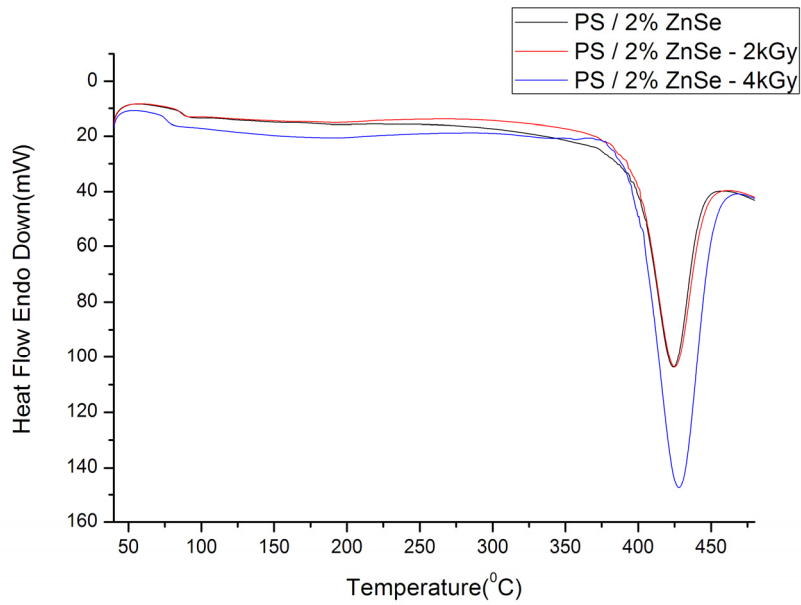


**Fig.9.14: DSC curves of PS / 2 % ZnSe and irradiated PS / 2 % ZnSe.**

#### 9.4.2 TGA analysis

Thermogravimetry is a technique in which the mass of a substance is measured as a function of temperature or time, while the substance is subjected to a controlled temperature program. The TGA analysis of the samples were carried out between 40°C and 600 °C at a heating rate of 20°C/min in nitrogen atmosphere. TGA curves of the pure EVA and irradiated EVA are shown in Fig.9.15. Thermal degradation of pure EVA and irradiated EVA presents a two step thermal decomposition. The first step of decomposition is in between 300°C and 380°C, which corresponds to thermal decomposition of vinyl acetate  $(-\text{CH}_2-\text{CH}_2(\text{O}(-\text{COCH}_3)-))_m$  and double bonds in the polymer backbone. The second step between 380°C and 500°C corresponds to the degradation of ethylene segments  $(-\text{CH}_2-\text{CH}_2-)_n$ . Almost same thermal behaviour is observed by Pistor V et al. [26] when they studied the effect of organophilic montmorillonite clay (OMMT) in EVA. In the first step around 17% of the weight is lost, but the major portion of the weight is lost in the second stage, which is around 83%. A close observation in the TGA curves reveals that there is a slight increase in the thermal stability of the irradiated EVA as compared to pure EVA. This may be due to the creation of more compact three-dimensional crosslinking networks which is more stable against formation of gaseous products on heating due to electron irradiation [27]. Similar behaviour is also observed in the case of EVA / 2% ZnSe and irradiated EVA / 2% ZnSe composites.

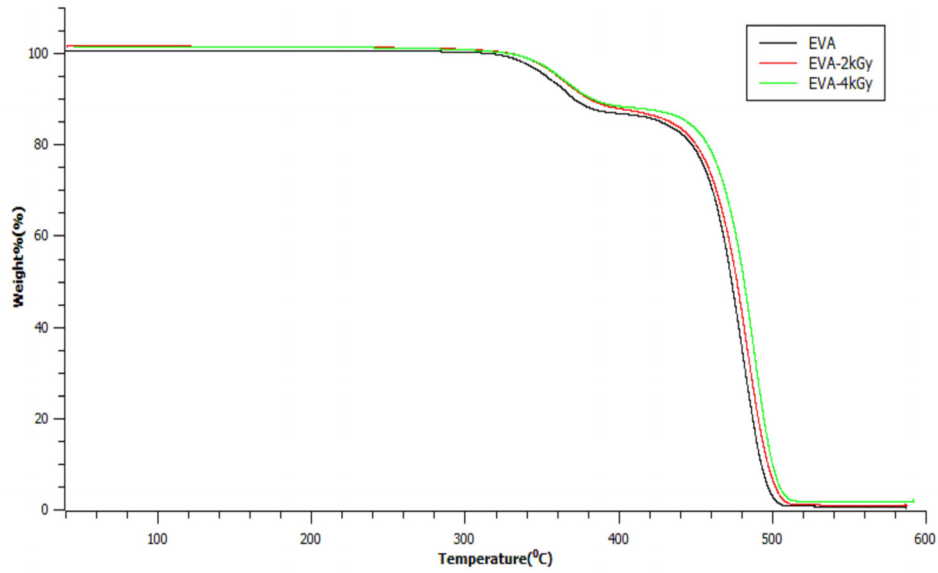


**Fig.9.15: TGA curves of pure EVA and irradiated EVA**

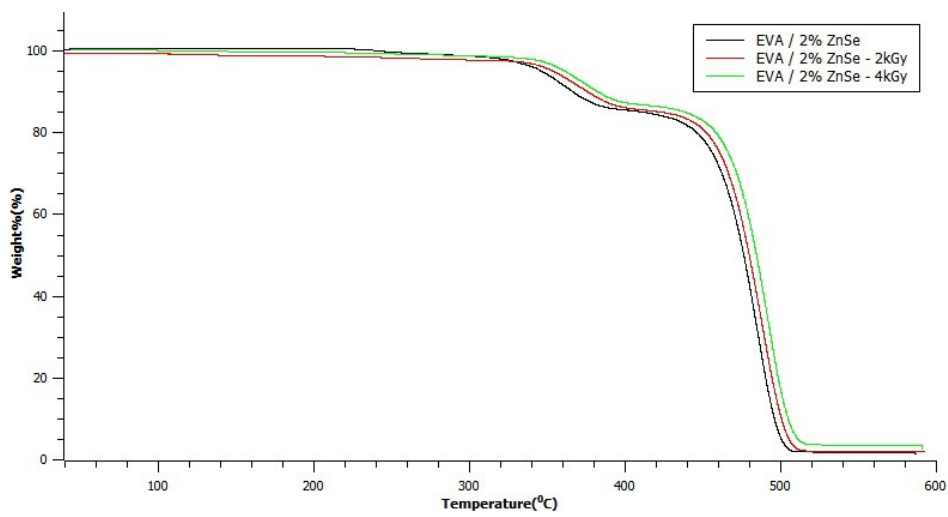


**Fig.9.16: TGA curves of EVA / 2% ZnSe and irradiated EVA / 2% ZnSe**

Effect of irradiation (doses of 2 kGy and 4 kGy) on the TGA curves of pure polystyrene and EVA / 2% ZnSe have also been done using STA 6000 thermal analyser in nitrogen atmosphere at the rate of 20°C / minute. Instead of two stage decomposition in EVA composites, one stage decomposition occurs in the case of polystyrene composites. From the figure, it is clear that there is a slight increase in the onset temperature decomposition of the pure EVA and EVA / 2% ZnSe at 2kGy and 4kGy doses. The enhanced thermal stability by the electron irradiation may be due to the increase in the charge carriers. The same effect is observed by Shah A H et al. [28] by the addition of multiwalled carbon nanotubes in polystyrene.

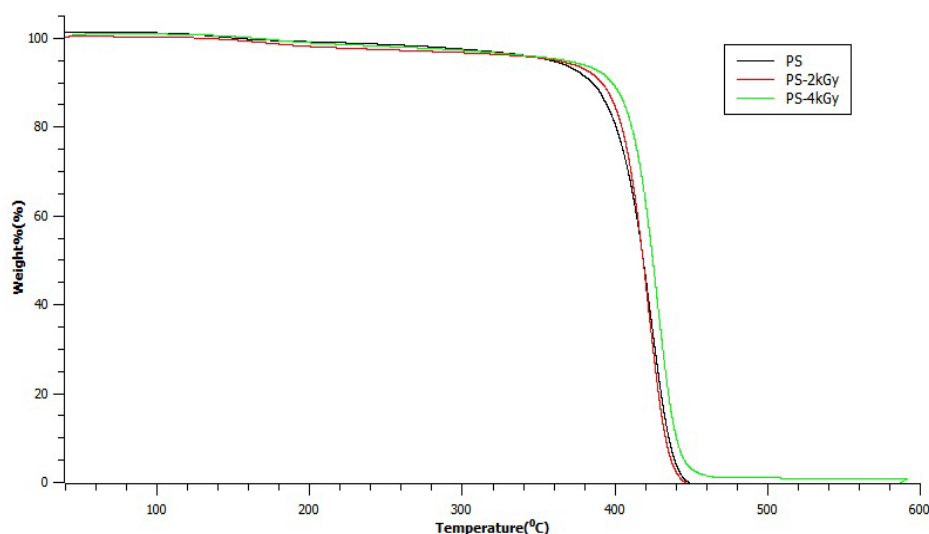


**Fig.9.18: TG curves of pure PS and irradiated PS**

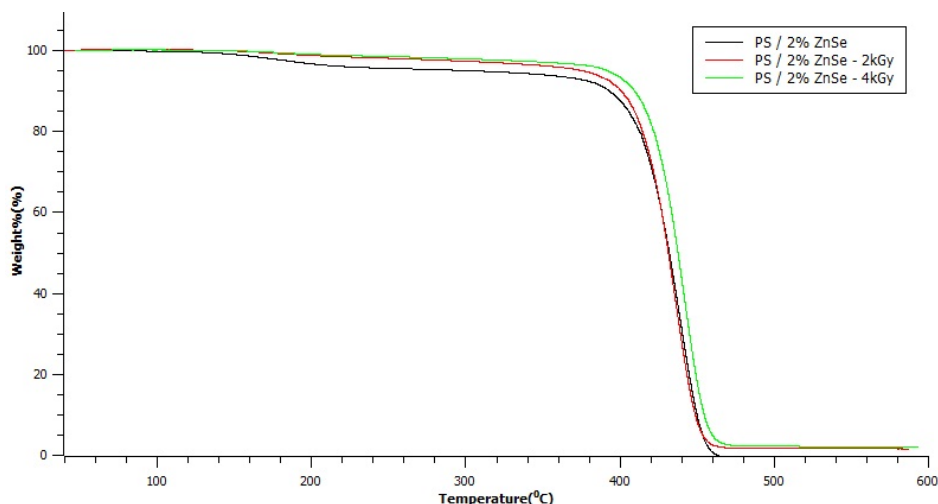


**Fig.9.17: TG curves of PS / 2% ZnSe and irradiated PS / 2% ZnSe**

## 9.5 Conclusion

Effect of electron irradiation on the electrical and thermal properties of the pure EVA and EVA / 2% ZnSe nanocomposites as well as pure PS and PS / 2 % ZnSe PS have been done for 2 kGy and 4 kGy doses. It is found that the dielectric constant of the pure PS, EVA and their nanocomposites increases with increase in dose. However, the percentage of the enhancement of dielectric constant in the nanocomposites was found to be higher than that of pure polymer. AC conductivity of the samples was also increasing with increase in frequencies. The thermal properties of the samples have also been studied. The melting point and the thermal properties of the samples found to increase with increase in the electron irradiation doses.



## Reference

- [1] Tummala R R and Rymaszewski E J. Microelectronic Packaging Handbook. Van Nostrand Reinhold. New York, 1989.
- [2] Radium I, Putri, R I, and Siswanto S, International Journal of Engineering and Technology, 2012, 12, 6,5.
- [3] Fan Z and Lu J G, J.Nanosci. Nanotechnol, 2005,5, 1561.
- [4] Murakami T N, Fukushima Y, Hirano Y, Tokuoka Y, Takahashi M, Appl. Surf. Sci., 2005, 249 , 425.
- [5] Homann T, Hotje U, Binnewies M, Borger A, Becker K D, Bredow T, Solid State Sci.,2006, 8, 44.
- [6] Maria C Tamargo, II-VI Semiconductor Materials and their Applications, Taylor and Francis, New York, 2002, 113.
- [7] Kasap S, Handbook of Electronic and Photonic Materials, Springer, Berlin, 2007.
- [8] Bouffard S, Gervais B, Leroy C, Nucl. Instrum. Methods B 1995, 105,1.
- [9] Singh J P, Singh R, Ghosh S, Tripathi A, Kabiraj D, Gupta S, Som T, Kumar R, Arora S K, Asokan K, Avasthi D K, Kanjilal D, Mishra N C, Mehta G K., Nucl. Instrum. Methods B 1999, 156, 206.
- [10] Abd- El Khader F H, Said G, Attia G and Abo-El Fadl A M., Egypt J.Phys. Vol 37, No 2, pp 111 (2006)
- [11] Mishra R, Tripathy S P, Sinha D, Dwivedi K K, Ghosh S, Khathing D T, Muther M, Fink D , Chung W H, Nucl.Instrum. Methods B. 2000, 168,59.
- [12] Davenas J, Boiteux G, Xu X L, Adem E, Nucl. Instrum. Methods B. 1988,32,136.
- [13] Tarev B, Physics of Dielectric Materials, Russia, 1975.
- [14] Bibo Wang, Lei Song, Ningning Hong, Qilong Tai, Lu H, Hu Y, Radiation Phys. And Chem., 2011, 80,1275.

- [15] Soltani Z, Ziaie F, Ghaffari M, Afarideh H, Ehsani M, Radiation Phys. And Chem., 2013, 83,79.
- [16] Maria Porubska, Ivica Janigova, Klaudia Jomova, Ivan Chodak, Radiation Phys. And Chem., 2014, 102,159.
- [17] Joykumar Singh T H, Ganesh Sajeev K, Siddappa S, Bhat V, Jour. of Polymer Sci., Part B, Polym. Phys., 42, 1299.
- [18] Raghu S, Kilarkaje S, Sanjeev G, Nagaraja G K, Devendrappa H, Radiation Phys. And Chem., 2014, 98,124-131.
- [19] Siddappa K, Ganesh K M, Balakrishna, Ramamurthi S S, Soni H C, Shrivastava P, Sheth Y, Hemanani R, Radiat. Phys. Chem. 1998,51,4-6, 441.
- [20] Abel-Hamid H M, Radwan R M, Ashour A H, Ion beam induced changes in electrical resistivity of polymer films : the case of unplasticized poly(vinyl chloride). J. Phys. D: Appl.Phys. 35 (2002) 1183.
- [21] Chandra S, Annapoorni S, Singh F, Sonkawade R G, Rana J M S, Ramola R C, Low temperature resistivity study of nanostructured polypyrrole films under electronic excitations. Nucl. Instrum. Methods B (2010) 268, 62.
- [22] Nanda, Pradyot, Maity, Sankar, Pandey, Namitha, Ray, Ruma, Thakur, Tarafdar A K., Sujata. Conductivity enhancement in polymer electrolytes on gamma irradiation. Radiat. Phys. Chem. 80(2011) 22.
- [23] Ferloni P, Magistris A, Chiodeli G, Faucitano A, Buttafava A, Effect of gamma-radiation on the polymer electrolyte P(EO)<sub>8</sub> LiClO<sub>4</sub>. Radiat. Phys. Chem. 40(1992). 367.
- [24] Faker M, RazaviAghjeh M K, Ghaffari M, Seyyedi S A, European Polymer Journal, 2008,44,1834.
- [25] Tianxi Liu, European Polymer Journal, 2003 , 39, 1311.
- [26] Pistor V, Lizot A, Fiorio R, Zattera A J, Polymer, 2010, 51, 5165

- [27] Jamaliah Sharif, Khairul Zaman Mhd Dahlan, Wan Md Zin Wan Yunus, Radiation Physics and Chemistry, 2007,76,1698
- [28] Shah A H, Rizvi T Z, Measurement, 2013, 46, 1541

.....❧.....

# Chapter 10

## SUMMARY AND CONCLUSION

<i>Contents</i>	10.1 <i>Introduction</i>
	10.2 <i>Summary</i>
	10.3 <i>Conclusions</i>

### 10.1 Introduction

This chapter gives a glimpse of the summary and conclusion of the work carried out. The study reveals the effectiveness of II-VI semiconductor nanomaterials as fillers in polystyrene (PS) and poly (ethylene-*co*-vinyl acetate) (EVA) matrices in enhancing thermal, dielectric and optical properties. The possibility of improvement in the electrical and thermal properties of nanocomposites by electron irradiation is also investigated and reported as part of this research.

### 10.2 Summary

This thesis focuses mainly on the development of nanocomposite films based on poly (ethylene co-vinyl acetate) and polystyrene with zinc oxide (ZnO), zinc selenide and cadmium selenide (CdSe) as semiconductor nanofillers for various applications in optoelectronic industry. The contents of various chapters in this thesis are summarised in the following sections.

In Chapter 1, major types of nanocomposites, their constituents, methodology of nanocomposite preparation etc. are explained. The optoelectronic applications of different polymer nanocomposites are also discussed along with a brief description of previous studies done in this field. Literature regarding the nanocomposite structures based on polystyrene and EVA are reviewed. Previous work reported on II-VI semiconductor nano materials embedded in different polymer matrices are also detailed in this chapter. The scope and objectives of the present study are also listed.

Semiconductor nanomaterials in II-VI group used for these experiments were synthesised by hydrothermal / solvothermal methods. The nanopowder obtained was purified and the particle size was evaluated and confirmed by a transmission electron microscope. Zinc oxide (ZnO), cadmium selenide (CdSe) and zinc selenide (ZnSe) nanopowders were then used to synthesise the polymer nanocomposites.

Poly(ethylene-*co*-vinyl acetate) EVA / ZnO composites were prepared by solution casting method with toluene as the solvent for EVA. Nanocomposites with different weight percentages (1,2 and 4 %) of ZnO were prepared after ultrasonication to provide proper filler dispersion. Scanning electron microscope images showed homogeneous dispersion of nano ZnO in the polymer matrix. Optical absorption spectra of the composites gave a large transparency window between 500nm and 1600nm. Band gap of the composites was determined from Tauc plot and found that band gap energy got reduced to 3.97eV by the addition of 4% ZnO. Thermal stability was

found to increase with filler concentration. Photopyroelectric studies showed that thermal conductivity, diffusivity and effusivity increased with ZnO filler concentration. Tensile strength and peel resistance of the prepared composites were increased by 1% incorporation of ZnO.

EVA/ZnSe nanostructures were made in varying percentages of ZnSe by solution casting after direct probe sonication. Microscopic evaluation of ZnSe and EVA/ZnSe composites was done by TEM and SEM. FT-IR and refractive index studies were done to evaluate the nanocomposite's chemical and physical properties. Tauc Plot and Urbach plot were made and it was found that band gap decreases and Urbach energy increases with ZnSe filler incorporation. Dielectric constant, dielectric loss and AC conductivity measurements were carried out at different frequencies. From TG-DTA analysis, it was found that thermal stability improves with nano ZnSe. Thermal conductivity also increased, as found from photopyroelectric studies.

EVA/CdSe nanocomposite materials of different concentrations of CdSe nanoparticle (1%, 2% and 4%) have been prepared successfully by ultrasonication and solution casting. The dielectric constant and dielectric loss were found to be decreasing with increasing frequency remaining almost constant at higher frequencies, but increasing with increase in filler concentration. The band gap of the nanocomposites decreased with increase in the amount of CdSe, but the Urbach energy was found to increase. The onset decomposition temperatures of pure EVA, EVA / 1% CdSe, EVA / 2% CdSe and EVA / 4% CdSe are

298°C, 326°C, 338°C and 352°C respectively. The thermal conductivity of nanocomposites was found to increase with increasing filler concentration. The tensile strength of nanocomposites was found to decrease by the addition of CdSe nanomaterials. On the addition of CdSe, the elongation properties also get reduced. Peel resistance of the nanocomposite increased with 1%CdSe.

In situ-polymerisation of styrene monomer mixed with ZnO nanomaterials was done to prepare the nanocomposite. Scanning electron microscopy confirmed the dispersion of nano ZnO in the polystyrene matrix. UV-Vis absorbance spectra and Tauc plot and Urbach studies were utilised to study the band gap and Urbach energy of the nanocomposite. Raman, FTIR and laser induced fluorescence spectra were obtained and the effect of incorporation of the ZnO filler was analysed. Dielectric studies and AC conductivity studies at varying frequencies were done to find the effect of nanomaterials. Photopyroelectric study was carried out to find the thermal parameters of the prepared PS/ZnO nanocomposite. Thermal conductivity was found to reduce with ZnO filler incorporation.

Chapter 7 explains the synthesis and characterisation of polystyrene-zinc selenide system. Studies were carried out on these thin film nanocomposites with different (1%, 2%, 4%) filler concentrations. Morphological studies and dielectric studies of the nanocomposites were carried out. UV absorption and Raman spectra were used to find optical properties and TG-DTA evaluation was done to identify the thermal behaviour. Onset decomposition temperature of the samples was found to

increase by increasing the filler concentrations. Thermal effusivity, diffusivity, conductivity and specific heat capacity of the samples were studied by photopyroelectric method.

Chapter 8 deals with the influence of cadmium selenide (CdSe) on polystyrene polymer matrices. Solvothermal method was used to synthesize nanoparticles whereas nanocomposites were prepared by in situ polymerization method. Dispersion of the CdSe was studied using SEM analysis. Thermal stability of the composites was found to increase with increasing filler concentration. It was found that both dielectric constant and loss decreased by increasing frequency. UV-Vis-NIR spectroscopy was used to record the optical absorption of the samples and the band gap of the samples was plotted using Tauc's method. It is evident from the Tauc plot that band gap decreased with increasing dopant concentration, which means that the conductivity increases with increasing filler concentration.

The effect of electron irradiation on various properties of virgin polystyrene and EVA matrices and their nanocomposite derivatives based on ZnSe nanocomposites are described in Chapter 9. Thermal stability and the conductivity of the pristine samples and ZnSe composites were found to enhance by increasing the doses of electron irradiation.



### 10.3 Conclusions

The conclusions from the investigations can be stated as follows:

#### **Synthesis and preparation:**

- Hydrothermal and solvothermal processes can be employed as a simple preparation method to synthesise ZnO, ZnSe and CdSe nanoparticles.
- Solution casting of ethylene vinyl acetate copolymer with required ultrasonication can be used for making thin film nanocomposites with uniform thickness.
- In-situ polymerisation of styrene with the nanomaterial dispersed in the monomers can be used for making homogeneous thin films.

#### **Characterisation and optical studies**

- TEM images and SEM images of the morphology of nanoparticles and nanocomposites confirmed that the synthesis/preparation method was reliable.
- FTIR, Raman and LIF spectra confirmed the presence of various chemical groups and their characteristic vibrations and peaks.
- UV-VIS-NIR spectra of the nanocomposites showed the characteristic absorptions, the Tauc and Urbach plots exhibited the decreased bandgap energy and increased Urbach energy with the incorporation of nanofillers.

### **Dielectric Studies**

- The dielectric constant and dielectric loss of the nanocomposites decrease at higher frequencies. With increase of doping, the dielectric properties exhibited slight increase at all frequencies. At a particular frequency, the dielectric constant is found to decrease with increase of temperature.
- AC conductivity of the nanocomposites increases with increasing frequency. At frequencies near 100 kHz, the doped and undoped materials showed much difference in conductivity. At higher doping the conductivity increased exponentially at higher frequencies.

### **Thermal analysis**

- The thermal stability of the nanocomposites was found to increase with semiconductor nano doping. The polystyrene and ethylene vinyl acetate matrices showed enhanced thermal stability and prolonged decomposition characteristics.
- Enhanced thermal conductivity is noticed in ethylene vinyl acetate samples, whereas the thermal conductivity is reduced in polystyrene matrices. Specific heat capacity, thermal effusivity and diffusivity showed considerable variation with the nanofiller incorporation.

### **Mechanical properties**

- The effect of incorporation of nanofillers on ethylene vinyl acetate was measured. The peel resistance of EVA with nanomaterials improved at very low (1%) loading on all substrates.

### **Electron irradiation**

- Dielectric constant, AC conductivity and thermal stability of the II – VI semiconductor nanocomposites exhibited good improvement on electron irradiation.

In nutshell, the thermal, optical, electrical properties of Ethylene vinyl acetate and polystyrene matrices are improved by the addition of ZnO, ZnSe and CdSe nanoparticles. Electron irradiation on the nanocomposites has a synergistic effect on polymers. Since the properties of the nanoparticles depend on the size, EVA and PS nanocomposite can be utilized effectively for optoelectronic device fabrications by varying the size and concentrations of nanoparticles dispersed in the matrix.

.....✪✪.....

## List of Abbreviations

$\epsilon_0$	-	Permittivity of free space
$\epsilon_r$	-	Dielectric constant
$\mu\text{V}$	-	Microvolt
$\text{mW}$	-	Milliwatt
$\text{W}$	-	Watt
$\text{J}$	-	Joule
$\text{K}$	-	Kelvin
$\text{Kg}$	-	Kilogram
$\text{nm}$	-	Nanometer
$\mu\text{m}$	-	Micrometer
$\mu_0$	-	Permeability of free space
$\text{\AA}$	-	Angstrom
$\theta$	-	Theta
$\Delta$	-	Delta
$\omega$	-	Omega
$\text{g}$	-	Gram
$\lambda$	-	Wavelength
$\alpha$	-	Thermal diffusivity
$k$	-	Thermal conductivity
$e$	-	Thermal effusivity
$C_p$	-	Specific Heat capacity
$\text{eV}$	-	Electron Volt
$E_g$	-	Band gap
$E_u$	-	Urbach energy
UV-Vis-IR	-	Ultraviolet Visible Infrared
FT-IR	-	Fourier Transform Infrared

*List of Abbreviations*

---

TGA	-	Thermogravimetric
DTA	-	Differential thermal analysis
DSC	-	Differential scanning calorimetry (DSC),
PPE	-	Photopyroelectric
PNC	-	Polymer Nanocomposite
PS	-	Polystyrene
EVA	-	Ethylene Vinyl Acetate
ZnO	-	Zinc Oxide
ZnSe	-	Zinc Selenide
CdSe	-	Cadmium Selenide
LIF	-	Laser Induced Fluorescence
CNC	-	Cellulose Nano Crystal
CNT	-	Carbon Nano Tube
TEM	-	Transmission Electron Microscopy
SEM	-	Scanning Electron Microscopy
ASTM	-	American Society for Testing and Materials
PANI	-	Polyaniline
PTP	-	Polythiophene
PPy	-	Polypyrrole
PVDF	-	Poly-Vinylidene Fluoride
OPV	-	Organic Photovoltaic
OLED	-	Organic Light Emitting Diodes
PVA	-	Poly Vinyl Alcohol
PP	-	Poly Propylene
PLA	-	Poly Lactic Acid
ICP	-	Intrinsically Conducting Polymers
CPC	-	Conductive Polymer Composite

.....❧.....

## ||| List of Publications |||

### Publications

- [1] **Jose Sebastian**, Eby T Thachil, Jobin Job Mathen, Augustine J. Edakkara, Nelson Kuriakose, Joby Sebastian, Ginson P. Joseph (2015) Preparation and Characterization of ZnSe/EVA Nanocomposites for Photovoltaic Modules: *Journal of Minerals and Materials Characterization and Engineering* **3**, 215-224.
- [2] **Jose Sebastian**, Eby T. Thachil, Jobin Job Mathen, J. Madhavan, Prince Thomas, Jacob Philip, M. S. Jayalakshmy, Shahrom Mahmud, Ginson P. Joseph (2015) Enhancement in the Electrical and Thermal Properties of Ethylene Vinyl Acetate (EVA) Co-Polymer by Zinc Oxide Nanoparticles: *Open Journal of Composite Materials* **5**, 79-91.
- [3] **Jose Sebastian**, Eby T. Thachil, Jobin Job Mathen, Prince Thomas, Jacob Philip, Ginson P. Joseph (2015) Polymer nanocomposite based on EVA for enhanced thermal and electrical properties. (Communicated to Journal of Polymer Research)
- [4] **Jose Sebastian**, Eby T. Thachil, Jobin Job Mathen, Prince Thomas, Jacob Philip, Ginson P. Joseph (2015) Effect of ZnO nanofillers in electrical and optical properties of Polysterene films (Communicated to Materials Research Bulletin)
- [5] **Jose Sebastian**, Eby T. Thachil, Jobin Job Mathen, Prince Thomas, Jacob Philip, Ginson P. Joseph (2015) Effect of electrical, thermal and optical properties of CdSe on Polysterene films (Communicated to Materials Characterizations)

### Presentations

- [1] *Electrical and Thermal behaviour of ZnO / EVA Polymer Nanocomposites* : **Jose Sebastian**, Augustine J. Edakkara, Jobin Job Mathen, Joseph Madhavan, S.E Al Garni, Ginson P. Joseph; Sixth International Conference on Optical, Optoelectronic and Photonic Materials and Applications (ICOOPMA 14), **27<sup>th</sup> July – 1<sup>st</sup> August 2014**, organized by The Faculty of Engineering at the **University of Leeds, England, UK.**

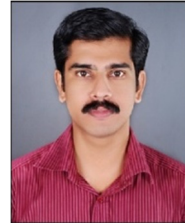
- [2] *Dispersion of ZnO into Polyethylene Vinyl Acetate and electrical and thermal behaviour of their Nanocomposites: Jose Sebastian, Augustine J.Edakkara, Jobin Job Mathen, GinsonP.Joseph; International Materials, Industrial and Manufacturing Engineering Conference (MIMEC 2013) during 4-6 December 2013, Johor Bahru, Malaysia Organized by Dept. of Materials, Manufacturing and Industrial Engineering, Universiti of Teknologi Malaysia.*
- [3] *Synthesis and characterizations of Polyethylene Vinyl Acetate/ ZnSe nanocomposites: Jose Sebastian, Jobin Job Mathen Augustine J.Edakkara, Joseph Madhavan, Ginson P. Joseph; International Materials, Industrial and Manufacturing Engineering Conference (MIMEC 2013) during 4-6 December 2013, Johor Bahru, Malaysia Organized by Dept. of Materials, Manufacturing and Industrial Engineering, Universiti of Teknologi Malaysia.*
- [4] *Studies on the Optical, Thermal and Electrical behavior of Polystyrene – ZnSe Nanocomposite for Electronics Applications; Jose Sebastian, Eby T Thachil, Jacob Philip, Santhosh Kumar R, Prince Thomas, Ginson P. Joseph; International conference on Emerging Advanced Nanomaterials (ICEAN 2012) during 22-25 October 2012, Brisbane, Australia.*
- [5] *Synthesis and Physico-Chemical properties of Polyvinylalcohol – CdSe Nanocomposite as Electrically Conductive Adhesive ; Jose Sebastian, Eby T Thachil, Jacob Philip, G. Ramalingam, Augustine J Edakkara, Jobin Job Mathen, GinsonP.Joseph; International conference on Emerging Advanced Nanomaterials(ICEAN 2012) during 22-25 October 2012, Brisbane, Australia.*
- [6] *Electrical and Optical Properties of ZnO / Polystyrene Composites: Jose Sebastian, Eby Thomas Thachil, Jeeba Sunny, Jobin Job Mathen, Ginson Joseph; 28 June to 03 July, 2015 in Singapore held at Suntec Singapore Convention & Exhibition Centre organized by Materials Research Society of Singapore.*
- [7] *Electrical and Thermal Properties of ZnO –EVA Nanocomposites Films Jose Sebastian, Eby Thomas Thachil, Ginson Joseph, Eighth International Conference on Materials for Advanced Technologies (ICMAT 2015), 28 June to 03 July, 2015 in Singapore held at Suntec Singapore Convention & Exhibition Centre organized by Materials Research Society of Singapore.*

.....✂.....

## Curriculum Vitae

### Jose Sebastian

Lecturer in Polymer Engineering  
Mahatma Gandhi University College of Engineering  
Muttom, Thodupuzha. 685587  
Ph: 09447980555 E- mail: joseuce@gmail.com



### Personal Details

Date of Birth : 27-02-1979.  
Sex : Male.  
Religion : Christian, RCSC.  
Qualification : B. Tech, M. Tech (Polymer Technology)  
Teaching Experience : 11 years.  
Residence Address : Pampara (H), Muttom P O, Thodupuzha.

.....✍.....